HIGHWAY RESEARCH RECORD

Number 67

Bituminous Materials and Mixes

7 Reports

Presented at the
43rd ANNUAL MEETING
January 13-17, 1964

HIGHWAY RESEARCH BOARD
of the
Division of Engineering and Industrial Research
National Academy of Sciences—
National Research Council
Washington, D. C.
1965

Department of Materials and Construction

John H. Swanberg, Chairman
Chief Engineer, Minnesota Department of Highways, St. Paul

BITUMINOUS DIVISION

William H. Goetz, Chairman
Joint Highway Research Project, Purdue University
Lafayette, Indiana

Lloyd F. Rader, Vice-Chairman
Department of Civil Engineering
University of Wisconsin, Madison

COMMITTEE ON CHARACTERISTICS OF BITUMINOUS MATERIALS AND MEANS FOR THEIR EVALUATION

(As of December 31, 1963)

J. York Welborn, Chairman
U. S. Bureau of Public Roads, Washington, D. C.

Stephen H. Alexander, Research Center, Monsanto Chemical Company, St. Louis, Missouri
Edwin J. Barth, Asphalt Consultant, New York, New York
John H. Barton, Director, Chemical and Bituminous Laboratories, Missouri State Highway Department, Jefferson City
James V. Evans, Marketing Technical Service Department, American Oil Company, Chicago, Illinois
Harry K. Fisher, Consulting Engineer, Washington, D. C.
J. H. Goshorn, Managing Engineer, The Asphalt Institute, Columbus, Ohio
W. H. Gotolski, Associate Professor, Department of Civil Engineering, Pennsylvania State University, University Park
F. C. Gzemski, The Atlantic Refining Company, Research and Development Department, Philadelphia, Pennsylvania
W. J. Halstead, Physical Research Division, U. S. Bureau of Public Roads, Washington, D. C.
James H. Havens, Director of Research, Kentucky Department of Highways, Lexington
Arnold J. Hoiberg, Assistant Director, The Flintkote Company, Whippany, New Jersey
J. O. Izatt, Senior Engineer, Shell Oil Company, New York, New York
Robert E. Meskill, Humble Oil and Refining Company, Houston, Texas
W. G. O'Harra, Engineer of Materials, Arizona State Highway Department, Phoenix
Vytautas Puzinauskas, Assistant Research Engineer, The Asphalt Institute, University of Maryland, College Park
J. C. Reed, Supervising Engineer, Bureau of Testing and Materials, New Jersey State Highway Department, Trenton
E. O. Rhodes, Pittsburgh, Pennsylvania
F. S. Rostler, Director of Research, Golden Bear Oil Company, Bakersfield, California
R. J. Schmidt, California Research Corporation, Richmond
H. E. Schweyer, Department of Chemical Engineering, University of Florida, Gainesville
Vaughn Smith, Vice President, American Bitumuls Asphalt Company, San Francisco, California
D. E. Stevens, California Crude Oil Sales Company, San Francisco
E. G. Swanson, Staff Materials Engineer, Colorado Department of Highways, Denver
Edmund Thelen, Manager, Colloids and Polymers Laboratory, Franklin Institute, Philadelphia, Pennsylvania

R. N. Traxler, Texas Transportation Institute, Texas A & M College, College Station
W. B. Warden, President, Miller-Warden Associates, Raleigh, North Carolina
Frank M. Williams, First Assistant Engineer of Tests, Ohio State University, Columbus
L. E. Wood, Department of Civil Engineering, Purdue University, Lafayette, Indiana

COMMITTEE ON BITUMINOUS SURFACE TREATMENTS

(As of December 31, 1963)

William H. Goetz, Chairman
Joint Highway Research Project
Purdue University, Lafayette, Indiana

D. W. Anderson, South Dakota Department of Highways, Pierre
E. W. Bauman, Managing Director, National Slag Association, Washington, D. C.
J. E. Bell, Assistant to Engineering Director, National Crushed Stone Association, Washington, D. C.
C. W. Chaffin, Supervising Chemical Engineer, Materials and Tests Division, Texas Highway Department, Austin
Robert A. Crawford, Assistant Research Engineer, South Dakota Department of Highways, Pierre
Leslie B. Crowley, Senior Consultant (HQ USAF) Directorate of Civil Engineering, DCS/Operations, Department of the Air Force, Washington, D. C.
John B. Dunbar, District Engineer, The Asphalt Institute, Montgomery, Alabama
Bob M. Gallaway, Research Engineer, Civil Engineering Department, Texas Transportation Institute, Texas A & M College, College Station
Moreland Herrin, Associate Professor of Civil Engineering, Department of Civil Engineering, University of Illinois, Urbana
Phillip L. Melville, Civil Engineering Branch, Engineering Division, Military Construction, Office, Chief of Engineers, Department of the Army, Washington, D. C.
William H. Mills, Consulting Engineer, Atlanta, Georgia
J. W. Reppel, Engineer of Maintenance, Ohio Department of Highways, Columbus
James M. Rice, Highway Research Engineer, Division of Physical Research, U. S. Bureau of Public Roads, Washington, D. C.
Ernest Zube, Supervising Materials and Research Engineer, California Division of Highways, Sacramento

COMMITTEE ON MECHANICAL PROPERTIES OF BITUMINOUS PAVING MIXTURES

(As of December 31, 1963)

Lloyd F. Rader, Chairman
Department of Civil Engineering
University of Wisconsin, Madison

Harry C. Bower, American Bitumuls & Asphalt Company, Baltimore, Maryland
T. W. Cavanaugh, Engineer of Materials, Connecticut State Highway Department, Portland
A. B. Cornthwaite, Division Managing Engineer, Atlantic Gulf Division, The Asphalt Institute, Washington, D. C.
Ladis H. Csanyi, In Charge, Bituminous Research Laboratory, Iowa State University, Ames
Joseph F. Goode, Highway Physical Research Engineer, Physical Research Branch, U. S. Bureau of Public Roads, Washington, D. C.

Donald I. Inghram, Senior Engineer of Physical Tests, Nebraska Department of Roads, Lincoln

Bernard F. Kallas, The Asphalt Institute, University of Maryland, College Park

W. H. Larsen, Chief, Bituminous and Chemical Section, U. S. Army Engineer Waterways Experiment Station, Corps of Engineers, Vicksburg, Mississippi

Phillip L. Melville, Civil Engineering Branch, Engineering Division, Military Construction, Office, Chief of Engineers, Department of the Army, Washington, D. C.

Fred Moavenzadeh, Associate Professor of Civil Engineering, Ohio State University, Columbus

Carl L. Monismith, University of California, Berkeley

O. A. Philippi, Construction Administrative Engineer, Texas Highway Department, Austin

C. K. Preus, Materials and Research Engineer, Minnesota Department of Highways, St. Paul

James H. Schaub, Head, Department of Civil Engineering, West Virginia University, Morgantown

B. A. Vallerga, Vice President, Golden Bear Oil Company, Bakersfield, California

Ellis G. Williams, District Engineer, The Asphalt Institute, Louisville, Kentucky

Ernest Zube, Supervising Materials and Research Engineer, California Division of Highways, Sacramento

George H. Zuehlke, Materials Tests Engineer, State Highway Commission of Wisconsin, Madison

ERRATA

In Highway Research Record Number 67, the fourth and fifth entries of the "Contents" page should read as follows:

Contents

Rheological Response of Bituminous Concrete

CHARLES A. PAGEN
Assistant Professor of Civil Engineering, The Ohio State University

This research is part of a continuing effort to develop more rational methods of flexible pavement design. This study has evaluated in the laboratory the temperature-dependent viscoelastic response of five bituminous concrete mixes representing several major categories used in road surfacing. The complicated dependence of the mechanical properties of bitumen-aggregate compositions on the principal variables of loading time and temperature were separated to yield time functions and functions of temperature.

The validity of the time-temperature superposition concept to these materials was verified to a satisfactory degree of accuracy by aggrement between data obtained from dynamic tests and values predicted by superposition of compression creep measurements over a range of temperature from 0 to 120 F at stress levels in the linear viscoelastic range. This made it possible to define the properties of the bituminous concrete mixes by three general functions: the dependence of the magnitude and phase of the complex modulus on reduced frequency and the temperature dependence of the temperature shift factor, a_T. Experimental verification of the phenomenological linear viscoelastic response of bituminous concrete was obtained by unconfined dynamic and creep experiments to a useful degree of approximation.

The experimental results of complex and creep moduli cover approximately twelve decades of reduced frequency and time, respectively. The time-temperature superposition principle used in this study allowed the viscoelastic data to be extended from 10^{-6} to 10^{6} seconds, a range normally inaccessible by conventional experimental methods. This principle also allows the creep and dynamic strength moduli of bituminous concrete mixtures to be evaluated at any intermediate temperature within the tested experimental range by a relatively few tests. Methods are also presented to incorporate the mechanical properties of the material, evaluated by use of the thermodynamic and rheologic concepts advanced in this study, into pavement design procedures.

•EFFECTIVE UTILIZATION of engineering materials must start with a complete understanding of the materials involved. As new materials are developed, and as the use of existing ones are extended, the evaluation of their engineering properties becomes more significant. The study of the mechanical properties of bituminous concrete is by no means an easy task. This is due to the complex composition of the material, and the variety of environmental and loading conditions under which this material must function. Engineering is an applied science and the ability to simplify and idealize is a requirement to achieve workable solutions to practical problems. The evaluation of the temperature-dependent rheological properties of bitumen-mineral aggregate compositions is no exception, and some degree of idealization is inevitable even in the most sophisticated solutions.

Despite the fact that highway pavements have been constructed from the earliest civilizations, all methods of flexible pavement design have the common disadvantage of

Paper sponsored by Committee on Mechanical Properties of Bituminous Paving Mixtures.

lacking a completely rational basis. The procedure used at this time consists of applying one of several design methods. These design empiricisms rely on past experience, economics, judgment of the design engineer, and correlations of pavement performance with laboratory tests.

In recent years there has been an increase of interest in the development of a theoretical method for the design of flexible pavement structures. This growing interest in a more rational design procedure has evolved from the limitations imposed by the empirical methods in extrapolating beyond the boundaries of previous experience to additional pavement-climate-load problems. If design procedures are to be used beyond their assigned limitations, it seems that theoretical, rather than empirical, methods would provide a better foundation for such extensions.

One of the important requirements for the development of a rational method of flexible pavement design is a procedure which evaluates the mechanical properties of the components of such a layered system under any type of applied load, at any environmental or loading condition. A step in this direction has been taken in this study which has evaluated the complicated dependence of the mechanical properties of five bituminous concrete mixtures representing several major categories used in road surfacing on the important variables of loading time and environmental temperature.

The present study was concerned with defining the rheological response of bituminous concrete over a wide range of loading times or frequencies and with evaluating the temperature dependence of these properties. The linear viscoelastic response of high polymers has been successfully investigated by using the concepts of rheology (1, 2, 3, 4) and a great deal of fundamental information has been developed in this area. Analyses of the viscoelastic behavior of bituminous concrete mixes have been performed using rheologic concepts (5, 6, 7, 8) and this basic research has served as a valuable reference to asphalt technologists in establishing the nature of bituminous concrete. The temperature dependence of the viscoelastic response of bitumens and high polymers has been studied using time-temperature superposition concepts (9, 10, 11). However, the concepts of the kinetic theory and time-temperature superposition techniques or method of reduced variables (1, 12) at the time this study was started have not been extensively applied to the analysis of the mechanical response of bituminous concrete in the time and frequency domains. This paper is concerned with the validity of the application of these useful concepts to bituminous compositions. Therefore, experimental data are presented which compare the rheological moduli of bituminous mixes evaluated by unconfined creep and dynamic tests on the phenomenological level.

Experimental results of two types of test data are presented and discussed: (a) the results of constant load tests used to determine the transient response of the mixture, and (b) the results of direct dynamic and resonant vibration tests of the same material. An essential part of the study is a presentation of the mathematical relations necessary to evaluate the rheologic response of the material by a generalized Voigt linear viscoelastic model for both types of tests.

The objective of this study was to analyze the method of reduced variables concerning the effect of temperature on the mechanical behavior of thermally sensitive materials such as bituminous concrete. The purpose of applying this concept was to determine if time and temperature may have an approximately equivalent effect on the viscoelastic response of bituminous mixes, and if it would be possible to predict the response of the mixture by a relatively few experiments for any temperature within the tested range and at loading times or frequencies both longer and shorter than are normally obtained experimentally. The specific goal of the study was to define the time and temperature dependent mechanical properties of bituminous mixes over a wide range of environmental and loading conditions.

EXPERIMENTAL TECHNIQUES

To evaluate the mechanical properties of the dense-graded asphaltic concrete mixes, two basic types of tests were performed. Creep and dynamic tests allowed the mechanical properties of these pavement materials to be determined independently by each type of test. The applicability of the linear viscoelastic theory and time-temperature super-

position concept to represent the response of asphaltic concrete to a useful degree of approximation was also investigated by both types of tests.

Sinusoidal-Stress Dynamic Tests

To supplement the creep tests and provide information about the dynamic response of bituminous concrete mixes at very short loading time intervals, direct dynamic tests were performed in which the stress varied periodically with a sinusoidal alternation at a frequency, ω. In the dynamic tests a periodic stress was applied to the unconfined specimens and the resulting axial and circumferential strains were recorded using the electronic recorder. This sinusoidal stress was applied by a repetitional loading machine (Fig. 1) designed and built at The Ohio State University's Engineering Experiment Station (13). The equipment consists of an electrical constant speed motor which drives a sinusoidal cam of double eccentricity through a set of interchangeable gears, by which it is possible to vary the frequency of applied load. The sinusoidal stress applied to the samples was measured by a load cell connected to the electronic recorder. Two pairs of SR-4 strain gages were attached to the specimens, one pair attached vertically and the other pair attached horizontally to measure the vertical and lateral strains of the test samples, respectively. The two pairs of strain gages were attached to each specimen at mid-height at diametrically opposite points on the periphery of the test cylinders.

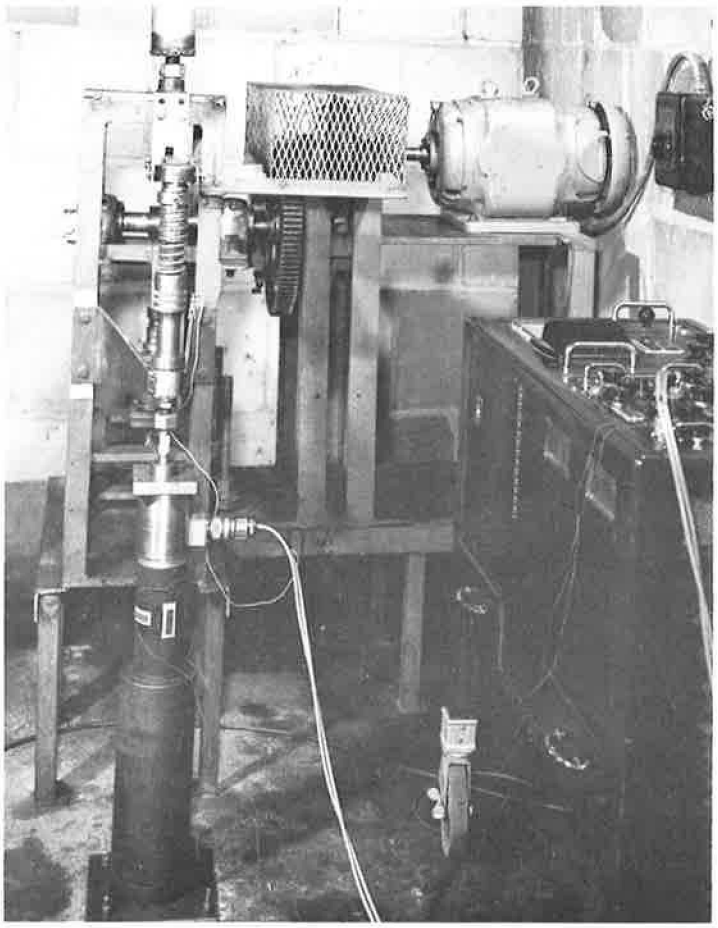

Figure 1. Dynamic test equipment.

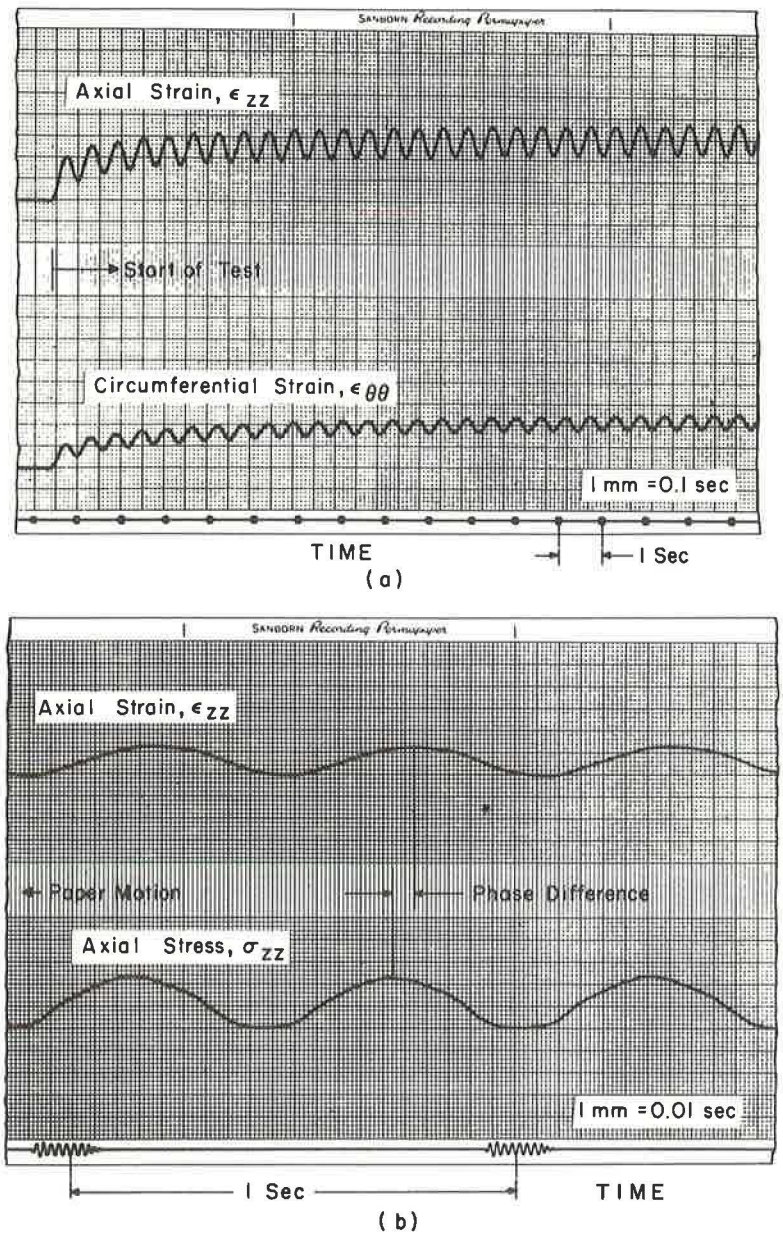

Figure 2. Dynamic test recordings: (a) strain and (b) stress.

Figure 2 shows an actual recording of the stress and strains in a dynamic test. All tests were conducted under isothermal conditions at several frequencies and stress levels. The samples were enclosed in rubber triaxial membranes and placed in a constant temperature water bath for several hours before and during testing. A new sample was used in each test to eliminate any variations due to changes in physical properties as a result of previous testing (14).

Compression Creep Tests

In the creep tests conducted, a constant axial load was quickly applied to the unconfined samples without impact and kept constant throughout the test by a soil consolidation apparatus shown in Figure 3. Continuous recordings of the axial and circumferential strains were obtained by an electronic recorder. A typical test recording of the axial and circumferential strain measured by SR-4 gages, obtained by the electronic recorder, is shown in Figure 4. Vertical deformation of the samples under load was also checked by a linear displacement transducer and by Ames dials. Tests were performed under controlled temperature conditions at several loads at eleven temperatures from 0 to 120 F. The samples were instrumented and strains recorded in a manner similar to the procedure for the identical mixes used in the dynamic tests.

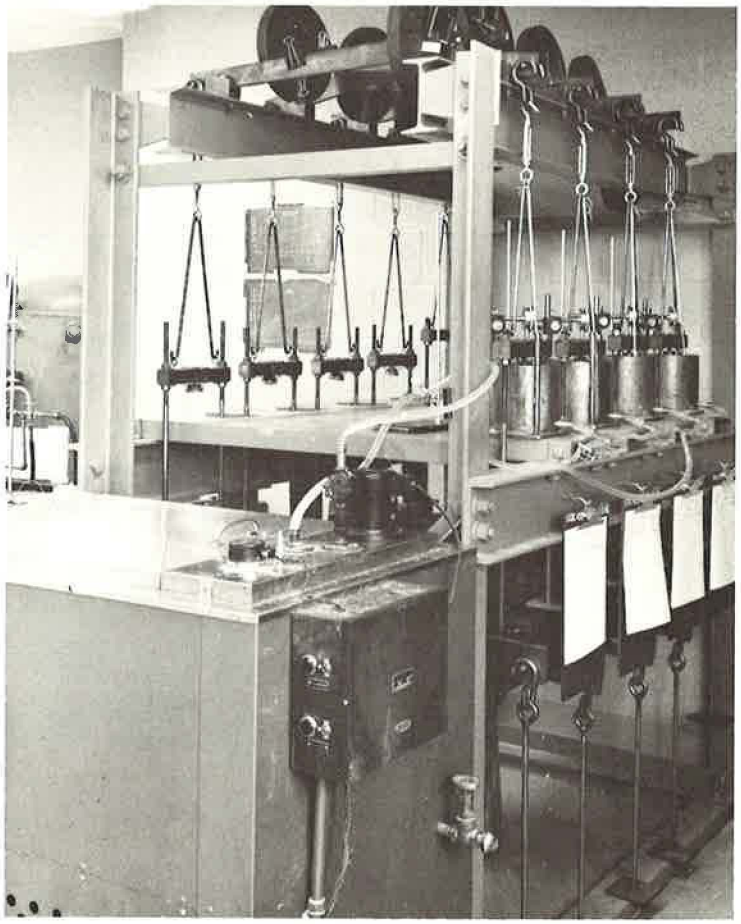

Figure 3. Creep test equipment.

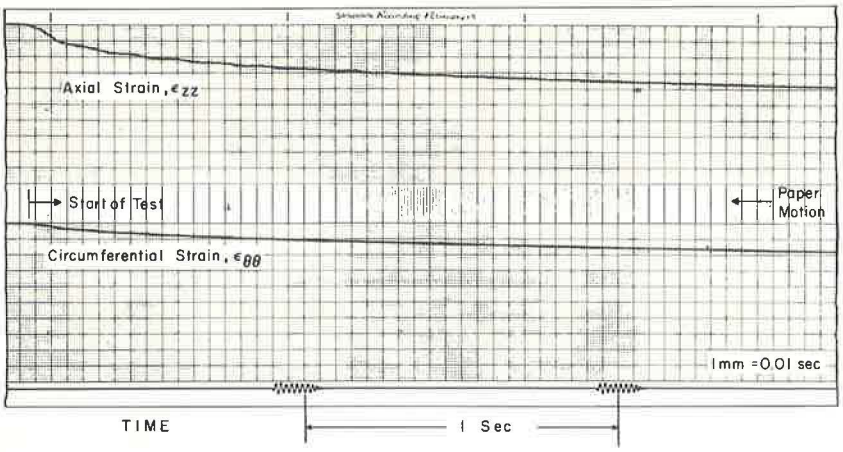

Figure 4. Creep test recordings.

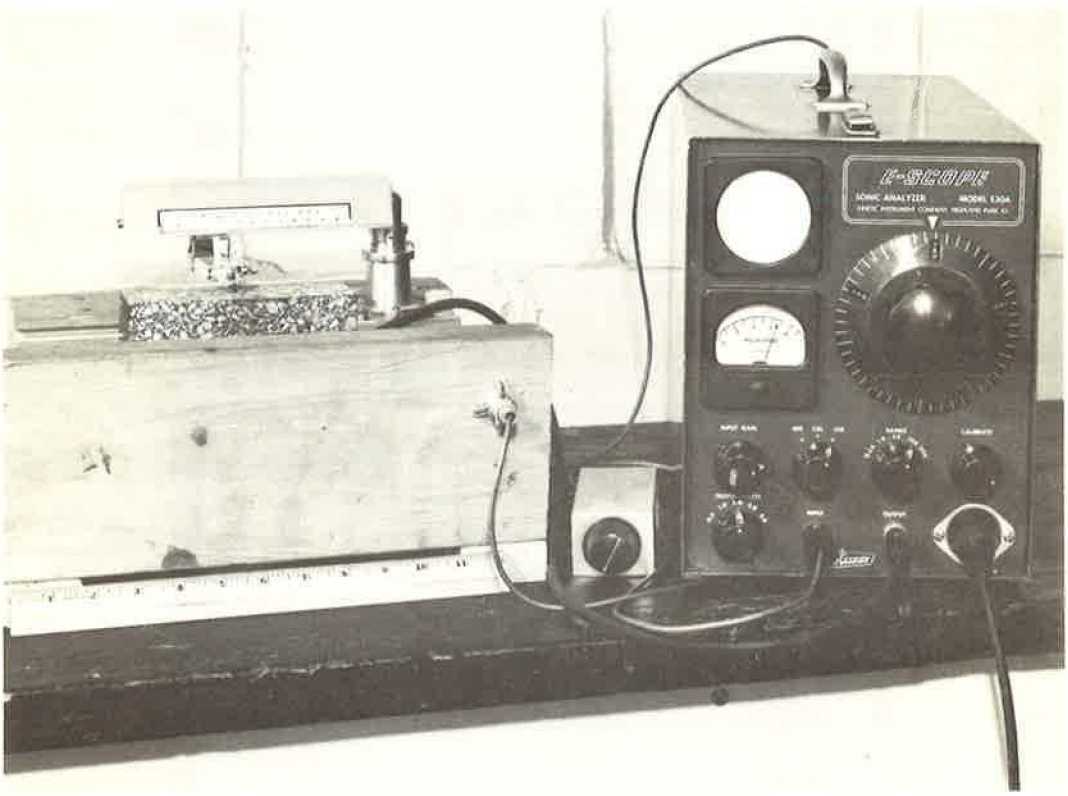

Figure 5. Sonic equipment showing E-scope and testing frame.

Sonic Dynamic Tests

Dynamic resonant frequency tests were also performed on prismatic specimens sawed from the cylindrical samples. The two properties measured in the sonic experiments to characterize the dynamic behavior of the materials were the real component of the complex modulus and the phase angle. The determination of $E_1(\omega)$ and ϕ_E from the resonant frequency vibrations was performed following ASTM Designation C 125-60 and procedures found in other similar references (15, 16). Figure 5 is a photograph of the resonant frequency test in progress showing the sonic apparatus.

PREPARATION OF SAMPLES

To obtain the maximum homogeneity and isotropy in the clyindrical samples, a gyratory compactor was used to mold the specimens. Proportioning of the aggregates and asphalt was performed on the basis of weight. The crushed Columbus and AASHO limestone aggregates were first separated into various sieved sizes, oven-dried and then combined into individual batches with exact proportions. The batches were heated for 8 hr along with the mixing bowls and molds in an oven maintained at 325 F. The exact amount of asphalt which had been heated to 275 F was combined with the heated aggregates, and then thoroughly mixed in a mechanical mixer for a minimum of 2 min or until the aggregate surface was coated with asphalt. The mix was placed in the gyratory compactor mold using a standard procedure which required the mix to be placed in two layers and each layer to be spaded vigorously 25 times. A fixed axial pressure was applied to the samples in the gyratory compactor and maintained constant while the gyration angle of 2° was set and the desired number of gyrations were applied. The samples which measured 2.8 in. in diameter and approximately 6 in. in height were stored before testing at room temperature until age effects (17) had become negligible. Tables 1 through 4 summarize the density and void analyses of the samples, asphalt content and aggregate gradations used, as well as the gyratory compaction details. Included in these tables are the identification tests performed on the bitumens: penetration, specific gravity, and the kinematic viscosity measured by a sliding plate microviscometer. A complete description of the preparation of samples and physical properties of the materials used may be found elsewhere (18).

The degree of homogeneity of the specimens used in this study was analyzed by evaluation of the bulk densities of all cylindrical samples and also small cubes sawed from representative samples. To determine degree of isotropy of the samples, the ultimate compressive strength of the sawed cubes was obtained by performing a constant-rate-of-deformation test on different planes of the cubes. Analyses of bulk densities and ultimate compres-

TABLE 1

DENSITY AND VOID ANALYSIS

Analysis	Mix Designation				
	300	500	700	800	900
Avg. bulk density of samples	2.35	2.28	2.26	2.28	2.34
Max theoretical density	2.40	2.35	2.42	2.39	2.35
Sp gr of total agg.	2.61	2.55	2.58	2.59	2.59
Percent of max theoretical density	97.90	96.90	93.40	95.30	99.50
Vol of voids (% total vol)	2.10	3.10	6.60	4.70	0.50
Vol of total agg. (% total vol)	84.90	84.30	83.50	83.00	84.20
Vol of bitumen cem. (% total vol)	13.00	12.72	10.30	12.60	15.20
Percent of agg. voids	15.1	15.7	16.5	17.0	15.8
Percent of agg. voids filled	86.2	81.0	62.4	74.1	96.3

TABLE 2

SPECIFIC GRAVITY AND PENETRATION GRADE OF BITUMEN USED

Commercial Penetration Limits	Type	Sp Gr	Actual Penetration[a]
85 - 100	AA	1.0209	84
85 - 100	A	1.0309	86
100 - 120	L	1.0295	102

[a] Of 100 g in 5 sec at 77 F.

TABLE 3

COMPACTION DETAILS, BITUMEN CONTENT AND BULK SPECIFIC GRAVITY OF MATERIALS

Analysis	Mix Designation				
	300	500	700	800	900
Mixture type	A	B	C	B	D
Bitumen type	100 - 120 L	85 - 100 AA	85 - 100 A	85 - 100 A	85 - 100 A
Bitumen (% by wt)	5.7	5.7	4.7	5.7	6.7
Gyratory compaction pressure (psi)	244	244	244	244	244
No. gyrations	30	45	45	45	45
Gyratory angle (deg)	2	2	2	2	2
Avg bulk sp gr	2.35	2.28	2.26	2.28	2.34

TABLE 4

BITUMINOUS CONCRETE MIXTURE PROPORTIONS

Type of Material	Passing Sieve	Retained on Sieve	Percent[a]	Percent[b]	Wt per Mix (g)
(a) Type A - Columbus Limestone					
Crushed limestone	1/2 in.	3/8 in.	10.7	10.1	141
	3/8 in.	No. 4	16.5	15.6	218
	No. 4	No. 10	20.5	19.3	270
	No. 10	No. 20	16.5	15.6	218
	No. 20	No. 40	13.7	12.9	180
	No. 40	No. 80	11.7	11.0	154
	No. 80	No. 200	7.8	7.3	104
Crushed limestone filler	No. 200	—	2.6	2.5	35
Total	—	—	100.0	94.3	—
Bitumen cement	—	—	—	5.7	80
Total	—	—	—	100.0	1,400
(b) Type B - AASHO Materials					
AASHO coarse	3/8 in.	No. 4	18.4	17.4	244
AASHO coarse sand	No. 4	No. 10	22.9	21.6	302
	No. 10	No. 20	18.4	17.4	244
	No. 20	No. 40	15.3	14.4	201
AASHO fine sand	No. 40	No. 80	13.2	12.4	173
	No. 80	No. 200	8.8	8.3	117
Limestone filler	No. 200	—	3.0	2.8	39
Total	—	—	100.0	94.3	—
Bitumen cement	—	—	—	5.7	80
Total	—	—	—	100.0	1,400
(c) Type C - Columbus Limestone and Natural Sand					
Crushed limestone	3/8 in.	No. 4	18.5	17.6	244
	No. 4	No. 10	23.0	21.9	302
	No. 10	No. 20	18.5	17.6	244
Coarse sand	No. 20	No. 40	15.2	14.5	201
Fine Sand + limestone	No. 40	No. 80	13.1	12.5	173
	No. 80	No. 200	8.7	8.4	117
Limestone filler	No. 200	—	3.0	2.8	39
Total	—	—	100.0	95.3	—
Bitumen cement	—	—	—	4.7	65
Total	—	—	—	100.0	1,385
(d) Type D - Columbus Limestone and Natural Sand					
Crushed limestone	3/8 in.	No. 4	18.4	17.2	244
	No. 4	No. 10	23.0	21.4	302
	No. 10	No. 20	18.4	17.2	244
Coarse sand	No. 20	No. 40	15.2	14.2	201
Fine Sand + limestone	No. 40	No. 80	13.1	12.2	173
	No. 80	No. 200	8.9	8.3	117
Limestone filler	No. 200	—	3.0	2.8	39
Total	—	—	100.0	93.3	—
Bitumen cement	—	—	—	6.7	95
Total	—	—	—	100.0	1,415

[a]By wt of aggregate. [b]By wt of total mix.

sive strengths of the experimental mixtures showed the specimens prepared for this study were quite homogeneous and isotropic.

LINEAR VISCOELASTIC THEORY

Phenomenological Treatment of Linear Viscoelastic Behavior

The classical elastic theory deals with the response of purely elastic materials where, in accordance with Hooke's law, stress is directly proportional to strain. However, elastic materials are idealizations. Real materials existing in nature generally show stress, temperature, and time anomalies. A viscoelastic material is one which exhibits both elastic and viscous characteristics, and stress is related to strain by a function of time in the linear viscoelastic range. To describe the response of such a material using the model representation, a mechanical system is used consisting of Hookean springs and Newtonian dashpots connected in series or parallel in various configurations.

The mechanical behavior of materials may be approximated by models composed of a finite number of linear springs and dashpots such as the Kelvin, Maxwell, and Burgers models (19, 20) and have been employed by many engineers. However, if the mechanical behavior of engineering materials is observed closely, it is realized that these models are too simple and cannot adequately depict the response of real materials. Several authors (21, 22) have suggested that it is possible to represent the response of viscoelastic bodies using more refined models consisting of a larger number of elements in the model. The generalized Voigt and Maxwell models consisting of n + 1 and n number of elastic and viscous elements are shown in Figures 6a and 6b, respectively.

The generalized Voigt model used in this study shows instantaneous elasticity, E_o, Newtonian flow with viscosity, η_o, and n different retardation times, τ_i, due to n Kelvin elements connected in series. The Kelvin element with retardation time, τ_i, has a spring with elasticity, E_i, and a dashpot with viscosity, η_i. The retardation time, τ_i, is equal to η_i/E_i and has units of time. Under a constant stress the generalized Voigt model exhibits creep behavior; the creep compliance, $J_c(t)$, used in this study is defined as the constant axial stress, σ, divided by the time-dependent axial strain, $\epsilon_{zz}(t)$:

$$J_c(t) = \frac{1}{E_o} + \frac{t}{\eta_o} + \sum_{i=1}^{n} \frac{1}{E_i}\left(1 - e^{-t/\tau_i}\right) \qquad (1)$$

Such a model under given conditions has constant parameters defining the material properties. However, if an outside factor, such as temperature, influences the response of the material, the elements of the model will be functions of temperature.

A continuous model can be constructed starting from the generalized Voigt model which consists of a single spring, a single dashpot, and an infinite number of Kelvin units connected in series. In the continuous model, the Kelvin units with retardation times between τ and $\tau + d\tau$ will contribute to the compliance. The function $L(\tau)$ is called the distribution function of retardation times or retardation spectrum, where $0 < \tau < \infty$. The creep behavior of such a model may be obtained from the creep compliance of the generalized Voigt model. Using the logarithmic

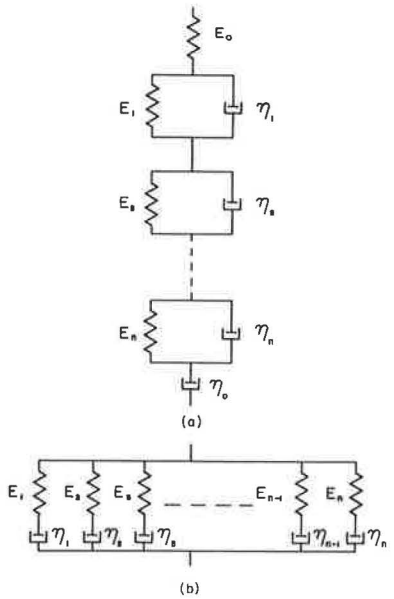

Figure 6. Complex mechanical models: (a) generalized Voigt model and (b) generalized Maxwell model.

distribution function, $L(\ln \tau)$, the creep response can be represented by the following equation:

$$J_c(t) = \frac{1}{E_o} + \frac{t}{\eta_o} + \int_{-\infty}^{\infty} L(\ln \tau)\left(1 - e^{-t/\tau}\right) d(\ln \tau) \qquad (2)$$

Once the retardation spectrum has been evaluated by creep experiments for a linear viscoelastic material, the dynamic response of the material, such as the complex modulus, can be obtained (1, 22).

Similar concepts may be used to evaluate the transverse modulus, $T_c(t)$, which is defined as the constant axial stress divided by the time-dependent circumferential strain, $\epsilon_{\theta\theta}(t)$. The complete theory reviewed for the creep compliance remains valid for all moduli and compliances.

Dynamic Response of Materials

In the previous section, static tests were considered in which the applied stress is essentially a step function and equal to zero up to a given instant and then changes discontinuously to a finite value. The response of materials is also considered in another type of test in which the stress varies sinusoidally with time, $\sigma = \sigma_o \sin \omega t$, and the material undergoes axial and lateral sinusoidal strains, $\epsilon = \epsilon_o \sin(\omega t - \phi)$, at the same frequency as the stress but lagging the stress by a phase angle (6, 23).

The concept of the complex modulus applied in this study to define the viscoelastic response of materials is based on the fact that when a sinusoidal excitation is applied to a material, the response of the material will also be sinusoidal, but out-of-phase with the stress by a phase angle.

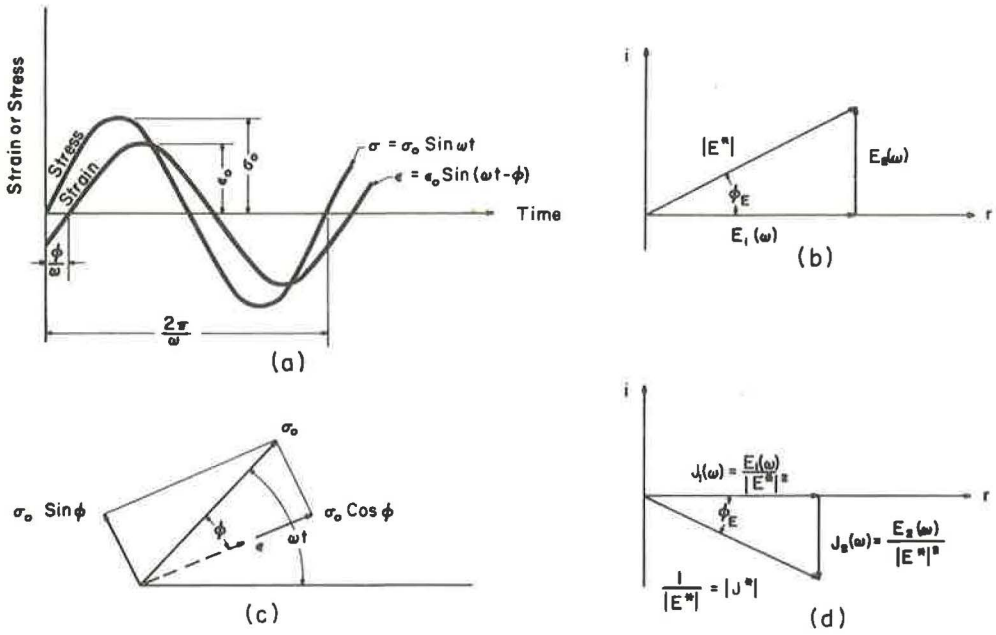

Figure 7. Dynamic viscoelastic response and vectorial resolutions: (a) steady-state response of viscoelastic material to sinusoidal strain or stress, (b) vectorial resolution of modulus components in sinusoidal deformation, (c) rotating vector representation, and (d) vectorial resolution of compliance components in sinusoidal deformation.

A linear viscoelastic material subjected to a sinusoidal stress will reach a steady-state condition after a limited number of cycles, and the amplitude of the stress, σ_o, divided by the amplitude of the strain, ϵ_o, is equal to the absolute value of the complex modulus, $|E^*|$. The phase lag, ϕ, shown in Figure 7, is the angle by which the stress leads the strain.

If a given sinusoidal stress is imposed on a material, the measurement of the amplitude of the stress and strain, as well as the angle by which the strain lags the stress, will define the response of the material at a frequency, ω. Evaluation of ϕ and $|E^*|$ at all frequencies will completely define the viscoelastic response of the material (4). The complex modulus of a material is a complex number and may be resolved into a real and imaginary part or an absolute value and phase angle:

$$E^* = E_1(\omega) + j\,E_2(\omega) \tag{3}$$

and

$$E^* = |E^*|\,e^{j\phi} \tag{4}$$

The dynamic data may also be expressed in terms of a complex compliance which is the reciprocal of the complex modulus as shown in Figure 7:

$$J^* = J_1(\omega) - j\,J_2(\omega) \tag{5}$$

The real and imaginary components of the complex compliance can be represented by the continuous Voigt model (22):

$$J_1(\omega) = \frac{1}{E_o} + \int_{-\infty}^{\infty} L(\ln\tau)\,\frac{1}{1+\omega^2\tau^2}\,d(\ln\tau) \tag{6}$$

$$J_2(\omega) = \frac{1}{\omega\,\eta_o} + \int_{-\infty}^{\infty} L(\ln\tau)\,\frac{\omega\tau}{1+\omega^2\tau^2}\,d(\ln\tau) \tag{7}$$

These equations require a knowledge of the spectrum over a wide range of the frequency scale. In principle, $L(\ln\tau)$ may be obtained from the experimental data of Eqs. (2), (6) or (7). If this is true, the dynamic response of the material can be evaluated at the same temperature using the retardation spectrum as an intermediate value in the calculations.

One important problem is how the $L(\ln\tau)$ functions are calculated from the creep functions, which are presented in graphical form in this study and applied to predict the dynamic response of the material. Because the exact methods are of limited use, the approximate methods suggested by Widder and Leaderman were used in this study (1, 6).

Three-Dimensional Viscoelastic Response

The complete theory developed for the complex elastic modulus, E^*, is also valid for all other complex moduli and compliances. Thus, similar relations may be written for the complex shear modulus, G^*, complex bulk modulus, K^*, and the complex Poisson's ratio, ν^*. The evaluation of two independent complex moduli of an isotropic, homogeneous, linear viscoelastic material allows the formation of general stress-strain equations similar in form to equations for the classical elastic body (1, 7). These equations will differ from the elastic equations in one important respect: all quantities in them are functions of frequency. In these equations E^*, ν^*, G^*, and K^* are the complex moduli of the material, and σ^* and ϵ^* are Fourier transforms of the stress and strain, respectively. A specific complex modulus used in this study is the transverse modulus, T^*, which relates the axial stress to the transverse strain.

TIME-TEMPERATURE SUPERPOSITION CONCEPT

The time-temperature superposition principle whereby phenomenological viscoelastic data at one temperature can be transformed to another temperature by a multiplicative transform of the experimental time scale was independently suggested by several authors (1, 4, 6, 9). This concept shows it may be possible to extend creep viscoelastic moduli such as E_c (t), T_c (t), or the complex moduli obtained at a given temperature to loading times both longer and shorter than can normally be obtained by experimentation. The superposition principle was used in this study to evaluate the extreme portions of the loading time scale and also to determine the creep and dynamic moduli at any intermediate temperature in the experimental range.

By use of the previously discussed concept, master curves of E_c (t), T_c (t), ϕ_E, ϕ_T, $|E^*|$, and $|T^*|$ were developed from the experimental data covering a relatively small portion of the time scale but over a wide range of the temperature scale. Refinements of this procedure are treated in the literature (9).

The empirical criterion for fulfilling the preceding conditions required that the shape of individual creep or dynamic tests data evaluated at different temperatures should coincide, within experimental error, after a horizontal shift along the logarithmic time axis. The horizontal temperature shift factor, a_T, must be evaluated empirically for each temperature, but the requirement of superposition does not permit an arbitrary selection in this choice because in both the dynamic and creep tests, the same value of a_T must be used to bring E_c (t), T_c (t), and the magnitude and phase of the complex moduli into superposition for a given temperature change.

When the criterion is not met, the applicability of reduced variables in this convenient form must be rejected. A material which meets the criterion has been called thermorheologically linear (1, 9) and is defined as one in which a change in experimental temperature alters only the position of the viscoelastic functions on the time or frequency scales and not the general shape of the curves. Even when the response of the material is only approximately thermorheologically linear, it allows the viscoelastic response of the material to be represented by two functions instead of a complex three-dimensional representation in time and temperature space.

The reduction scheme must be slightly altered to make it theoretically more satisfactory. A factor $T_o P_o/TP$ enters into the coordinate scheme because of the entropy-spring nature of the stored elastic energy in the material as explained by the kinetic theory of rubberlike elasticity and theory of Rouse (1, 9, 24). T_o is the standard reference temperature, P_o is the density of the material at this temperature, and P is the density at the absolute experimental temperature, T. The kinetic theory suggests that the equilibrium modulus is proportional to the absolute temperature, and the quantity $T_o P_o/TP\ E_c$ (t) should be governed by the superposition principle rather E_c (t). The factors of density and absolute temperature result in small vertical shifts of the viscoelastic moduli.

In regions of the time scale where the rheological moduli are changing rapidly with time, it is possible to match adjacent curves empirically without first applying a vertical shift as suggested by theory. Slightly different values of a_T will, of course, be obtained in each case. In sections where the viscoelastic function is flat, the influence of the vertical shift is more significant. However, the vertical factor is clearly indicated by the theoretical considerations.

Experimental moduli of thermorheologically linear materials may now be reduced to a standard reference temperature, T_o, of the master curve. The effect of a temperature increase from T_o to T on a double logarithmic plot consists of a shift of the creep modulus vertically by the factor, ln $(T_o P_o/TP)$, and horizontally by the temperature shift factor, ln a_T.

It is suggested that if one of the viscoelastic functions of bituminous concrete obeys the time-temperature relations stated previously, all other viscoelastic functions such as E_c (t), J_c (t), and the complex moduli should obey similar time-temperature relations. The results of the experimental investigation of this concept are included in the subsequent sections.

EXPERIMENTAL RESULTS

The experimental results on the macroanalytical level are presented in graphical and tabular form in an attempt to verify that to a useful degree of approximation, the bituminous mixes used in this study may be represented by thermorheologically linear materials under the experimental conditions investigated. The use of the linear viscoelastic theory to depict the response of bituminous concrete under load was also studied by both dynamic and transient tests.

Creep Tests

The objective of the creep tests was to obtain continuous recordings of the axial and transverse strain over a wide range of the time and temperature scales. For the response of a material to be described by the linear viscoelastic theory to a useful degree of approximation, the creep moduli in a constant stress test must be approximately independent of the stress level in the linear viscoelastic range.

In Figure 8 typical results of several unconfined creep tests are plotted for the 500 series mix. Only the axial stress has been varied in the experiments by simple multiples. Each individual strain curve was obtained by testing three samples under identical conditions and averaging the experimental data. Inspection of the data reveals that the vertical strain data, ϵ_{ZZ}, are almost proportional to the stress levels at all times, showing that the linear viscoelastic theory is a satisfactory approximation to the response of this material. The creep modulus, E_c (t), at any given time, has approximately the same value for all four stress levels tested. It is suggested that the linear viscoelastic theory will provide a higher level of approximation than the elastic theory to represent the creep response of the material over a range of temperature

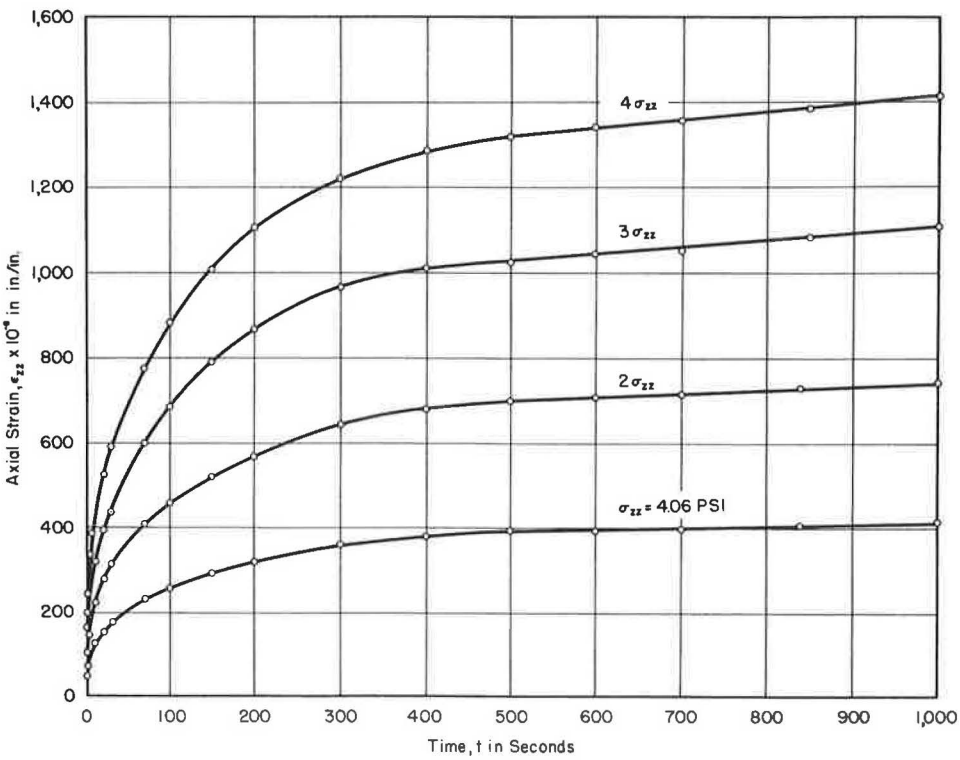

Figure 8. Viscoelastic response of bituminous concrete obtained from unconfined creep tests at four stress levels.

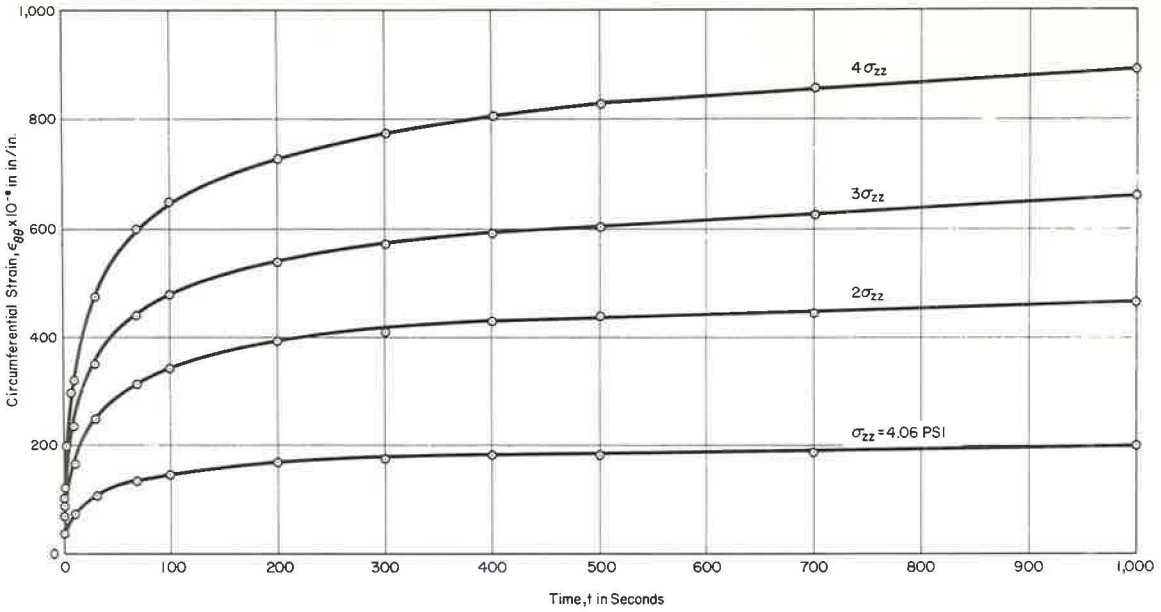

Figure 9. Circumferential strain obtained from creep tests at four stress levels.

TABLE 5

DYNAMIC EXPERIMENTAL RESULTS[a]

Variables			$\lvert E^* \rvert \times 10^6$ (psi)					ϕ_E (deg)					$\lvert T^* \rvert \times 10^6$ (psi)					ϕ_T (deg)				
Freq. (rad/sec)	Temp. (°C)	Axial Stress (psi)	300	500	700	800	900	300	500	700	800	900	300	500	700	800	900	300	500	700	800	900
10.8	36.1	4.06	0.163	0.140	0.318	—	—	41.4	36.1	26.4	—	—	0.290	0.253	0.330	—	—	49.2	39.5	39.1	—	—
		8.12	0.147	0.129	0.253	—	—	34.8	34.3	24.7	—	—	0.259	0.346	0.333	—	—	46.6	46.3	34.1	—	—
	25.0	4.06	0.412	0.256	0.567	0.329	0.386	29.2	27.2	21.2	28.9	28.1	0.807	0.812	1.136	0.878	0.812	39.5	28.4	28.2	30.3	37.1
		8.12	0.398	0.223	0.441	0.405	0.439	27.3	30.1	25.7	33.4	27.9	0.876	0.888	1.102	1.201	0.903	37.5	36.6	36.6	37.1	31.4
		16.24	0.364	0.206	0.610	0.357	0.465	26.3	27.0	26.3	33.0	32.0	0.874	0.874	1.036	0.822	1.208	35.9	36.5	40.6	34.7	31.1
	5.4	16.24	1.330	1.315	1.333	—	—	19.3	18.8	18.2	—	—	5.461	4.343	3.812	—	—	22.1	20.3	22.8	—	—
		32.48	1.632	1.120	1.290	—	—	20.7	17.0	20.7	—	—	4.836	5.912	3.60	—	—	20.7	24.2	24.2	—	—
21.6	36.1	4.06	0.256	0.152	0.221	—	—	38.6	38.3	21.4	—	—	0.460	0.512	0.301	—	—	41.1	42.4	32.1	—	—
		8.12	0.162	0.103	0.274	—	—	37.4	30.7	23.6	—	—	0.402	0.344	0.351	—	—	44.9	40.2	38.5	—	—
	25.0	4.06	0.380	0.232	0.563	0.486	0.460	24.2	28.0	25.7	31.7	28.9	0.621	0.812	1.791	1.043	1.156	34.2	32.9	29.0	39.0	33.6
		8.12	0.440	0.247	0.551	0.552	0.518	24.9	27.8	25.6	25.4	28.2	0.820	0.839	1.540	1.296	1.174	34.9	29.6	28.1	36.9	32.6
		16.24	0.464	0.351	0.418	0.504	0.502	26.6	29.1	20.5	27.2	26.5	0.990	0.991	0.975	1.165	0.963	32.9	34.8	32.7	36.5	36.1
	5.4	16.24	1.755	1.380	2.011	—	—	15.8	14.1	14.3	—	—	6.018	4.803	3.263	—	—	18.6	24.0	23.5	—	—
		32.46	1.390	1.092	1.911	—	—	16.5	16.2	15.4	—	—	5.149	4.210	3.561	—	—	25.3	17.5	20.2	—	—
86.4	25.0	4.06	0.648	0.397	0.477	0.624	0.698	15.6	26.0	19.6	19.8	23.9	0.972	0.772	2.360	1.622	1.540	24.5	15.5	21.6	17.4	21.6
		8.12	0.570	0.338	0.574	0.616	0.610	22.5	27.6	15.0	18.0	19.6	1.362	0.859	2.295	1.807	1.642	20.1	25.1	20.1	28.2	24.8

[a]Absolute values of complex moduli $\lvert E^* \rvert$ and $\lvert T^* \rvert$ and respective phase angles ϕ_E and ϕ_T for 300, 500, 700, 800, and 900 mixes as designated.

and loading time conditions. Using the linear viscoelastic assumption, the maximum deviation from the average value of ϵ_{zz} by the four vertical strain curves is 10 percent. An identical procedure was used to evaluate the circumferential strains, $\epsilon_{\theta\theta}$, from the same constant stress tests performed on the 500 series mixes. The circumferential strains at four stress levels shown in Figure 9 also illustrated that the linear viscoelastic theory is a good approximation to depict the response of bituminous concrete at low stress levels and for the conditions investigated.

Direct Dynamic Tests

The results of the direct dynamic tests are summarized in Table 5 in terms of the absolute values of the complex moduli, $|E^*|$ and $|T^*|$, and their respective phase angles, ϕ_E and ϕ_T. Besides the 500 mix, four other bituminous concrete mixtures, namely the 300, 700, 800, and 900 mix designations, were investigated in the dynamic experiments. The principal variables studied in this phase of the experimentation were frequency, temperature, stress level, and type of bituminous mixture.

Several important facts are brought out by the inspection of the data, the most important being that the magnitude and phase of the complex modulus $|E^*|$ seem to be independent of the stress level and depend only on mix type, temperature and frequency. If the amplitude of the applied stress is double, the resulting amplitude of axial strain is also approximately doubled so that $|E^*|$ is unchanged. Similar results are noted for $|T^*|$ to demonstrate the linear viscoelastic nature of bituminous concrete.

Resonant Vibration Experiments

The results of the sonic dynamic experiments are summarized in Table 6. The real component and phase angle of the complex elastic and shear moduli were obtained from the experimental results and used to evaluate $|E^*|$ and ϕ_E. The magnitude and phase of E* and T* evaluated by both methods of dynamic tests will be used to study interrelations among the viscoelastic functions.

Evalutation of Thermorheologically Linear Response of Bituminous Concrete

The experimental data of the constant stress tests of the 500 series mix are presented in Figure 10. The creep modulus, E_C (t), has been evaluated at eleven experimental temperatures varying from 0 to 120 F as indicated and plotted on logarithmic plots vs time. The experimental stress levels used were chosen to be sufficiently low (as compared to the ultimate strength of the material) to be within the range for which the linear viscoelastic theory might produce a good approximation for the material at the temperature of test. The stress levels varied from 2 to 90 psi at 120 and 0 F, respectively. A summary of the stress levels used at each temperature in the creep and dynamic tests is presented in Table 7. It was necessary to vary the stress levels at each temperature as it was noted that the upper limit of the linear viscoelastic range is a function of temperature.

TABLE 6
SONIC EXPERIMENTAL DATA[a]

Specimen No.	Length (in.)	Base (in.)	Thickness (in.)	Weight (lb)	Resonant Frequency		C	B	$E_1(\omega)$ x 10^6 (psi)	ϕ_E (deg)	$E_2(\omega)$ x 10^6 (psi)	$\lvert E^* \rvert$ x 10^6 (psi)	$G_1(\omega)$ x 10^6 (psi)	ϕ_G (deg)	$G_2(\omega)$ x 10^6 (psi)	$\lvert G^* \rvert$ x 10^6 (psi)
					Flexural N(cps)	Torsional N'(cps)										
317	5.88	2.37	0.97	1.159	2,185	2,505	0.274	0.0363	1.54	10.1	0.275	1.57	0.264	15.1	0.072	0.274
325	5.87	2.24	1.12	1.261	2,720	2,890	0.196	0.0441	1.84	11.9	0.389	1.88	0.464	7.0	0.055	0.467
337	5.88	2.21	1.10	1.271	2,479	2,180	0.208	0.0523	1.56	14.3	0.398	1.61	0.316	10.3	0.057	0.321
562	6.10	2.20	0.90	0.994	2,281	1,650	0.382	0.0752	1.91	9.1	0.305	1.93	0.204	4.9	0.015	0.204
537	5.94	1.93	0.94	0.885	2,259	1,762	0.388	0.0635	1.76	9.2	0.284	1.78	0.174	7.5	0.023	0.174
570	5.08	2.31	1.02	0.984	3,220	2,205	0.160	0.0474	1.61	11.4	0.324	1.64	0.236	6.0	0.025	0.237
710	5.92	2.33	0.98	1.058	2,453	2,910	0.270	0.0601	1.70	6.3	0.188	1.71	0.538	18.6	0.182	0.568
713	6.03	2.15	0.81	0.885	2,165	2,241	0.512	0.0930	2.12	7.9	0.294	2.14	0.414	15.8	0.117	0.431
706	5.95	2.26	1.01	1.070	2,392	2,627	0.265	0.0564	1.62	9.1	0.258	1.63	0.415	16.2	0.124	0.457

[a]Magnitude and phase of complex moduli obtained from torsional and resonant frequencies using bituminous concrete mixtures 300, 500, and 700 measured at 25 C.

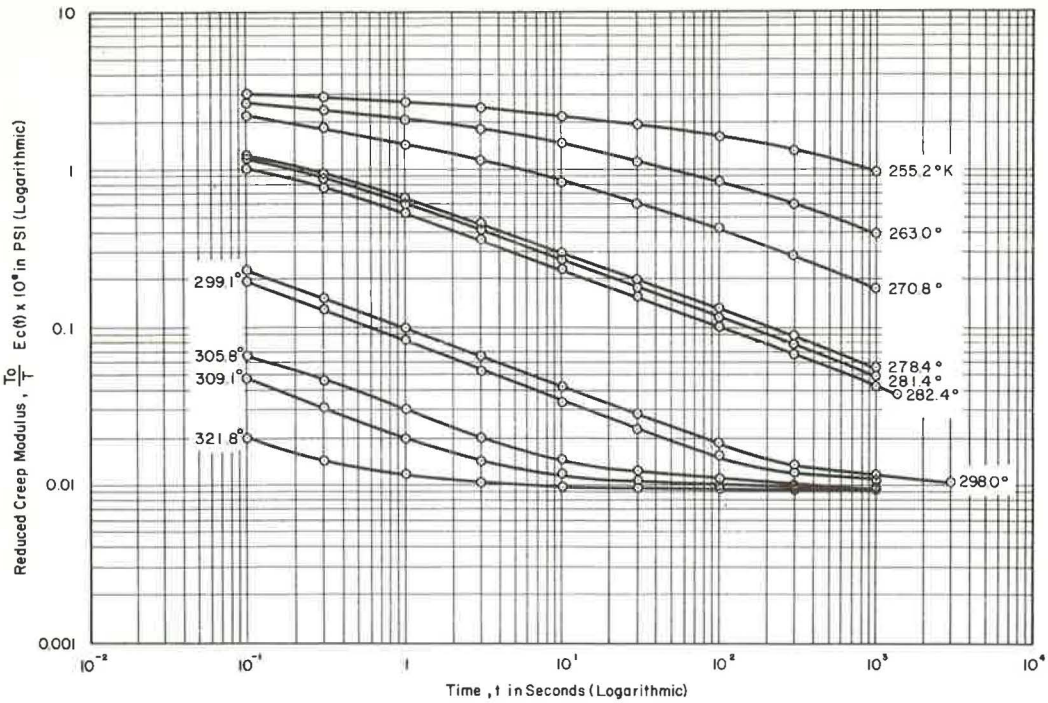

Figure 10. Axial creep modulus reduced to 298 K vs time at indicated temperatures.

TABLE 7

STRESS LEVELS IN LINEAR VISCOELASTIC RANGE AT EXPERIMENTAL TEMPERATURES

Temperature (°K)	Temperature (°F)	Axial Load (lb)	Axial Stress (psi)
255.2	0	550	89.29
263.0	14	500	81.17
270.8	28	450	73.05
278.4	41.7	400	64.94
281.4	47.1	312.5	50.73
282.4	49	312.5	50.73
298.0	77	100	16.24
299.1	79	100	16.24
305.8	91	37.5	6.09
309.1	97	25	4.06
321.8	120	12.5	2.03

A reference temperature, T_O, equal to 77 F or 298 K, was arbitrarily selected within the experimental temperature range. The creep functions were first reduced by the absolute temperature factor, T_O/T, which enters into the coordinate scheme due to entropy-spring nature of the stored elastic energy. The density factor, P_O/P, has been omitted from the calculations as it approaches unity and is within the experimental error of the tests. Each creep function at a given temperature was obtained by testing three samples under identical conditions and averaging the axial and circumferential strain data.

Investigation of the eleven creep functions in Figure 10 shows that a change in the experimental temperature shifts only the position of the reduced creep moduli with respect to the logarithmic time scale, and the general shapes of the curves are not altered when the experimental temperature is changed. The horizontal distance between each pair of adjacent curves was measured and found to be the same within experimental error. Thus, portions of the adjacent viscoelastic functions are essentially parallel lines and have the same numerical values of E_C (t) at different portions of the logarithmic time scale. A change in temperature has shifted only the position of the viscoelastic modulus function on the logarithmic time scale as all retardation times have the same temperature dependence to provide experimental verification that the bitumen-aggregate mixes used in this study may be represented by thermorheologically linear materials.

The viscoelastic data plotted in Figure 10 may now be used to extend the experimentally accessible time scale of the creep modulus obtained at 298 K by developing single

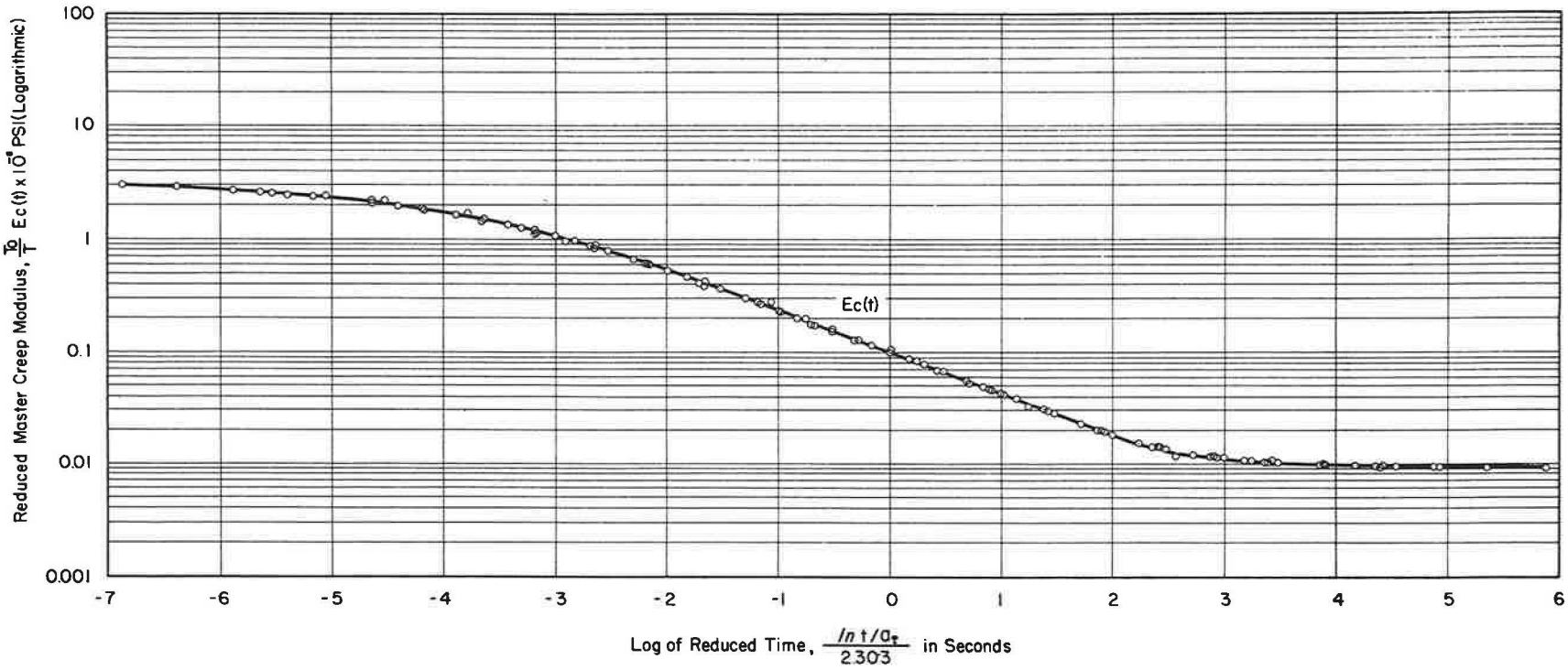

Figure 11. Composite master creep modulus obtained by time-temperature superposition principle, representing viscoelastic behavior over extended time scale at 298 K.

or master creep function at this temperature. Since time and temperature have been shown to have an equivalent influence on the creep moduli in Figure 10, it was possible to shift the remaining ten reduced creep modulus curves to the chosen reference temperature by transforming them horizontally along the time axis until the experimental curves superimpose on the reference curve at 298 K to give a fairly smooth plot as shown in Figure 11. In this figure the time scale of the experimental curve was extended beyond the practical experimental range, and now extends from 10^{-6} to 10^{6} seconds or approximately 12 days. The composite curve represents the behavior of the bituminous mix at a single temperature, T_o; the master curve is actually composed of segments of the eleven creep functions which were evaluated at different temperatures.

The experimental transverse creep functions, T_c (t), determined at the same eleven temperatures are plotted in Figure 12. The equivalence of time and temperature effects on the viscoelastic properties of bituminous concrete can again be noted from the experimental plots. The transverse creep functions were shifted vertically by the T_o/T factor. The density factor was again omitted from the reduction scheme. The master transverse creep function at 298 K shown in Figure 13 was obtained by superposition of the eleven individual creep functions and now covers an extensive range of the time scale.

The experimental creep moduli, E_c (t) and T_c (t), have been reduced vertically by the factor T_o/T before application of the superposition concept to develop the master curves. This procedure was used in this study as it seemed to produce the smoothest master viscoelastic functions. Although master curves of E_c (t) and T_c (t) were also

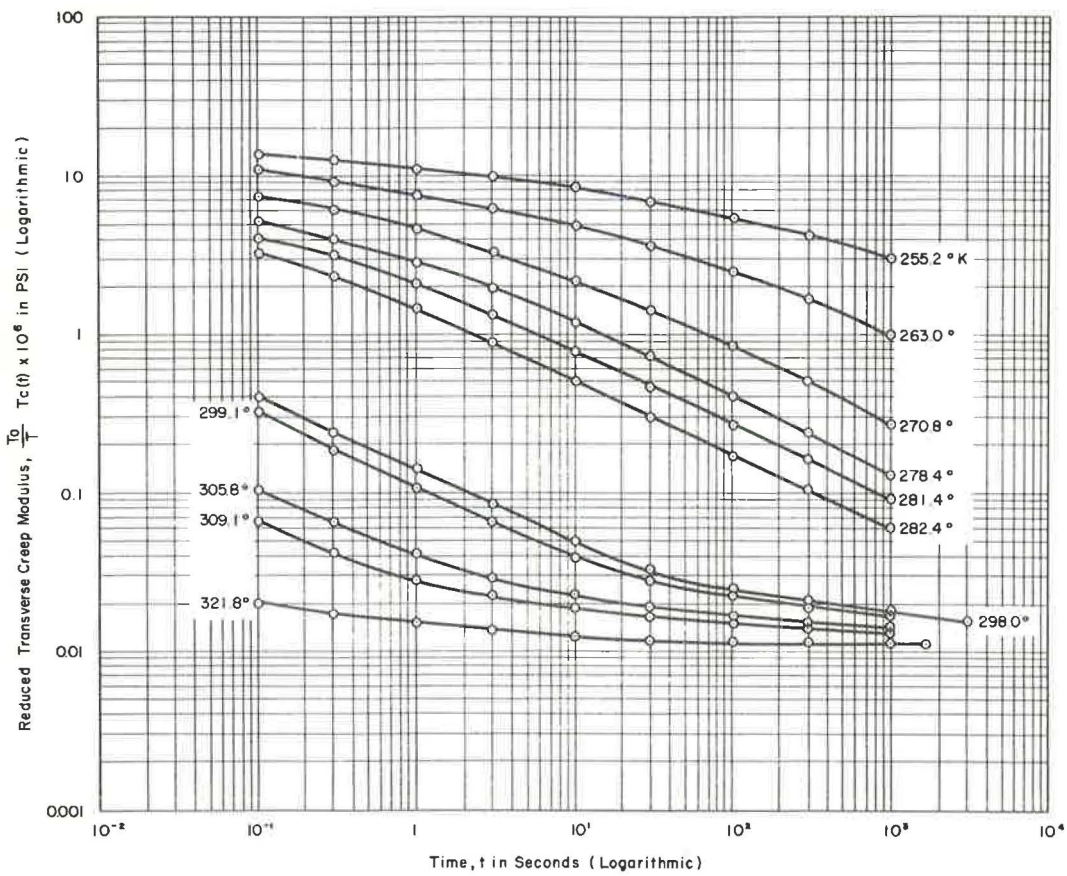

Figure 12. Transverse creep function reduced to 77 F vs time at eleven temperatures.

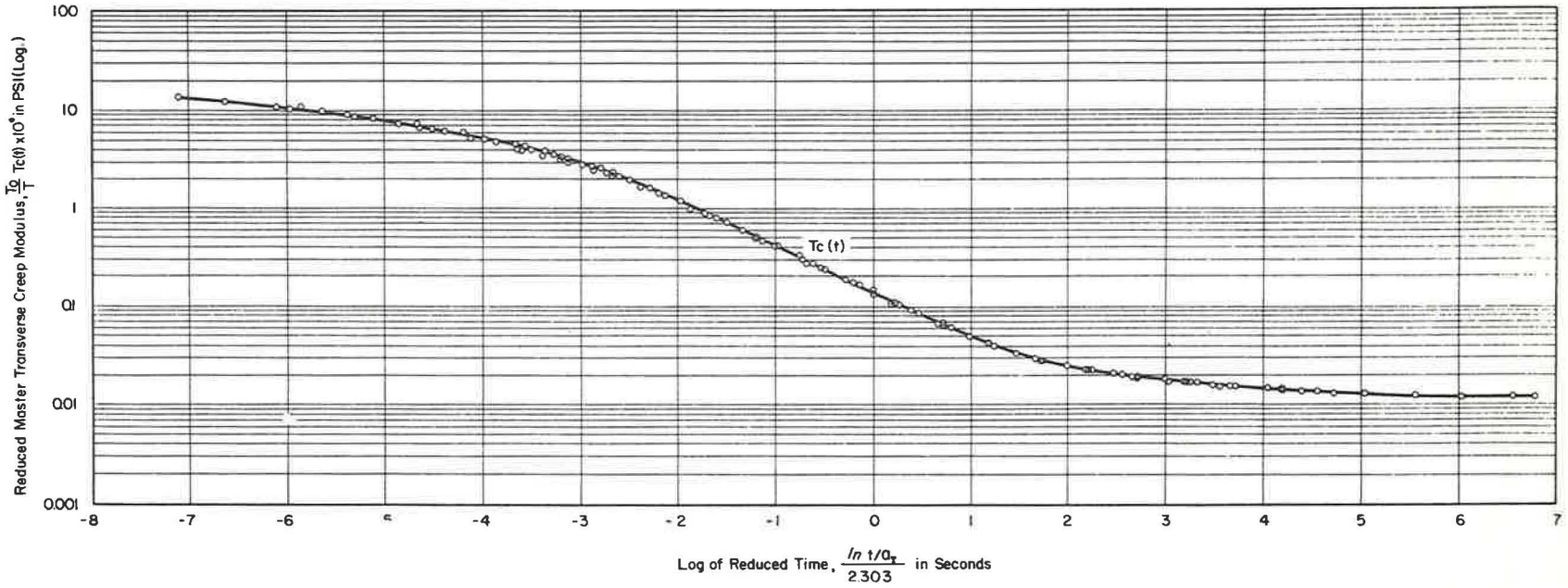

Figure 13. Composite master transverse creep function at 77 F.

obtained by neglecting the T_o/T and P_o/P factors, these curves were not as smooth or continuous. Perhaps this procedure of treating the data may be applied in many cases. However, due to the limitations of the experimental equipment and magnitude of the T_o/T shift, more refined experimentation is necessary at this time to evaluate this interesting concept.

Temperature Dependence of Shift Factor, a_T

The temperature dependence of the shift factor, a_T, was evaluated by plotting the relative horizontal shifts to obtain coincidence of adjacent creep modulus curves vs the experimental temperature differences of the viscoelastic curves. These values were obtained from Figures 10 and 12. The temperature reduction function, f (T), has been constructed in Figure 14 by plotting the time shifts between experimental curves vs temperature intervals of Figures 10 and 12 for $T_o/T\ E_c$ (t) and $T_o/T\ T_c$ (t), respectively.

The choice of 298 K as the standard reference temperature, T_o, is purely arbitrary and is based on convenience. It is interesting to note that by selecting the lowest temperature in the experimental range as T_o, the master curve is developed for exceedingly long loading times. However, if the short time response of the material is of interest, the master curve in this range can be developed by designating 120 F as T_o.

In Figure 14 the experimental results from E_c (t) and T_c (t) have been plotted and a straight line used to approximate f (T) for the 500 series bituminous concrete mixture. It well be shown later that the same f (T) will also be applicable to shift the magnitude and phase of E* and T* evaluated in this study. The good correlation of f (T) evaluated from both viscoelastic creep moduli and used to shift the absolute value and phase of the complex moduli in the frequency domain seems to indicate that if one characteristic viscoelastic function is controlled by the time-temperature relations, then all other viscoelastic functions of the same material are controlled by the same relations.

The temperature shift function has also been evaluated from the experimental data of E_c (t) and T_c (t) that were not first reduced vertically by the temperature factor, T_o/T. A straight line was again used to approximate f (T). An equation was developed for the shift factor, $a_T = 10^{40.6 - 0.1360\ T}$, which is only slightly different from the corresponding equation in Figure 14.

The master creep functions, E_c (t) and T_c (t), were determined at 298 K by plotting $T_o/T\ E_c$ (t) vs ln t/a_T and $T_o/T\ T_c$ (t) vs ln t/a_T, respectively. Once the temperature shift function and master creep functions are evaluated for a reference temperature, the master curves can be readily shifted to any other temperature from 0 to 120 F by application of the appropriate values of ln a_T and vertical temperature factor.

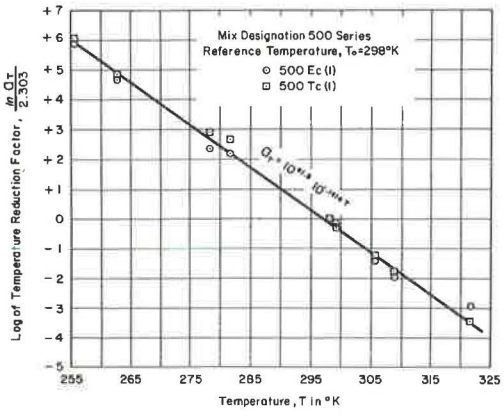

Figure 14. Temperature dependence of shift factor, a_T, evaluated from reduced axial and transverse creep moduli.

Thus, starting from a complicated dependence on both temperature and time as illustrated in Figures 10 and 12, these two independent variables can be separated to yield a viscoelastic function of time alone at a standard reference temperature, and a temperature function. The temperature reduction function, f (T), and the viscoelastic functions, E_c (t) and T_c (t), can be used to completely define the material at any time and experimental temperature within the tested range. Figures 11 and 13 represent E_c (t) and T_c (t) as they would have been measured at temperature T_o over a large range of the time scale. In a rheologic study, the temperature and time dependent response of a material may also be dealt with by including the independent variable of temperature as well as time in the rheological equation of state used to depict the quantitative mechanical behavior of the material.

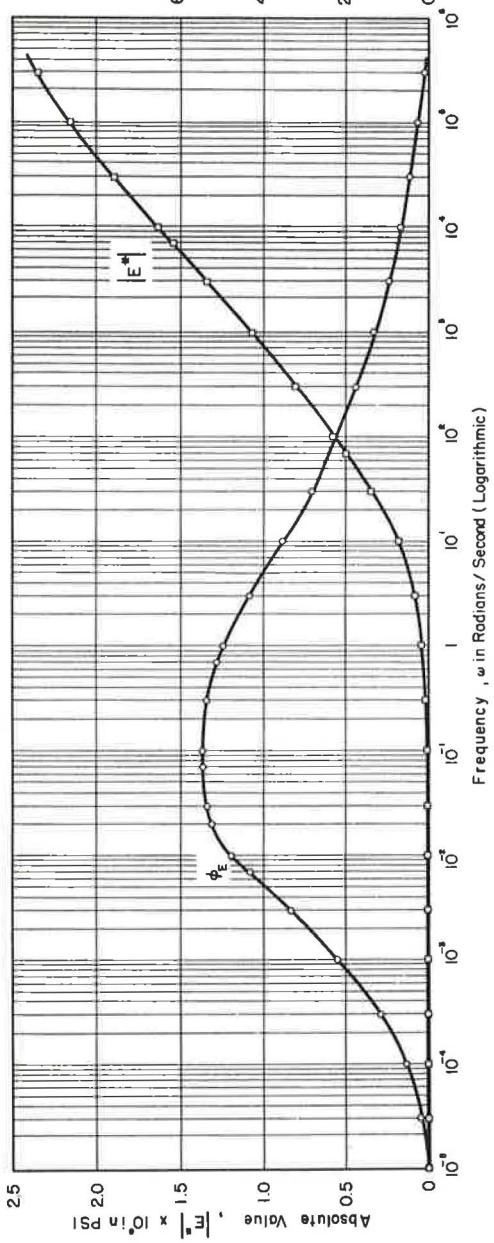

Figure 15. Magnitude and phase angle of complex elastic modulus, E*, as function of angular frequency at 77 F.

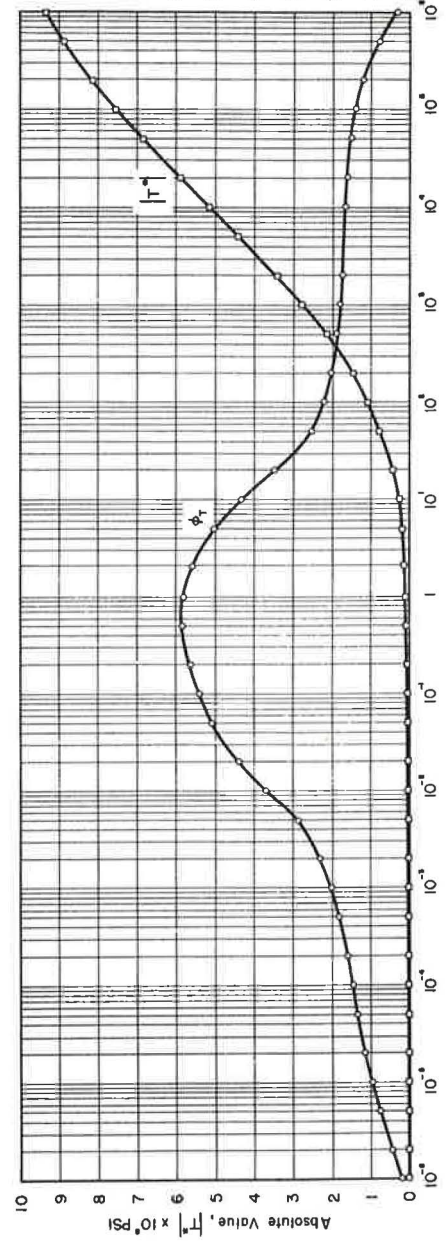

Figure 16. Absolute value and phase of complex transverse modulus, T*, at 77 F.

Prediction of Complex Moduli

Generalized mechanical models were used in this study to represent the response of real materials because this method allows the mechanical response of bituminous concrete to be adequately represented, and it is possible to deal directly with the viscoelastic functions rather than using a model consisting of a finite number of elements only to approximate the complicated response of the material. The highest degree of accuracy in representing the viscoelastic response was obtained in this case by use of the infinite Voigt model.

The distribution functions of retardation time were calculated from the creep experimental results, and by use of the interrelations among the viscoelastic functions, a method to evaluate the complex moduli of the material from the compression tests is available. The real and imaginary parts of E* and T* were calculated using the first- and second-order approximation methods suggested by Leaderman and Widder (1, 6). The master creep functions were first used to evaluate retardation spectra, $L(\ln \tau)$, which were then used to determine the storage and loss components of the complex moduli and compliances by similar approximate methods. At any specified temperature and frequency, the dynamic response of a material is defined by either $J_1(\omega)$ and $J_2(\omega)$ or alternately by $|E^*|$ and ϕ_E. The two methods of representing the complex moduli are equivalent and related to each other. Figure 15 is a plot of the absolute value of the complex elastic modulus, $|E^*|$, and its phase angle, ϕ_E, vs angular frequency at 298 K obtained from the master creep curve of Figure 11 using the previous relations. To develop similar functions at any temperature in the static experimental range from 0 to 120 F, the appropriate value of $\ln a_T$ from Figure 14 and temperature factor may be selected and used to transform the dynamic viscoelastic function to the temperature desired. An identical result could be obtained by first developing the master creep viscoelastic function in the time domain at the desired temperature T_i, and then transforming the creep function to frequency domain at this temperature. Thus, the same values of $|E^*|$ and ϕ_E can be obtained by two methods using the same value a_T. Figure 16 is a plot of $|T^*|$ and ϕ_T vs angular frequency at 298 K. These viscoelastic functions were obtained from the master transverse creep curve in Figure 13 by the approximate interrelations between viscoelastic functions.

Correlation of Creep and Dynamic Data

By comparing the direct dynamic and sonic test data presented in Tables 5 and 6 and the values of the magnitude and phase of the complex moduli predicted by creep tests, the correlation of results may be observed between both types of experimentation. Values of $|E^*|$, $|T^*|$, ϕ_E, and ϕ_T evaluated by creep and dynamic tests may be compared at the common experimental temperatures and frequencies. By applying the appropriate values of a_T and temperature factor to either the dynamic or creep data or simultaneously to both, the magnitude and phase or the real and imaginary components of E* and T* evaluated by dynamic tests and the corresponding viscoelastic functions calculated by creep tests were compared directly in the frequency domain over a range of temperatures for the 500 series mix.

The agreement between the dynamic viscoelastic functions predicted by creep tests, which are continuous functions of frequency, and the values of the magnitude and phase of E* and T* over the range of temperatures was considered to be good in 90 percent of the analyses of the data performed.

The good agreement in this type of experimentation between the experimental values of the magnitude and phase of the complex moduli evaluated by creep and dynamic tests provides another verification of the ability of the linear viscoelastic assumption to describe the response of bituminous concrete mixtures. It also provides verification of the application of the time-temperature superposition concept to this material, because the creep and dynamic test data were obtained in entirely different time intervals.

Investigation of f (T) evaluated from the creep experimental data and used for the dynamic test results seems to indicate that f (T) determined from one characteristic function may be used to obtain the temperature dependence of the other characteristic creep and dynamic viscoelastic functions for a given material. A satisfactory correla-

tion of f (T) evaluated from E_c (t) and T_c (t) and checked by the directly evaluated values of the magnitude and phase of the complex moduli E* and T* can be noted from the experimental data.

The proposed methods may now be applied to evaluate the response of bituminous concrete at any time or frequency and temperature in the experimental range by interpolation, and to extend the data to cover by extrapolation ranges of time not possible by conventional laboratory methods.

Analogous creep and dynamic experiments, calculations, and graphical procedures were performed on the 300 series bituminous concrete mixture. These calculations are not presented here in detail due to space limitations and may be found elsewhere (18). An analysis of this data also indicated the validity of the time-temperature superposition and linear viscoelastic concepts to the creep and dynamic experimental results of the 300 series mixture.

DISCUSSION

Significance of Results

The experimental results suggest that at low stress levels and for the conditions tested, the assumption of linear viscoelastic behavior is applicable to bituminous concrete. The experimental phase of this study also indicated that the time-temperature superposition concept can be applied to the mechanical properties of bitumen-aggregate compositions to a useful degree of accuracy. For a design engineer who is interested in the mechanical properties of bituminous mixes over a large range of environmental and loading conditions, the equivalence of time and temperature on the viscoelastic response, even when approximate, means an important simplification.

These concepts when properly applied, however, do provide a higher level of approximation than the present elastic theory. Whereas the elastic theory provides valuable information regarding stresses and strains in bituminous pavements under fast-moving wheel loads at freezing temperatures, the effects of slowly applied or static loads at relatively high temperatures cannot be accurately considered by the elastic idealization. In addition, the progressive accumulation of small irrecoverable deformations under repeated wheel loads and subsequent rutting of the bituminous pavement in the vehicle wheelpath cannot be accounted for by the elastic theory. Fatigue effects and plastic flow of flexible pavement surface courses parallel to the direction of traffic are other examples of the inelastic behavior of this engineering material. Thus, a more rational method of flexible pavement design must incorporate the effects of loading time or frequency and temperature on the stress-strain properties of the materials. If the concepts advanced in this study do not provide a sufficiently high degree of accuracy, more sophisticated approaches can be developed. However, the complexities due to the linear viscoelastic and time-temperature superposition concepts are now troublesome when applied to practical problems.

The relationship of original viscosity to temperature for two typical bitumens is shown in Figure 17.

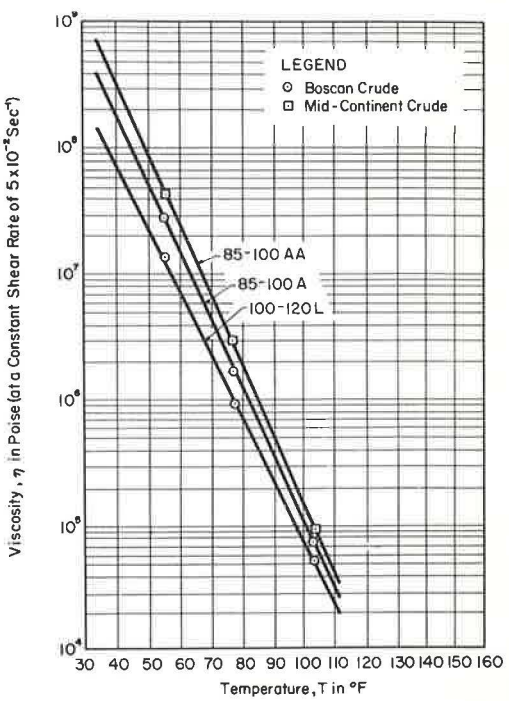

Figure 17. Original bitumen viscosity vs temperature.

Application of the previously discussed principles to the mechanical properties of pavement materials in thickness design procedures are more tentative at this time than their immediate application to bituminous concrete mixture strength evaluation and comparison. These concepts may, however, prove to be more significant in the future, and the elastic layered-system design theories which are available today may be supplemented by future viscoelastic theories which will also include the temperature-dependent properties of the material. Any analysis will be complicated by the many variables that enter into pavement design methods and evaluation.

When only one type of experimental method is available to evaluate mixture strength, covering only a limited portion of the time or frequency scale, the concepts investigated allow the viscoelastic functions to be traced out over a much larger effective range by varying the experimental temperature. For the bituminous concrete studied, an increase in temperature corresponds to an increase in the time or a decrease in the frequency scale in its effect on the viscoelastic functions of the material. This reduction scheme must be used judiciously with regard to the reservations of the theories which support it, and when properly applied, yields plots in terms of reduced variables which can be used with confidence to predict the viscoelastic functions.

Viscoelastic data obtained from one type of experimental measurement are, in principle, sufficient to define all time-dependent properties within the range of linear response, provided the experimental time scale is varied over an exceedingly wide range. In practice, however, it is usually not possible to cover at a single temperature the full time scale required to characterize the transitions of the material. By application of the time-temperature relations over a range of temperatures, the complete transitions of bituminous concrete have been evaluated.

Three-Dimensional Response

The concepts developed in previous sections defining the response of linear viscoelastic materials in one direction can also be extended to analyze their behavior in the three-dimensional case. The experimental data have indicated that if one fundamental property of a thermorheologically linear material follows the time-temperature relations, then all other fundamental properties obey the same relations.

The stresses or strains in two mutually perpendicular directions are related by a linear differential equation in the time domain and by algebraic relations in the frequency domain. Thus, having obtained E* and T* for a given material, the other complex moduli of the material ν^*, G*, K* can be easily obtained. In fact, all equations which are valid for the Hookean solid remain valid for the linear viscoelastic material when expressed in terms of complex moduli, and the three-dimensional response of the material in the frequency domain can be defined over a wide range of temperatures. To evaluate the viscoelastic behavior in the time domain, the inverse transform of the response in the frequency domain is taken (25, 26).

CONCLUSIONS

The major objective of this study was to obtain a better understanding of the mechical properties of bituminous concrete mixtures, which are used over an extensive range of environmental and loading conditions. The following are the major conclusions of the investigation:

1. The experimental data indicate the mechanical properties of the dense bituminous concrete mixtures investigated can be expressed by the linear viscoelastic theory to a useful degree of approximation under the conditions investigated.
2. Experimentation of the phenomenological level has demonstrated that the time-temperature superposition principle is valid for the bitumen-aggregate compositions tested to a satisfactory level of approximation.
3. Time and temperature were shown to have an equivalent effect on the viscoelastic properties of the materials studied, and the number of experiments needed to define the response of the material over a wide range of temperature and time can now be greatly reduced. By use of the time-temperature relations, it was possible to project the ex-

perimental viscoelastic functions to loading times both shorter and longer than can normally be obtained experimentally, and for any intermediate temperature within the tested temperature range.

ACKNOWLEDGMENTS

The author would like to thank Professor Robert F. Baker for his services as adviser of the dissertation from which this paper was partially developed, as well as his valuable suggestions concerning the content of this study. This study was completed at The Ohio State University during tenure of a fellowship awarded by the National Bituminous Concrete Association, whose continued interest and cooperation are gratefully acknowledged. Special thanks are due to the staff of the Transportation Engineering Center of The Ohio State University for its efforts in the preparation of this paper, and especially to Sandy Geiger for typing the manuscript.

REFERENCES

1. Stuart, H. A., Ed., "Die Physik der Hochpolymeren." Springer-Verlag, Berlin (1956).
2. Payne, A. R., "Sinusoidal-Strain Dynamic Testing of Rubber Products." ASTM Mater. Res. Std. (Dec. 1961).
3. Leaderman, H., "Elastic and Creep Properties of Filamentous Materials and Other High Polymers." Textile Foundation, Washington, D. C. (1943).
4. Alfrey, T., "Mechanical Behavior of High Polymers." International Pub., New York (1948).
5. Baker, R. F., "Pavement Design Using Rheologic Concepts." Proc. Internat. Conf. on the Structural Design of Asphalt Pavements, Ann Arbor (1962).
6. Eirich, F. R., Ed., "Rheology, Theory and Applications." Academic Press, New York (1961).
7. Papazian, H. S., "The Response of Linear Viscoelastic Materials in the Frequency Domain." Proc. Internat. Conf. on the Structural Design of Asphalt Pavements, Ann Arbor (1962).
8. Pister, K., and Monismith, C. L., "Analysis of Viscoelastic Flexible Pavements." HRB Bull. 269, pp. 1-15 (1960).
9. Ferry, J. D., "Viscoelastic Properties of Polymers." John Wiley and Sons, New York (1961).
10. Krokosky, E. M., Andrews, R. D., and Tons, E., "Rheological Properties of Asphalt/Aggregate Compositions." Paper presented at Annual Meeting of ASTM (163).
11. Brodnyan, J. G., "Use of Rheological and Other Data in Asphalt Engineering Problems." HRB Bull. 192, pp. 1-19 (1958).
12. Bergen, J. I., Ed., "Viscoelasticity-Phenomenological Aspects." Academic Press, New York (1960).
13. Papazian, H. S., Pagen, C. A., and Baker, R. F., "The Rheological Properties of Bituminous Concrete." Report 172-1, Ohio State Univ. (1961).
14. Burgers, J., and Scott Blair, C., "Report on the Principles of Rheological Nomenclature." Proc. Internat. Rheological Cong., Holland (1948).
15. Pickett, G., "Equations for Computing Elastic Constants from Flexural and Torsional Resonant Frequencies of Vibration of Prisms and Cylinders." Proc. ASTM (1945).
16. Spinner, S., and Tefft, W., "A Method for Determining Mechanical Resonance Frequencies and for Calculating Elastic Moduli from These Frequencies." Proc. ASTM (1961).
17. Brown, A. B., and Sparks, J. W., "Viscoelastic Properties of a Penetration Grade Paving Asphalt at Winter Temperatures." Proc. AAPT (1958).
18. Pagen, C. A., "An Analysis of The Thermorheological Response of Bituminous Concrete." Ph. D. Diss., Ohio State Univ. (1963).
19. Reiner, M., "Deformation and Flow." H. K. Lewis and Co., London (1949).

20. Freudenthal, A. M., "The Inelastic Behavior of Engineering Materials and Structures." John Wiley and Sons, New York (1950).
21. Bland, D. R., "The Theory of Linear Viscoelasticity." Pergamon Press, London (1960).
22. Gross, B., "Mathematical Structure of the Theories of Viscoelasticity." Herman and Co., Paris (1953).
23. Ley, B. J., Lutz, S. G., and Rehberg, C. F., "Linear Circuit Analysis." McGraw-Hill, New York (1959).
24. Rouse, P. E., "A Theory of the Linear Viscoelastic Properties of Dilute Solution of Coiling Polymers." Jour. Chem. Phys. (1953).
25. Churchill, R. V., "Operational Mathematics." 2nd Ed., McGraw-Hill, New York (1958).
26. Truxal, J. G., "Automatic Feedback Control System Synthesis." McGraw-Hill, New York (1955).

Determination and Treatment of Asphalt Viscosity Data

A. W. SISKO
Research and Development Department, American Oil Company, Whiting, Indiana

A simple and convenient cone-plate viscometer has been developed for asphalts. It determines viscosities from 10^2 to greater than 10^{10} poises at temperatures from below 32 to 156 F and at shear rates from 10^{-3} to 10^2 sec^{-1}, requires no more than 1.5 g of sample, and may be used with or without a recorder. Three asphalts have been studied in detail. When the viscosities at various shear rates and temperatures are shifted to a selected reference temperature, they yield a master curve covering a wider range of shear rates than is possible by direct measurement. The master curve correlates shear rates and temperature encountered in service, in stability tests, and in viscosity measurements for specification purposes. A simple equation fits the master curve well and can be combined with the Walther equation to give an equation describing the dependence of viscosity on both shear rate and temperature.

•THE STRENGTH of a bituminous material, in service at a particular temperature, is dependent on the mechanical properties of the asphalt at that temperature. Relevant properties are the elasticity and viscosity, and instruments for their determination have been designed (1, 2, 3). However, these instruments are complicated and for many situations, such as in deformation by rutting (4), for creep under steadily applied loads, and for specification purposes (5), the viscosity sufficiently describes the mechanical behavior of the asphalt. A difficulty with viscosity measurements is that asphalts, in service and in stability tests, encounter shear rates and temperatures covering ranges too wide to be duplicated with a single viscometer. The difficulty can be overcome by the use of a viscometer that covers as much of these ranges as is practical and by treatment of the viscosity data with methods that in effect extend the data to cover the desired ranges of shear rates and temperatures.

The requirements for such a viscometer are that it be rugged, preferably require small samples (such as those recovered from thin film tests), and because asphalts are non-Newtonian fluids be operable over a range of shear rates. Parallel-plate (6) and cone-plate viscometers (7, 8) meet these requirements. However, cone-plate instruments have the advantages of a wider range of shear rates and of requiring neither the sample density nor weight. These advantages and the absence of a suitable commercial instrument prompted the development of a simple and rugged cone-plate viscometer that can be used with or without a recorder.

CONE-PLATE VISCOMETER

Description

Cone-plate viscometers provide means for determining the drag produced by a sample sheared between the cone and the plate. In this instrument, torques are applied to the cone by weights and angular velocities of the cone are measured.

Paper sponsored by Committee on Characteristics of Bituminous Materials and Means for Their Evaluation.

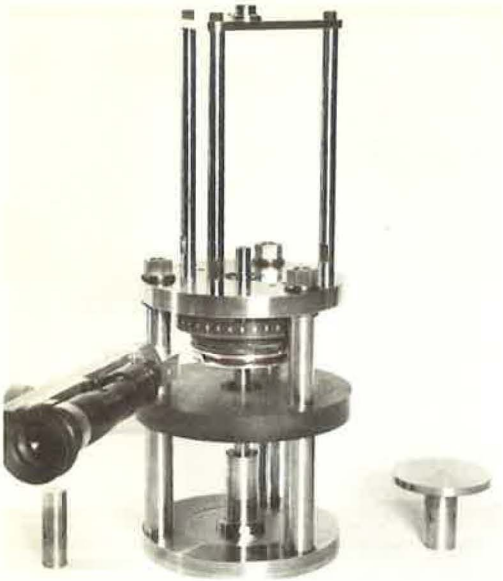

Figure 1. Viscometer.

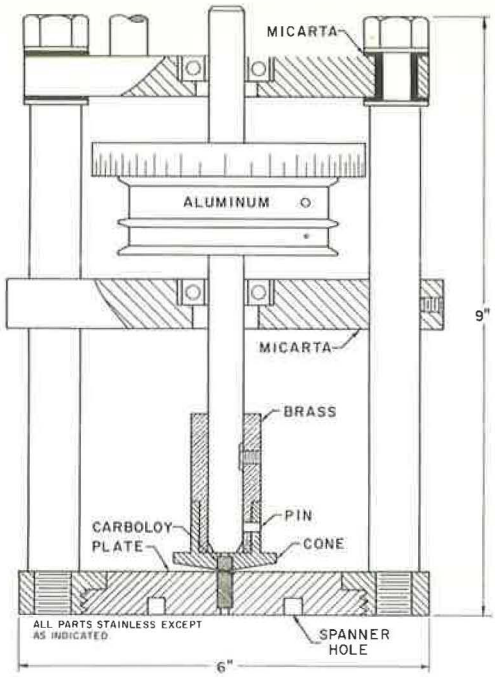

Figure 2. Assembly view of viscometer.

The viscometer (Fig. 1) consists of a stainless steel frame, composed of three plates and support rods, containing a central vertical shaft. Above the frame are three rods and a plate with a bubble level for supporting and leveling the instrument in a thermoregulated bath. Construction details are shown in Figure 2. Precision bearings (SKF 6201 Y/C782) align the central shaft radially but allow free vertical movement. The top plate is electrically insulated from the support rods by micarta washers and sleeves. The middle plate is made of micarta. The bottom plate consists of a ring, into which is threaded a precision ground plate. A pulley and a cone are attached to the vertical shaft. The pulley is slotted to receive the knotted end of a cord. About five turns of cord are wrapped around the pulley and led over a second pulley at the edge of the laboratory bench.

Torques are produced by hanging weights (10 to 25,000 g have been used) from the free end of the cord. Angular velocity is measured by timing the displacement of a drum dial on the instrument pulley. The dial is read by sighting through either a 10-power microscope mounted on the instrument or a cathetometer. Alternatively, a galvanometer light focused on a small mirror attached to the shaft and reflected to a frosted glass scale could be used for observing motion of the cone. Angular velocity might also be determined by recording the output of a rotary variable differential transformer at the top of the shaft.

The cones have large apex angles but differ in diameter. In Figure 2 the cone angle is exaggerated. The cone tip and plate center are made of wear-resistant Carboloy. Cone diameters are approximately 1.9, 3.8, and 7.6 cm, and the respective sample requirements are approximately 0.002, 0.02, and 1.5 g. Cone selection is based on temperature and viscosity; the large cone is used at high temperatures or for materials with low viscosities, and the small cone below 40 F or for very viscous materials.

A sample is prepared for measurement by placing it on the plate beneath the raised cone, and then letting the cone settle. An ohmmeter, placed across the top and bottom plates, indicates when the cone and the plate are in contact. Applying a hot plate to the base and a kilogram weight to the top of the shaft shortens loading time. The instrument is then cooled to room temperature and finally mounted in a temperature-

regulated bath with the bottom of the micarta plate approximately 1 in. above the thermostatted liquid.

Calculations

Viscosity, η, is determined as a function of shear rate, D, or shear stress, S. These are given by:

$$\eta = \frac{S}{D} = \frac{3\,T\,\psi}{2\,\pi\,R^3\,\Omega} \tag{1}$$

$$D = \frac{\Omega}{\psi} \tag{2}$$

$$S = \frac{3T}{2\,\pi\,R^3} \tag{3}$$

in which T is torque in dyne centimeters, ψ is cone angle in radians, R is cone radius in centimeters, and Ω is angular velocity in radians per second. Viscosity, shear rate, and shear stress are in poises, reciprocal seconds, and dynes per square centimeter, respectively. In an actual run, angular velocities are measured in degrees per second for various loads in grams.

The effects of various construction errors have been analyzed (8). Errors arise from friction, drag at the edge of the cone, misalignment of cone and shaft axes, and rounding of the cone tip. Because these errors cannot be completely eliminated, the instrument is calibrated with a liquid of known viscosity. National Bureau of Standards Oil P at 30 C, with viscosity of 461.2 poises, was used. Data for Oil P with the medium cone are shown in Figure 3. Friction prevents the plotted line from passing through the origin. The equation of the line is

$$\omega = -0.490 + 0.2481\,L \tag{4}$$

in which ω is angular velocity in degrees per second and L is weight in grams. Solving for L at zero angular velocity gives the weight, f, required to overcome friction (1.98 g for the medium cone). The shear stress is

$$S = \frac{3\,r\,g\,(L - f)}{2\,\pi\,R^3} = k_1(L - f) \tag{5}$$

in which r is the pulley radius plus the cord radius and g is the gravitational constant.

Errors other than from friction are incorporated into an effective cone angle, calculated from the slopes of Figure 3:

$$\psi = \eta\,\frac{d\Omega}{dS} = \frac{461.2\,(2\pi)}{k_1\,(360)}\,\frac{d\,\omega}{d\,L} \tag{6}$$

The effective cone angle is within 6 percent of the value determined by measurement with a sine bar and precision gage blocks. This difference affects only the non-Newtonian portion of the flow curve and is negligible for the asphalts studied. Shear rate in degrees per second is given by

$$D = \frac{2\,\pi}{360\,\psi} = k_2 \tag{7}$$

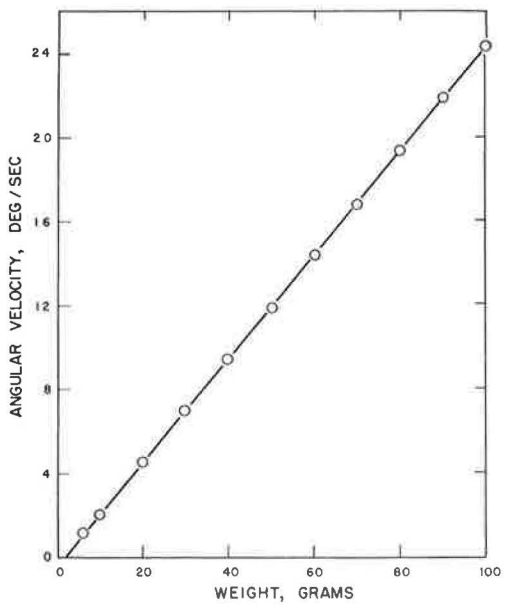

Figure 3. Calibration of instrument.

Constants for the three cones are given in Table 1. For construction purposes, angles are in the range 0.45 to 0.50 degrees. The range of the instrument may be further extended by using cones of larger angles.

TABLE 1

CONE CONSTANTS

Cone	Radius (cm)	Angle (rad)	f(g)	k_1	k_2
Small	0.850	8.622×10^{-3}	3.96	2009	2.015
Medium	1.905	8.016	1.98	249.2	2.177
Large	3.812	8.086	2.53	31.09	2.159

Results and Discussion

In viscosity determinations on asphalts, complications arise due to thixotropic, elastic, and normal stress effects. Thixotropy results in a decrease in viscosity with time of shearing. Elasticity is evidenced by sample strain without flow immediately after application of the torque. The normal stress effect causes the sample to creep out of the gap between the cone and the plate. At high temperature the three phenomena are less serious. The instrument is operated to minimize these complications. A run is started with a heavy weight, before going to lighter weights, to reduce thixotropic effects. A similar procedure is effective with the parallel-plate viscometer (9). Weights are removed after each reading to minimize rotation and give the operator time to record the data. The effect of elasticity is reduced by allowing the cone to rotate at least 1° after each weight application before angular displacement is timed. Normal stress effects are minimized by making measurements with a minimum rotation of the cone.

Data for a typical run on a 57-penetration paving asphalt at 77 F are shown in Table 2. The data cover a 660-fold range of shear rates with less than ½ rev of the cone. Fracture occurs within the asphalt, not at the asphalt-metal interface.

Comparisons were made of viscosities determined with the parallel-plate and cone-plate instruments. Figure 4 gives results obtained at two temperatures on a paving asphalt using the medium cone. The agreement between the two viscometers is good. The data demonstrate the wider range covered by the cone-plate instrument. Use of the large cone would have extended the data at 122 F to below 10^{-2} sec^{-1}.

When cooled from mixing and sampling temperatures, asphalts slowly develop an internal structure. This phenomenon, steric hardening, also occurs in samples stored in the viscometer. Figure 5 shows how the viscosity of an asphalt held in the viscometer at 77 F for 3, 18, and 65 hr before running at 77 F increases with time. At high shear rates, differences in viscosity are less than at low shear rates, indicating that shear breakdown (thixotropy) is greatest for the sample with the most developed internal structure. For routine use, standard holding times of 0.5 hr at 77 F or of 1 hr at 39.2 F have been adopted.

TREATMENT OF DATA

Extensive measurements were made on three paving-grade asphalts. Inspection properties of the asphalts are given in Table 3. Asphalts A and B were prepared

TABLE 2

RESULTS OF TYPICAL TEST WITH VISCOMETER[a]

Weight (g)	Deg	Time (sec)	D (sec^{-1})	η (poises)	S ($dynes/cm^2$)
300	2	825.0	5.28×10^{-3}	1.41×10^{7}	7.44×10^{4}
100	1	1,370.1	1.59	1.54	2.45
300	1	378.2	5.76	1.29	7.43
500	1	209.1	1.04×10^{-2}	1.19	1.24×10^{5}
1,000	1	83.9	2.59	9.60×10^{6}	2.49
2,000	3	81.3	8.03	6.20	4.98
4,000	6	45.7	2.86×10^{-1}	3.48	9.95
8,000	20	33.9	1.28×10^{0}	1.56	2.00×10^{6}
12,000	55	34.1	3.51	8.52×10^{5}	2.99
16,000		sample fractured			

[a]Sample of 57-penetration paving asphalt.

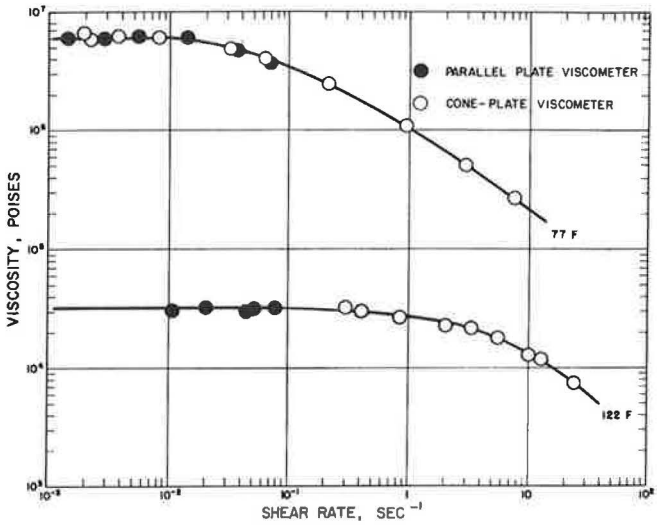

Figure 4. Comparison of parallel-plate cone-plate viscometer.

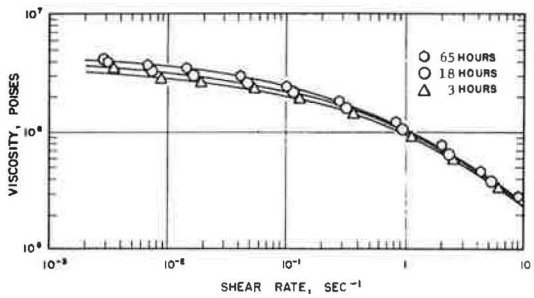

Figure 5. Dependence of viscosity on sample age.

by reduction of Midcontinent and Venezuelan crudes. Asphalt C was prepared by oxidation of a reduced Venezuelan crude. Viscosities for the asphalts are shown in Figures 6, 7, and 8.

Each asphalt forms a family of curves of the same general shape. The curves extrapolate to limiting viscosities at low shear rates and to a common slope at high shear rates. The similarity suggests that the data can be combined in single master curves, one for each asphalt, by vertical and horizontal shifts. The shifts are easily accomplished when the data are plotted on tracing paper having log-log coordinates. This is a common procedure in rheology and has been used for dynamic mechanical properties of asphalts (10, 11).

Vertical shifts are made to obtain coincidence of the limiting viscosities at a selected reference temperature. The amount of shift is determined from a plot of limiting viscosity against temperature. In Figure 6, for example, limiting viscosities are readily found from the data

TABLE 3

INSPECTION PROPERTIES OF ASPHALTS

Asphalt	Penetration[a]	Viscosity (poises)	
		At 275 F	At 250 F
A	55	6.99	15.2
B	60	6.48	13.6
C	154	2.91	6.70

[a] Of 100 g at 77 F in 5 sec.

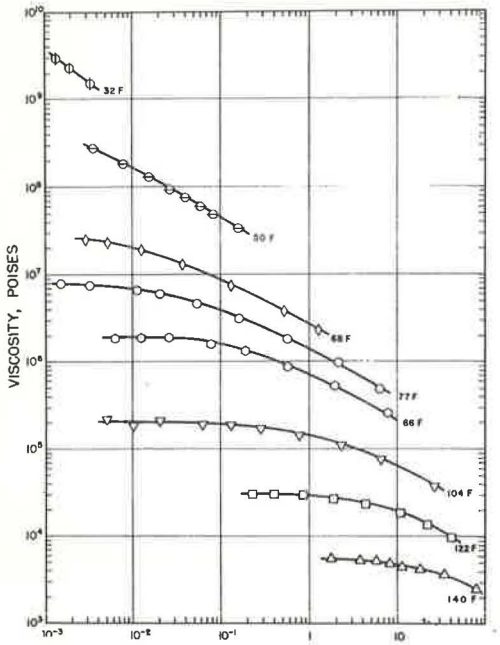

Figure 6. Flow curves for asphalt A.

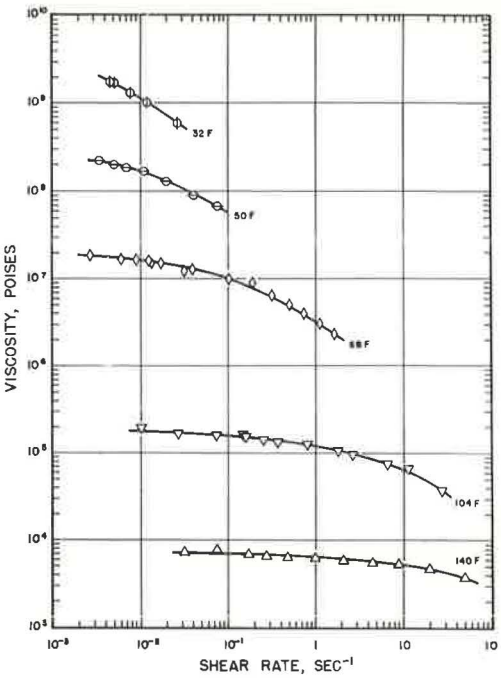

Figure 7. Flow curves for asphalt B.

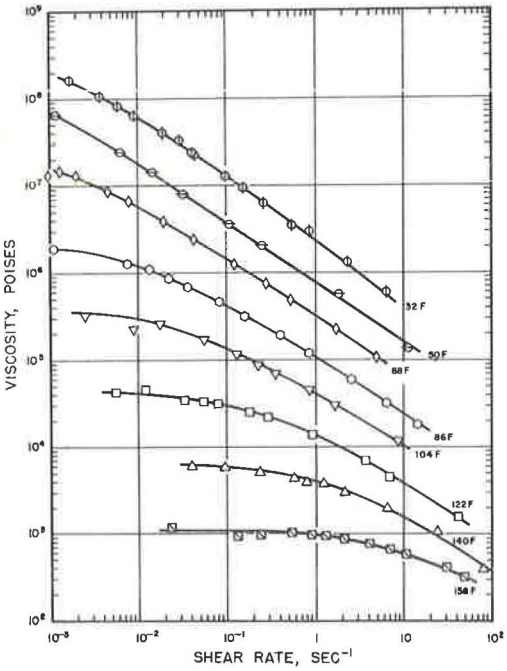

Figure 8. Flow curves for asphalt C.

at temperatures from 77 to 140 F. These limiting viscosities and capillary viscometer data at 250 and 275 F (where non-Newtonian flow is negligible) are plotted on a graph with coordinate spacings based on log log 100η and log T (Walther coordinates), in which T is absolute Fahrenheit temperature. Such a plot is shown in Figure 9 for asphalt A. Generally these plots are straight lines or are slightly curved. Limiting viscosities at other temperatures are found by interpolation or extrapolation. Reference temperatures for asphalts A, B, and C were arbitrarily selected at 77, 68, and 86 F.

Horizontal shifts are needed after application of the vertical shifts to obtain coincidence of the individual curves at high shear rates. Figure 10 shows the amount of horizontal shift required. Curves with factors greater than 1 are shifted to the right, those with factors less than 1 are shifted to the left. The direction of the shifts shows that non-Newtonian flow begins at higher shear rates as temperature is increased.

Master curves obtained by these shifts appear in Figures 11, 12, and 13. The

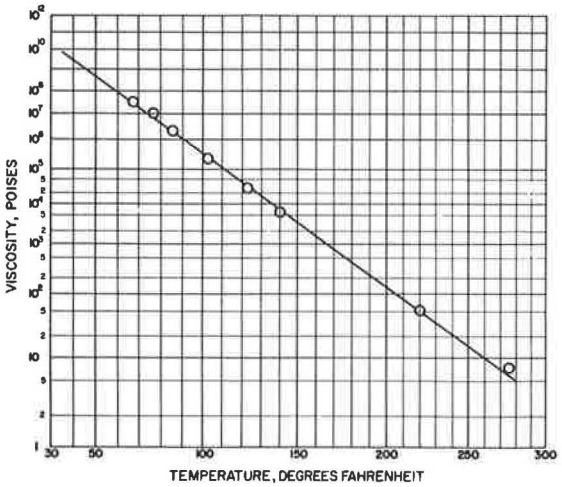

Figure 9. Effect of temperature on initial viscosity of asphalt A.

coordinates are reduced viscosity, resulting from the vertical shift, and reduced shear rate—the product of the horizontal shift factor α and the shear rate. The curves cover wider ranges of shear rates than is possible with any one viscometer. Starting with a master curve and applying the shifts yields viscosities over the complete range—from the limiting viscosity at low shear rates to the limiting slope at high shear rates—at temperatures where the limiting conditions are relatively inaccessible to experimental measurement.

An equation in good agreement with the flow curves in Figures 6, 7, and 8 has been found. At any temperature, the fluidity φ (reciprocal of the viscosity) is the sum of the limiting fluidity at low shear rates φ_0 and a fluidity that has a power dependence on shear rate:

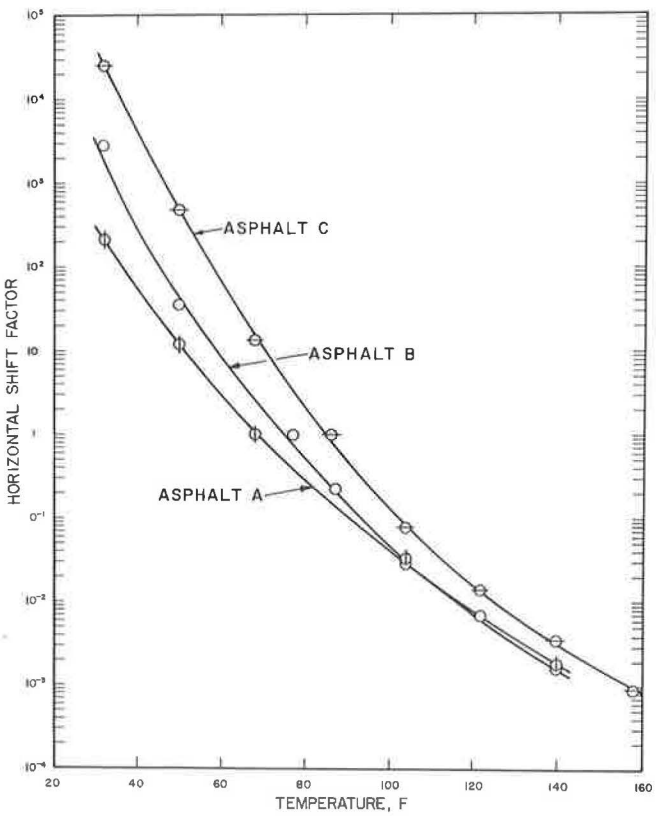

Figure 10. Horizontal shift factors for asphalts.

$$\varphi = \varphi_0 + bD^n \tag{8}$$

In this equation, b and n are constants with n the limiting slope at high shear rates when log fluidity is plotted as a function of log shear rate. In terms of viscosity the equation becomes

$$\eta = \frac{\eta_0}{1 + \eta_0 bD^n} \tag{9}$$

in which η_0 is the limiting viscosity at low shear rates. When the constants are known for the reference temperature, flow curves at other temperatures can be calculated from the more general equation:

$$\eta = \frac{\eta_0}{1 + CD^n} \tag{10}$$

in which $C = \eta_0^* b^* \alpha^n$. Constants η_0^*, b^*, and n are those for the reference flow curve; η_0 and α are values appropriate to the temperature for which the flow curve is to be calculated.

At the reference temperature, where $\alpha = 1$, the equation of the master curves in Figures 11, 12, and 13 has the constants given in Table 4. These data are insufficient for assessing how generally the narrow range of n, found here, applies to other asphalts. The agreement between the calculated master curve and the data for each asphalt, over 5 to 10 decades of shear rate, is generally good.

The dependence of η_0 on temperature is given by the Walther equation (12):

$$\log \log 100\,\eta_0 = a - m \log T \tag{11}$$

in which a and m are constants. In the absence of phase changes the Walther equation has been found reliable for most asphalts in the temperature range 150 F and below, and for many asphalts the equation is a good approximation up to temperatures of 275 F. Walther constants are given in Table 5.

The dependence of viscosity on both shear rate and temperature is given by the equation:

$$\log \log 100\,\eta\,(1 + CD^n) = a - m \log T \tag{12}$$

This equation yields a family of curves, one for each temperature, on plots of viscosity as a function of shear rate (such as appear in Figures 6, 7, and 8) or a family of curves, one for each shear rate, on Walther plots.

Curves of the second type are shown in Figures 14, 15, and 16. The plots are easily interpolated to find viscosities at intermediate shear rates. Asphalt C is appreciably non-Newtonian at the specification temperature of 140 F and this behavior could interfere with agreement between the different vacuum capillary viscometers used at 140 F. Much of the curves in Figures 14, 15, and 16 can be found by plotting viscosities inter-

TABLE 4

CONSTANTS OF EQUATION OF MASTER CURVES

Asphalt	η_0^*	b*	n
A	8.33×10^6	6.05×10^{-7}	0.692
B	2.00×10^7	2.70×10^{-7}	0.700
C	2.40×10^6	9.71×10^{-6}	0.691

TABLE 5

WALTHER CONSTANTS

Asphalt	a	m
A	11.0712	3.7081
B	10.9104	3.6505
C	10.3381	3.4661

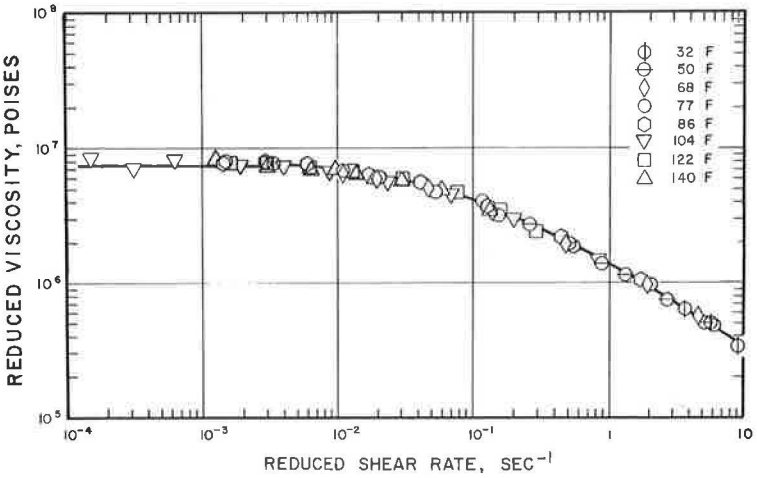

Figure 11. Master curve for asphalt A.

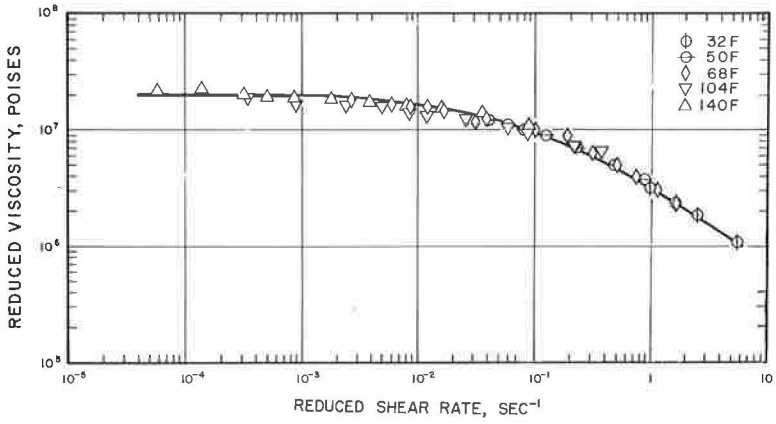

Figure 12. Master curve for asphalt B.

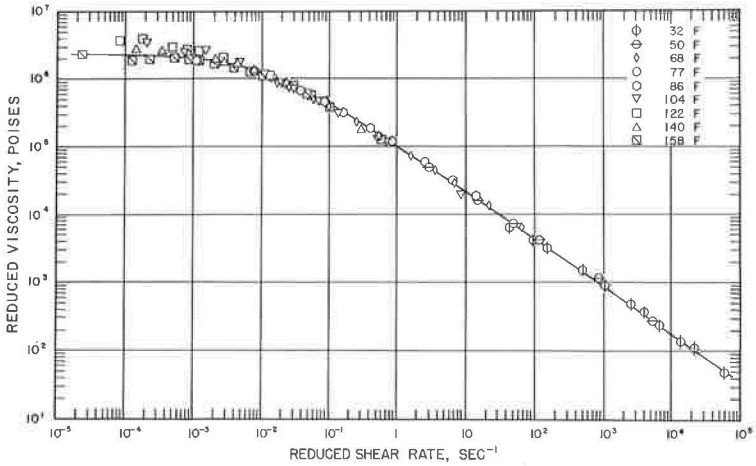

Figure 13. Master curve for asphalt C.

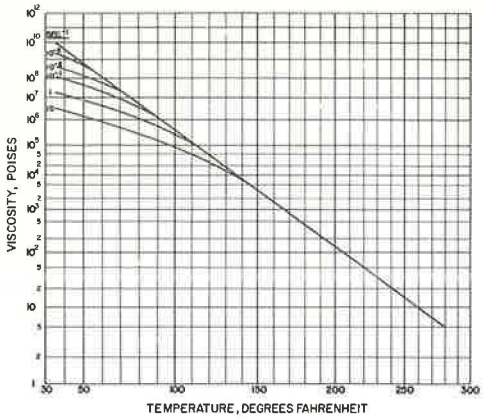

Figure 14. Effect of shear rate and temperature on viscosity, asphalt A.

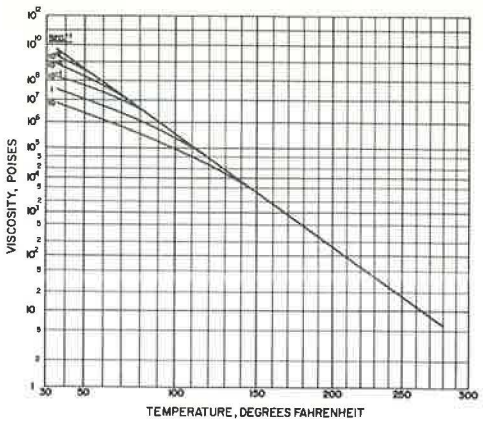

Figure 15. Effect of shear rate and temperature on viscosity, asphalt B.

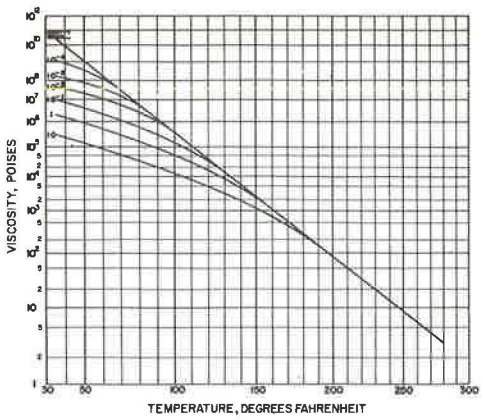

Figure 16. Effect of shear rate and temperature on viscosity, asphalt C.

polated from flow curves at different temperatures, thereby offering a simpler but limited method for portraying the effect of both shear rate and temperature on viscosity.

CONCLUSION

A cone-plate viscometer and an operating procedure for minimizing the complications of elasticity and time-dependent flow have been developed for asphalts. The instrument covers a wider range of shear rates with small samples than do other asphalt viscometers.

Two methods of treating the data are attractive. One method requires shifting viscosities determined at various shear rates and temperatures to yield a master curve at some reference temperature; the other simply displays the data on a plot of viscosity against temperature as a family of curves, one for each shear rate.

A simple equation describing asphalt flow is combined with the Walther equation to yield the dependence of viscosity on both temperatures and shear rate. Either the combined equation or the master curve technique describes asphalt flow over a range of shear rates and temperatures wide enough to include most conditions encountered

in service, in stability tests, and in viscosity measurements for specification purposes.

ACKNOWLEDGMENTS

The author wishes to thank L. C. Brunstrum for helpful suggestions and A. T. Jancosek for careful experimental work and calculations.

REFERENCES

1. Lammiman, K. A., and Roberts, J. E., Lab. Pract., 10: 816 (1961).
2. Thrower, En N., Jour. Sci. Instr., 38: 69 (1961).
3. Philippoff, W., Jour. Appl. Phys., 24: 685 (1953).
4. Speer, T. L., Brunstrum, L. C., Evans, J. V., Ott, L. E., and Sisko, A. W., Proc. AAPT, 32: 236 (1963).
5. Welborn, J. Y., and Halstead, W. J., Public Roads, 31: 243 (1962).
6. Griffin, R. L., Miles, T. K., Penther, C. J., and Simpson, W. C., ASTM Spec. Tech. Publ. 212 (1957).
7. Higginbotham, R. S., Jour. Sci. Instr., 27: 139 (1950).
8. Markovitz, H., Elyash, L. J., Padden, F. J., Jr., and De Witt, T. W., Jour. Colloid Sci., 10: 165 (1955).
9. Fink, D. F., and Heithaus, J. J., ASTM Spec. Tech. Publ. 309 (1961).
10. Brodnyan, J. G., "Use of Rheological and Other Data in Asphalt Engineering Problems." HRB Bull. 192, pp. 1-19 (1958).
11. Gaskins, F. H., Brodnyan, J. G., Philippoff, W., and Thelen, E., Trans. Soc. Rheology, 4: 265 (1960).
12. Walther, C., Oil Kohle, 1: 71 (1933).

Stress Relaxation of Bituminous Concrete in Tension

EDGAR F. DAVIS, EDWARD M. KROKOSKY, and EGONS TONS
Respectively, Research Assistant and Assistant Professors of Civil Engineering, Massachusetts Institute of Technology

Asphaltic concrete has been largely studied in compression. The evaluation of rheological properties of asphaltic concrete in tension aids in completing a picture of this complicated material system. A simple test method, employing a constant rate of extension was used to determine the relaxation behavior of certain asphalt-aggregate mixtures. Experimental results were then compared with compression test results conducted in the same manner. Nonlinear viscoelastic behavior was experienced in both types of tests and the effect of temperature and strain on nonlinearity was determined. In tension the nonlinearity increased with decreasing temperature, whereas in compression the reverse was true. A possible explanation for reversal of the temperature dependence of the nonlinearity involves interparticle friction and low-temperature "stress-riser" effects.

•THE SUITABILITY of asphaltic concrete for use as a pavement material seems to be related to its rheological behavior. Therefore, a thorough knowledge of the time and temperature dependent properties of this composite is indispensable.

A complete picture of rheological behavior of a material has to include both tensile and compressive properties. Researchers have been active in the area of compression evaluation (1, 2, 3, 4, 5); the evaluation of tensile rheological behavior to date has gone unchallenged.

PURPOSE AND SCOPE

The primary purpose of this study was to investigate the rheological properties of asphaltic concrete by tension tests at constant strain rates. A secondary purpose was to evaluate effects of asphalt content and microaggregates on the stress relaxation behavior.

Approximately 150 tensile specimens were tested employing the following variables:

1. Three asphalt contents: 5.5, 6.5 and 7.5;
2. Four temperature conditions: -20, +20, +77, and +120 F;
3. Three rates of deformation: 0.02, 0.2, and 2.0 in./min; and
4. Three microaggregate combinations: 5 percent limestone, 5 percent asbestos, and 2.5 percent limestone plus 2.5 percent asbestos.

The amount of stress relaxation that occurred during the constant extension tests was computed using the same analysis performed by Krokosky (1) for asphaltic concrete in compression. Certain comparisons were made between the rheological data observed in tension and those observed in compression.

Paper sponsored by Committee on Mechanical Properties of Bituminous Paving Mixtures.

SAMPLE PREPARATION AND TESTING

Composition and Size of Specimens

The mix design conformed to a typical Commonwealth of Massachusetts Type I, top-course asphaltic mixture with ½-in. maximum size aggregate. Mix characteristics and proportions are summarized in Tables 1 and 2, Figures 1 through 3, and Appendix A. This mix has been used extensively by the Civil Engineering Materials Research Laboratory at Massachusetts Institute of Technology for various testing programs. The code designations for the various specimen compositions are given in Table 3. The specimens used were 2 in. in diameter and 5 in. high. The 1-in. additional length was required because the type of grips used had a collar that extended ½ in. onto the specimen (Figs. 4, 5 and 6).

TABLE 1

AGGREGATE GRADATION

Sieve Size		Wt (g)	Accum. Wt (g)	Retained (%)	Passed (%)
Passed	Retained				
½ in.	⅜ in.	72.5	72.5	8.5	91.5
⅜ in.	No. 4	213.0	285.5	34	66
No. 4	No. 10	181.0	466.5	55	45
No. 10	No. 20	72.5	539.0	63.5	36.5
No. 20	No. 40	100.0	639.0	75.4	24.6
No. 40	No. 80	100.0	739.0	87	13
No. 80	No. 200	63.0	802.0	94.5	5.5

TABLE 2

MIX PROPORTIONS

Component	5.5% Asphalt		6.5% Asphalt		7.5% Asphalt	
	% by Wt	Wt (g)	% by Wt	Wt (g)	% by Wt	Wt (g)
Coarse agg.[a]	52	466.5	51.5	466.5	50.9	466.5
Fine agg.[b]	37.5	335.5	37.0	335.5	36.6	335.5
Microagg.[c]	5.0	44.8	5.0	45.3	5.0	45.8
Asphalt	5.5	49.2	6.5	58.9	7.5	68.8
Total	100.0	896.0	100.0	906.2	100.0	916.6

[a]Retained on No. 8 sieve. [b]Passing No. 10 sieve.
[c]Passing No. 20 sieve (74 μ or smaller).

Specimen Fabrication

Mold equipment and specimen materials were heated at 300 F before compaction. The mold was insulated by 3 in. of asbestos during compaction to insure that the compacting temperature would not fall rapidly. Aggregate and asphalt were proportioned by adding the asphalt to the aggregate on a direct reading scale. Mixing was done by hand for 2 min in a mixing bowl. A mechanical kneading compactor was used to consolidate the hot mix. The kneading compactor is thought to impart the action most comparable to that of rubber-tired traffic (10). Figures 4 and 5 show the manual type of kneading compactor used. The specimen was compacted in six layers with 50-load applications at 500 psi for each layer.

To remove the specimen from the mold, the "push-out" method described in ASTM D1560-58T (11) was used. After cooling, the specimens were glued with epoxy into

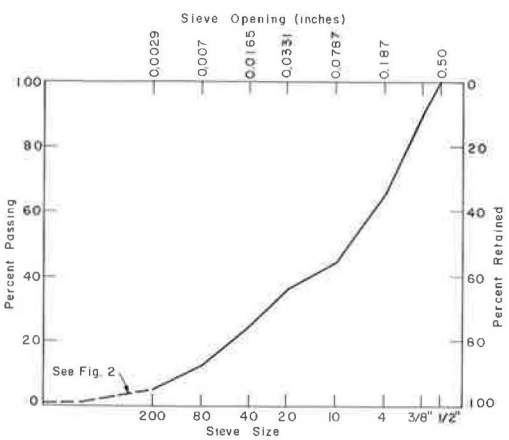

Figure 1. Aggregate gradation used.

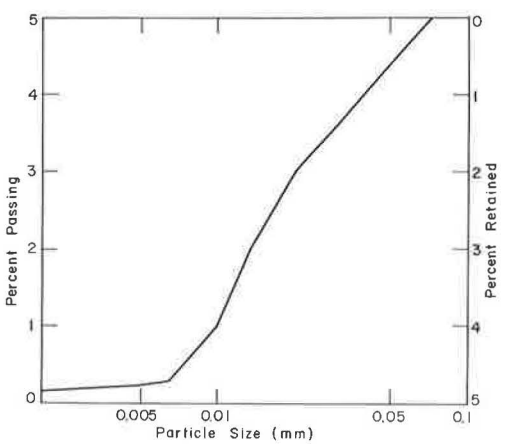

Figure 2. Particle size distribution for limestone microaggregate.

tensile caps which were 2-in. brass "cleanout" covers (Figs. 6 and 7). Appendix B discusses the capping specimen and the glue resins used. Before testing, the specimens were allowed to cure in air for 24 hr.

Test Procedures

The specimens were tested at different rates of strain by a universal testing machine which provides a continuous record of load and deformation.

TABLE 3

CODE DESIGNATION FOR MIXES

Code Letter	Microaggregate	Asphalt Content (%)[a]	Microagg. Content (%)[a]
A-1	Asbestos	5.5	5
A-2	Asbestos	6.5	5
A-3	Asbestos	7.5	5
LS-1	Limestone	5.5	5
LS-2	Limestone	6.5	5
LS-3	Limestone	7.5	5
ALS-1	Asbestos-Limestone	5.5	2.5-2.5
ALS-2	Asbestos-Limestone	6.5	2.5-2.5
ALS-3	Asbestos-Limestone	7.5	2.5-2.5

[a]By total weight of mix.

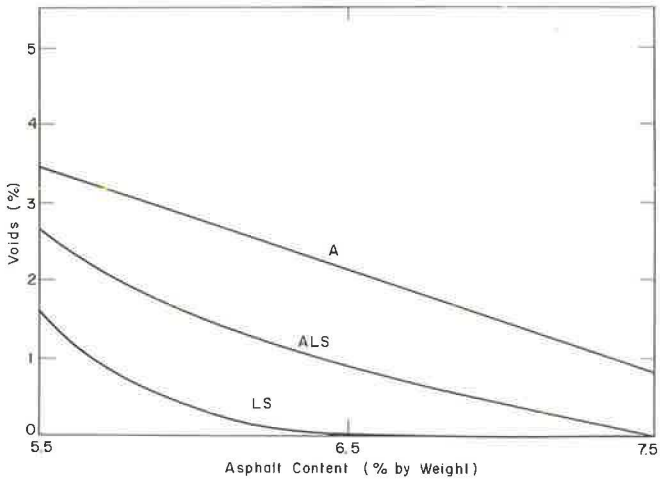

Figure 3. Comparison of voids for different asphalt contents and different microaggregates.

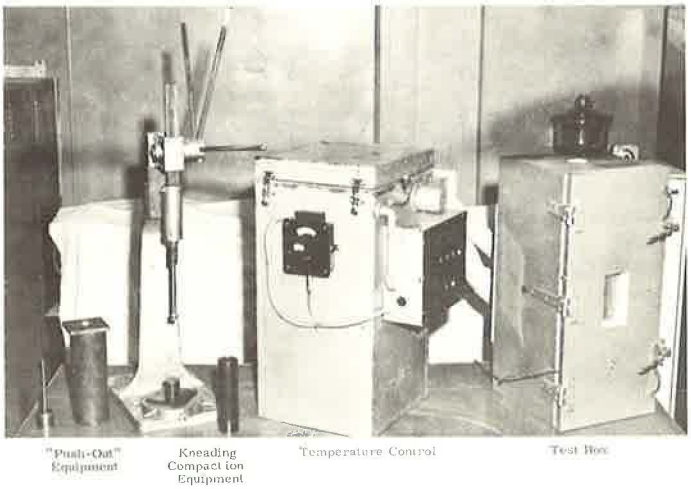

Figure 4. Special compaction and test equipment.

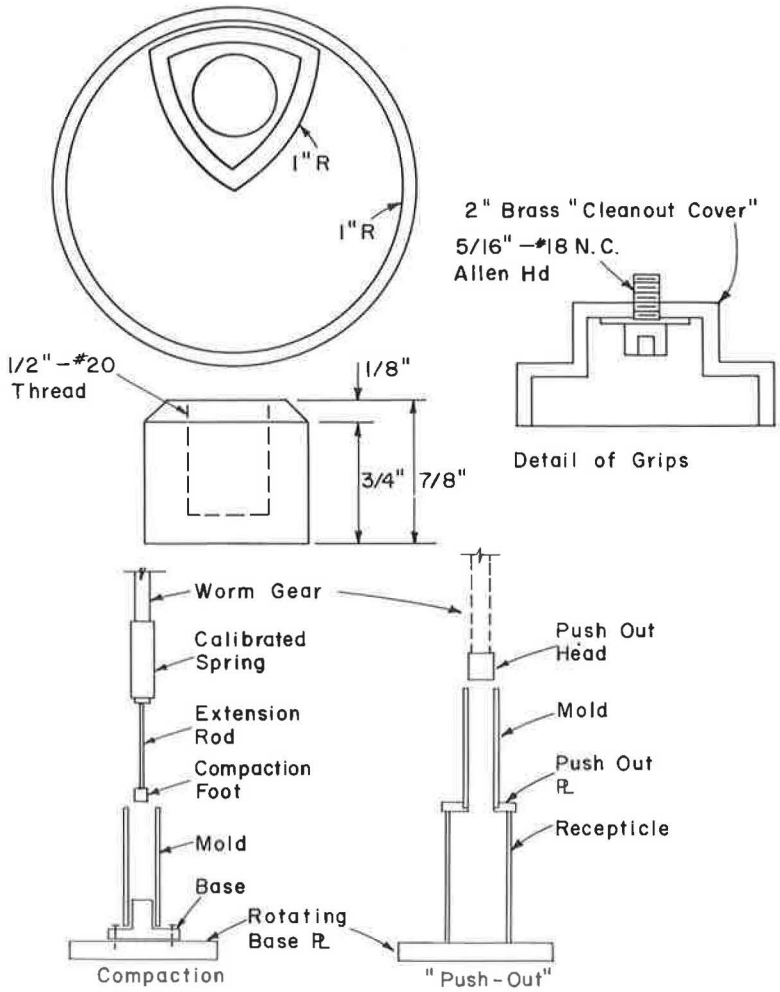

Figure 5. Details of compaction foot, cap grips and fabrication schemes.

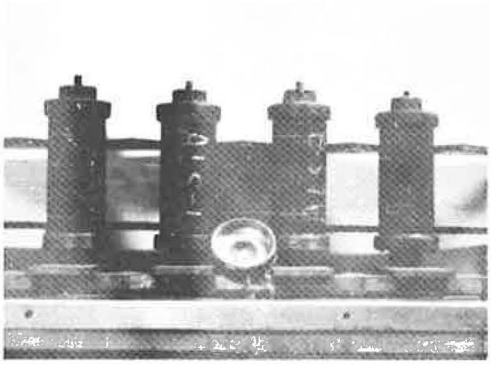

Figure 6. Capping apparatus.

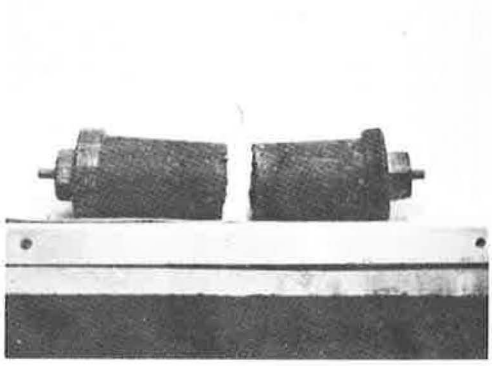

Figure 7. Typical tension failure.

Temperature was controlled by a temperature control unit and an insulated test box (Fig. 4) which was positioned in the testing machine by screw jacks. Before being placed in the test box, the specimens were conditioned for 2 hr at the test temperature, using laboratory oven or refrigeration facilities.

RESULTS

Tension Testing Program

For each of the 150 tests a recorded trace of stress vs time (strain) was made (Fig. 8). For each type of specimen, curves were plotted for different strain rates at a given temperature (Fig. 9). Figure 10 shows the results of seven similar specimens tested under identical conditions, but by different laboratory personnel. Specimens 1, 2 and 3 were made and tested by one team.

To estimate the reproducibility when different personnel prepare and test the specimens, as well as the inherent reproducibility, the straight-line projections of these upper portions of the stress strain curves with the origin of coordinates translated horizontally were compared (Fig. 10). The translation of the curves eliminated the lower portion of transition, as shown in Figure 8, which is usually caused by slack in the test system. The average value of modulus or slope in Figure 10 is 76,000 psi, with extreme values ranging from 66,000 to 90,000 psi, or deviations from the average of -10,000 psi (13 percent) and +14,000 psi (18 percent). For the first three of the specimens mentioned previously which were tested by the same personnel the average is 70,000 psi, with extremes of 66,000 and 72,000 psi, or deviation of -4,000 psi (6 percent) and +2,000 psi (4 percent).

Therefore, in the tensile studies for the equipment and methods previously discussed the reproducibility of results is within ±20 percent, using different personnel to prepare the samples and to within ±10 percent, when the same personnel are used to prepare all the samples.

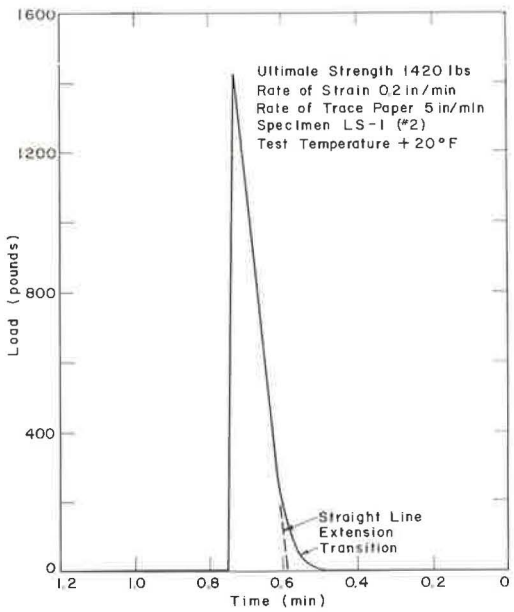

Figure 8. Typical test trace.

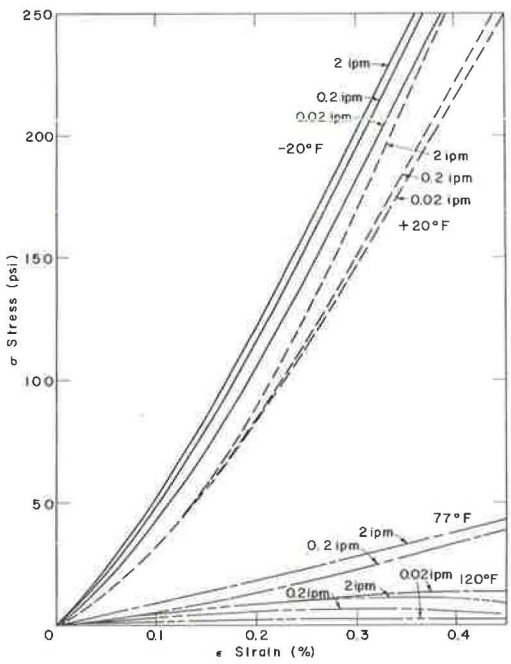

Figure 9. Stress-strain curves for twelve A-1 specimens.

NOMENCLATURE

σ = stress,
ϵ = strain,
$\dot{\epsilon}$ = strain rate,
t = time,
T = temperature,
$F(\epsilon, t)$ = constant rate of extension modulus (strain dependent),
S (t) = constant strain rate modulus (nonstrain dependent),
$\Gamma(\epsilon, T)$ = factor expressing deviation from linear viscoelastic behavior,
m = factor relating F(t) and E (t),
E_r (t) = stress relaxation modulus,
τ = relaxation time,
H = relaxation spectrum in extension, and
a_T = horizontal shift factor.

RHEOLOGICAL THEORIES

Comparison of Compression and Tension Tests

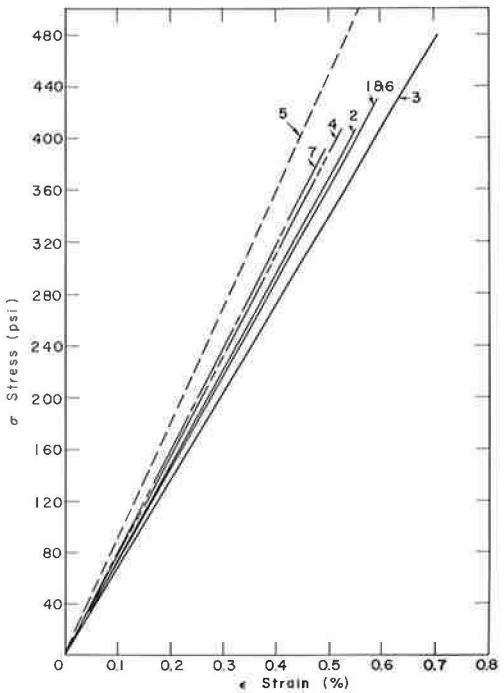

Figure 10. Typical stress-strain curves for seven LS-1 specimens at +20 F, 0.2 in./min.

Some polymer materials obey the laws of linear viscoelasticity; i.e., their behavior can be described by a series of Hookean springs and Newtonian dashpots. As a result of this linearity, a unique stress relaxation modulus can be determined at any low constant strain. Therefore, in a linear viscoelastic material, modulus E_r (t) is only a function of time and not a function of strain.

Other materials, e.g., crystalline polymers, filled polymers and certain rubbers, are nonlinear in their viscoelastic behavior. It should be noted also that fillers can alter the properties of a linear viscoelastic material so as to impart to them certain nonlinear characteristics. Asphalt-aggregate mixtures are in this category. Some asphalts are linear viscoelastic materials; however, the introduction of filler (aggregate) imparts to them certain nonlinear characteristics.

Of major interest, therefore, is the degree to which a material such as asphalt, when filled with aggregate and tested in tension, will exhibit nonlinear behavior. It was previously concluded (1) after conducting constant rate of compression, creep and stress relaxation tests (in compression) that:

> The introduction of the large volume (80%) of solid filler (aggregate) into an asphalt which is ordinarily a linear viscoelastic material produces a material with nonlinear and pseudo-viscoelastic material properties.

Although the asphalt aggregate composite retains some of the properties of the viscoelastic cementing agent, the difference between the viscoelastic response of the asphalt alone and that of the composite seems to be a strong function of the type of test employed. The more aggregate displacement involved, the greater is the difference between the viscoelastic properties of the composite and of the asphalt.

> The Γ function, in a sense a correction factor, which represents deviations from ideal linear viscoelastic behavior, plays a more important role as the behavior of the aggregate is more involved in the deformation. The more the aggregate is involved,

> the greater the dependence of Γ on various factors such as stress or strain, time and temperature. In the constant rate of compression test, where the aggregate is moved forcibly, Γ is a function of strain and temperature; in the creep test, where the aggregate motion is less forced, Γ is a function only of temperature; but in the direct stress-relaxation test, where there seems to be no aggregate motion required, there are indications that the Γ function is not required. (1)

In a constant rate of compression test (which is of greatest interest because it is simply a reversal of the constant rate of extension test employed in this study), the composite shows nonlinear behavior, where Γ varies with strain and temperature. In compression the deformation is continuously forced, which involves displacing particles that offer resistance, and as a result there is a strain dependence. At the higher temperatures, where viscosity of the asphalt binder is low, the nonuniform sized aggregate particles are able to move easily past each other. As the temperature decreases, two effects occur: (a) the viscosity of the asphalt increases, which hinders the aggregate particles from slipping by each other, and (b) the aggregate particles are forced to move in larger aggregate combinations. Thus, the details of the aggregate motion depend on the temperature and, as a consequence, the Γ functions should be temperature dependent.

One of the questions to be resolved by the tensile tests is the nature of the nonlinear function when the asphalt sample is subjected to tension. There is a possibility that the system is linear when tested in tension. It must be remembered that there are inherent differences between the tensile and compression tests. In compression there is more likelihood of a sharing of the stress between the particles and the asphalt with the aggregate transmitting some stress to the asphalt. In tension the majority of stress is transmitted through the asphalt and asphalt would be transmitting the stress to particles. One of the objects of this study was to see if the nonlinear correction factor is affected by the differences in stress transmission.

Some Theoretical Considerations

Constant Rate of Extension Test and Stress Relaxation. —For a constant rate of extension tests at small values of strain, linear viscoelastic behavior can be represented by the relation:

$$\Gamma(\epsilon)\, S(t) = \frac{\sigma(\epsilon, t)}{\epsilon} \tag{1}$$

in which

$\Gamma(\epsilon)$ = correction factor which is strain dependent only,
$S(t)$ = constant strain rate modulus which is only a function of time (Hookean modulus),
(t) = time,
σ = stress, and
ϵ = strain.

Smith (12) found that if a material is subjected to various finite rates of loading, during the time of loading it will be undergoing some relaxation; the slower the test the greater will be the relaxation.

Various empirical modifications of equations from linear theory have at times been used for representing certain types of nonlinear viscoelastic behavior. For the purposes here, a correction factor called Γ has been applied to Eq. (1) so that this equation will fit observed or predicted nonlinear behavior (1, 16). Equation (1) also indicates that for large strains (in this case strains greater than 0.1 percent), the time and stress functions are separable. Thus, it is reasonable to assume that $S(t)$ (assuming $S(t) \cong F(\epsilon, t)$ as ϵ approaches zero) can be written in the form (16):

$$\sigma(\epsilon, t) = \epsilon \cdot F(\epsilon, t) = \Gamma(\epsilon) \cdot \epsilon \cdot S(t) \quad (2a)$$

$$\log \sigma(\epsilon, t) = \log \left[\Gamma(\epsilon) \cdot \epsilon \right] + \log S(t) \quad (2b)$$

in which

$\Gamma(\epsilon)$ = a correction factor or deviation from linearity and is seemingly a function only of strain, approaching unity as the strain approaches zero; and
$F(\epsilon, t)$ = experimental constant strain rate modulus (non-Hookean modulus).

If Γ is only due to stress-strain it should be independent of time. If independent of time it should also be independent of temperature, according to the time-temperature superposition principle.

The validity of Eq. (2a) can be determined by plotting isostrain curves, obtained from calculations based on arbitrarily selected strain values, on log σ vs log t, thereby separating strain and time effects. The slope of the isostrain curve is a measure of relaxation. The vertical separation between isostrain curves is a measure of $\log \Gamma(\epsilon) \cdot \epsilon$. If the isostrain curves are parallel, then the data can be represented by Eq. (2a).

The vertical separation of isostrain curves, plotted as log $F(\epsilon, t)$ vs log t is the quantity $\Gamma(\epsilon)$ which should approach unity as ϵ approaches zero. If these isostrain curves are shifted vertically, the relative value $\Gamma(\epsilon)$ can be determined.

It is possible to write $\Gamma(\epsilon)$ as $\Gamma(\epsilon\, t, T)$. $\Gamma(\epsilon)$ is a deviation effect from linearity or correction factor, which could just as well be a function of time and temperature as well as of strain. To determine its dependence it would be necessary to hold two of these quantities constant and vary the third. Equation (2) shows that, if $\Gamma(\epsilon)$ is temperature independent, isothermal stress-strain curves at a constant time must yield parallel curves when plotted as log σ vs log ϵ, because the shape of the curves represents $\Gamma(\epsilon)$. If the isochronal curves resulting from the plotting of log σ vs log ϵ for arbitrary fixed times at a constant temperature are parallel (i.e., in relation to the σ axis), this would indicate that $\Gamma(\epsilon)$ is not a function of time.

The relation between the constant strain rate modulus S (t) and the stress relaxation modulus E_r (t) has been developed by Smith (12):

$$E_r(t) = S(t)\ (1 + m) \quad (3)$$

in which

$$m = \frac{d \log S(t)}{d \log t}$$

In this report, "m" was taken as the slope of the best straight line drawn through the superimposed isostrain curves in the log $F(\epsilon, t)$ vs log t plot when these have been shifted vertically to the lowest common strain base (see Fig. 16).

By shifting these E (t) curves along the log time axis, a master curve covering a much wider range of log time can be constructed, as explained in the following discussion.

Time-Temperature Superposition Principle.

Horizontal Shift Concept.—The possibility of time-temperature superposition was first suggested by Leaderman (13) and was applied to experimental data in an explicit numerical manner by Tobolsky (14). In brief, the principle is that the effect of temperature on viscoelastic properties can be expressed by multiplying (or dividing) the time scale by a constant factor at each temperature. The practical range of stress relaxation measurement during a test is usually from 10 to 10^5 sec. However, by applying the principle of superposition, the relaxation curves obtained at different temperatures can be shifted horizontally on log scale of time, thus extending the coverage of time to a far greater range. In the area of asphaltic pavement design, this principle is very useful because the loading conditions on pavement vary considerably, ranging from static load on parking lots to dynamic load on highways and runways.

Time-temperature superposition can be expressed as follows:

$$E_{r,T}(a_T(T) \cdot t) = E_{r,T_o}(t) \tag{4}$$

in which a_T is a shift factor which is a ratio of relaxation moduli at temperature T and T_o. The principle is still empirical and has to be proved for each material. The application of this principle to asphalt-aggregate system seems to be justified from previous work (1).

Physical Significance of a_T. —The shift factor, a_T, has been defined for polymer viscoelasticity as primarily the temperature dependence of a segment mobility or friction coefficient on which the rates of all configuration arrangements depend (15). It is not known whether the introduction of aggregate filler of macro-size into the polymer can seriously affect the a_T values. However, work by Landel (16) on polyisobutylene and glass beads indicates that for this type of system (approximately 38 percent by volume of glass beads) there is increased average segmental friction coefficient for longer segments of the molecule as the result of adsorption of the polymer on the bead surface. Whether this is applicable in asphalt which has lower average molecular weight in the continuous phase is questionable.

Distribution of Relaxation Times. —To approximate more closely the viscoelastic behavior of real viscoelastic materials, the concept of a distribution of relaxation times was introduced. In this approach the number of Maxwell models theoretically increases without limit. This results in a continuous spectrum in which each infinitesimal contribution to rigidity is defined as $H\,d\ln t$ (logarithmic time scale) (17) associated with the relaxation times whose logarithms lie in the range between $\ln t$ and $\ln t + d\ln t$ (in which t is some characteristic relaxation time).

Computation of Relaxation Spectrum. —Several methods exist by which the distribution of relaxation times can be computed by exact and approximate relationships. Most of the approximate methods involve derivatives of the initial function or of related functions. For the most part these approximate methods involve the measurement of the slope of the initial functions that are usually known.

This paper depends on Alfrey's rule (17) which is considered to be a first approximation method. The general expression for this is given as:

$$\left.\frac{-dE_r(t)}{d\ln t}\right|_{t=\tau} = H \tag{5}$$

Therefore, the relaxation spectrum at $t = \tau$ is obtainable in the first approximation as the negative slope of the relaxation modulus. Equation (5) is usually sufficiently accurate only if H changes very slowly with time.

RESULTS OF RHEOLOGICAL ANALYSIS

Stress-Strain Curves

Typical stress vs strain curves are shown in Figure 9 for A-1 specimens at four temperatures and three constant rates of strain. Theoretically, the amount of separation between curves for the three rates of strain at each temperature is a measure of the relaxation that occurs at that temperature; there is more opportunity for relaxation at the higher temperatures (1). The spread between +20 and +77 F curves suggests the need for tests at about +40 F in any subsequent study.

Isostrain Curves

Figures 11 and 12 show isostrain curves plotted for log σ vs log t for A-1 specimen at -20 and 120 F. These curves are obtained by selecting arbitrarily a number of strain values (in this case, 0.1, 0.2, 0.3 and 0.4 percent and determining for each strain value a stress at each strain rate. The time required to reach the selected strain at each strain rate is given by $\epsilon/\dot{\epsilon}$, in which ϵ is strain and $\dot{\epsilon}$ is strain rate. At each

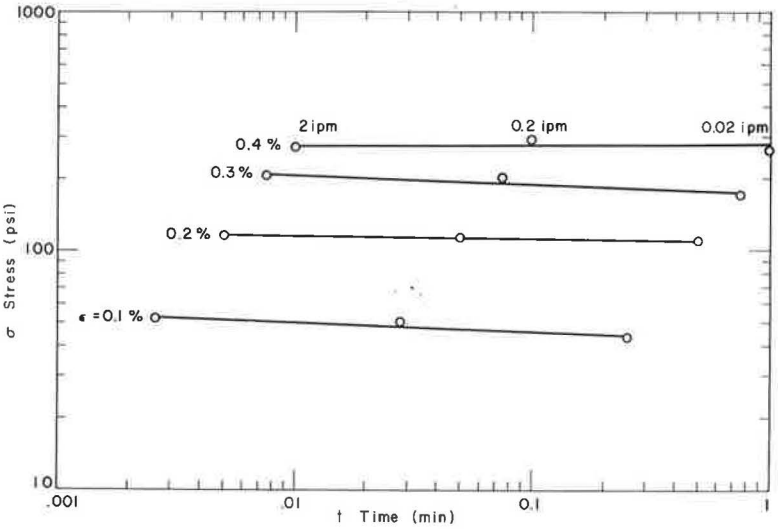

Figure 11. Isostrain curves on log σ vs log t for A-1 specimens at -20 F.

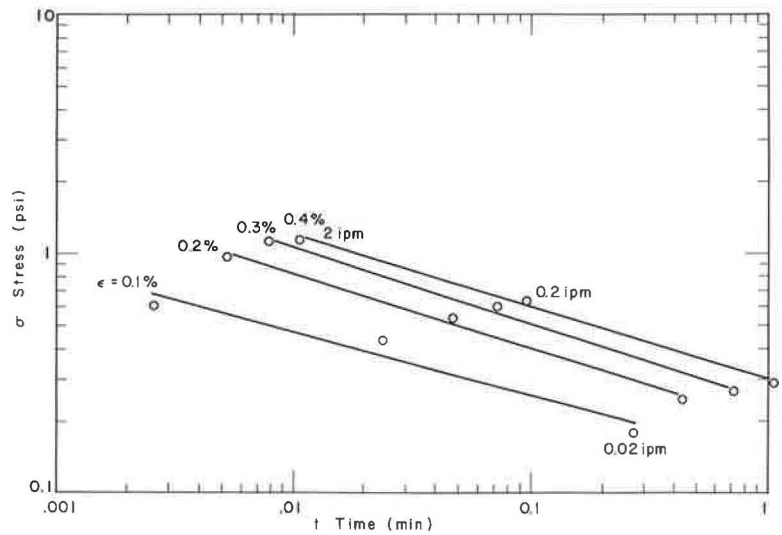

Figure 12. Isostrain curves on log σ vs log t for A-1 specimens at +120 F.

temperature the best straight line through each set of three points representing three strain rates is drawn, resulting in a family of straight lines of isostrain.

In the case chosen for illustration, A-1, the points lie fairly close to the best straight lines and the curves are nearly parallel. A review of all such data gathered for this study results in the conclusion that stress-strain data fit Eq. (2) for elongations up to 0.4 percent (strain).

Isochronal Curves

From the data presented in the isostrain curves it is possible to obtain isochronal curves by selecting time values arbitrarily and plotting corresponding values of σ and

ϵ as log σ vs log ϵ. Figure 13 shows isochronal plots of A-1 specimens at 120 F. At each temperature level, the isochrones are substantially parallel, indicating that $\Gamma(\epsilon)$ can be considered independent of time. On each isochronal curve a line with a 45° slope has been drawn to indicate Hookean behavior so that $\Gamma(\epsilon)$ = unity.

Isothermal Curves

By using the same data as in the isochronal curves, it is possible to plot isothermal curves at constant time values. Figure 14 shows isothermal plots on log σ vs log ϵ of A-1 specimens at three times, 0.01, 0.05 and 0.20 min. Although at first glance these curves appear somewhat parallel because of the small scale involved, they are substantially unparallel, having straight, convex and concave configurations. Thus, $\Gamma(\epsilon)$ is a function of temperature.

Determination of Some Values

Value of $F(\epsilon, t)$. —$F(\epsilon, t)$, the constant strain rate modulus, is related to stress according to Eq. (2a). Absolute values for this modulus are determined simply by dividing the stress data of figures such as 11 and 12 by corresponding fixed strain values. The top portions of Figures 15 and 16 show isostrain curves of log $F(\epsilon, t)$ vs log t at the various temperature levels.

Relative Values of $\Gamma(\epsilon)$. —If the log $F(\epsilon, t)$ vs log (t) curves of Figures 15 and 16 are shifted to the same strain base, 0.1 percent, the relative value of $\Gamma(\epsilon)$ can be determined. Figure 16 shows some typical curves after they have been shifted for the A-1 specimens to the 0.1 percent strain base. Figure 17 presents $\Gamma(\epsilon, T)$ or vertical shift values, for two types of specimens at four temperature levels.

The variation of $\Gamma(\epsilon, T)$ with temperature shows considerable scatter as indicated by Figure 17. There are some trends, however: in three types of specimens (A-2, LS-2, ALS-1) $\Gamma(\epsilon, T)$ increases with a decrease in temperature, in two others (A-1, LS-3) this tendency is substantially the same though some temperatures are transposed,

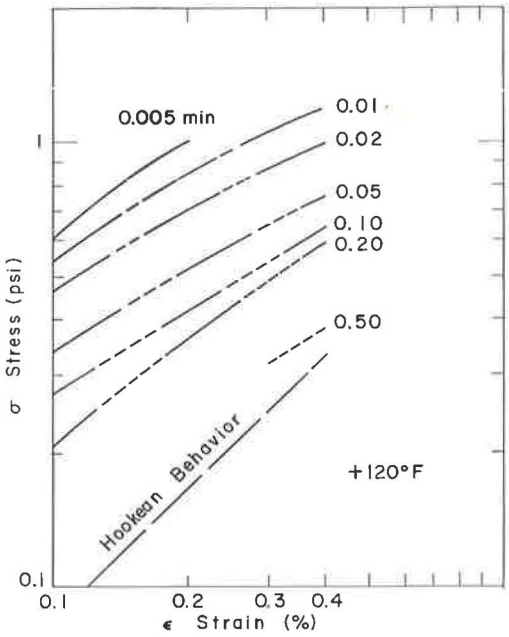

Figure 13. Isochronal curves of log σ vs log ϵ for A-1 specimens at +120 F.

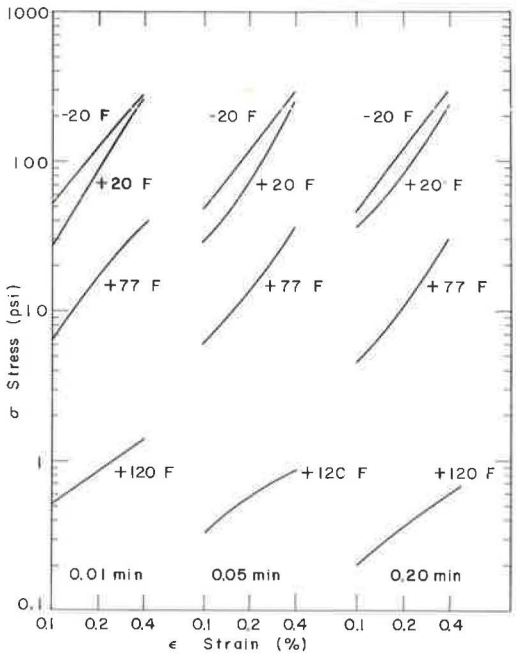

Figure 14. Isothermal curves on log σ vs log ϵ for A-1 specimens at constant times.

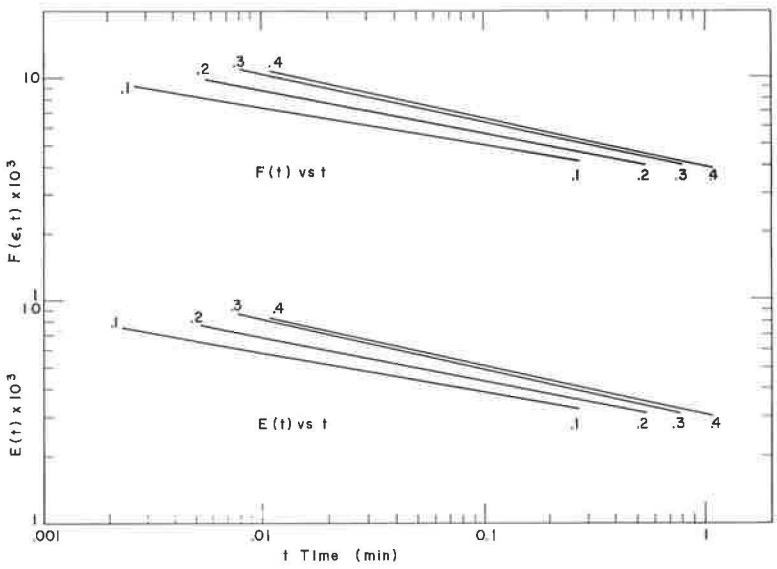

Figure 15. Isostrain curves of log F (t) vs log t and log E (t) vs log t for A-1 specimens at +77 F.

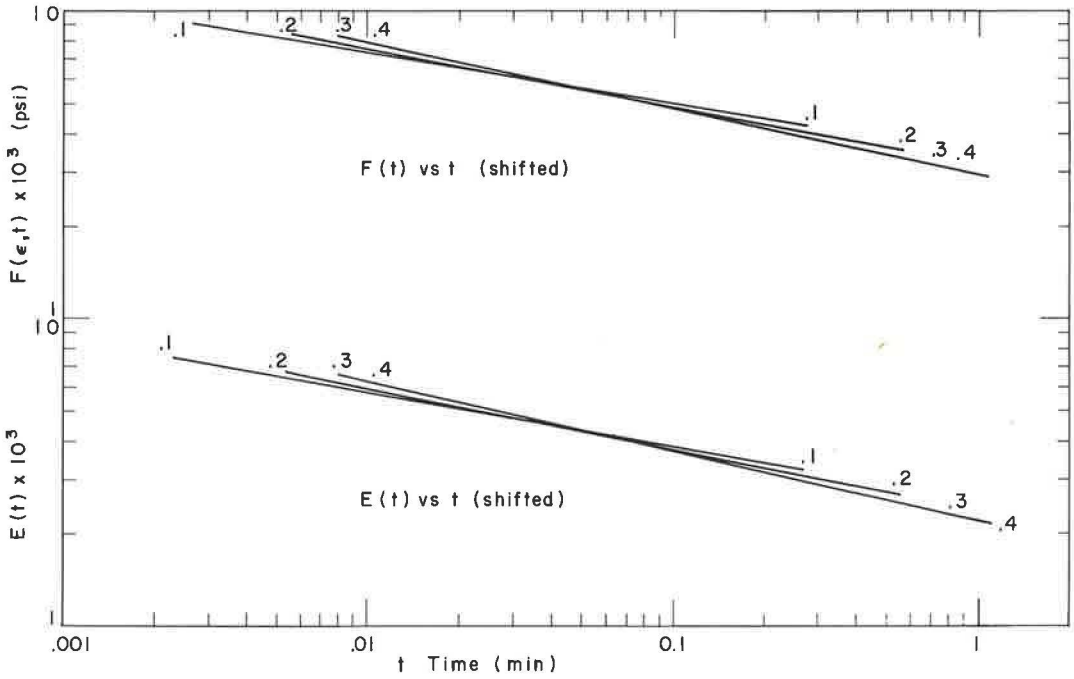

Figure 16. Isostrain curves of A-1 specimens at 77 F shifted vertically, base = 0.1 percent strain.

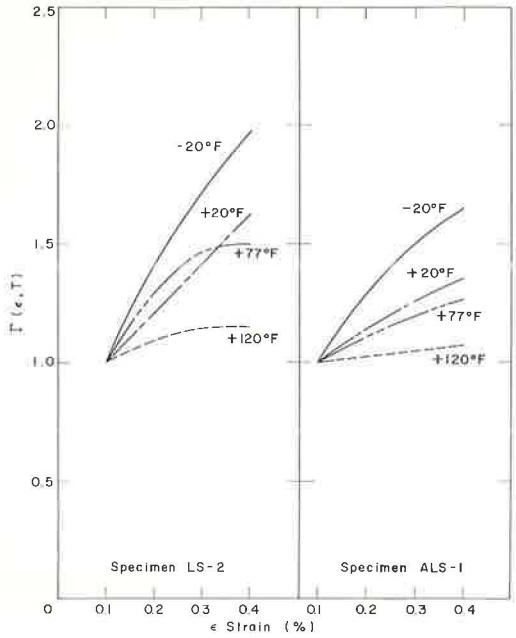

Figure 17. $\Gamma(\epsilon, T)$ vs ϵ at constant temperatures for specimens LS-2 and ALS-1, base = 0.1 percent strain.

in two (LS-1, ALS-3) the curves are completely scrambled, and in the remaining two (A-3, ALS-2) the tendency is for a decrease in $\Gamma(\epsilon, T)$ with a decrease in temperature, with some temperatures transposed. From this analysis it may be concluded that $\Gamma(\epsilon, T)$ tends to increase with a decrease in temperature, that low asphalt contents seem to promote this tendency and that the type of mineral filler seems to have no effect whatsoever in this regard.

Value of $E_r(t)$. —The value of $E_r(t)$ is obtained from the isostrain curves of log $F(\epsilon, t)$ vs log t through Eq. (3) (m being the slope of each isostrain curve). Because all isostrain curves have been constructed as straight lines, the corresponding m values are constants independent of strain. Figure 15 shows the resulting isostrain curves of log $E_r(t)$ vs log t for specimen type A-1. The greatest differences between E (t) and $F(\epsilon, t)$ occur at the higher temperatures, because m increases with temperature.

A qualitative evaluation of $E_r(t)$ over a large number of decades of time can be achieved by a horizontal shift procedure employing the principle of time-temperature superposition. To achieve this, A-1 isostrain curves of log $E_r(t)$ vs log t are shifted vertically and superimposed on a base strain, 0.1 percent, as shown at the bottom of Figure 16. Next, the shifted curves are averaged by drawing a straight line through these vertically shifted curves, resulting at each temperature in a single straight line which represents the stress relaxation of specimen A-1, at a given temperature, as shown in Figure 18. Figures 18

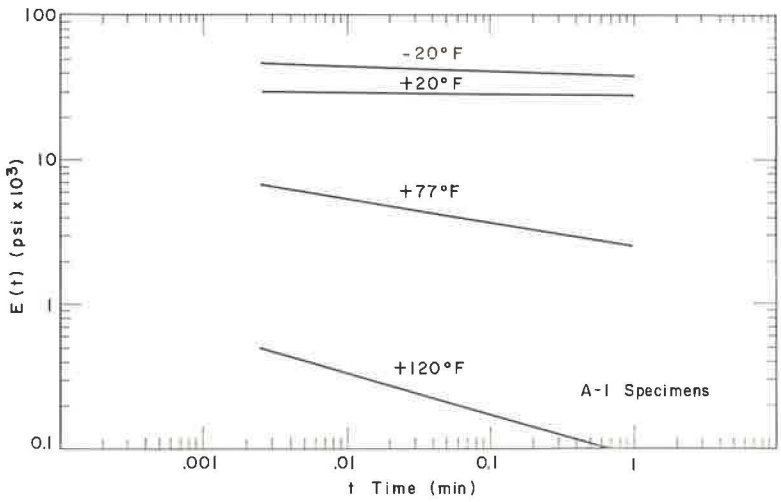

Figure 18. Locus of vertically shifted isostrain curves of log E (t) vs log t for A-1 specimens.

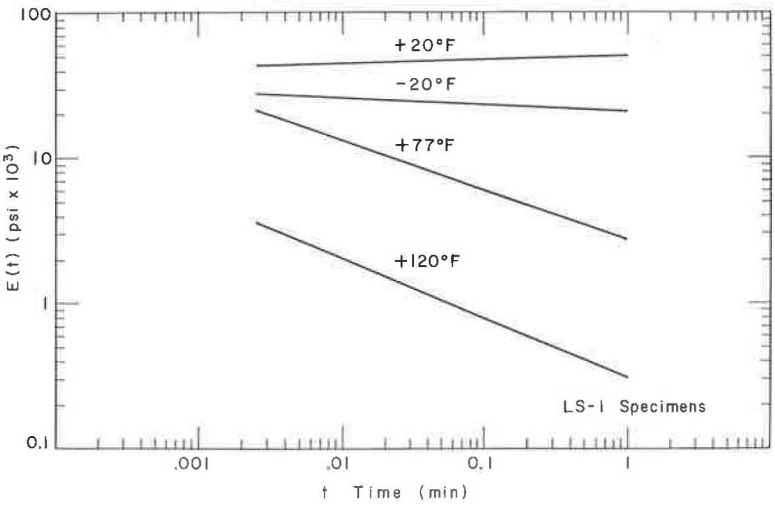

Figure 19. Locus of vertically shifted isostrain curves of log E (t) vs log t for LS-1 specimens.

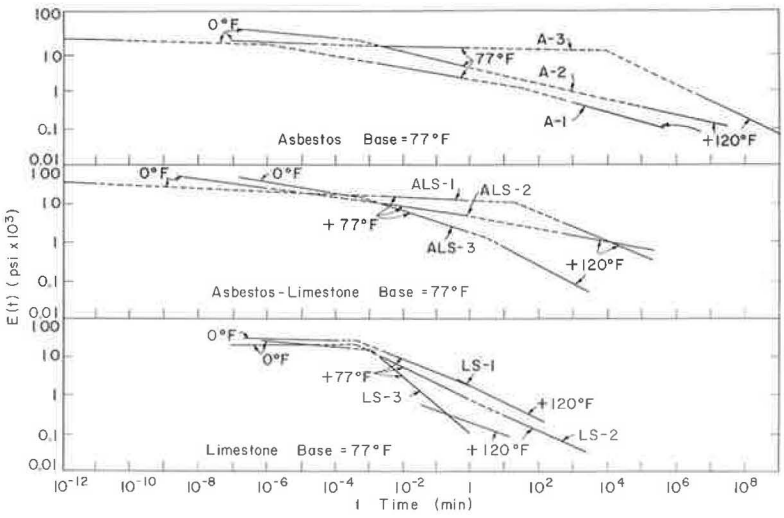

Figure 20. Locus of individual stress relaxation curves shifted horizontally.

and 19 show these curves for two specimen types. In each figure, four curves represent the four temperature levels. In some cases it was necessary to interpolate a 0 F curve because of some reversals that occurred between the -20 and +20 F curves. This reversal was also noted when the ultimate strength was measured because of a larger stress-riser effects at lower temperatures due to the aggregates in the system.

For each specimen type a master curve has been constructed (Fig. 20) by choosing the +77 F curves as a base and shifting the others horizontally along the log t axis over as many decades of time as needed to form the base smooth curve. Although the resulting master curves are not as complete or as smooth as desired, they are sufficient to indicate the factors of interest here; i.e., the relative values of a_T and the slopes of the E_r (t) curves as a function of the microaggregate.

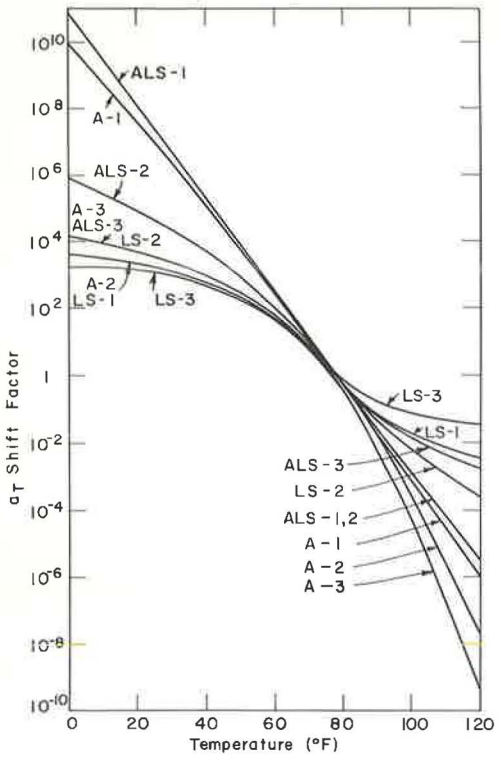

Figure 21. Horizontal shift factor (a_T) vs temperature for all specimens.

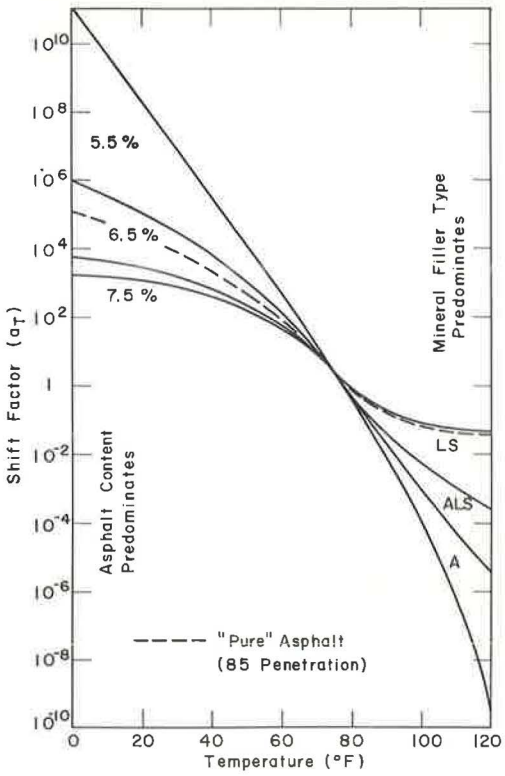

Figure 22. Schematic representation of Figure 21, including curve for pure asphalt.

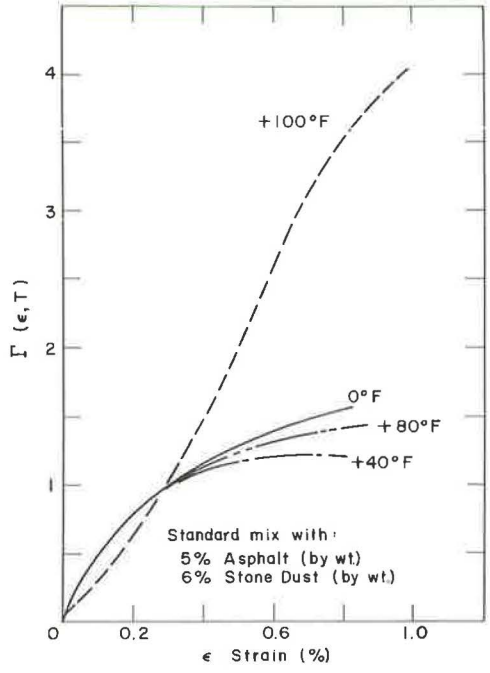

Figure 23. $\Gamma(\epsilon,T)$ vs ϵ for constant rates of compression tests, base = 0.3 percent (1).

The amount of horizontal shift, or shift factor designated a_T, can be plotted against temperature (Fig. 21). Figure 22 is a schematic representation of Figure 21 and points up the influence of the microaggregate, which predominates at high temperature (+120 F), and the influence of asphalt content, which predominates at low temperature (0 F). This figure indicates the degree of sensitivity of the tensile test procedure to mineral filler. Shown also in Figure 22 is a shift factor curve for pure asphalt, which is in approximate agreement with the shift factors of the asphalt aggregate mixtures used in this study.

DISCUSSION OF RESULTS

Nonlinearity Factor

The vertical shifts indicate that the $\Gamma(\epsilon)$ factor is a function of ϵ and T, but not of t, as was also found for compression (1). Plotting $\Gamma(\epsilon, T)$ against ϵ has resulted in the curves of Figure 17 with

a general appearance similar to those shown in Figure 23, which were previously noted by one of the authors (1), who likened them to the appearance of stress-strain curves obtained by subjecting compacted saturated Ottawa sand to shear, which are also independent of time, as shown in Figure 24 (18).

It was noted (1) that "when the filler becomes the predominant portion of the mixture, then it should be expected that its properties would begin to resemble those of granular materials." As the asphalt binder phase exhibits linear viscoelasticity, the aggregate must contribute nonlinear characteristics to the composite. As the temperature of the composite increases, the asphalt becomes more liquid and the aggregate phase dominates the physical properties. Thus, in compression tests, increasing temperature increases nonlinearity and the $\Gamma(\epsilon, T)$ factor, as can be seen from Figure 23.

However, the curves of Figure 19 give strong indication that for tensile tests, $\Gamma(\epsilon, T)$ increases with decreasing temperature. Figure 25 compares constant rate of strain tests in tension and compression. Comparable tensile data were obtained by interpolation. These data reaffirm the conclusion that in tension, $\Gamma(\epsilon, T)$ vs strain behaves in an opposite manner than in compression.

The asphalt (phase) in tension supports almost all of the applied tensile stress. At higher temperatures, the asphalt matrix is more ductile and the introduction of aggregate into the asphalt system results in less of a stress-riser effect. As the temperature decreases, however, the presence of the aggregates is felt more strongly and at lower temperatures the asphalt matrix is subjected to high internal stresses which lead to the nonlinearity encountered.

This stress-riser effect must also be present in compression but nonlinearity-induced interparticle friction at high temperatures in compression is evidently far more serious and as a consequence adds more to nonlinearity than the stress-riser effects. Figure 25 is a rough comparison of the nonlinearity effects at different temperatures and modes of deformation.

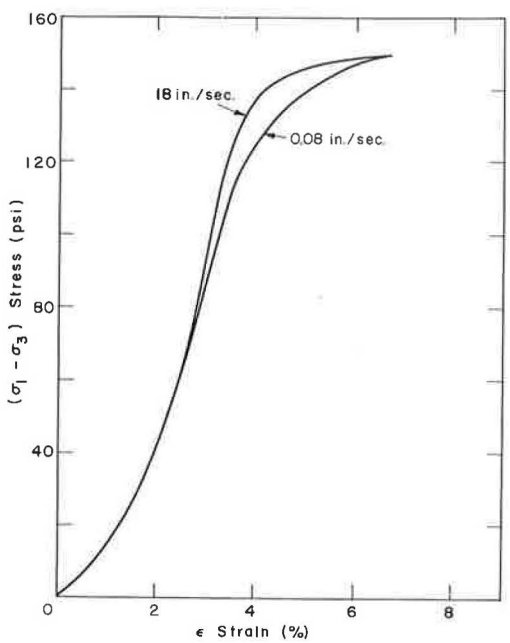

Figure 24. Stress vs strain for saturated Ottawa sand at two rates of loading (18).

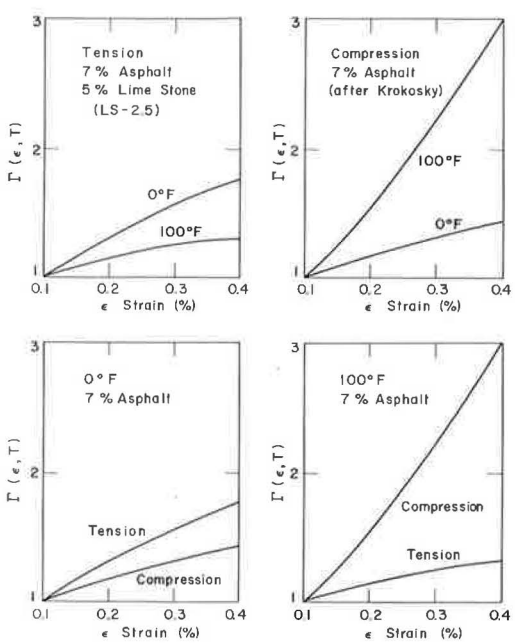

Figure 25. $\Gamma(\epsilon, T)$ vs ϵ for tension and compression at 0 and 100 F.

Horizontal Shift

The scope and limitations of the horizontal shift procedure and its relation to theoretical discussion have been indicated.

The fact that $\Gamma(\epsilon, T)$, in this case a vertical shift, is a function of temperature but not of time would seem to be a violation of the time-temperature superposition principle. However, this effect has been noted in some rubber-filled systems (19). This vertical shift phenomenon seems to be related to the inherent stiffness of the matrix. Whether it affects the relaxation rates, i.e., horizontal shift magnitudes, is not known at this time.

However, the reliability of the horizontal shift depends on three factors (17):

1. Smoothness of the master curves;
2. Magnitude of a_T which must superimpose all viscoelastic functions; and
3. Temperature dependence of a_T which must have a reasonable form.

Figure 22 shows that the a_T curve for pure asphalt (1) corresponds closely with those for specimens of a high asphalt content. In compression tests this would imply relaxation of the asphalt rather than movement of aggregate particles. In tension, it indicates that a horizontal shift can be performed to determine a_T. Figure 20 indicates that a degree of smoothness has been obtained in the master curves, although overlap of the isotherms has not been achieved to any great extent due to the large differences in the temperature levels. This takes care of the first and third factors for reliability of the horizontal shift. The second factor is resolved in the next section.

Microaggregate Effect on Stress Relaxation

Does the microaggregate act strictly as an inert filler or does it contribute decidedly to the overall rheological behavior of the composite? Figure 22 indicates that a_T is affected by both asphalt content and microaggregate. Above 80 F the type of microaggregate has a definite effect on the horizontal shift factor, a_T, whereas below 80 F the asphalt content seems to predominate. However, recent tests (compression stress relaxation) with one type of microaggregate and different asphalt contents indicate that a_T is not a function of asphalt content (Fig. 26).

Therefore, in all probability the a_T functions pictured in Figure 22 are affected by the type of microaggregate. Above 80 F there is a definite trend; a_T increases with increasing asbestos content. This implies that there is adsorption and some change in the "segmental" or molecular mobility which would alter the stress relaxation characteristics. This is in keeping with an initial physical interpretation of a_T in which this factor is related to segment mobility.

Therefore, in the case of asbestos microaggregates where there is some chance of molecular adsorption of asphalt to the microaggregate there is a decided effect on the a_T function. The asbestos mixes exhibit high tensile stability at higher temperatures or longer loading times. In other words, it takes longer for stress to relax out of this system with asbestos in it because of increased internal friction. This is manifested in the a_T values which cover a longer number of time decades for a corresponding temperature change (Fig. 21). The more decades of time covered, usually the less is the slope of the $E_r(t)$ curve, and therefore, the smaller the height of the distribution of relaxation times. (Using the first approximation method the slope of the stress relaxation curve determines the height of the distribution function.)

CONCLUSIONS

These conclusions are based on one given aggregate gradation, three asphalt contents and three microaggregate combinations:

1. The compacted mixes tested to failure at a constant rate of extension exhibited simple nonlinear viscoelastic behavior (stress and strain were not proportional).
2. The nonlinearity did not affect the spectrum of relaxation time.
3. The method proposed by Smith (12), separating strain and time effects to evaluate the nature of nonlinearity, was found to be applicable.

4. The nonlinearity factor depended on strain and temperature.

5. At low temperatures the nonlinearity factor was higher. This is thought to be due to stress-riser effect of aggregates in the composite.

6. Mixes containing asbestos as microaggregate showed lesser amount of relaxation.

7. The temperature dependence of a_T was found to be comparable to pure asphalt, suggesting that the stress relaxation is still largely dependent on the asphalt phase.

PRACTICAL APPLICATIONS

The basic reason why this study has been undertaken was to enable evaluation of the nonlinearity of asphalt-aggregate mixtures so that accurate phenomenological model could be constructed. If the nonlinearity is simple in nature (i.e., only strain-dependent), the proper corrections can be made on the linear viscoelastic functions. Interconvertibility could be carried out on the linear viscoelastic portion of the data so that the behavior of the pavement under all loading conditions could be predicted from one type of test.

If simulation by analog computers is employed, an accurate model would be very useful. The computer model could be subjected to the large variety of loads, temperatures and subbase conditions that pavement would be required to withstand during its life. The inelastic or nonrecoverable portion of the load could then be computed and an evaluation of the rutting and stability of a pavement could be made for a given pavement life.

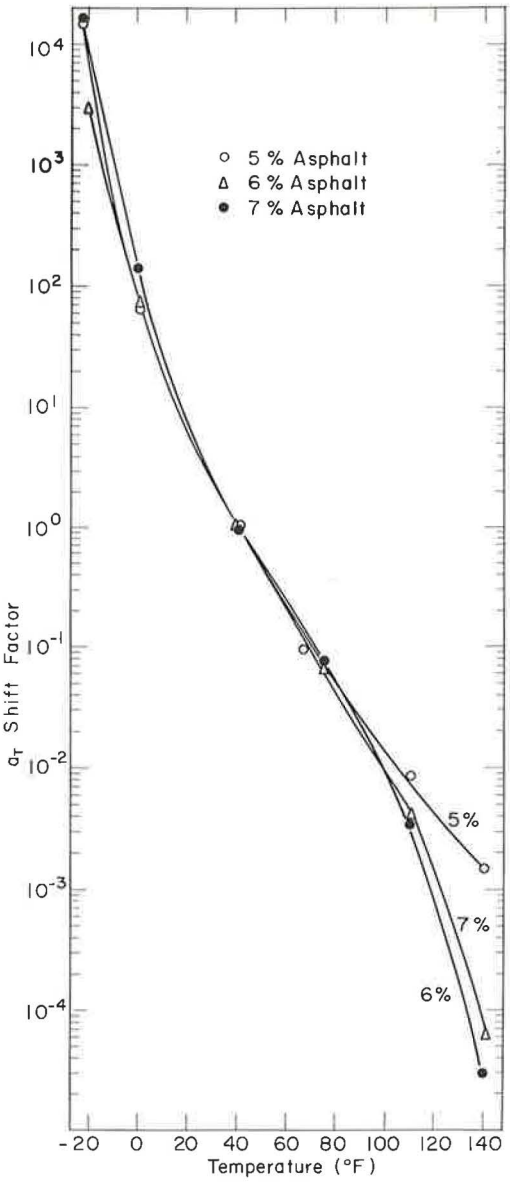

Figure 26. Shift factor a_T for compression stress relaxation (20).

OTHER RECOMMENDATIONS FOR FUTURE WORK

1. Of prime interest is a direct relaxation test for comparison with specimens already tested by this alternate method. Comparison of the a_T values and the slope of the relaxation curves determined by both methods would be of interest.

2. The use of microparticles of increased adsorption would be desirable to extend and improve stability of asphalt mixtures at higher temperatures.

3. A fundamental study of solid particle movement in a viscous medium subjected to tension and compression would be desirable to develop a deeper insight into asphalt aggregate stabilities and particle motion.

4. A greater number of aggregate gradations and types of microaggregates would aid in determining the nonlinear effects and the shift factors as a function of these variables.

ACKNOWLEDGMENTS

The study described in this paper was supported by funds of the Joint Highway Research Project established at the Massachusetts Department of Public Works for research in the field of highway engineering. Additional data were taken from a previous project sponsored by the Johns-Manville Products Corp.

The authors wish to express their thanks to Robert K. Ashworth, Jr., who assisted with the preparation and testing of specimens, to Jong P. Chen who aided with phases of the rheological study and to C. W. Christiansen who machined portions of the testing apparatus.

REFERENCES

1. Krokosky, E. M., "Rheological Properties of Asphalt/Aggregate Compositions." Part II, M.I.T. Civil Eng. Dept. Rept. R62-32 (Aug. 1962).
2. Secor, K. E., and Monismith, C. L., "Analysis of Triaxial Test Data on Asphalt Concrete Using Viscoelastic Principles." Proc. HRB, 40: 295-314 (1961).
3. Pister, K. S., and Monismith, C. L., "Analysis of Viscoelastic Flexible Pavements." HRB Bull. 269, pp. 1-15 (1960).
4. Papazian, H. S., "Response of Linear Viscoelastic Materials in the Frequency Domain." Transportation Eng. Center, Ohio State Univ., Report 172-2.
5. Wood, L. E., "The Stress-Deformation Characteristics of Asphaltic Mixtures Under Various Conditions of Loading." Ph. D. Diss., Purdue Univ. (Aug. 1956).
6. Henault, G., "Properties of Microaggregates in Bituminous Concrete." M. S. Thesis, M.I.T. (June 1961).
7. Tons, E., and Henault, G., "Evaluation of Microaggregates by Smith Triaxial Test." HRB Bull. 329, pp. 48-61 (1962).
8. "Mix Design Methods for Hot-Mix Asphalt Paving." Asphalt Inst., Manual Ser. 2 (April 1956).
9. "Preparation of Test Specimens of Bituminous Mixtures by Means of California Kneading Compactor." ASTM Designation: D1561-58T, ASTM Std. 1961, Pt. 4.
10. Vallerga, B. A., "Laboratory Compaction of Bituminous Mixtures." Proc. AAPT, Vol. 20 (1951).
11. "Resistance to Deformation and Cohesion of Bituminous Mixtures by Means of Hveem Apparatus." ASTM Designation: D1560-58T, ASTM Std. 1961, Pt. 4.
12. Smith, T. L., "Non-linear Viscoelastic Response of Amorphous Elastomers to Constant Strain Rates." Trans. Soc. Rheology, Vol. 6 (1962).
13. Leaderman, H., "Elastic and Creep Properties of Filamentious Materials and Other High Polymers." Textile Found., Washington, D. C. (1943).
14. Tobolsky, A. V., "Properties and Structure of Polymers," John Wiley and Sons, New York (1960).
15. Williams, M. L., Landel, R. F., and Ferry, J. D., "The Temperature Dependence of Relaxation Mechanisms in Amorphous Polymers." Jour. ACS, 77: 3701-3707 (July 1955).
16. Landel, R. F., "The Dynamic Mechanical Properties of a Model Filled System: Polyisobutylene—Glass Beads." Trans. Soc. Rheology, Vol. 2 (1958).
17. Ferry, J. D., "Viscoelastic Properties of Polymers." John Wiley and Sons, New York (1961).
18. Whitman, R. V., and Healy, K. A., "Shear Strength of Sands During Rapid Loadings." Proc. ASCE, 88 (SM2) (April 1962).
19. Smith, T., Private Communication.
20. Krokosky, E. M., and Chen, J. P., "Viscoelastic Analysis of the Marshall Test." M.I.T. Civil Eng. Dept. Rept. R63-41 (Nov. 1963).

Appendix A

MIX DESIGN

The mix conformed to Massachusetts Type I specification for top-course asphaltic concrete.

Mix Characteristics

The coarse aggregate was Massachusetts rhyolite, a fine-grained, hard, crushed rock with low absorption characteristics. The fine aggregate was clean quartz sand with small amounts of mica. The microaggregate was one of the following three:

1. Limestone—limestone microaggregate of commercial grade, containing primarily $CaCO_3$ (high calcium limestone), with gradation shown in Figure 2.
2. Asbestos—hydrous magnesium silicate called "chrysotile" because of its fibrous structure. Fiber diameter varied from 7.06×10^{-8} to 11.8×10^{-8} inch.
3. A combination of 50 percent each of these two.

The binder was steam-refined asphalt obtained from the ESSO Refinery, Everett, Mass., which uses a Venezuelan crude. The properties of the asphalt were penetration, 85-100 (ASTM D5-52); softening point, 110 to 120 F (ASTM E28-51); and viscosity at 0, 40, 80, and 100 F of 2.8×10^{10}, 1.1×10^{8}, 1.2×10^{6}, and 2.7×10^{5} poises, respectively. The specific gravities of these various components are as follows: coarse aggregate, 2.66 (ASTM C127-59); fine aggregate, 2.63 (ASTM C128-59); asbestos, 2.52 (ASTM C188-44); limestone, 2.73 (ASTM C188-44); and asphalt, 1.008 (ASTM D70-52). The specific surface areas for the asbestos, limestone and 50 percent combination of the two are 7, 250, 2, 500 and 4, 875 sq cm/g, respectively.

Densities and Void Contents of Compacted Mix

Specific gravities were obtained by following ASTM Test D188-53, except that the void contents were computed on the basis of solid volumes, using the following formula to obtain maximum theoretical specific gravity:

$$G_a = \frac{100}{\frac{P_{W_1}}{G_1} + \frac{P_{W_2}}{G_2} + \frac{P_{W_3}}{G_3} + \frac{P_{W_4}}{G_4}} \qquad (6)$$

in which

G_a = maximum theoretical specific gravity of solid,

P_{W_1}, P_{W_2}, P_{W_3}, P_{W_4} = percent by weight that each component is of total, and

G_1, G_2, G_3, G_4 = specific gravity of each component.

The void contents for different mixes are given in Figure 3.

Appendix B

CAPPING OF TEST SPECIMENS

It was discovered that the 2-in. brass cover, an ordinary plumbing cleanout cap, when properly tapped and fitted (see Figs. 4 and 5) served quite well as a test specimen holder. The cap was designed for a load of 3,000 pounds, more than adequate for the range of loads in this study.

The epoxy glue which secured the specimen in the cap was very critical in the overall test procedure and had to function properly at extreme temperatures and loading conditions. The mixture finally arrived at through experimentation comprised Epon (Shell) Resin 828, 55 percent by weight; Epon (Shell) Resin 871, 36 percent by weight; and D. T. A. curing agent, 9 percent by weight.

The Resin 828 supplies strength; the 871 supplies toughness against impact. The proportion of curing agent is such as to allow a proper set in a few hours while avoiding the brittleness that results from a flash set.

It is recommended that the end of the test specimen and the specimen sides for about $\frac{1}{2}$ in. from the top be roughened with sandpaper and the loose material removed before the gluing operation. Caps are cleaned by heating and scraping.

Effects of Asphalt Viscosity on Physical Properties of Asphaltic Concrete

GANDHARV RAJ BAHRI and LLOYD F. RADER
Respectively, Graduate Student and Professor of Civil Engineering, University of Wisconsin

This laboratory study investigated the effects of variations of mixing viscosity and compacting viscosity of asphalt on the physical properties of asphaltic concrete as measured by Marshall testing apparatus. The effects of varying the mineral filler content were also determined. Mixing temperatures were varied between 260 and 350 F in increments of 30 F. Marshall stability specimens were compacted by a mechanical compactor at temperatures in increments of 30 F ranging from 200 F to a temperature 30 F below the corresponding mixing temperature.

The viscosity-temperature relationship of the single 85-100 penetration grade asphalt cement used was established and each of the mixing and compacting temperatures was related to the asphalt viscosity. The same aggregates were used throughout the investigation, but two filler-bitumen ratios were investigated with the same asphalt content. The asphaltic concrete was of coarse-graded aggregate type for surface course conforming to gradation limits of Wisconsin State Highway Commission specifications.

The experimental results showed that variations in the mixing and compacting viscosities of asphaltic concrete produced changes in Marshall stability, flow value, specific gravity, and voids of the compacted mixtures. Some of these differences were large enough to warrant attention to selection and control of proper mixing and compacting viscosities. "Optimum" mixing viscosity and "optimum" compacting viscosity are suggested for the asphaltic concrete mixtures investigated. The results showed that changes in the ratio of mineral filler to asphalt cement affect the optimum mixing and compacting viscosities of asphalt for the asphaltic concrete paving mixtures investigated.

•THE IMPORTANCE of proper viscosity of asphalt during both mixing and compacting operations of hot-mix asphaltic concrete pavements is recognized. For improved qualitative control of pavement construction, it is essential that the asphalt be at proper viscosity at the times of mixing the asphalt and aggregates in the plant and of compacting the paving mixture by paving and finishing machines and rollers on the paving project.

A fundamental measure of fluidity of asphalt in hot mixes is on the basis of viscosity which is the inverse of fluidity. Viscosity also varies inversely with temperature, i.e., the higher the temperature, the lower the viscosity.

PURPOSE AND SCOPE

The purpose of this investigation is:

1. To study the effects of variations in mixing viscosity and in compacting viscosity of the asphalt on physical properties of compacted asphaltic concrete by the Marshall test;

Paper sponsored by Committee on Mechanical Properties of Bituminous Paving Mixtures.

2. To determine the effects of filler-bitumen (F/B) ratio on the results obtained;
3. To establish "optimum" mixing viscosity and "optimum" compacting viscosity for the asphaltic concrete mixtures investigated.

The experimental work reported consisted of the mixing, compacting, and testing of specimens of Wisconsin State Type 3 bituminous concrete surface course mix (1) using the Marshall test apparatus. The mixing was done at 30 F increments through a 260 to 350 F range. Both asphalt and aggregate were heated to the same mixing temperature. Five different compaction temperatures at 30 F increments were chosen between 200 and 320 F to simulate a range of temperature that might occur during pavement construction at the commencement of knockdown rolling on hot-mix projects where 85-100 penetration grade asphalt cements are used. The compaction temperature varied from a minimum of 200 F to a peak value 30 F below the corresponding mixing temperature (Table 1). No reheating was done after the materials were mixed.

The viscosity-temperature relationship of the asphalt cement used was established and each of the mixing and compaction temperatures was related to the asphalt viscosity. Four specimens were molded at each of the combinations of mixing and compacting temperatures. Two filler-bitumen (F/B) ratios were used with the same asphalt content.

SELECTION OF MATERIALS

Aggregates

Pit run gravel from Brown Pit, Baraboo, Wis., was used. The gravel was crushed; about 66 percent of coarse aggregate consisted of dolomite and 34 percent was igneous material. The sand was a mixture of igneous and dolomite material.

Pulverized limestone dust from the Waukesha Limestone Company was used as mineral filler. It had 81.7 percent passing the No. 200 sieve and a specific gravity of 2.823 by ASTM Designation: D854-58. Limestone dust passing the No. 200 sieve had a specific gravity of 2.844.

Bitumen

The bitumen was an 85-100 penetration grade asphalt cement produced by the Texas Company at Casper, Wyo. At 77 F, it had a specific gravity of 1.030 and a ductility of 110+ cm. The viscosity-temperature relationship is shown in Figure 1. A Saybolt Furol viscometer was used

TABLE 1

Mixing Temp (° F)	Mixing Viscosity (SSF)	Compacting Temp (° F)				
		320	290	260	230	200
350	34.5	x	x	x	x	x
320	54.0	—	x	x	x	x
290	105	—	—	x	x	x
260	250	—	—	—	x	x
Compacting Viscosity (SSF)		54	105	250	640	2000

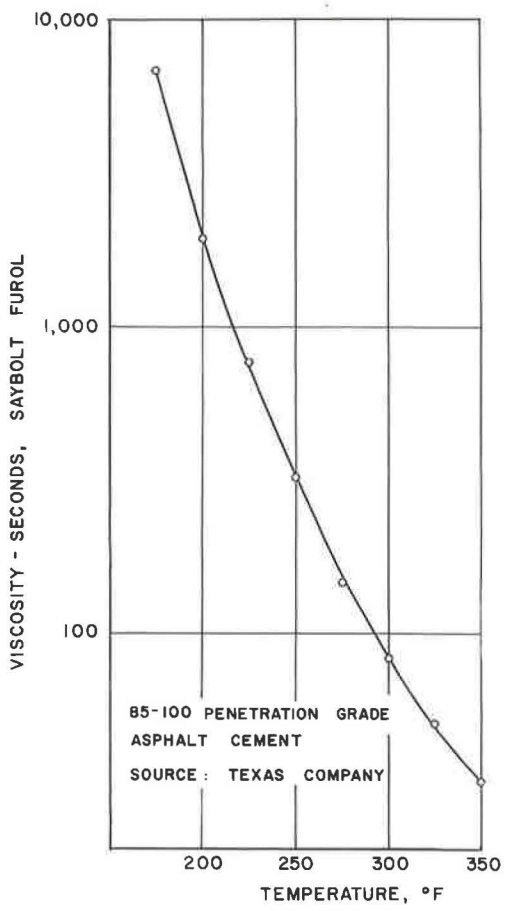

Figure 1. Viscosity-temperature relationship for asphalt cement.

TABLE 2

VISCOSITY OF ASPHALT CEMENT BY SAYBOLT FUROL VISCOMETER METHOD[a]

Test Temp (° F)	Viscosity (SSF)		
	Test 1	Test 3	Avg.
250	318.0	322.5	320.3
275	148.5	144.5	146.5
300	83.0	82.5	82.8
325	52.0	50.0	51.0
350	33.5	32.5	33.0
375	23.5	23.5	23.5

[a]Viscosity at 77 F by sliding plate microviscometer, 1.212 X 10^6 poises at FS = 1,000 ergs/sec/cu cm.
[b]By ASTM Method E102-62.

TABLE 3

VISCOSITY OF ASPHALT CEMENT VACUUM CAPILLARY VISCOMETER METHOD[a]

Test Temp (° F)	Capillary Tube No.	Diam Tube (cm)	Vacuum (cm Hg)	Time (sec)	K	Viscosity (poises)	Avg. Viscosity (poises)
175	2	0.1004	30	67.8	2.172	147.50	—
	4	0.0987	30	69.0	2.120	146.00	146.75
200	1	0.1141	10	44.0	0.919	40.40	—
	1	0.1141	10	45.0	0.919	41.30	40.85
225	2	0.1004	10	22.2	0.705	15.65	—
	4	0.0987	10	21.2	0.685	14.55	15.10
250	1	0.1141	10	7.5	0.917	6.87	—
	1	0.1141	10	7.0	0.917	6.42	6.65

[a]Viscosity at 77 F by sliding plate microviscometer, 1.212 X 10^6 poises at FS = 1,000 ergs/sec/cu cm.

for viscosity determination (Table 2) in the high temperature range (250 to 350 F), and the viscosity between 175 and 250 F was measured by a vacuum capillary viscometer (Table 3). The mixing and compacting viscosities were interpolated from Figure 1 for the various mixing and compacting temperatures investigated.

MIXING AND COMPACTING VISCOSITIES (TEMPERATURES)

The mixing and compacting viscosities investigated (with corresponding temperature values) are given in Table 1. The "x" marks indicate the combinations of mixing viscosities and compacting viscosities at which Marshall specimens of asphaltic concrete were molded and tested.

PAVING MIXTURE

A coarse-graded aggregate type of mix for surface course conforming to gradation limits of Specification No. 3, 1957, Wisconsin State Highway Commission (1), was used. The aggregate gradation curves are shown in Figure 2. Two designed gradations were investigated: one with a limestone dust content of 8.0 percent by weight of total aggregate, which corresponds to usual practice, and a second with a limestone dust content of 11.5 percent by weight of total aggregate. These values correspond to 8.6 and 11.3

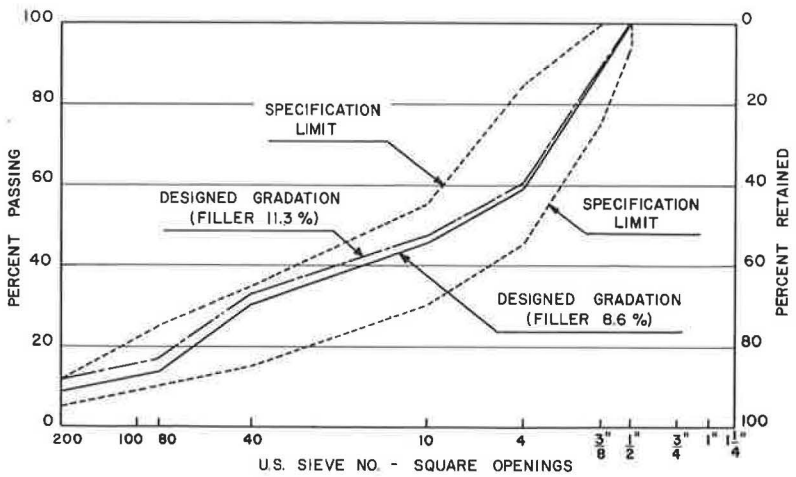

Figure 2. Aggregate gradation curves for asphaltic concrete mixtures.

percent mineral filler passing No. 200 sieve by weight of total mix, respectively, considering the blended aggregate. The F/B ratios by weight were 1.81 and 2.38, respectively, when filler is taken as material passing No. 200 sieve. The corresponding F/B ratios by volume were 0.66 and 0.87, respectively. The maximum size of coarse aggregate was ½ in. Controlled grading of the aggregate was maintained during the molding of the specimens by separating the aggregate into different size fractions and then recombining according to the design proportions.

An asphalt content of 4.75 percent by weight of the total mixture was used throughout the investigation on the basis of previous studies using the same aggregate and mix gradation. This asphalt content also conforms to current practice of the Wisconsin State Highway Commission for these materials and results in a mixture that yields test values satisfying the established criteria of the Commission.

PREPARATION OF MARSHALL SPECIMENS

The method of mixing, molding and testing Marshall specimens conformed in general to ASTM Designation: D1559-60T (2), except for variations in mixing viscosity and compacting viscosity and except that a compaction machine, built for the Wisconsin State Highway Commission testing laboratory, was used in place of hand compaction. Compaction was by 50 blows of the hammer of each side of the specimen at the rate of approximately 50 blows in 66 sec. The specimen molds were rotated during compaction at a rate of one revolution for each 50 blows of the hammer. The hammer weighed 10 lb and had a flat horizontal striking face. The height of drop was 18 in. During compaction, the specimen molds rested on a steel plate mounted on a concrete pedestal. Careful attention was paid to mixing and compacting temperatures in molding the specimens. No reheating of the mix was done after mixing. The standard test temperature of 140 F was carefully controlled.

DATA AND DISCUSSION OF RESULTS

Effects of Mixing Viscosity on Mixture Containing 8.6 Percent Mineral Filler

Stability. —Figure 3 shows the relationship of mixing viscosity (in seconds, Saybolt Furol (SSF)) to stability and also the relationship of mixing temperature to stability. The trend of all curves is the same at different compaction viscosities from 2,000 to 54 SSF (compaction temperatures from 200 to 320 F). Each curve has a peak and a trough when the mixing viscosity is decreased from 250 to 34.5 SSF (mixing temperature from 260 to 350 F).

Each peak is assumed to indicate the optimum mixing temperature for the corresponding compacting temperature. The stability increases as the mixing temperature is increased from 260 to 290 F (viscosity decreasing from 250 to 105 SSF). The stability decreases when the mixing temperature is raised to 320 F (viscosity 54 SSF). Further rise in mixing temperatures from 320 to 350 F (viscosity decreasing from 54 to 34.5 SSF) results in increased stability values.

The peaks and troughs in Figure 3 for 8.6 percent filler asphaltic concrete com-

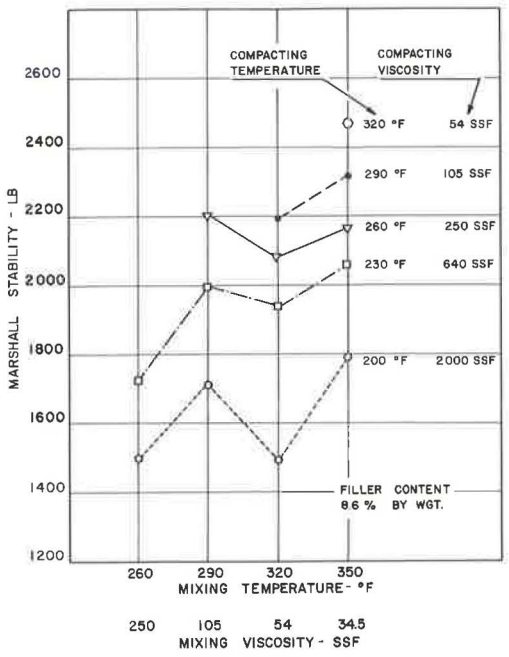

Figure 3. Effects of mixing viscosity (mixing temperature) on Marshall stability.

pare favorably with the peaks and troughs shown by Lehmann and Adam (3, Figs. 3 and 4), especially for 137 penetration asphalt from Talco crude. The viscosity-temperature curve (Fig. 1) for the Texas Company 85-100 penetration grade asphalt also compares closely with one for 137 penetration asphalt from Talco crude (3, Fig. 2). Lehmann and Adam also give an explanation concerning these relationships involving peaks and troughs. In a similar manner, the results of this investigation for the 8.6 percent filler asphaltic concrete mixture may be explained: At a mixing temperature of 260 F (viscosity 250 SSF) the asphalt is not fluid enough for proper coating and mixing with aggregate particles so the lowest values of stability are obtained. However, the aggregate and asphalt temperatures are high enough at 290 F (asphalt viscosity 105 SSF) to permit droplets of asphalt to envelop particles of aggregates on contact resulting in intimate coating and uniform dispersion of materials. This increases the stability values. Further rise in the mixing temperature to 320 F (viscosity 54 SSF) makes the asphalt extremely fluid so that instead of coating the particles to uniform thickness it merely lubricates the particles, causing excessive movements under dynamic impact of the compaction hammer. This results in a drop in stability at mixing temperature of 320 F as compared with 290 F. Further rise in stability value when the mixing temperature is increased to 350 F (viscosity 34.5 SSF) could well be attributed to the hardening or oxidizing of asphalt which results in change in consistency.

From this discussion it follows that a proper control over the mixing viscosity and compacting viscosity should be exercised for asphaltic concrete. The asphalt must be at proper viscosity (or fluidity) at the time of mixing to promote intimate mixing and coating (not lubricating) and proper dispersion of materials. The viscosity of the contained binder at time of compaction must be low enough so that a considerable portion of compactive effort exerted is not expended in overcoming the greater resistance offered by the higher viscosity of binder at lower temperatures.

Considering the stability values up to a compaction temperature of 260 F, the highest value of stability (2,200 lb) is obtained when the mixing is done at 290 F (viscosity 105 SSF) with compaction at 260 F (viscosity 250 SSF). This appears to be an excellent combination of mixing temperature and compacting temperature. A value of 2,184 lb is obtained for a mixing temperature of 320 F (mixing viscosity of 54 SSF) and a compacting temperature of 290 F (compacting viscosity of 105 SSF), which appears also to be a satisfactory practical combination of mixing and compacting temperatures.

Figure 4 shows the contours of stability values at intervals of 100 lb with mixing tem-

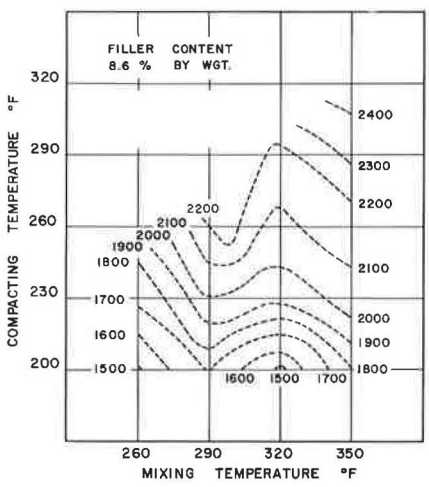

Figure 4. Stability contours showing effects of variations in mixing and compacting temperatures.

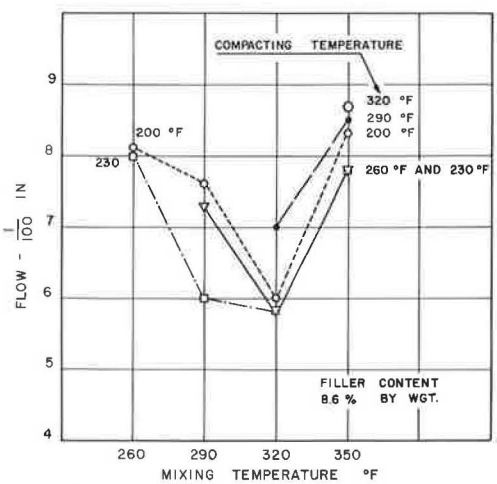

Figure 5. Effects of mixing temperature on flow.

perature and compacting temperature as the coordinate axes. In the drawing of these contours it is assumed that the stability varies linearly between two different stability levels. These contours indicate that higher compaction temperatures are required at mixing temperatures of 260 and 320 F to provide the same stability values as at a mixing temperature of 290 F. Thus, a compaction temperature of 210 F is required with mixing at 290 F to give the same stability (1,800 lb) as obtained at compaction temperatures of 245 and 220 F with mixing done at temperatures of 260 and 320 F, respectively. There is not much difference in the compaction temperatures for mixing temperatures of 290 and 350 F for equal stabilities, the compaction temperatures at 350 F being slightly lower than those at 290 F.

Flow. —Figure 5 gives the relationship between mixing temperature and flow. The general trend of all curves is the same. Each curve has a trough at a mixing temperature of 320 F. Within the limits of compacting temperatures from 200 to 290 F, the lowest values of flow are obtained at a mixing temperature of 320 F.

Specific Gravity. —In Figure 6 mixing viscosity and mixing temperature are plotted against specific gravity. The specific gravity values are not appreciably affected by variations in the mixing viscosity. The specific gravity values peak at mixing viscosity of 105 SSF for compacting viscosities of 250, 640 and 2,000 SSF. An interesting comparison may be made between these peak values and those shown by Lehmann and Adams (3, Fig. 6).

For compacting temperatures up to 260 F (viscosity 250 SSF), the highest value of specific gravity is obtained at a mixing temperature of 290 F (viscosity 105 SSF). An equal value is also obtained for compacting temperature of 290 F (viscosity 105 SSF) with a mixing temperature of 320 F (mixing viscosity 54 SSF).

Figure 7 shows the contours of specific gravity at intervals of 0.005 with mixing temperature and compacting temperature as the coordinate axes. It has been assumed that the specific gravity varies linearly between two different specific gravity levels. These contours indicate that the specific gravity increases as the mixing temperature is increased from

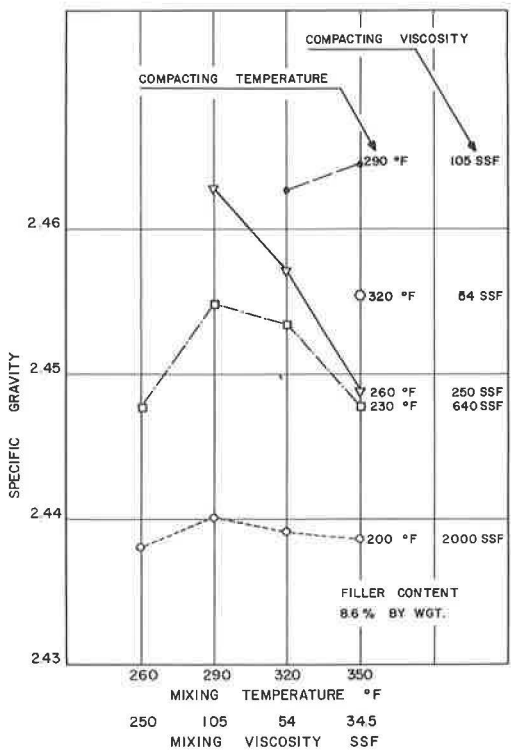

Figure 6. Effects of mixing viscosity (mixing temperature) on specific gravity of asphaltic concrete.

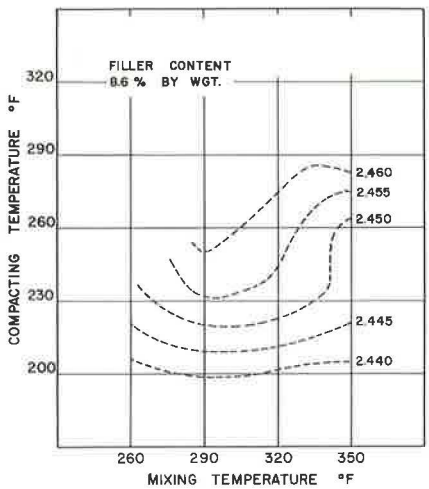

Figure 7. Specific gravity contours of asphaltic concrete showing effects of variations in mixing and compacting temperatures.

260 to 290 F (viscosity 250 to 105 SSF). Further rise in mixing temperatures from 290 to 350 F results in a decrease in specific gravity values. This is in contrast to stability values shown in Figures 3 and 4 where the values increase as the mixing temperature is increased from 320 to 350 F. Thus, an increase in stability value may not be related to increase in density.

Voids in Total Mix. —Figure 8 gives the plot of mixing temperature vs percent voids in total mix. Apparent specific gravity of the aggregate was used for the computation of voids. The discussion of specific gravity values pertains also to voids in total mix.

Voids in Mineral Aggregate. —The percentage of voids in mineral aggregate (VMA) is an important criterion to study in design of mixtures because it indicates the amount of space available for asphalt in compacted mixtures. Minimum VMA values are significant because they indicate the combination of materials and methods of fabrication at which the mineral particles are arranged to occupy the smallest volume for a given amount of compaction. For compaction temperatures up to 260 F, the lowest values of VMA are obtained at a mixing temperature of 290 F (viscosity 105 SSF), the curves forming a trough (Fig. 9). Because low values of VMA are desirable, the combination of 290 F mixing temperature with 260 F compacting temperature is good; also, 320 F mixing temperature with 290 F compacting temperature gives a similar value.

Voids Filled with Bitumen. —Figure 10 shows the relationship between mixing temperature and percent voids filled with bitumen (VFB). Within the limits of mixing temperatures (260 to 350 F) and compacting temperatures (200 to 320 F), the VFB lie between 75.0 and 80.8 percent. An increase in VFB when the mixing temperature is raised from 260 to 290 F is followed by a decrease in values up to a mixing temperature of 350 F, excepting at a compaction temperature of 290 F and where there is a slight increase in VFB at a mixing temperature of 350 F over that obtained at mixing temperature of 320 F.

For compaction temperatures up to 260 F, the highest values of VFB are obtained at a mixing temperature of 290 F, the curves peaking at this temperature. The highest value of VFB is obtained at mixing and compacting temperatures of 350 and 290 F, respectively. This value (80.8 percent) is only 0.4 higher than the value at the mixing temperature of 290 F with compaction done at 260 F or the value obtained at the 320 F mixing temperature with 290 F compacting temperature.

Effects of Compacting Viscosity on Mixture Containing 8.6 Percent Mineral Filler

Graphs showing the relationship between compacting viscosity (or compacting temperature) and physical properties of asphaltic concrete by the Marshall test method are shown in Figures 11 to 16. These graphs are based on the same data as plotted in Figures 3 to 10 or where mixing viscosity (or mixing temperature) was plotted as abscissa.

Compaction studies by Parker (11) for a similar asphaltic concrete wearing course mixture gave similar trends for Marshall stability, specific gravity, percent voids in total mix, and percent voids filled with bitumen for increases in compaction temperature.

Stability. —Figure 11 gives the plot of compacting viscosity as abscissa vs Marshall stability as ordinate, as well as that of compacting temperature as abscissa against Marshall stability. All curves follow the same pattern. There is an increase in the stability value as the compacting temperature is increased from 200 to 320 F (viscosity decreased from 2,000 to 54 SSF). This increase is the greatest from a compacting temperature of 200 to 230 F (viscosity 2,000 to 640 SSF). As the compaction temperature is raised, the binder viscosity is reduced. Therefore, less resistance is offered to the compactive effort, resulting in higher stability values.

Neglecting the mixing temperature of 350 F, which is considered high for present-day practice, the highest value of stability is obtained at a compaction temperature of 260 F (viscosity 250 SSF) with mixing at 290 F (viscosity 105 SSF). This value is higher than stability obtained at a mixing temperature of 350 F (viscosity 34.5 SSF) with compaction at 260 F (viscosity 250 SSF). It can also be seen from Figure 11 that compaction temperature at 290 F (viscosity 105 SSF) is satisfactory with mixing temperature of 320 F (mixing viscosity of 54 SSF).

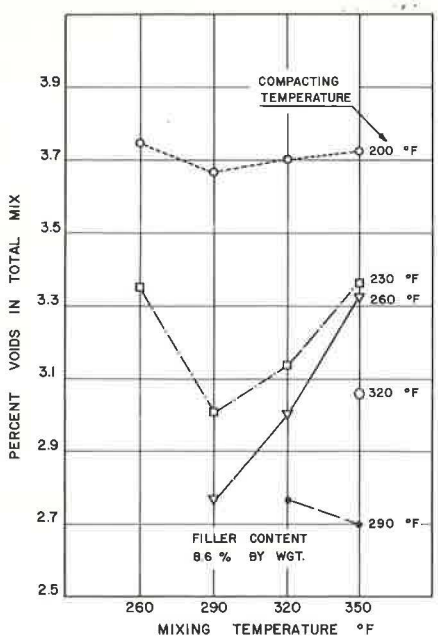

Figure 8. Effects of mixing temperature on percent voids in total mix.

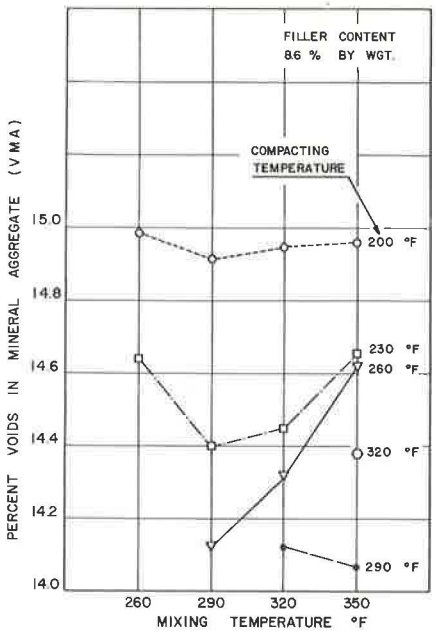

Figure 9. Effects of mixing temperature on percent VMA.

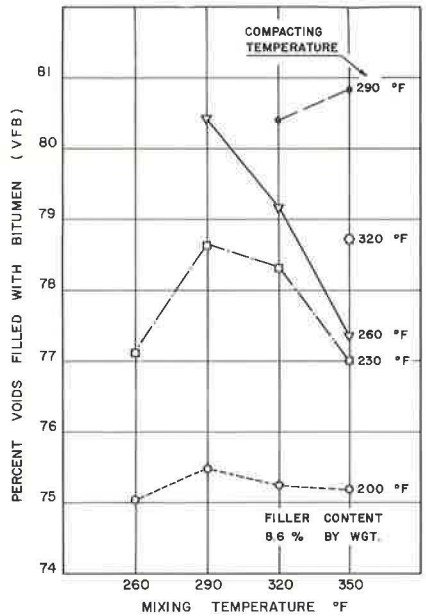

Figure 10. Effects of mixing temperature on percent VFB.

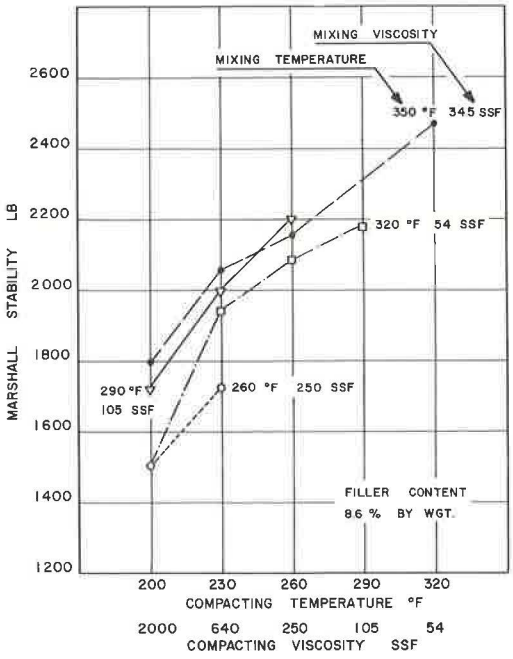

Figure 11. Effects of compacting viscosity (compacting temperature) on Marshall stability.

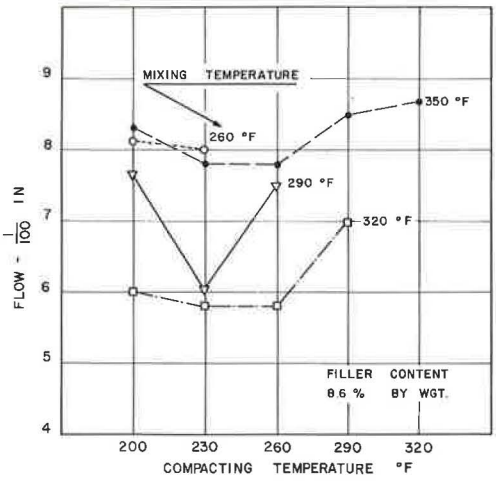

Figure 12. Effects of compacting temperature on flow.

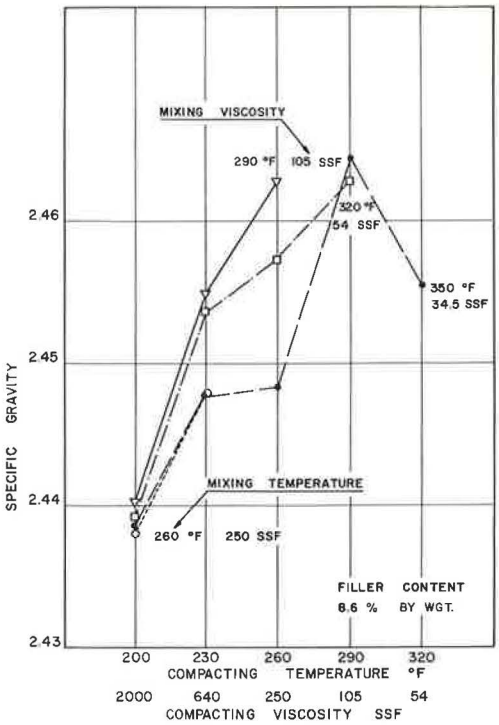

Figure 13. Effects of compacting viscosity (compacting temperature) on specific gravity of asphaltic concrete.

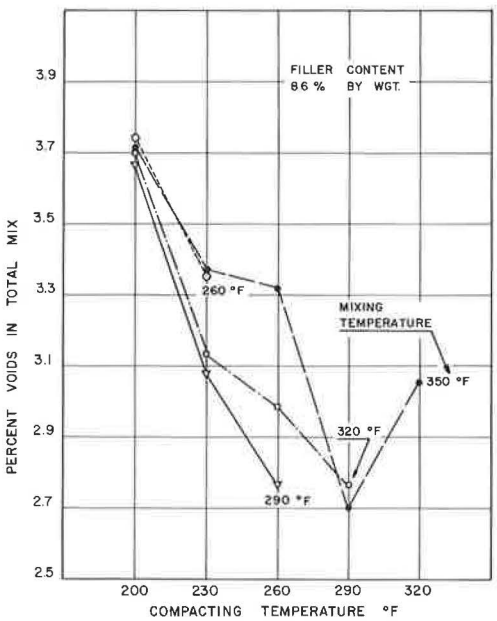

Figure 14. Effects of compacting temperature on percent voids in total mix.

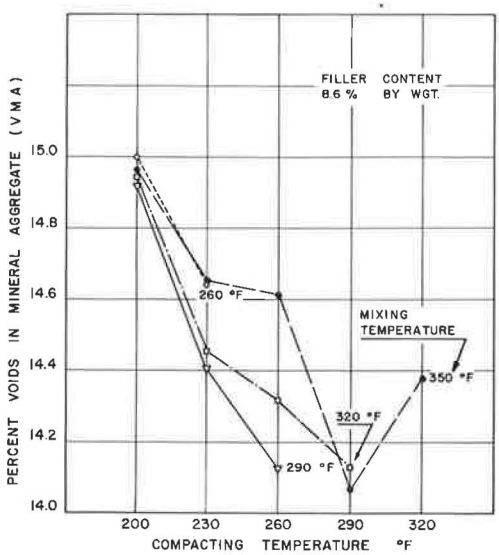

Figure 15. Effects of compacting temperature on percent VMA.

Flow. —The relationship between compacting temperature and flow is given in Figure 12. At any mixing temperature, there is no appreciable change in flow values (in units of 0.01 in.) within the limits of compacting temperatures, the maximum variation being 1.7 for a mixing temperature of 290 F. Within the limits

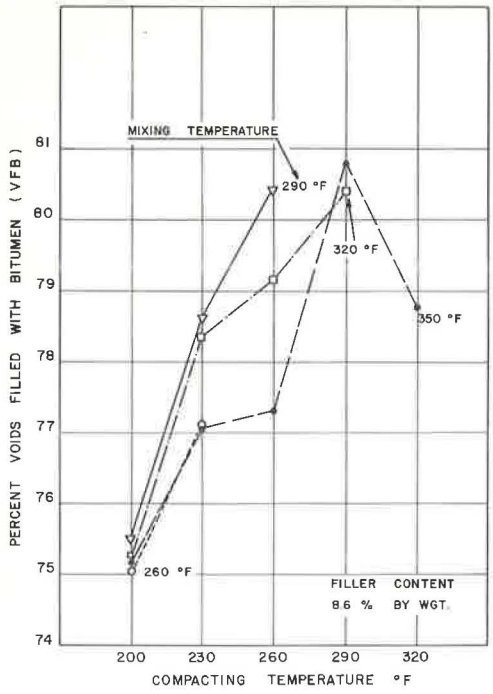

Figure 16. Effects of compacting temperature on percent VFB.

of mixing and compacting temperatures investigated, the flow values lie between 5.8 and 8.7. Minimum values of flow are obtained at the mixing temperature of 320 F.

Specific Gravity. —In Figure 13 the plot of compacting viscosity vs specific gravity is given as well as the relationship of the compacting temperature to specific gravity for the same data. There is an increase in specific gravity values as the compacting temperature is increased to 290 F (viscosity decreased to 105 SSF). This increase is steepest for compacting temperatures between 200 and 230 F (viscosity 2,000 to 640 SSF). As the compacting temperature is increased to 320 F (viscosity 54 SSF) there is a decrease (0.009) in specific gravity at mixing temperature of 350 F (viscosity 34.5 SSF). These results can be explained as follows: At low compacting temperatures, the viscosity of the contained asphalt is very high (viscosity at 200 F of 2,000 SSF). A considerable portion of the compactive effort is expended in overcoming the resistance offered by high binder viscosity and does not contribute to the compaction of the mix. This results in decreased densities at low compacting temperatures. However, at a compacting temperature of 320 F (with mixing at 350 F), viscosity of the contained asphalt appears to be very low (54 SSF), so that the mix displaces under the compactive effort, and the compaction is, therefore, not fully effective. This results in a decrease in specific gravity when the compacting temperature is increased from 290 to 320 F (viscosity decreased from 105 to 54 SSF).

The practice of many highway organizations is to specify roadway density requirements as a function of laboratory density, such as 98 percent of laboratory density. In view of the variation of specific gravity values of laboratory compacted mixtures with compacting viscosity of the asphalt (Fig. 13), it is suggested that a requirement should be placed in specifications to control the compacting viscosity of asphalt when forming laboratory briquets for use in checking pavement density. This would eliminate errors caused by employing too high a compacting viscosity (too low a compacting temperature) when molding the laboratory briquets (3).

Voids in Total Mix. —Figure 14 shows the relationship of the compacting temperature to percent voids in total mix. There is no appreciable change in the voids for the mixture tested as the compacting temperature is increased from 200 to 320 F. For the mixing temperatures (260 to 350 F) and compacting temperatures (200 to 320 F) used in molding specimens, the void values range between 2.70 and 3.74 percent, giving a total variation of about 1.0 percent only. As the compacting temperature is increased from 200 F there is a decrease in voids up to a compacting temperature of 290 F, after which there is a slight increase (0.35 percent voids) as the compacting temperature is raised to 320 F at a mixing temperature of 350 F.

The decrease in voids is due to the ability of the less viscous asphalt to fill up more of the aggregate voids as the compacting temperature is raised, the compactive effort remaining the same throughout the series. At high compacting temperatures, however, there may be excessive movement of the mix due to lubricating action of the binder. The full compactive effort may not, therefore, be effective. This increases the void contents at high compacting temperatures.

Voids in Mineral Aggregate. —Figure 15 shows the plot of compacting temperature vs percent VMA. As the compacting temperature is increased from 200 to 290 F, there is progressive decrease in VMA. Further rise in compacting temperature to 320 F with mixing at 350 F results in a slight increase (0.31 percent VMA). Lowest value of VMA is obtained at a compacting temperature of 290 F with mixing at 350 F. This percent value is only 0.06 lower than the VMA at mixing and compacting temperatures of 290 and 260 F, respectively, or the VMA at mixing and compacting temperatures of 320 and 290 F, respectively.

Voids Filled with Bitumen. —Figure 16 gives the relationship between compacting temperature and percent VFB. As the compacting temperature is increased from 200 to 230 F, there is an average increase of 2.55 percent VFB. This is followed by further increase in VFB as the compacting temperature is raised to 290 F. At the mixing temperature of 350 F, a further increase in compacting temperature from 290 to 320 F results in a decrease of 2.05 in percent VFB values. With a mixing temperature of 350 F and compaction at 290 F, the highest VFB value of 80.8 percent is obtained. This value is 0.4 higher than percent VFB obtained at mixing and compacting temperatures of 290 and 260 F, respectively.

Effects of Mixing Viscosity on Mixture Containing 11.3 Percent Mineral Filler

Properties of the mixture containing 11.3 percent mineral filler are discussed, as well as the effects on the results of a relatively high F/B ratio.

Stability. —Figure 17 gives the plots of mixing viscosity and mixing temperature vs Marshall stability for 11.3 percent mineral filler. The general trend of all curves is the same. There is an increase in the stability values as the mixing temperature is raised from 260 to 350 F (viscosity decreased from 250 to 34.5 SSF). This increase is at a low rate from 260 to 290 F (viscosity from 250 to 105 SSF), but the values increase more rapidly when the mixing temperature is increased from 290 to 350 F (viscosity from 105 to 34.5 SSF).

It may be noted that this increase in the stability value as the mixing temperature is increased from 260 to 350 F at filler content of 11.3 percent is in contrast to the results obtained with filler content of 8.6 percent (Fig. 3). For 8.6 percent filler, the curves have a peak at 290 F and a trough at 320 F as the mixing temperature is increased from 260 to 350 F. These results may be explained as follows: As the filler content is increased from 8.6 to 11.3 percent (asphalt content being the same), the viscosity of asphalt-filler binder is increased. Higher mixing temperatures are, therefore, required for proper coating, good mixing and uniform dispersion of materials. Thorough mixing is evidently not obtained at low mixing temperatures of 260 and 290 F (asphalt viscosities of 250 and 105 SSF), resulting in lower stabilities than at mixing temperatures of 320 and 350 F (viscosities of 54 and 34.5 SSF). The increased stabilities at 350 F may be attributed to hardening of asphalt.

It is also seen from Figure 17 that at very low compaction temperatures (or high compaction viscosities) there is no

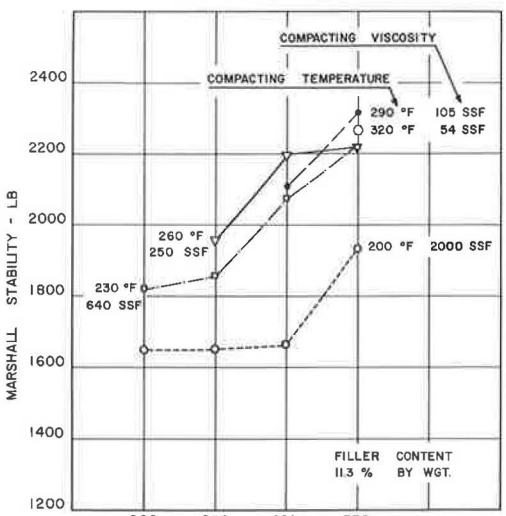

Figure 17. Effects of mixing viscosity (mixing temperature) on Marshall stability.

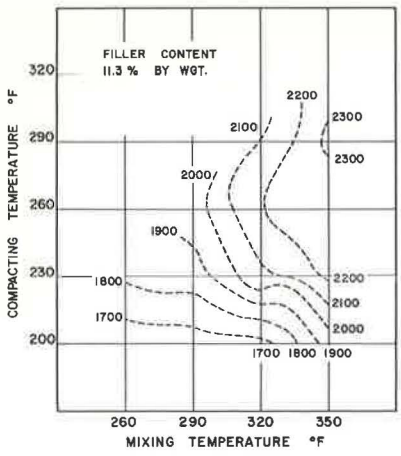

Figure 18. Stability contours showing effects of variations in mixing and compacting temperatures.

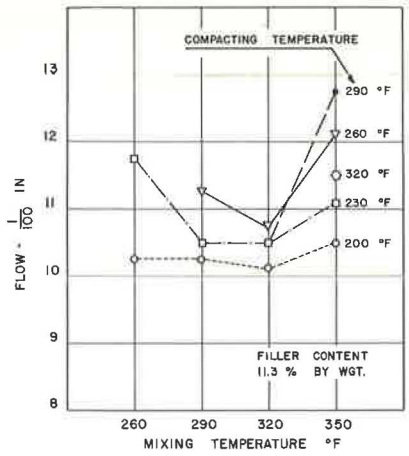

Figure 19. Effects of mixing temperature on flow.

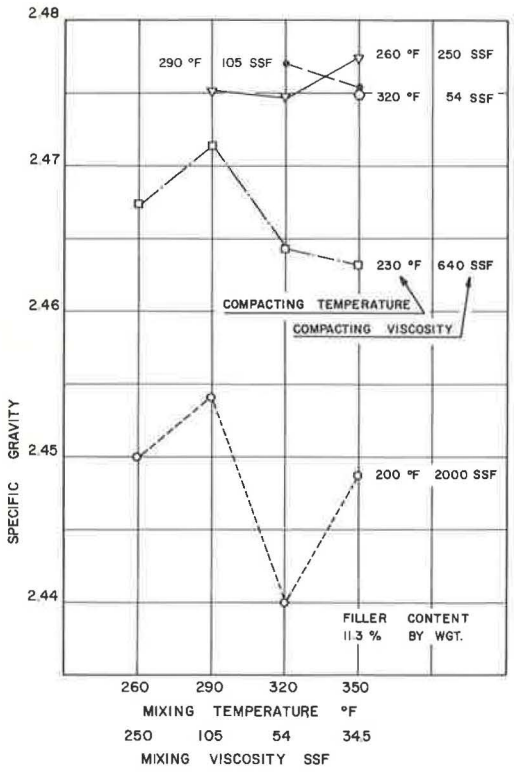

Figure 20. Effects of mixing viscosity (mixing temperature) on specific gravity of asphaltic concrete.

appreciable difference in the stability values as the mixing temperature is increased from 260 to 290 F (viscosity from 250 to 105 SSF).

Up to a mixing temperature of 320 F, the highest stability value is obtained at a mixing temperature of 320 F (viscosity 54 SSF) with compaction done at 260 F (viscosity 250 SSF). This value is 20 lb lower than at mixing and compacting temperatures of 350 and 260 F, respectively.

Figure 18 shows the stability contours at 100-lb intervals with filler content of 11.3 percent. These contours show that for a constant compacting temperature, the stability values increase as the mixing temperatures are increased. The lower portion of this figure indicates that for equal stability, the compaction temperatures should be progressively increased as the mixing temperature is decreased from 350 to 260 F. Thus, compaction temperatures of 211, 222, and 227 F are required for same stability (1,800 lb) at mixing temperatures of 320, 290, and 260 F, respectively. Also, with mixing temperatures of 350 and 320 F, a stability value of 2,000 lb is obtained when compaction is done at temperatures of 290 and 224 F, respectively. The upper portion of the figure indicates that for a constant mixing temperature of 320 F, there is a peak in stability values at about 260 F compacting temperature. Above this peak, there is a reversal be-

cause increased compacting temperature produces a lower stability value when the mixing temperature is kept constant (e.g., the stability values at 260 and 290 F for a mixing temperature of 320 F).

Flow. —In Figure 19 the graph showing the relationship between mixing temperature and flow is given. The general trend of all curves is the same as noted with 8.6 percent filler content in Figure 5, but the flow values are greater for the 11.3 percent filler mixture.

Specific Gravity. —Figure 20 gives the plots of mixing viscosity and mixing temperature vs specific gravity. The general trend of all curves is the same up to a mixing temperature of 320 F (viscosity 54 SSF). The specific gravity increases as the mixing temperature increases from 260 to 290 F (viscosity from 250 to 105 SSF) after which there is a decrease in the values as the mixing temperature is raised to 320 F (viscosity 54 SSF). Further increase in mixing temperature to 350 F (viscosity 34.5 SSF) produces variable results. It is interesting to compare the peak in curves obtained at 290 F (105 SSF mixing viscosity) with results published by Lehmann and Adam (3, Fig. 6), where a peak is shown at 85 SSF mixing viscosity for percent theoretical specific gravity for laboratory compacted briquets.

Figure 21 shows the contours for specific gravity for the 11.3 percent filler mixture at intervals of 0.005 with mixing temperatures and compacting temperatures as the coordinate axes. For a constant mixing temperature, specific gravity is increased as the compacting temperature is raised.

Voids in Total Mix. —Figure 22 shows the relationship between mixing temperature and percent voids in total mix for 11.3 percent mineral filler. The change in voids as the mixing temperature is varied between 260 and 350 F is slight, less than 0.6 percent at equivalent compaction temperatures. A decrease in voids as the mixing temperatures are increased from 260 F (viscosity 250 SSF) to 290 F (viscosity 105 SSF) is followed by some increase up to 320 F (viscosity 54 SSF). It is interesting to compare this trough in values of percent voids in total mix with the peak of values given by Lehmann and Adam (3, Fig. 6).

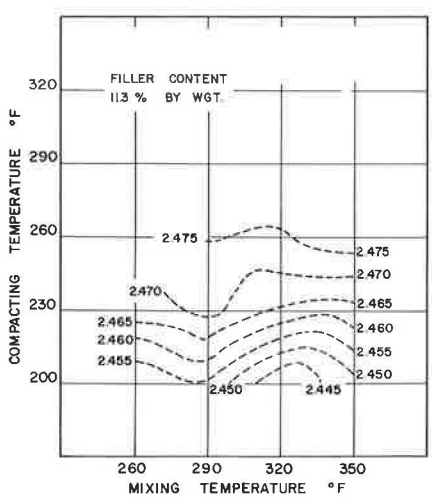

Figure 21. Specific gravity contours of asphaltic concrete showing effects of variations in mixing and compacting temperatures.

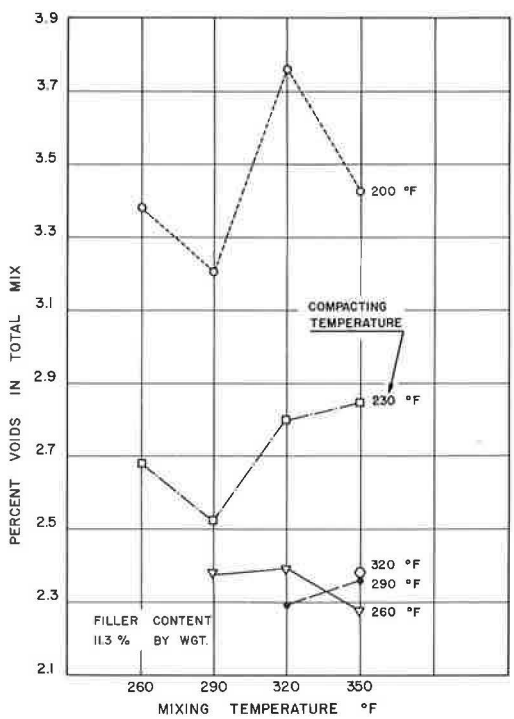

Figure 22. Effects of mixing temperature on percent voids in total mix.

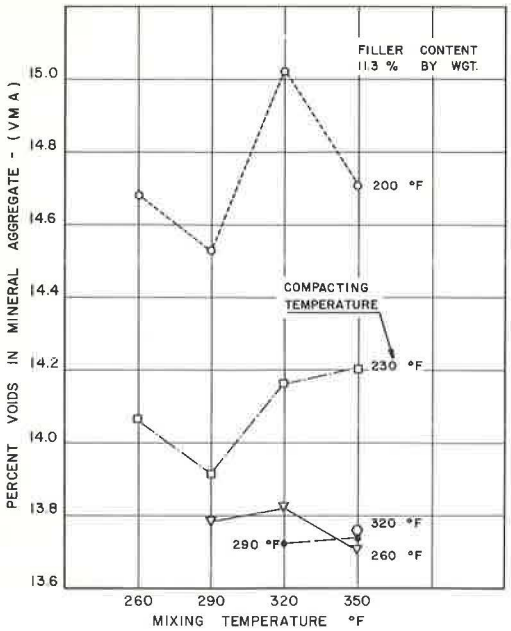

Figure 23. Effects of mixing temperature on percent VMA.

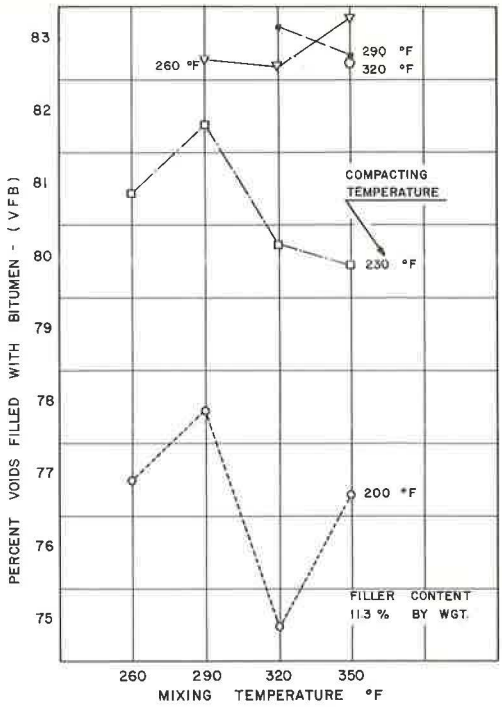

Figure 24. Effects of mixing temperature on percent VFB.

There is very little difference in values as the mixing temperature is further increased to 350 F, excepting at a compaction temperature of 200 F where the percent voids decreases by 0.25.

Voids in Mineral Aggregate. —Figure 23 gives the plot of mixing temperature vs percent VMA. The maximum change in percent VMA at the same compaction temperature is only 0.5 as the mixing temperature is varied between 260 and 350 F. For compacting temperatures up to 260 F, a trough of low values of VMA occurs at 290 F. The combination of 320 F mixing temperature with 290 F compacting temperature gives a low value of VMA of 13.72.

Voids Filled with Bitumen. —The relationship between mixing temperature and percent VFB is shown in Figure 24 for 11.3 percent mineral filler. The total variation in VFB values is about 1½ times the variation at filler content of 8.6 percent, the values varying between 74.9 and 83.4 percent. As the mixing temperature is increased from 260 to 290 F, there is an increase in VFB. Further rise in mixing temperature up to 320 F results in a decrease in values. For further increase in mixing temperature up to 350 F, the trends are variable. For compaction temperature equal to or greater than 260 F the percent VFB values lie within 0.7 as the mixing temperature is varied between 290 and 350 F.

Effects of Compacting Viscosity on Mixture Containing 11.3 Percent Mineral Filler

Graphs for the mixture containing 11.3 percent mineral filler are considered where the compacting viscosity (or compacting temperature) is plotted against the various physical properties. These graphs are based on the same data as plotted in Figs. 17 to 24 where mixing viscosity (or mixing temperature) was plotted as abscissa.

Stability. —Figure 25 shows the relationship of compacting viscosity and temperature as abscissa against Marshall stability as ordinate for the 11.3 percent mineral filler mixture. There is an appreciable increase in the stability as the compacting tempera-

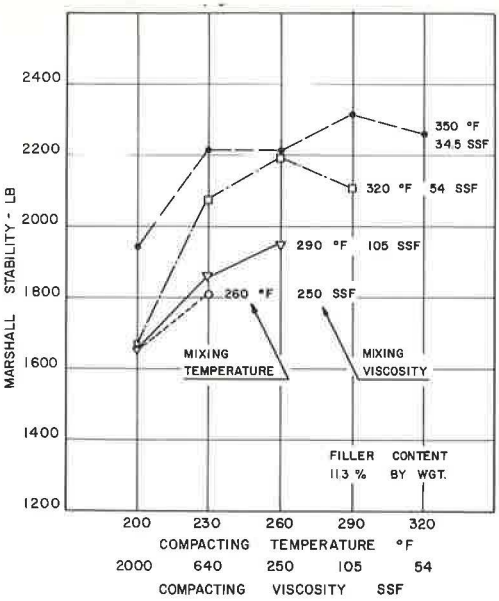

Figure 25. Effects of compacting viscosity (compacting temperature) on Marshall stability.

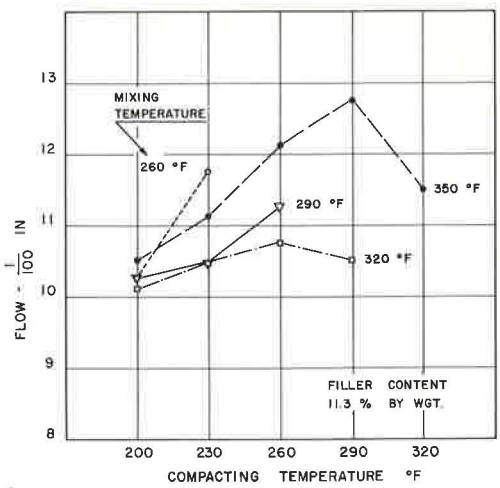

Figure 26. Effects of compacting temperature on flow.

ture is increased from 200 to 260 F (viscosity decreased from 2,000 to 250 SSF). At a mixing temperature of 320 F (viscosity 54 SSF), the peak of the curve is at a compacting temperature of 260 F (viscosity 250 SSF). At a mixing temperature of 350 F (viscosity 34.5 SSF), the stability is highest at a compacting temperature of 290 F (viscosity 105 SSF) after which there is a decrease in stability of 54 lb as the compacting temperature is increased to 320 F (viscosity 54 SSF). There is a decrease of 90 lb in stability at a mixing temperature of 320 F when the compacting temperature is raised from 260 to 290 F (viscosity decreased from 250 to 105 SSF).

Flow. —The results for the mixture containing 11.3 percent mineral filler for compacting temperature vs flow are plotted in Figure 26. Within the limits of mixing and compacting temperatures, the variation in flow is less than 2.7, the values lying between 10.1 and 12.8. There is an increase in the flow as the compacting temperature is increased from 200 to 260 F. This is followed by a slight decrease in flow at a mixing temperature of 320 F. At a mixing temperature of 350 F, there is a decrease in flow of 1.2 as the compacting temperature is raised from 290 to 320 F. Minimum values of flow are obtained at the mixing temperature of 320 F, as is also the case for the mixture with the filler content of 8.6 percent (Fig. 12).

Specific Gravity. —Figure 27 gives the relationship between compacting viscosity and specific gravity as well as between compacting temperature and specific gravity. As the compacting temperature is increased from 200 to 260 F (viscosity decreased from 2,000 to 250 SSF), there is an increase in specific gravity values. Further rise in compacting temperature to 320 F (viscosity 54 SSF) results in a slight decrease in specific gravities at a mixing temperature of 350 F (viscosity 34.5 SSF).

The reasons for this increase in specific gravities as the compacting temperature is increased to a certain value followed by decrease in the values with further rise in compacting temperature have already been explained in the discussion on the mixture with 8.6 percent filler content.

It may be noted from comparison of Figures 25 and 27 that although there is a slight increase in specific gravity when the compacting temperature is increased from 260 to 290 F with mixing at 320 F, the corresponding stability decreases by 90 lb. Also at mixing temperature of 350 F, an increase in compacting temperature from 260 to 290 F results in a very slight decrease in specific gravity (0.0023) but the stability increases by 100 lb. These show a lack of direct stability-density correlation.

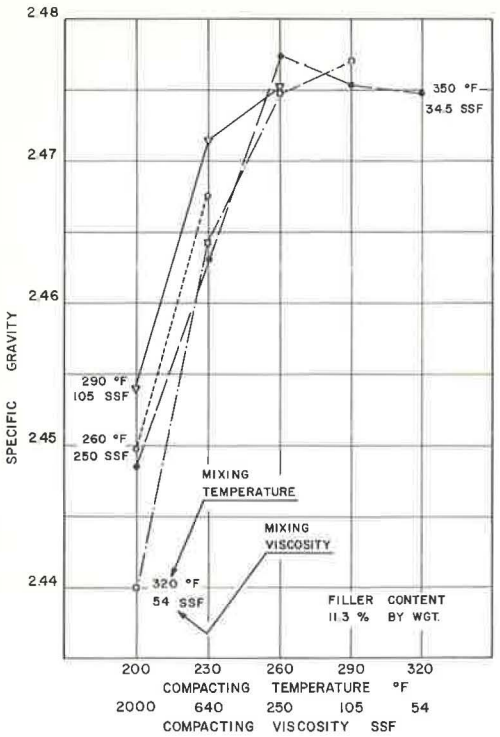

Figure 27. Effects of compacting viscosity (compacting temperature) on specific gravity of asphaltic concrete.

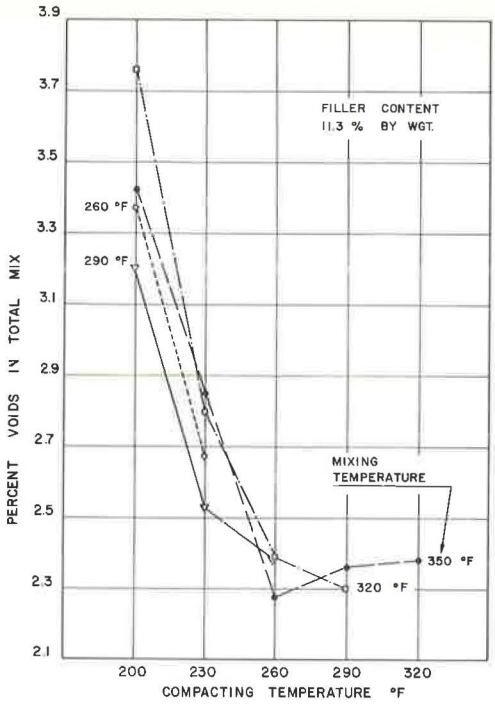

Figure 28. Effects of compacting temperature on percent voids in total mix.

Voids in Total Mix. —In Figure 28 the relationship between compacting temperature and percent voids in total mix is shown for 11.3 percent mineral filler. Within the limits of mixing and compacting temperatures, the void values lie between 2.3 and 3.8 percent, giving a maximum variation of about 1.5 percent voids. There is a steep decrease in voids as the compacting temperature is raised from 200 to 230 F, the average decrease being 0.7 percent voids. The amount of change in voids reduces with further rise in compacting temperatures to 320 F. At the mixing temperature of 350 F there is practically no difference in voids as the compacting temperature is increased from 260 to 320 F.

Voids in Mineral Aggregate. —Figure 29 gives the plot of compacting temperature against percent VMA for 11.3 percent mineral filler. The VMA values lie between 13.7 and 15.0 percent, giving a maximum variation of 1.3 percent within the range of mixing and compacting temperatures used in this study. There is a decrease in the VMA as the compacting temperature is increased from 200 to 290 F, excepting for the mixing temperature of 350 F where there is a very slight increase (0.09 percent VMA) as the compacting temperature is raised from 260 to 320 F. The combination of 290 F compacting temperature with 320 F mixing temperature gives a low value of VMA.

Voids Filled with Bitumen. —Figure 30 shows the relationship between compacting temperature and percent VFB. The VFB values range between 74.9 and 83.4 percent, as the compacting temperature is varied between 200 and 320 F with the mixing temperature ranging between 260 and 350 F. The increase in VFB values is greatest when the compacting temperature is increased from 200 to 260 F. An increase in compacting temperature from 260 to 320 F results in a small decrease in VFB (0.6 percent VFB) at the mixing temperature of 350 F. Relatively high values of VFB are obtained at a mixing temperature of 320 F with a compacting temperature of 290 F, as well as at temperatures of 290 and 260 F, respectively.

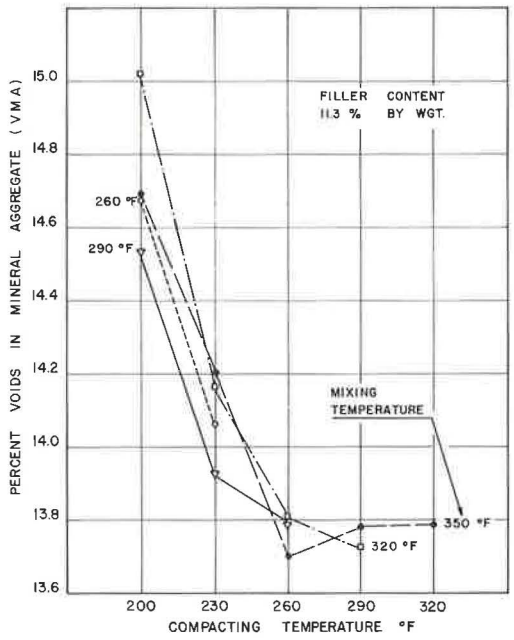

Figure 29. Effects of compacting temperature on percent VMA.

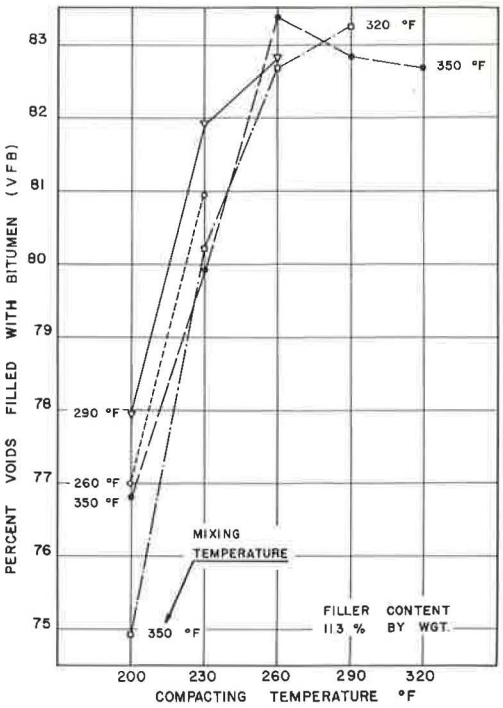

Figure 30. Effects of compacting temperature on percent VFB.

Effects of Increasing Filler-Bitumen Ratio

As mentioned before, the effects of mixing and compacting viscosities on the properties of asphaltic concrete were studied with two filler contents, keeping constant the asphalt content of 4.75 percent by weight of total mix. A filler content of 8.6 percent by weight of total mix (considered normal in the asphaltic concrete mix investigated) was used in one set of specimens, whereas the filler content of 11.3 percent (considered relatively high) was used in the other set of specimens.

Stability.—The increase in F/B ratio by weight from 1.81 to 2.38 (filler content from 8.6 to 11.3 percent by weight of total mixture) results in an increase in the stability values at mixing temperatures of 260, 320, and 350 F, and a decrease at mixing temperature of 290 F. This is readily seen in Figure 31 (see also Figs. 3 and 17). Taking the average of the stability values at different compacting temperatures at specified mixing temperatures, this increase is 119 lb (7.1 percent), 86 lb (4.5 percent), and 32 lb (1.5 percent) at mixing temperatures of 260, 320, and 350 F, respectively. At a mixing temperature of 290 F, there is a decrease of 150 lb (7.6 percent) in the value. The increase in stability may be due to the increase in the binder viscosity as the filler content is increased from 8.6 to 11.3 percent. Also, filler properties such as particle shape and particle-size distribution may affect the Marshall stability (4, p. 16). For the mixing temperature of 290 F, however, it is not clear as to why there is a decrease in stability values for the 11.3 percent filler mixture. Kallas and Puzinauskas (5, Fig. 12) reported variable results in Marshall stability values due to different concentrations of limestone dust mineral filler.

It is also seen from a study of Figure 25 for the 11.3 percent filler mixture that with high mixing and compacting temperatures (or low mixing and compacting viscosities) there is a drop in stability values. Thus, at a mixing temperature of 320 F (viscosity 54 SSF), the stability decreases by 91 lb as the compacting temperature is increased from 260 to 290 F. Also at a mixing temperature of 350 F (viscosity 34.5 SSF), the drop in stability is 54 lb as the compacting temperature is increased from 290 to 320

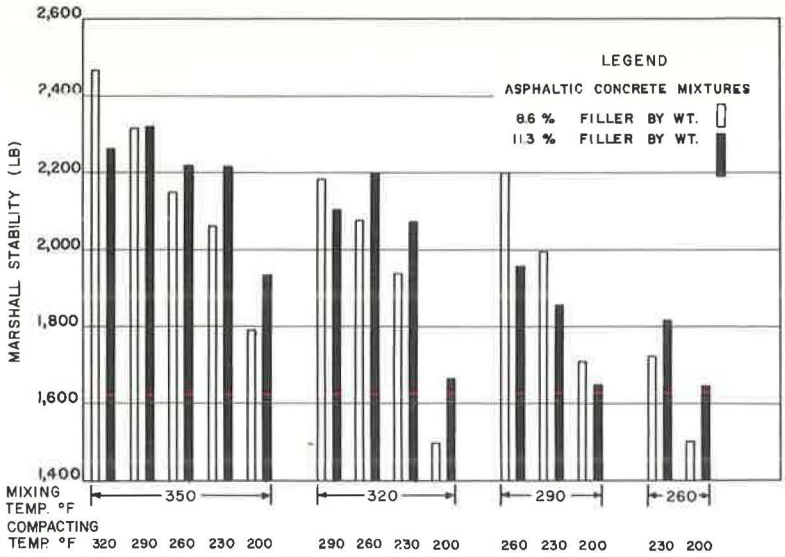

Figure 31. Comparison of Marshall stability values for asphaltic concrete mixtures with different filler contents for different mixing and compacting temperatures.

F. This is in contrast to the results shown in Figure 11 for the 8.6 percent filler mixture where at high mixing temperatures of 350 and 320 F, there is an increase in stability values as the compacting temperatures are increased from 260 to 320 F (compacting viscosities are decreased from 250 to 54 SSF).

The tendency of the Marshall stability-mixing viscosity curve to show a peak and a trough (Fig. 3) for 8.6 percent filler as the mixing viscosity is decreased (or mixing temperature increased) is eliminated when the filler content is increased to 11.3 percent. In the latter case (Fig. 17), there is a progressive rise in stability as the mixing viscosity is decreased from 250 to 34.5 SSF (or mixing temperature is increased from 260 to 350 F).

Lower mixing viscosities (or higher mixing temperatures) are desirable at high filler content so that there may be thorough mixing and uniform dispersion of the materials. The "optimum" mixing viscosity and the "optimum" compacting viscosity for stability depend on filler content.

Flow. —The flow values are considerably affected by the F/B ratios. The flow values increase as the filler content is increased from 8.6 to 11.3 percent (Figs. 5 and 19).

Specific Gravity. —Increase in mineral filler content from 8.6 to 11.3 percent by weight increases the specific gravity values. This increase in density indicates the void-filling property of the mineral filler (Figs. 6 and 20).

Voids in Total Mix. —The increase in mineral filler content results in a slight decrease in the voids in total mix (Figs. 8 and 22).

Voids in Mineral Aggregate. —At identical mixing and compacting temperatures, the VMA decrease as the mineral filler content is increased with one exception (Figs. 9 and 23).

Voids Filled with Bitumen. —At identical mixing and compacting temperatures, the VFB at the mineral filler content of 11.3 percent are higher than at the filler content of 8.6 percent with one exception (Figs. 10 and 24).

OPTIMUM MIXING AND COMPACTING VISCOSITIES

Within the range of mixing viscosities and compacting viscosities investigated in this study, a mixing temperature of 290 F (mixing viscosity of 105 SSF) is satisfactory at the filler content of 8.6 percent for the given gradation of aggregate and the given asphalt cement. For the mixing temperature of 290 F (viscosity 105 SSF), highest stabil-

ity and specific gravity values are obtained at the compacting temperature of 260 F (viscosity 250 SSF).

For comparison, a set of four specimens was prepared at a mixing temperature of 300 F (viscosity 82 SSF), with compaction done at 250 F (viscosity 335 SSF). The results are shown in Table 4. There is not much difference in the stability and density values when the mixing is done at temperatures of 290 and 300 F with compaction at 260 and 250 F, respectively; the stability and density are very slightly higher in the former, the difference being 10 lb for stability and 0.5 pcf for density values.

TABLE 4

MARSHALL TEST RESULTS FOR MIX CONTAINING 8.6 PERCENT FILLER

Property	At Mixing Temp 290 F and Compacting Temp 260 F	At Mixing Temp 300 F and Compacting Temp 250 F
Stability (lb)	2,200	2,190
Flow (0.01 in.)	7.5	6.8
Specific Gravity	2.463	2.456
Density (pcf)	153.67	153.22
Percent Voids in Total Mix	2.77	3.05
Percent VMA	14.02	14.38
Percent VFB	80.98	78.77

From this discussion it is seen that a mixing temperature range of 290 F (viscosity 105 SSF) to 300 F (viscosity 82 SSF) is satisfactory at a filler content of 8.6 percent with the aggregate gradation and asphalt cement used in this study.

At a filler content of 11.3 percent, the stability values at the mixing temperature of 320 F (viscosity 54 SSF) are higher than the values obtained when mixing is done at temperature of 290 F (viscosity 105 SSF) (Figs. 17 and 25). However, the average density with mixing temperature of 320 F is slightly lower than at the mixing temperature of 290 F.

A study of Figures 25 and 27 shows that at the filler content of 11.3 percent, mixing and compacting temperatures of 320 and 260 F (viscosity 54 and 250 SSF), respectively, are most satisfactory. However, mixing and compacting temperatures of 320 and 290 F (viscosity 54 and 105 SSF) are also satisfactory because the stability is only 91 lb smaller. At the compacting temperature of 260 F, the stability with mixing done at 320 F is 240 lb higher than the value at mixing temperature of 290 F, and 18 lb lower than at mixing temperature of 350 F. Mixing temperatures above 320 F are not recommended because of the danger of overheating and hardening the asphalt cement. However, there is not much difference in the density at mixing temperatures of 290, 320, and 350 F with compaction done at 260 and at 290 F (Fig. 20).

It is thus observed that an increase in filler content requires use of lower mixing viscosity (higher mixing temperature) for optimum stability and density values. In other words, the F/B ratio should be considered before arriving at an optimum mixing viscosity in the design and construction of asphaltic concrete. Also, the F/B ratio should be considered in selecting an optimum compacting viscosity for the design and construction of asphaltic concrete.

At the filler content of 8.6 percent by weight, the optimum mixing viscosity range of 82 to 105 SSF (300 to 290 F) is within the range of 75 to 150 SSF suggested by the Asphalt Institute (6). The corresponding mixing temperature range lies between 277 and 303 F for the asphalt cement used in this study for this viscosity range, the average temperature being 290 F.

At the mixing viscosity of 85 ± 10 SSF suggested in the Marshall stability test of ASTM Designation: 1559-60T (2), the temperature range varies between 293 and 303 F (Fig. 1). This mixing temperature range is satisfactory at the filler content of 8.6 percent, as can be seen from the previous discussion of results obtained by the Marshall test.

At the compacting viscosity of 140 ± 15 SSF suggested in the Marshall stability test of ASTM (2), the temperature varies between 275 and 283 F for the asphalt cement used in this investigation (Fig. 1). For the materials used in this investigation and for the mixture with 8.6 percent filler, a compacting temperature of about 260 F gave good results as measured by the Marshall test. The higher value between 275 and 283 F according to ASTM (2) would appear to be satisfactory (Figs. 3, 4, and 11).

At the filler content of 11.3 percent by weight, the optimum mixing viscosity as discussed previously is 54 SSF (or optimum mixing temperature of 320 F). This is outside the limits of 75 to 150 SSF suggested by the Asphalt Institute (or temperature range be-

tween 277 and 303 F). This optimum mixing viscosity is also below the ASTM value of 85 ± 10 SSF (or above temperature range of 293 to 303 F). However, Vokac (7) has noted that sheet asphalt with higher filler content required 50 to 100 SSF for mixing, whereas one-sized aggregate mixes, plant-mix macadam or sand asphalt could be mixed at temperatures corresponding to 125 to 250 SSF.

By comparing against the ASTM (2) compacting viscosity of 140 ± 15 SSF (temperature range 275 to 283 F), it is noted that the optimum compacting viscosity for the 11.3 percent filler mixture investigated is 250 SSF (optimum compacting temperature of 260 F). However, good results were also obtained for a compacting viscosity of 105 SSF (compacting temperature of 290 F). It appears that the ASTM compacting viscosity requirement falls within a range of compacting viscosities that would be suitable for this high filler content mixture.

Further research is required using a variety of aggregate types and gradations, different types of asphalts, and different F/B ratios to establish optimum mixing viscosity and optimum compacting viscosity for asphaltic concrete mixes.

CONCLUSIONS

Based on the materials and methods employed in this investigation, the following conclusions may be stated:

1. Variations in mixing viscosity of asphalt over a range of 34.5 to 250 SSF (temperature range from 350 to 260 F) gave significant differences in test results on asphaltic concrete specimens for Marshall stability, flow, specific gravity, percent voids in total mix, percent voids in mineral aggregate, and percent voids filled with bitumen.
2. Variations in compacting viscosity of asphalt over a range from 54 to 2,000 SSF (temperature range of 320 to 200 F), also gave significant differences in test results for the same properties.
3. Variations in the filler-bitumen ratio by weight from 1.81 to 2.38 in asphaltic concrete specimens gave some significant differences in the test values of physical properties for identical combinations of mixing viscosity and compacting viscosity of asphalt.

RECOMMENDATIONS

1. Selection of mixing viscosity and compaction viscosity values of asphalt for molding asphaltic concrete specimens should be based on optimum conditions consistent with practical paving plant and construction operations requirements for the production of durable pavements.
2. The filler-bitumen ratio should be considered in selecting optimum mixing viscosity and optimum compacting viscosity for the design and construction of asphaltic concrete.
3. The mixing viscosity and compacting viscosity of asphalt should be stated in reports giving results obtained by the Marshall stability test.
4. Control of the mixing and compacting viscosities of asphalt in the heating and mixing of materials and molding of asphaltic concrete specimens for the Marshall stability test should be required to obtain consistent and significant values of physical properties of asphaltic concrete mixtures.
5. A requirement should be placed in specifications to control the compacting viscosity of asphalt when forming laboratory briquets for use in checking pavement density to eliminate errors caused by employing too high a compacting viscosity (too low a compacting temperature) when molding laboratory briquets.

ACKNOWLEDGMENTS

Acknowledgment is made to the International Cooperation Administration and the Agency for International Development of the U. S. Government for the support given to Dr. Gandharv Raj Bahri of India as a participant in the teacher training program at the University of Wisconsin. The use of the facilities of the testing laboratory of the State Highway Commission of Wisconsin in conducting this investigation is also appreciated.

REFERENCES

1. State Highway Commission of Wisconsin, Standard Specifications for Road and Bridge Construction (1957).
2. American Society for Testing and Materials, "Resistance to Plastic Flow of Bituminous Mixtures by Means of the Marshall Apparatus." ASTM Designation: D 1559-60T, Book of Std., Pt. 4 (1961).
3. Lehmann, H. L., and Adam, V., "Application of Marshall Method to Hot Mix Design." ASTM Spec. Tech. Publ. 252, p. 27 (1960).
4. Kallas, B. F., Puzinauskas, V. P., and Krieger, H. C., "Mineral Fillers in Asphalt Paving Mixtures." HRB Bull. 329, pp. 6-29 (1962).
5. Kallas, B. F., and Puzinauskas, V. P., "A Study of Mineral Fillers in Asphalt Paving Mixtures." Proc. AAPT, 30:493 (1961).
6. The Asphalt Institute, "The Asphalt Handbook" (1960).
7. Vokac, R., Discussion of "Temperature Control of Hot Mixes." by H. G. Nevitt and J. A. Donaldson. Jour. Asphalt Tech., AAPT, 2(1):4 (1943).
8. Fink, D. F., and Lettier, J. A., "Viscosity Effects in Marshall Stability Test." Proc. AAPT, 20: p. 246 (1951).
9. Kiefer, R. W., "The Effect of Compaction Temperature on the Properties of Bituminous Concrete." ASTM Spec. Tech. Publ., 294:19 (1960).
10. Bahri, Gandharv Raj, "Investigations of Viscous Properties of Bituminous Materials and Mixtures and Bitumen—Filler Mortars." Unpublished Ph. D. Thesis, Univ. of Wisconsin (1962).
11. Parker, Charles F., "Steel-Tired Rollers." HRB Bull. 246, pp. 1-40 (1959).

Discussion

CHARLES F. PARKER, W. S. Hinman, Inc., Westbrook, Me. —The studies made by Dr. Bahri and Prof. Rader are in many ways similar to those shown by the writer (11). The purpose of this latter paper was slightly different and is more closely related to actual construction procedures, whereas Prof. Rader's paper is more closely associated with laboratory control.

The results of the compaction temperature studies shown (11) were presented to show the importance of this relationship and how critical this could be during actual construction. It was recommended that the diameter of steel-tired rollers be increased and widened to permit rolling at higher temperatures with less displacement or decompaction.

The procedure used by Bahri and Rader was similar to that used by the writer and was the standard Marshall procedure as has been described by Prof. Rader. The mix comprised 6.3 percent (of total mix) asphalt and the following gradations of aggregate: passing ½ in. sieve, 100 percent; No. 4, 68 percent; No. 10, 44 percent; No. 20, 31 percent; No. 40, 23 percent; No. 80, 13 percent; No. 200, 4.7 percent. The minimum mixing temperature was that required in the standard procedure, except when the tests were performed at higher temperatures than the standard; in this case all materials were brought to the temperature of the test before mixing. The results obtained by Bahri and Rader appear to support those we obtained.

In a paper (9) reporting on results using a Hveem kneading compactor rather than the Marshall method of compaction, Kiefer stated:

> A comparison of the results of this experimental program using kneading compaction with those of Parker...using impact compaction, shows that although the curves follow the same general trend....The changes in specific gravity, percent voids, stabilometer value and cohesimeter value using kneading compaction were about one half of those using impact compaction.

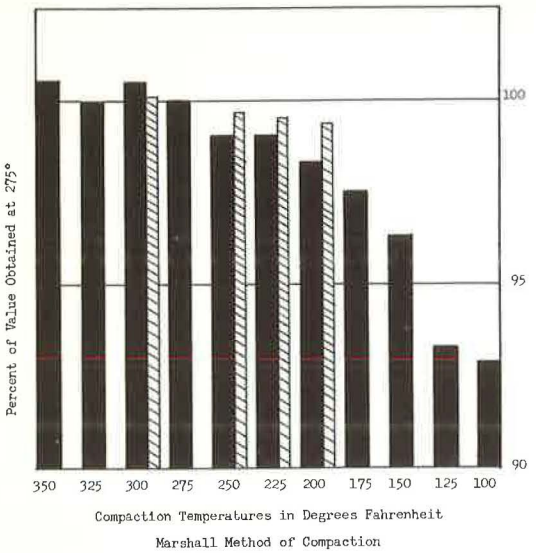

Figure 32. Effect of compaction at various temperatures on specific gravity; Rader results shown by hatched bars at 350F mixing temp. with filler content 8.6% by wt.

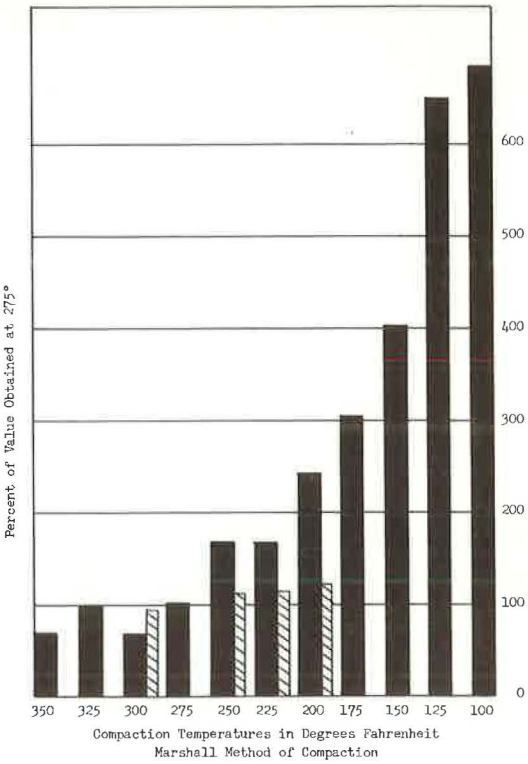

Figure 33. Effect of compaction at various temperatures on percent voids; Rader results shown by hatched bars at 350F mixing temp. with filler content 8.6% by wt.

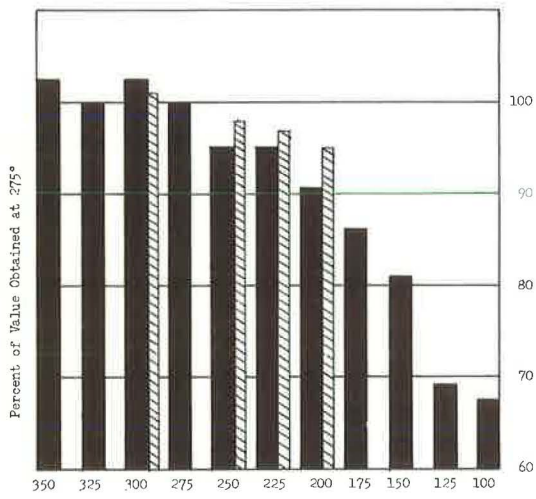

Figure 34. Effect of compaction at various temperatures on voids filled; Rader results shown by hatched bars at 350F mixing temp. with filler content 8.6% by wt.

In Figure 32, the values of Bahri and Rader for specific gravity are shown by the hatched bars; the shape of this curve corresponds very closely to the results obtained by the writer though the temperature range is not as broad as that investigated by the writer. In Figure 33, Prof. Rader's results for percent voids are again shown by the hatched bars and the trend is not quite as great as shown by our results. However, studies were made by the writer over a temperature range from 350 to 100 F as compared to the much narrower range of 300 to 200 F of Prof. Rader's paper. This low range (100 to 200 F) would seem to be of considerable importance in that it reflects to a great extent the results that may be obtained during cold weather construction, such as was described previously in a paper (12). In Figure 34, again the trend of our results for voids filled is very similar to those of Bahri and Rader and more extreme temperatures are covered by the writer. In Figure 35, the Bahri-Rader results for

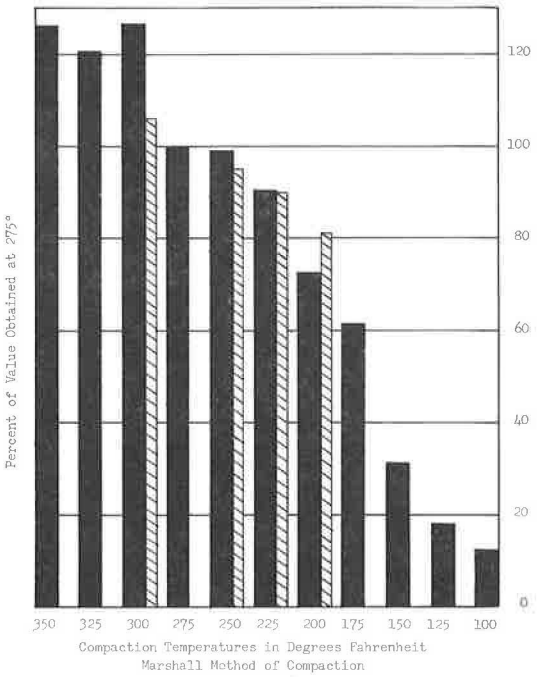

Figure 35. Effect of compaction at various temperatures on Marshall stability; Rader results shown by hatched bars at 350F mixing temp. with filler content 8.6% by wt.

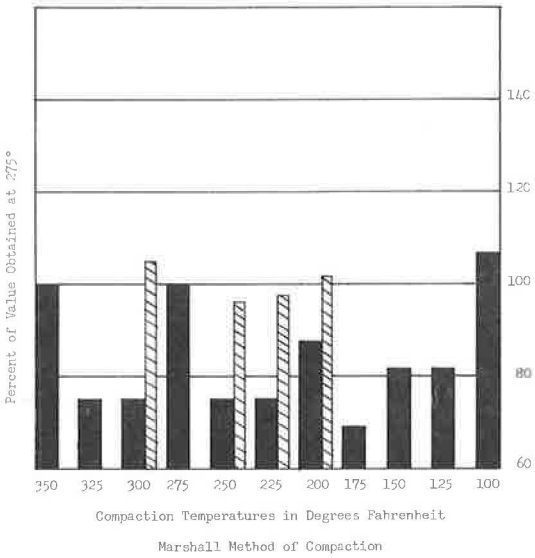

Figure 36. Effect of compaction at various temperatures on Marshall flow; Rader results shown by hatched bars at 350F mixing temp. with filler content 8.6% by wt.

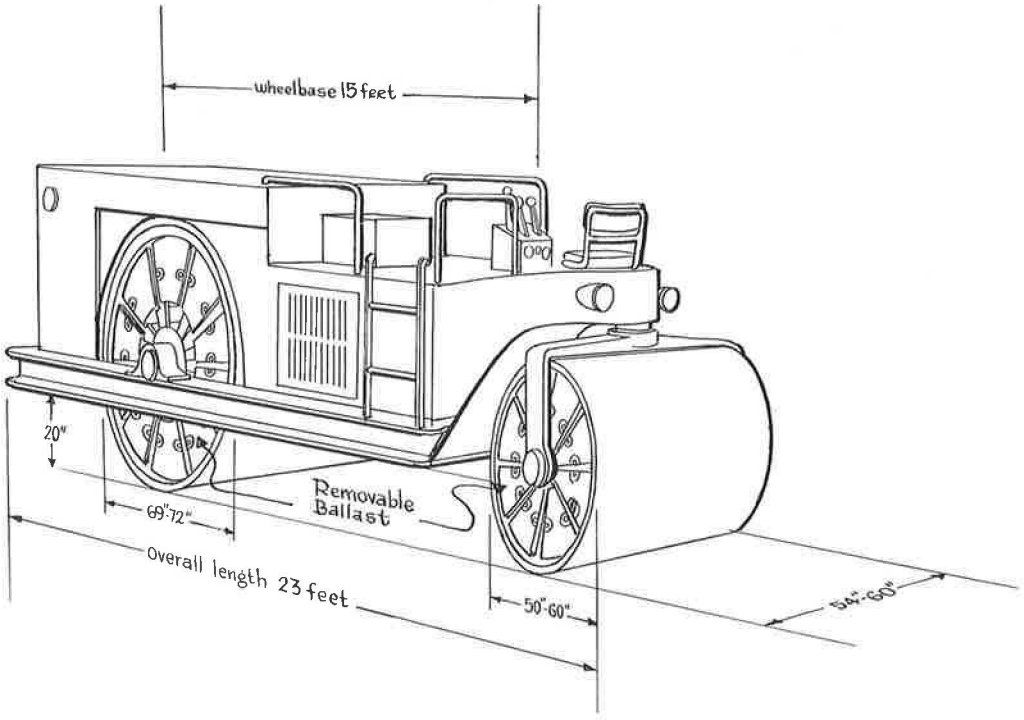

Figure 37. Artist's conception of roller.

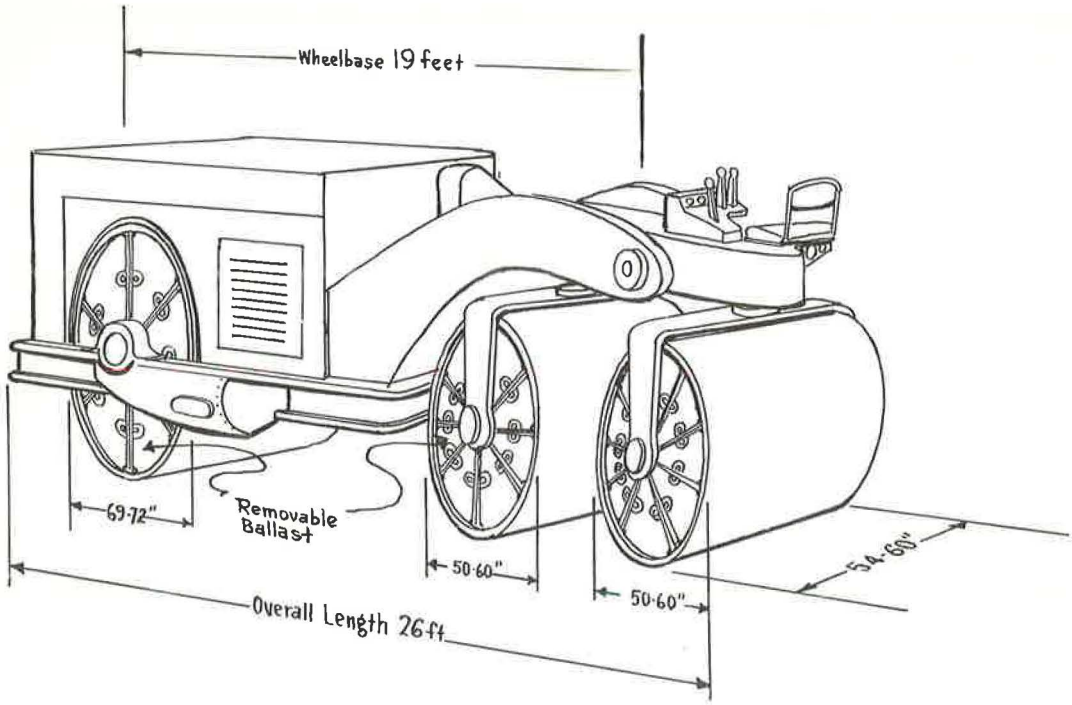

Figure 38. Artist's conception of roller.

Marshall stability, shown by the hatched lines are very similar to the results obtained by the writer, except in the high range of 300 F and the low range of 200 F. However, the general trend is practically identical. As shown in Figure 36, our results were somewhat erratic on this study of Marshall flow and nearly as much so in the results of the Bahri-Rader investigation.

Bahri and Rader have stated in their paper that for a mixture containing 8.6 percent mineral filler, "Considering the stability values up to a compaction temperature of 260 F, the highest value of stability (2,200 lb) is obtained when the mixing is done at 290 F (viscosity 105 SSF) with compaction at 260 F (viscosity 250 SSF). This appears to be an excellent combination of mixing temperature and compaction temperature." Our investigation indicated that the ideal compaction temperature was 275 F (11).

The writer agrees with Dr. Bahri and Prof. Rader that a selection of mixing viscosity and compaction viscosity values of asphalt for molding asphaltic concrete specimens should be based on optimum conditions consistent with the practical paving plant and construction operations and that a requirement should be placed in specifications to control the compaction viscosity of asphalt when forming laboratory briquettes for use in checking paving density.

Looking again at the practical side or the actual construction, it is important to have a requirement for compaction temperatures in the specification. This brings up the point that it is difficult to roll many of the so-called tender-type mixes by the conventional method of compaction, and that by increasing the diameter of the rollers, compaction may be completed at higher temperatures with less displacement or decompaction. Much the same effect is accomplished by pneumatic-tire rolling. In reality, changes in tire pressure varies the contact diameter of the rolls.

Figures 37 and 38 show an artist's conception of changes in design of steel-tired rollers that would permit compaction at higher temperatures by increasing the diameter of the rolls.

In conclusion, according to F. N. Hveem, "If more of our compaction rollers had six-foot wheels, many of our asphalt-compaction troubles would disappear" (13).

References

12. Parker, C. F., "Effect of Mix Temperature." HRB Spec. Rept. 54, pp. 28-33 (1960).
13. Day, Ray, "Pick Your Rollers for Top Blacktop Profit." Constr. Equip. and Mater. (Oct. 1963).

Viscoelastic Response of Asphalt Paving Slabs Under Creep Loading

K. E. SECOR and C. L. MONISMITH
Respectively, Assistant Professor of Civil Engineering, Chico State College, Chico, California, and Associate Professor of Civil Engineering, Institute of Transportation and Traffic Engineering, University of California, Berkeley

The results of an intensive study of the reactions of asphalt paving slabs subject to creep loads are the subject of this paper. The equipment employed in the slab research consists of a large spring base (approximately 4 ft square) inclosed in a constant-temperature cabinet. Several slabs compacted from the mixture selected for study were statically loaded on this base, and the resulting deflected shape of each was recorded against time by a system of linear variable differential transformers. Slabs were tested over a temperature range from 40 to 140 F. Each slab was subjected to stresses ranging from very low to very high to establish the linearity of its response pattern. Sufficient time was allowed between stress applications for the slab to regain its undeflected shape under the given ambient conditions.

The response of the test mixture in simple flexure was also evaluated by static bending tests on small beams (1 in. square by 12 in. long) sawed from compacted samples. The bending strains in both tension and compression were measured and used to compute a combined bending modulus as a function of time. The temperature dependence of the bending moduli was established by the application of the time-temperature superposition principle.

The time-dependent moduli derived from the simple flexure tests were used to predict the deflections which might be expected from the slab test procedures. This was done through the application of a numerical technique to classic elastic thin-plate theory. The procedures employed in this phase of the work were quite general in that no assumption of model properties was needed.

Also included in the paper is a discussion of the comparison between theoretical and measured values of slab deflections and their time dependence. Comments are also included concerning the linearity of material responses and the apparent validity of the basic theoretical assumptions underlying the work presented.

•IN THE PAST ten years considerable interest has developed in attempts to determine the time and temperature dependence of the physical properties of asphalt paving mixtures within the framework of viscoelastic theory. Ideally, the intent of this research would appear to be the development of additional analyses to broaden the scope of pavement design and permit consideration on a more rational basis of some aspects of loading which, at best, can only be qualitatively accounted for at present. Unfortunately, the extent to which this theory may be applied to a real material such as asphalt

Paper sponsored by Committee on Mechanical Properties of Bituminous Paving Mixtures.

concrete has yet to be properly defined. Sufficient data have been published, however, to indicate in a general way, at least, that this type of analysis may be feasible. For example, previous work at the University of California has indicated that the time-dependent behavior of asphalt concrete in compression can be approximated by simple models which are combinations of linear springs and dashpots (1, 2, 3). However, results of slab tests using this simplified approach (3) indicated considerable discrepancy between predicted and measured results. Research by Pister and Monismith (4), Papazian (5), Pagen (6), and Krokosky et al. (7) would indicate the necessity for use of a more generalized representation of linear behavior, behavior analogous to considering a model with either an infinite number of Kelvin elements in series or an infinite number of Maxwell elements in parallel. However, structural problems have been very difficult to solve by using this more generalized representation of material characteristics. In the last few years, particularly with the advent of electronic computers, some of these difficulties would appear to have been overcome.

The dependence of the viscoelastic properties of asphalt concrete on temperature has been shown by Monismith (4), Pagen (6), and Krokosky (7) to obey thermorheological principles similar to those developed for polymers. Krokosky (7), however, has questioned the applicability of linear response theory and has indicated that nonlinear theory which includes functions that are stress and strain dependent are more applicable. Whereas this latter data are of interest and importance, it would seem more appropriate first to define the limits of applicability of linear behavior before complicating the analysis still further with nonlinear functions.

As noted previously, rheologic studies of the material properties are (or should be) a preliminary step, although an important one, to the structural analysis of asphalt concrete pavements. At present only elastic methods of analysis are generally available to the engineer interested in the behavior of the pavement structure, and elastic methods fail to provide a sufficiently versatile tool for the study of many problems particularly associated with, though not necessarily limited to, this type of pavement.

Some limited data have previously been published (3) showing the reactions of actual asphalt paving slabs subjected to creep loads on a foundation of constant elastic properties. These data were compared with the performance predicted by a viscoelastic analysis predicated on an assumed four-element model. Although considerable error was evident between the theoretical predictions and measured data, sufficient correlation was found to warrant further work along similar lines. The results of a more intensive study of this type are presented here.

The research consisted of three distinct operations: (a) the determination of time-dependent elastic moduli considering differences in tensile and compressive behavior for beams prepared from a typical asphalt paving mixture, using simple creep bending tests performed over a range of temperatures; (b) the measurement of time-dependent deflection profiles for a series of slabs prepared from the same test mixture and subject to creep loading on a large spring base, again over a range in temperatures; and (c) the theoretical prediction of the slab deflection profiles from the results of the simple bending tests. Such a program has the possibility of providing a reasonably rigorous test of the ability of viscoelastic theory to reflect the action of the real material.

MATERIALS

A single asphalt concrete mixture was utilized for the investigations. The actual materials used have been employed in a number of previous studies and have been described in detail elsewhere (3).

The asphalt cement used in preparing test specimens was an 85-100 penetration

TABLE 1

IDENTIFICATION TESTS ON ASPHALT

Test	Result
Penetration at 77 F, 100 g, 5 sec	96
Penetration at 39.2 F, 200 g, 60 sec	24
Penetration ratio	25
Flash point, Pensky-Martens (° F)	445
Viscosity at 275 F (SSF)	138
Heptane-xylene equivalent	20/25
Softening point, ring and ball (° F)	110
Thin film oven test, 325 F, 5 hr:	
Weight Loss (%)	0.51
Penetration Retained (%)	53
Ductility of Residue at 77 F (cm)	100+

grade material. Results of standard identification tests on this asphalt are given in Table 1.

The aggregate used in the test mixture was a crushed granite from Watsonville, Calif., with a specific gravity of 2.92. A $\frac{3}{8}$-in. maximum size gradation conforming to the 1954 California Standard Specifications was employed for all specimens because the research was initiated before 1960. In 1960, new specifications for $\frac{3}{8}$-in. maximum aggregate grading were prepared by California. The gradation, together with both specification limits, is shown in Figure 1. It will be noted that the mix gradation also meets the 1960 specifications for all practical purposes.

Close control of gradation in the preparation of beam specimens was accomplished by screening the granite into individual size fractions and then recombining the size fractions in the amounts necessary to produce single specimens. The slabs were prepared at the Richmond, Calif. laboratories of the California Research Corp. The aggregate for the slabs (same granite as used in the beam specimens) was taken from the stocks of that organization, where it received care in batching comparable to that employed for the beams.

PREPARATION OF TEST SPECIMENS

Two types of test specimens were employed in the research described. For determination of viscoelastic bending moduli, 3- by $2\frac{1}{4}$- by 12-in. beams of the test mixture were prepared by kneading compaction. The details of the technique of mixing and compacting have been discussed in previous publications (8). The design asphalt content selected was 5.1 percent by weight of aggregate, a value already used in previous investigations with the same materials (3). The average density of the compacted specimens, as determined by water displacement, was approximately 152 pcf.

As a final step in the preparation of the bending specimens, each of the compacted beams was cut into four 1- by 1- by 12-in. sections with the aid of a diamond saw under conditions permitting close control over the dimensions of each of the beams.

The slab tests utilized thin "plates" of the test mixture approximately 40 by 40 in. square and slightly more than 1 in. deep. As mentioned previously, these slabs were prepared at the Richmond laboratories of the California Research Corp., where equipment suitable for the preparation of such large-scale specimens was available. The production of these slabs has been described in detail (3). After cooling, the compacted specimens were transported to the University of California laboratories for testing.

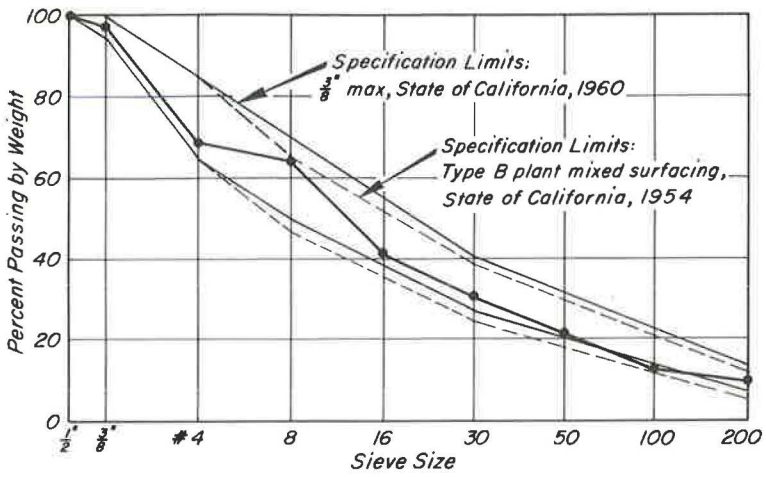

Figure 1. Grading curve, Watsonville aggregate.

It should be noted that these slabs were quite uniform in texture and thickness. Density measurements by water displacement on samples cut from the slabs after testing indicated unit weights of about 152.5 pcf, a value very close to that measured for the beam specimens.

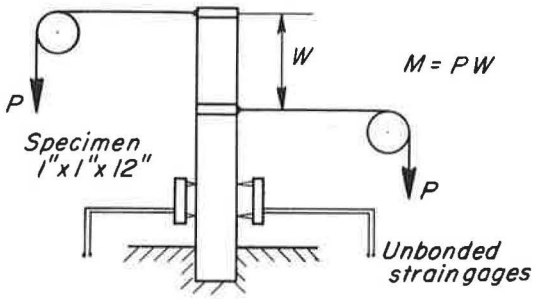

Figure 2. Schematic representation of test on slab mixture comparing creep behavior in tension and compression.

INSTRUMENTATION AND TEST TECHNIQUES

The apparatus employed in the bending creep tests is shown schematically in Figure 2. This test was performed with the beam in a vertical position, its lower end rigidly clamped against movement. A constant bending moment was then applied at the upper end of the beam by a system of pulleys and weights. Strains were measured on both the tension and compression sides of the specimen with unbonded strain gages. A continuous recording of the output of each gage was obtained through the use of an electronic strip-chart recorder. To insure uniform temperature conditions during the test, all measurements were conducted in a constant temperature room.

Two series of bending tests were performed, at 77 and 40 F, respectively. Unfortunately, the nature of the test procedure did not lend itself to measurements at elevated temperatures; the strength of a test specimen under such conditions would be inadequate to permit it to stand vertically unsupported. Each bending test was carried out for a period of 15 min, at a level of stress which induced relatively low strains (approximately 0.2 percent maximum).

The equipment used in the slab tests is shown in Figures 3 and 4; the details of its operation have been described previously (3). Approximately 1,600 coil springs, $\frac{7}{8}$ in. in diameter, provided the elastic foundation and were so arranged that the founda-

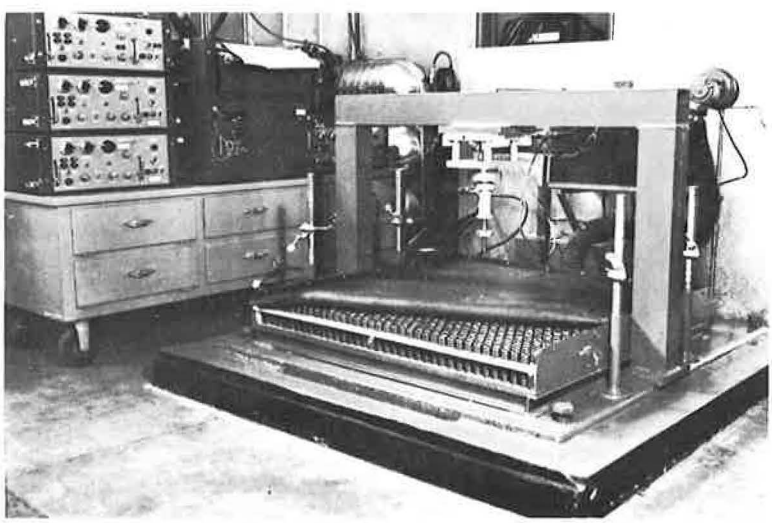

Figure 3. Slab testing device with rubber membrane stripped back to show spring base (pneumatic load cell hangs from center of reaction frame; electronic recorder for use with differential transformers appears in background).

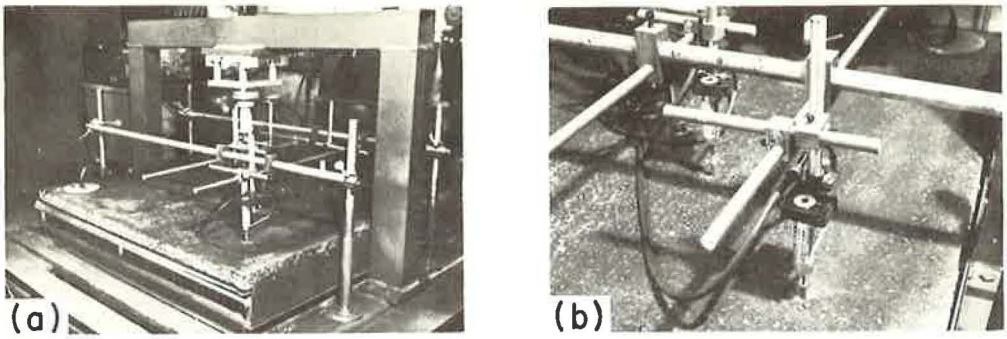

Figure 4. Slab test apparatus ready for operation: (a) Overall view of instrumented slab ready for testing, and (b) Close-up of differential transformer installation.

tion modulus of the system (k) was 200 psi per in. This value was verified by plate bearing tests. The entire foundation and slab system was designed for enclosure under an insulated cabinet equipped for accurate temperature control.

Loads for the slab tests were provided by a series of pneumatic cells, each constructed for a particular load range; a typical intermediate size is shown in Figure 3, attached to the steel frame used as a reaction member. Load for a given test was transmitted to the slab by a circular metal plate faced with rubber to simulate a flexible loaded area. The diameter of the load plate was varied with the test temperature to maintain an approximation of infinite boundary conditions for the slab.

Measurements of the deflected shapes of the loaded slabs were obtained by a series of linear variable differential transformers located along a radial line from the center of the slab, as shown in Figure 4. The outputs of these transformers were transmitted to an electronic strip-chart recorder located outside the test unit.

In performing a particular test, the slab was placed on the spring base and the transformers were positioned and calibrated. The unit was then covered and the temperature was raised to 140 F for 24 hr, to allow the slab to seat itself on the foundation. The temperature was then adjusted to the test level and the system was permitted to reach equilibrium before actual loading.

The research reported in this paper involved measurements on slabs tested at temperatures of 40, 77, and 140 F. Each slab was loaded a number of times, at successively higher levels of stress. One-half hour was allowed between loadings to permit the particular slab to recover completely (for all practical purposes) its undeformed shape. The load was maintained in each case for a period of 60 sec, and complete records were kept of variations in the deflected shape during that time.

BENDING TEST DATA

The results of the bending tests are shown in Figure 5, in which tensile and compressive strains are plotted against time for the measurements taken at both 40 and 77 F. Each curve shown represents the average of several specimens. Change in tensile and compressive properties (which become increasingly different) with time is clearly evident at both temperatures; at longer times the level of tensile strain is much greater than that of compressive strain. As is to be expected, the data indicate a material considerably stiffer at 40 F than at 77 F; however, the same general pattern of time-dependent behavior is noted.

In an earlier publication (3), a method for predicting slab performance from theoretical computations involving a four-element model was presented. The model properties employed in the computations were derived from the results of triaxial compression tests on the specimen material. However, the comparison of measured deflection profiles with those computed through theory showed considerable discrepancy.

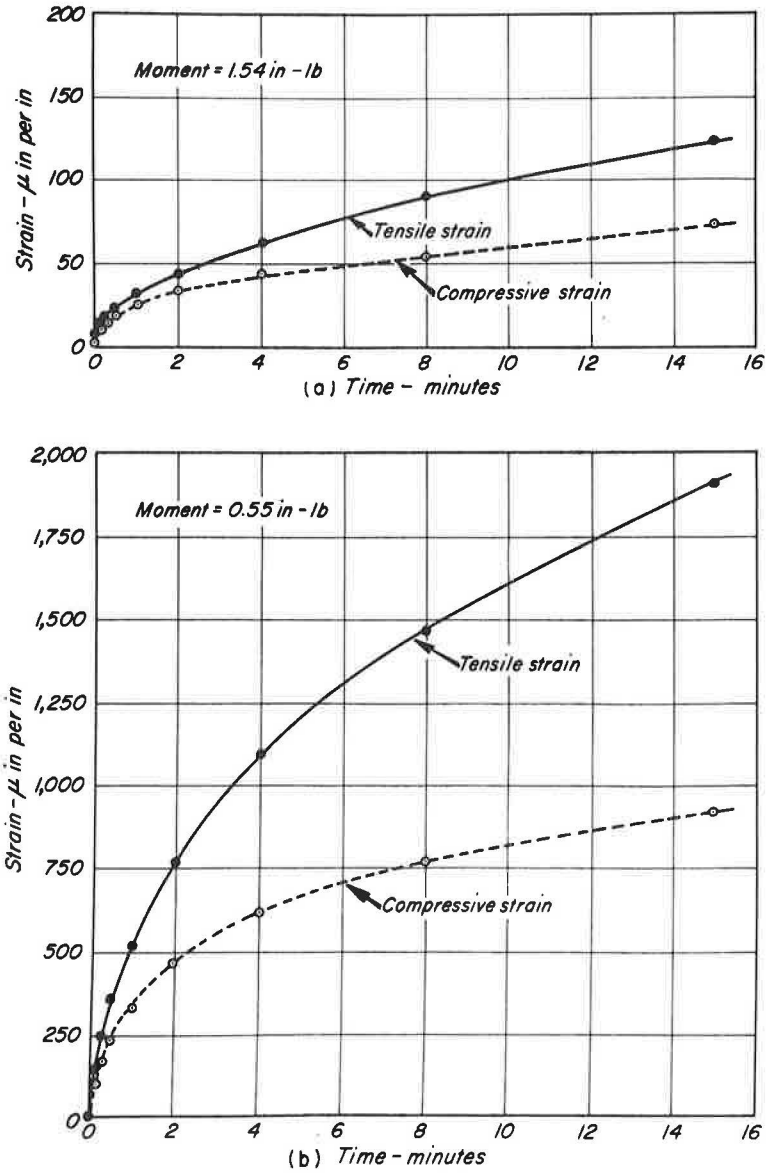

Figure 5. Comparison of tensile and compressive bending strains at (a) 40 F, and (b) 77 F.

One possible reason for this disagreement was a dependence on an assumption that the slab was composed of a material whose characteristics in tension were the same as in compression. Figure 5 clearly illustrates the error involved in this approach.

Establishment of analyses of the behavior of layered systems containing asphalt concrete involving the fewest possible assumptions should, among other things, consider the representation of the asphalt layer as a material with time-dependent properties differing in tension and compression. In addition, this representation should be based on properties measured separately in tension and compression. Unfortunately, this problem, from a mathematical standpoint, cannot be solved practically; thus, a simplified approach must be utilized. One technique is to make use of the relationship developed for pure bending of beams in which the beam material behavior obeys

Hooke's law but whose modulus in tension differs from that in compression (9). For this case

$$\frac{1}{R} = \frac{\epsilon t + \epsilon c}{h} \tag{1}$$

in which

R = radius of curvature of beam;
$\epsilon_t + \epsilon_c$ = maximum fiber strain in tension and compression, respectively; and
h = depth of beam (rectangular cross-section).

In addition, the following expression (9) can be applied to rectangular beams of the type considered here:

$$E_r = \frac{1}{I} \frac{M}{1/R} \tag{2}$$

in which E_r is reduced modulus of material, combining properties in tension and compression; M is applied moment; and I is moment of inertia of beam.

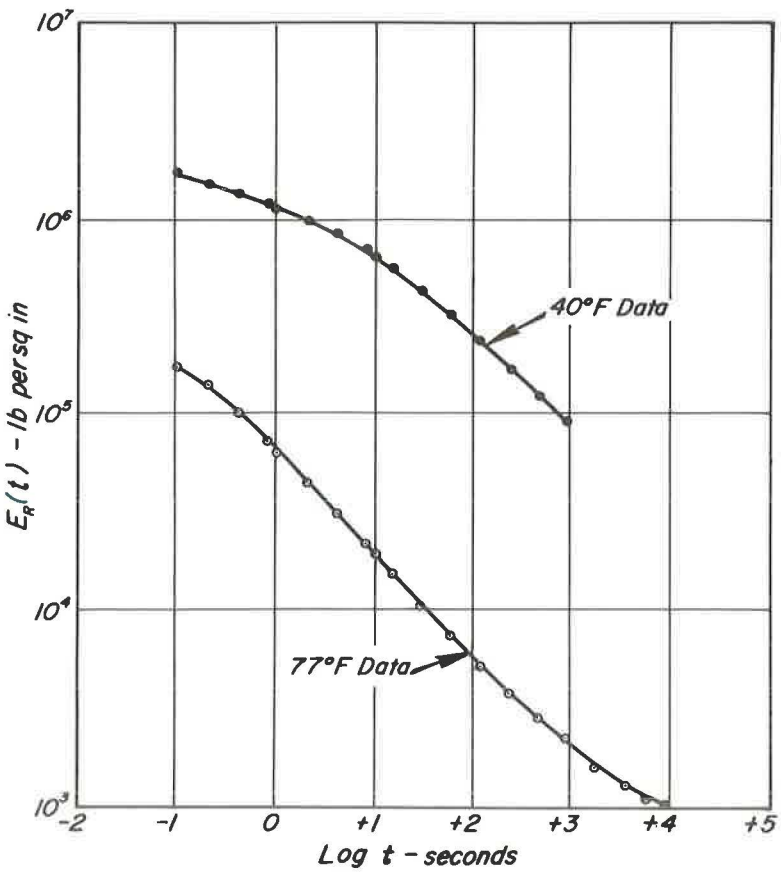

Figure 6. Reduced elastic moduli at 40 F and 77 F vs time.

As noted earlier, it is important to establish the limits, if any, of linear viscoelastic behavior for asphalt concrete. This is necessary to insure validity of certain of the techniques described below. Some data (3) have been published suggesting that the assumption of linear behavior may be acceptable at strains below about 0.3 percent. For this reason the bending test investigation was conducted at strains below this limit and the values of E_r are thus based on relatively small strains.

The data shown in Figure 5 were employed in conjunction with Eqs. (1) and (2) to produce the curves shown in Figure 6. In this figure, values of E_r for the test material at 40 and 77 F are plotted against time; again, a variation with time is evident. Due to the logarithmic character of the plots shown in Figure 6, no values for $t = 0$ (instantaneous moduli) are shown. Data were taken to supply such values, but the limitations of the recording equipment and test instrumentation employed did not permit the accuracy necessary for precise measurements at short times. Therefore, only approximate instantaneous moduli were obtained which are not included.

As has been mentioned, it was not feasible to make bending test determinations at temperatures above 77 F. This problem was handled by the time-temperature superposition principle (6, 10 and 11). In brief, the values of $E_r(t)$ shown in Figure 6 were first adjusted by a factor T_o/T, where T_o is an arbitrary reference temperature and T is a particular test temperature, both measured in absolute units. (This adjustment is based on the statistical theory of rubber-like elasticity; a full explanation of this subject is available in rheologic literature (11). For the work presented in this paper, the reference temperature T_o was selected as 298 K (77 F). A second theoretical correction factor, ρ_o/ρ, based on density changes with temperature, was neglected as being of small importance. This temperature correction shifts the curve slightly vertically.

After the data were adjusted by the T_o/T factor, a corrected plot was made of $T_o/T \cdot E_r(t)$ vs log time, similar to that already shown in Figure 6 for the basic $E_r(t)$ values. By inspection, a value was selected for the dimensionless factor a_T, which would permit horizontal translation (parallel to the time scale) of the 40 F data to permit coincidence with the 77 F data. It should be noted that the shift factor may be defined as:

$$a_T = t_T/t_o \qquad (3)$$

in which t_T is the time required to observe a phenomenon at temperature T, and t_o is the time required to observe the same phenomenon at some reference temperature T_o (10). A value of $\log a_T = 3.36$ was chosen for the bending data at 40 F by techniques which have been well described by Pagen (6). This number is in close agreement with those found by Monismith (12) for two other asphalt mixtures similar to the test material, as is shown in Figure 7.

Figure 8 is composite plot of $T_o/T \cdot E_r(t)$ vs log time at 77 F prepared from the shifted 40 F and the 77 F data. The curve shown represents a major portion of what might be considered a master plot of the reduced bending modulus over an extended time scale. If a_T can be defined for the test material at any temperature of interest, $E_r(t)$ for that temperature becomes available from Figure 8 by means of the time-temperature superposition technique. This concept was used to find values of $E_r(t)$ at 140 F to employ in conjunction with work on the slab deflection profiles. A value of $\log a_T = -4.0$ at 140 F was taken from Figure 7 by assuming a linear relationship between $\log a_T$ and temperature; this approach is supported by the other data shown in Figure 7 and by the work of Pagen (11).

The significance of the concept of reduced variables becomes more apparent when one considers the definition of a_T as indicated by Eq. (3) and the actual magnitude of the shift factor for 140 F as compared to 77 F. The number $\log a_T = -4.0$ indicates that a property defined at a time of 1 sec at 140 F would correspond to the same property defined at 10,000 sec (approximately 3 hr) at 77 F. In addition, the modulus (E_r) at a time of loading of 1 sec at 140 F could be obtained by entering the master curve at 77 F shown in Figure 8 at a time corresponding to 10,000 sec; this would give a value of $T_o/T \cdot E_r$ equal to 1,000 psi. Thus, E_r at 140 F corresponding to a time of loading of 1 sec would equal 1,050 psi.

SLAB TEST DATA

The data obtained from the slab test procedures were first checked for linearity by the procedure illustrated in Figure 9. This figure shows a plot of load vs deflection for one point on the surface of a slab tested at 77 F; the illustrative data are for a time of 20 sec after load application. Similar graphs were made for each point where deflections were measured at a given temperature; at each such point a family of curves was thus obtained, representing various times elapsed after the onset of loading. All curves had the general characteristics shown in Figure 9, indicating nonlinear deflections at small loads and good linearity in the higher stress ranges. Actually, the extent of nonlinearity illustrated in Figure 9 is an extreme case chosen for descriptive purposes; most of the test data exhibited this characteristic to a lesser degree.

The deviation from linearity shown in Figure 9 was thought to be a function of the test apparatus and not of the paving mixture being tested. This is supported

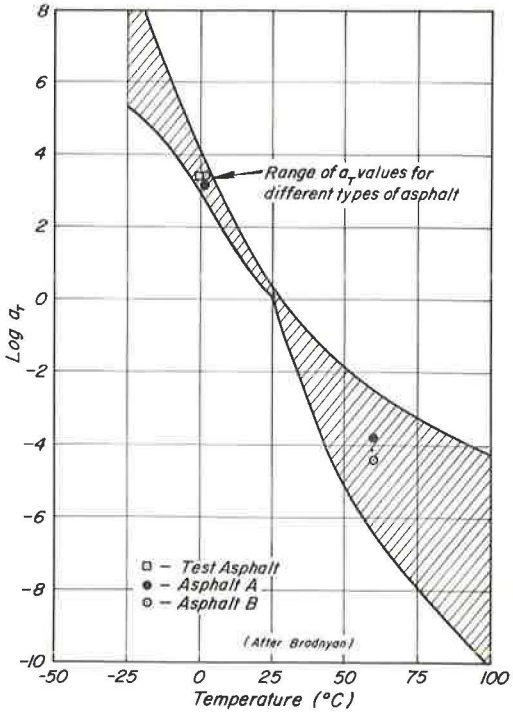

Figure 7. Temperature dependence of a_t values for various asphalts.

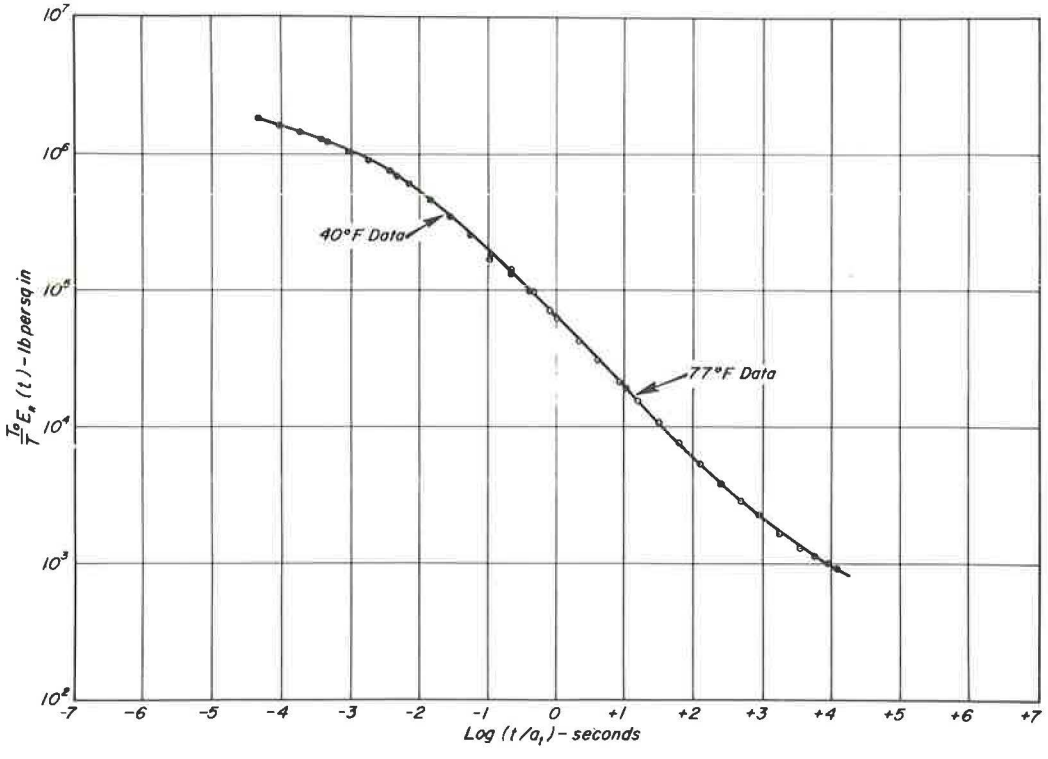

Figure 8. Reduced modulus vs time at 77 F (298 K).

by the fact that the load-deflection curves for the plate tests used to check the design foundation modulus exhibited the same type of performance. It would appear that the difficulty of securing a perfectly uniform contact between the test slab and the spring base resulted in this error. Of far more interest is the performance of the system at higher load levels, where linear responses were obtained in all cases.

To correct for the problem of seating error, all load-deflection data were adjusted to zero by the procedure illustrated in Figure 9. Typical results of this process are shown in Figure 10, where the complete load-deflection-time relationship for a particular point of measurement at 77 F is given.

From adjusted data such as are shown in Figure 10, it was possible to obtain slab deflection profiles for any load and elapsed time after load application. Inasmuch as the load-deflection relationships were linear within the test range in all cases (such profiles would change only in regard to the deflection scale for differences in load level at any particular point in time), only one magnitude of applied load at each temperature is presented herein.

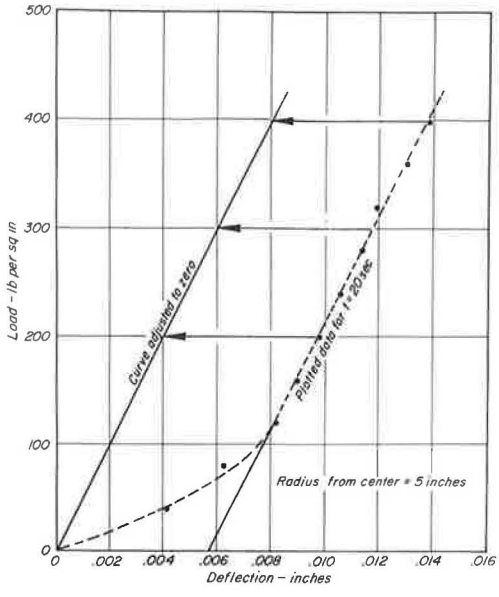

Figure 9. Typical adjustment of slab deflection data to eliminate zero error, 77 F.

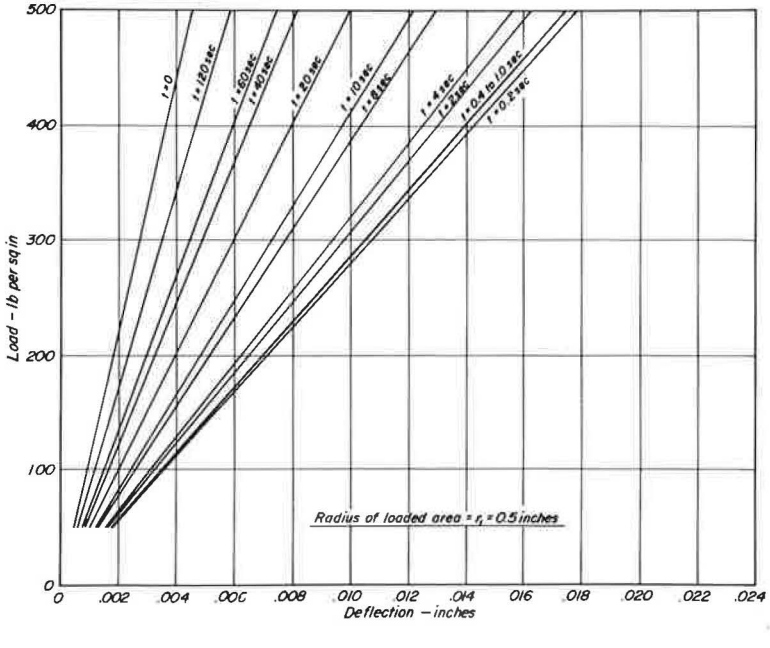

Figure 10. Typical corrected load-deflection-time relationship for point 5 in. from center of test slab, 77 F.

Figures 11 through 14 show measured deflection profiles at various times after loading for slabs at each of the three test temperatures. Also shown in each figure are the radius of the loaded area (r_1) and the intensity of stress (q_o). Figure 15 shows the deflection-time pattern for the centers of the slabs at each temperature.

Also shown in Figures 11 through 15 are deflection-time relationships predicted from the results of the bending tests. These computed values were obtained by applying the values of $E_r(t)$ at each test temperature to a known solution for the deflections of an infinite elastic plate on a Winkler foundation. This problem has been discussed in detail (13), hence only the resulting formulations need to be repeated here:

$$w(r) = \frac{q_o}{k} \int_0^\infty \frac{1}{\left[\left(\frac{\ell_o}{r_1}\right)^4 \lambda^4 + 1\right]} J_1(\lambda)\, J_o\left(\frac{\lambda}{r_1} r\right) d\lambda \qquad (4)$$

in which

λ = an integration variable,

$$\ell_o^4 = \frac{1}{k} \frac{E h^3}{12(1-\mu^2)},$$

E = elastic modulus of slab,

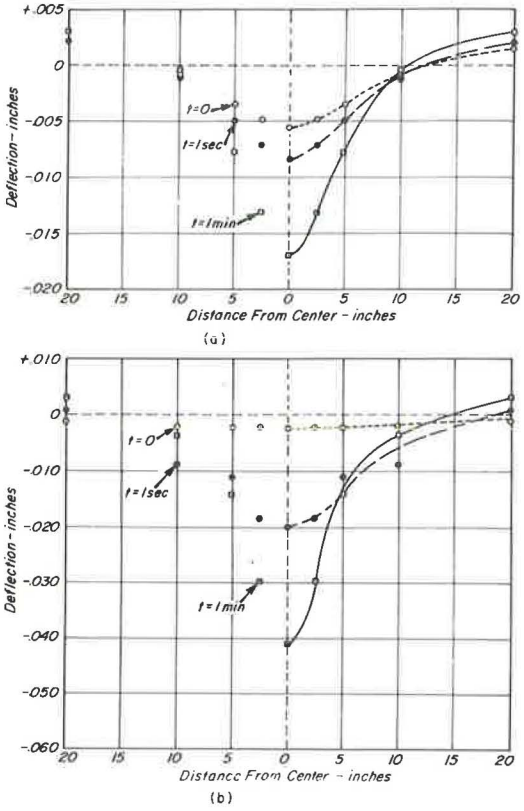

Figure 11. Deflection profiles at various times after load application at 40 F, q_o = 500 psi, r_1 = 0.5 in.: (a) theoretical, and (b) measured.

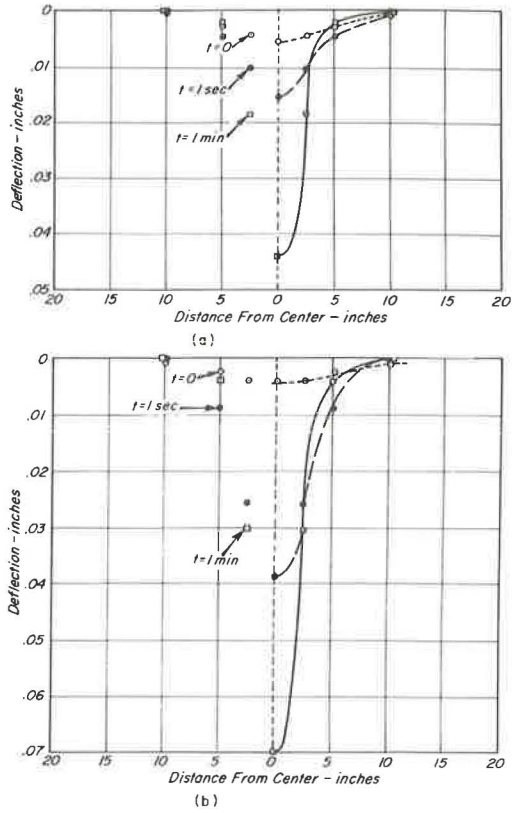

Figure 12. Deflection profiles at various times after load application at 77 F, q_o = 250 psi, r_1 = 0.5 in.: (a) theoretical, and (b) measured.

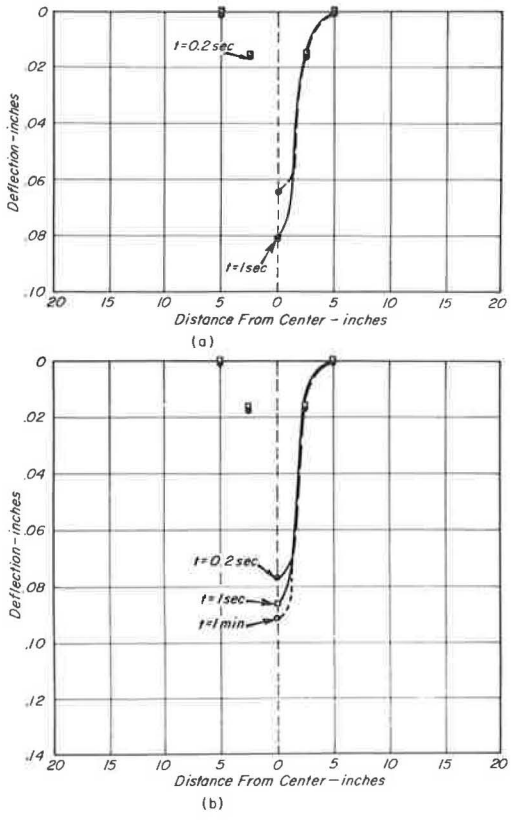

Figure 13. Deflection profiles at various times after load application at 140 F, q_o = 50 psi, r_1 = 1.0 in.: (a) theoretical, and (b) measured.

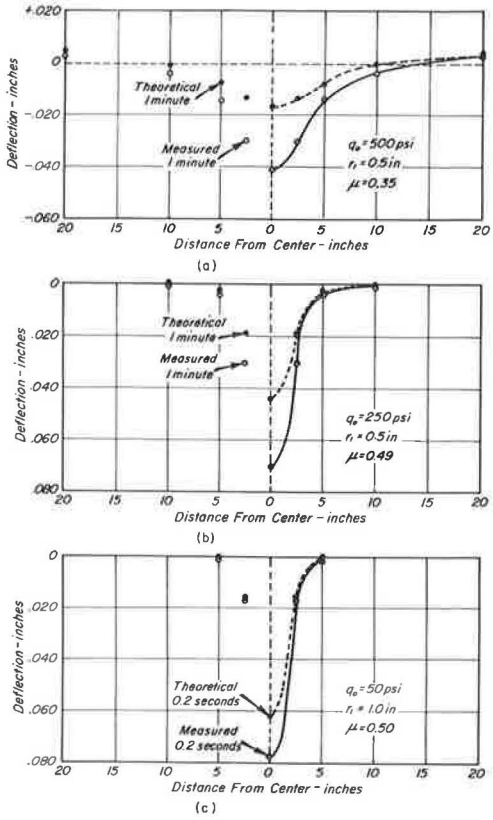

Figure 14. Typical comparisons of theoretical and actual deflection profiles: (a)at 40 F, (b)at 77 F, and (c) at 140 F.

h = slab thickness,
μ = Poisson's ratio of slab material,
r = distance from center of load, and
r_1 = radius of loaded area.

A discussion has been previously presented of the assumptions underlying Eq. (4) and the relation of these assumptions to the type of test reported herein (3). From the viewpoint of this paper, the two most important are those of (a) material properties of plate, the same in tension and compression, and (b) infinite boundary conditions. It is believed that the first of these two assumptions was satisfied by using the reduced moduli E_r in the computations. A discussion of the validity of the second will be dealt with later.

To these two should be added a third assumption, the dependence of Poisson's ratio, μ, on time of loading. In the previous work (3) and in the investigation discussed herein, μ has been assumed constant (time independent) at a particular temperature. Some data were presented previously (3) indicating μ to be essentially constant at high temperatures in a measurable time range; at low temperatures the data indicated μ to be somewhat time dependent. This could cause some differences between theory and measurement at low temperatures because the simple beam creep test is essen-

tially an analog computer for the development of $E_r(t)$. Because of the dimensions of the beam, however, Poisson effects do not influence the test results. In the plate (asphalt slab), on the other hand, the Poisson effect is present because of the biaxial state of stress.

As has been already mentioned, Eq. (4) was used with values of $E_r(t)$ to predict the slab deflection profiles. To obtain deflections for a particular temperature and time after load application, the appropriate E_r was selected from the results of the bending tests. The evaluation of the infinite integral was done numerically, using an IBM 7090 computer. Values for μ were taken from earlier work with the same material (3).

An inspection of Figures 11 through 14 indicates some disagreement between theoretical and measured deflection-time data. The disagreement is most severe at 40 F and least at 140 F. However, the essential ability of the viscoelastic approach to predict the changing shapes of the test slabs is also quite evident, particularly at the higher temperatures. Inasmuch as a purely elastic analysis would provide no means for predicting such changes in shape with time, the relative value of the two analytic systems is obvious.

It should be noted that the use of the modulus $E_r(t)$ as reported here considerably improved the predicted data in comparison with that published earlier, wherein only compression data were utilized. The improvement was most dramatic at 140 F. This phenomenon was to be expected because an assumption of the same behavior in tension and compression for asphalt paving mixtures at high temperatures is naturally poor.

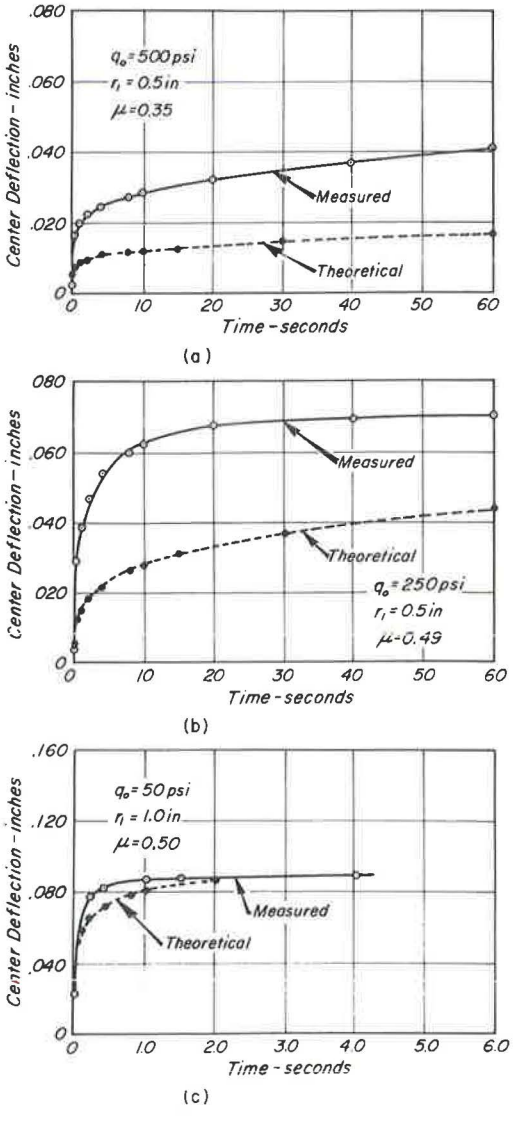

Figure 15. Comparison of measured deflections under centers of loaded slabs with deflections predicted from viscoelastic theory: (a) at 40 F, (b) at 77 F, and (c) at 140 F.

The disagreement between theoretical and measured profiles found at low temperatures was disappointing. However, inspection of these data indicates that the assumption of infinite slab boundaries was not entirely valid (Fig. 11). Theoretical analysis of the problem from the viewpoint of free boundary conditions, an assumption in line with actual test conditions, may possibly improve the comparison. Also, further investigation of the time dependence of μ may be worthwhile.

It is interesting to note that the above approach is similar to that proposed by various Shell researchers (14, 15), wherein a modulus corresponding to a particular time of loading is substituted in an existing elastic solution.

SUMMARY AND CONCLUSIONS

The work presented in this paper represents an evaluation of the usefulness of viscoelastic techniques in the analysis of the performance of structures prepared from asphalt paving mixtures. To provide adequate laboratory control of test conditions, the structure involved was necessarily simple; a similar analysis for a real flexible pavement would require a far more complex theoretical approach. Also, the comparison given here between measured slab performance and that predicted from theory was by no means perfect. Despite these drawbacks, it is felt that the results of this work cannot help but indicate that the viscoelastic approach provides an additional tool for analysis and design of asphalt concrete pavements. Continued investigations along such lines would seem definitely indicated.

ACKNOWLEDGMENTS

The authors wish to thank the staff of the California Research Corp., Richmond, Calif., for the preparation of the asphalt slabs tested in this investigation and George Dierking for his efforts in the preparation of the figures.

REFERENCES

1. Secor, K. E. and Monismith, C. L., "Analysis of Triaxial Test Data on Asphalt Concrete Using Viscoelastic Principles." Proc. HRB, 40: 295-314 (1961).
2. Secor, K. E., "Viscoelastic Properties of Asphaltic Paving Mixtures." D. E. Thesis, Univ. of California, Berkeley (1961).
3. Monismith, C. L., and Secor, K. E., "Viscoelastic Behavior of Asphalt Concrete Pavements." Proc. Internat. Conf. on the Structural Design of Asphalt Pavements, Univ. of Michigan (1963).
4. Pister, K. S., and Monismith, C. L., "Analysis of Viscoelastic Flexible Pavements." HRB Bull. 269, pp. 1-15 (1960).
5. Papazian, H. S., "The Response of Linear Viscoelastic Materials in the Frequency Domain with Emphasis on Asphalt Concrete." Proc. Internat. Conf. on the Structural Design of Asphalt Pavements, Univ. of Michigan (1963).
6. Pagen, C. A., "An Analysis of the Thermorheological Response of Bituminous Concrete." Ph. D. Thesis, Ohio State Univ. (March 1963).
7. Krokosky, E. M., Andrews, R. D., Jr., and Tons, E., "Rheological Properties of Asphalt/Aggregate Compositions." Paper presented at 66th Ann. Meeting, ASTM, Atlantic City, N.J. (June 23-28, 1963).
8. Monismith, C. L., Secor, K. E., and Blackmer, E. W., "Asphalt Mixture Behavior in Repeated Flexure." Proc. AAPT, 30: 188-222 (1961).
9. Timoshenko, S., "Strength of Materials, Part II, Advanced Theory and Problems." D. Van Nostrand and Co., New York (1950).
10. Landel, R. F., and Smith, T. L., "Viscoelastic Properties of Rubberlike Composite Propellants and Filled Elastomers." Amer. Rocket Soc. Jour. (May 1961).
11. Ferry, J. D., "Viscoelastic Properties of Polymers." John Wiley and Sons, New York (1961).
12. Monismith, C. L., "On the Viscoelastic Behavior of Asphalt Concrete." Unpublished report.
13. Timoshenko, S., and Woinowsky-Krieger, S., "Theory of Plates and Shells." McGraw-Hill, New York (1959).
14. Van der Poel, C., "Road Asphalt." Building Materials, Their Elasticity and Inelasticity, ed. by M. Reiner, pp. 361-443, Interscience Publishers, New York (1954).
15. Saal, R. N. J., "Mechanics of Technical Applications of Asphalt." Paper presented before Div. of Petroleum Chem., Amer. Chem. Soc., New York (Sept. 1960).

Modes of Failure and Strength of Asphalt Films Subjected to Tensile Stresses

KAMRAN MAJIDZADEH and MORELAND HERRIN
Respectively, Assistant Professor of Civil Engineering, University of Florida, and Professor of Civil Engineering, University of Illinois

The primary purpose of this investigation was to study the behavior of thin films of asphalts subjected to tensile stresses. A number of theories that might explain the behavior of asphalts or similar materials in thin films are reviewed and the advantages and disadvantages of each theory are discussed. To verify the hypotheses and theories related to tensile properties of asphalts, laboratory experiments were conducted on thin asphalt films under controlled test conditions. The variables studied, selected on the basis of theoretical consideration, were film thickness, rate of extension, temperature, and size of specimen.

The failure of mechanism of asphalt films can be placed in three categories—brittle fracture, tensile rupture, and shear flow—all of which are influenced by the variables studied. Equations are presented for predicting the limiting value of the film thickness corresponding to each type of failure. A hypothesis is also developed that explains this failure mechanism and the behavior of asphalts over a wide range of film thicknesses. It is also shown that two theories—the hydrodynamic theory and the theory of potential energy and cavities—could be used to predict the tensile strength of asphalts in thick and thin films, respectively.

•CRACKING and subsequent failure of bituminous surfaces can often be attributed to excessive tensile stresses induced in pavements by various causes. As a result of the bending of pavements under wheel loads, tensile stresses are developed depending on the relative positions of the load and the point of the pavement under consideration. Tensile stresses may also be developed in certain types of bituminous surfaces, such as surface treatments, as a result of the forward motion of the wheel which tends to dislodge the aggregates from the surface. Also, the nonuniform deformation of underlying surfaces often contributes substantially to these stresses. When these tensile stresses exceed the tensile strength of the asphalt present in thin films between the aggregates, the pavement will fail.

Failure of bituminous mixtures, which depends on the rheological behavior of asphalt, is due not only to simple tension or to simple shear alone, but also depends on the behavior of asphalt subjected to combined stresses. Thus, an understanding of the mechanism of failure and the rheological behavior of the material in simple tension, as well as in simple shear, is required for the final evaluation of any mix design. In turn, the rheological behavior of asphalts under tensile stresses is affected by many factors, including the rate of loading, temperature, and the thickness of the film separating the particles of the aggregate. Because the thickness of asphalt films is influenced by many factors and is expected to be variable in pavements, the strength of the mixture could be better predicted if the behavior of the material were known over a wide range of thicknesses.

Although asphalt is extensively used as a binder for many types of bituminous surfaces, some basic information concerning its behavior and its suitability for each type

Paper sponsored by Committee on Bituminous Surface Treatments.

of pavement is not yet available. A thorough investigation of tensile properties of asphalts in thin films should provide a part of the information required for predicting the behavior of binder in pavements. Such a study should lead to a better understanding of the behavior of asphalts in pavements and eventually to the development of a theoretical method of design.

STATE OF PRESENT KNOWLEDGE

Present knowledge of the tensile properties of asphalts in thin films is limited to studies conducted by Mack (18) and Wood (29, 30). These investigators have conducted a limited but worthwhile study of the behavior of thin films of asphalts under tensile stresses. However, the knowledge of similar behavior of other materials in thin films might be of significant value for obtaining more information about the theoretical behavior of asphalts. Extensive literature exists on the subject of adhesives and other materials. Thin films of asphalts subjected to tensile stresses should behave in a similar manner. Accordingly, a number of theories that might be applicable to asphalts have been investigated to determine if they explain the behavior of this material in thin films.

Strength-Thickness Rule

The "strength-thickness" rule which indicates the dependence of the tensile strength of materials on the magnitude of the film thickness, when tested in thin films, is well established. According to this rule, the tensile strength of thin films of a material, when tested in tension, increases as the thickness of the film decreases. Extensive experimental evidence is available to support the existence of such a rule in liquids, as well as in solids. In liquids, the theoretical and experimental works of Stefan (27) and Reynolds (24) with Newtonian liquid support the existence of such a relationship between strength and film thickness. Their research was later used for the study of non-Newtonian liquids. In solids, the tensile tests carried out by Crow (10) on soldered butt joints between copper rods indicate that the tensile strength increases very rapidly as the film thickness decreases. The existence of such a strength-thickness rule has also been confirmed for many different kinds of adhesives by McBain and Lee (19), Dietz (11), and Meissner and Bauldauf (21), Koehn (15) and other investigators.

Thus, according to the strength-thickness rule, the tensile strength of asphalt in thin films might be expected to vary with the film thickness. The result of investigations by Mack (18) indicates that the tensile strength of asphalts, when plotted on logarithmic scales, increases linearly to a maximum and then decreases as the film thickness continually decreases. On an arithmetic scale this relationship would be in the form of a curve that increases, levels off, and then decreases as the film thickness increases. The experiments on thin films of asphalts conducted by Wood (29, 30) indicate that tensile strength decreases rapidly as the film thickness increases and then eventually levels off with little change in the tensile strength at a film thickness of 200 μ.

A controversial point in the tensile strength-film thickness relationship is the existence of an optimum film thickness. The theoretical and experimental works of Mack (18) indicate the existence of a definite optimum film thickness in the very thin film range. This optimum film thickness varies with the type of asphalt, the viscosity and the temperature. According to this investigator, the theoretical explanation for the optimum film thickness is based on the energy requirement for breaking the bonds between the asphalt molecules. This optimum film thickness is reported to vary from 25 to 50 μ for different types of asphalts. Koehn (15) has reasoned differently as a result of his observations concerning the decrease of tensile strength in the region of very thin films. According to his explanation, the decrease of tensile strength of adhesives at a thickness of almost 10 μ is merely dependent on the lack of uniformity of the films. The presence of gaps or voids in the film or the metal-to-metal contact at the high points of the surface results in reduction of contact area. This could also cause stress concentration in the film. However, the result of an investigation by Wood (29, 30), who has tested asphalt films as thin as 10 μ, does not show that there is any optimum point in the film thickness.

Theories Explaining Strength-Thickness Rule

Many different thoughts and theories have been suggested to explain the strength-thickness relationship of asphalts and other materials in thin films which behave similarly under tensile stresses. These theories, ranging from a purely mathematical expression to simply an expression of thoughts, have failed to explain the behavior of these materials in the entire range of film thicknesses. Most of these theories have not yet been widely accepted and the usefulness of such theories has remained controversial. The most common of these theories are discussed subsequently.

Hydrodynamic Theory.—The strength-thickness relationship of materials tested in tension can be explained to some extent by the hydrodynamic theory, one of the first theories developed to explain the behavior of materials in thin films (21, 22, 24, 27). According to this theory, the flow behavior of thin layers of viscous materials, placed between two parallel plates and subjected to a pull, varies with the thickness of the layer. As the film thickness decreases, a larger stress is required to deform the material to a certain value. Furthermore, when a layer of Newtonian or non-Newtonian liquid is subjected to tension, in addition to deforming in the direction of the applied stress, it flows horizontally between the two parallel plates. In other words, horizontal shear forces are present (22). Because the inward movement of the material in contact with the two plates is prevented, the theory assumes that the flow perpendicular to the direction of the applied stress at any other plane is a parabolic function of the distance between the two plates. Therefore, the inward velocity of the flow, which is a parabolic function of the film thickness, is considerably smaller in the thinner films.

Because the reduction of deformation and flow is the basis of this theory, the hydrodynamic theory could be also named after the mechanism on which it is based. The theories of "restraint of deformation" or "reduction of plastic flow," which are encountered in the literature, are principally the same as the hydrodynamic theory (8, 14, 21, 26).

The hydrodynamic theory is credited to the experimental and theoretical works of Stefan (27) who measured the force necessary to separate, at a given rate, two circular glass disks immersed in a liquid. The mathematical derivation of this theory, which is rather difficult in Stefan's paper, has been simplified by Bikerman (4). For two parallel plates with radius of R, which are completely immersed in a Newtonian liquid with the viscosity equal to η, the relationship between the applied force, F, and the film thickness, H, can be written as follows:

$$F = \frac{dh}{dt} \frac{3\eta\pi R^4}{2H^3} \qquad (1)$$

If the two parallel plates are not immersed in the liquid, and the volume of material does not exceed the volume between the two plates, Eq. 1 can be written as follows:

$$F = \frac{dh}{dt} \quad \frac{3V^2\eta}{2\pi} \quad \frac{1}{H^5} \qquad (2)$$

in which V is the volume of material confined between two parallel plates.

Because Eq. 2 does not properly indicate the flow properties of non-Newtonian liquids, Scott (25) has developed a general formula for this class of materials. The flow of a non-Newtonian liquid that follows de Waele-Ostwald's law can be expressed by

$$\dot{\gamma} = \tau^n / K$$

in which n is a constant of the material and $\dot{\gamma}$ and τ are rate of shear and shear stress,

respectively. The term K is related to the viscosity of the material. When n = 1, the material is Newtonian liquid and K is equal to viscosity, η. Eq. 3 is Scott's formula derived for these materials. In this equation, the sign of the applied load has been reversed in order to be applicable to tensile forces rather than compressive forces.

$$F^n = \frac{dh}{dt} \frac{(2n)^n K (n+2) V^{\frac{3n+1}{2}}}{(3n+1)^n \pi^{\frac{n+1}{2}}} \frac{1}{H^{\frac{(5n+5)}{2}}} \qquad (3)$$

The basic equations thus obtained are adaptable to tests performed with different forms of loading. Strasburger (28) has used such a basic formula for the tests run by the constant velocity of separation. In this case, the term dh/dt in Eqs. 2 or 3 is a constant and is equal to the rate of extension set for the testing machine. In the same equations, it is deduced that

$$H = H_o + t\dot{\delta}$$

in which

H_o = initial thickness of material;

$t\dot{\delta}$ = Δh, the amount of deformation in t seconds of testing;

$\dot{\delta}$ = rate of extension; and

t = time of testing (sec).

Therefore, in a test run with a constant rate of extension, the only unknowns in Eqs. 2 or 3 would be t and F. Given the time of testing, t, the tensile force acting on the material is easily obtained.

The maximum tensile force that can be applied before the film fails is also easily obtained from these equations. So that this might be done, the amount of deformation of the film at the moment of failure ($t\dot{\delta} = \Delta h$) should be inserted in the equations. Moreover, in Eqs. 2 and 3 it is observed that the tensile strength is inversely related to the film thickness. When the film thickness decreases, a higher tensile force is required for the failure of the film. Furthermore, it is indicated that the type of material, viscosity, and rate of loading significantly influence the tensile strength of the film.

Limitations of Theory.—As stated previously, the hydrodynamic theory was founded on the assumption that a material flows slowly between two parallel plates when they are pulled apart. Flow may be considered to be a failure in shear. It is known that horizontal flow occurs as a result of a pressure difference built up in the material by application of external load. However, if the pressure difference is relieved by presence of cavities or air channels, the theory is no longer valid (6). Moreover, if, during the separation of the plates, the material forms into filaments or a number of threads and cavitation results, this theory would be invalid for the remainder of the experiment (2, 12).

Another limitation placed on the theory is Stefan's assumption concerning the rate of loading. For slow rates of loading, according to fundamental assumptions, materials flow laminarly and give way in shear. However, for rapid rates of loading the films rupture without any appreciable flow. The occurrence of a rupture in the film indicates that the failure is governed by tensile rather than shear flow alone. Because the viscous resistance increases with an increase in the rate of load application (23), the flow and deformation of the material between the parallel plates is considerably reduced in a fast rate of loading. Thus, for rapid rates of loading, the work required

to cause the flow of liquid by overcoming the viscous resistance is much greater than the work required to form two new surfaces (work of cohesion) (1). In this case, the failure occurs in tension and the theory is no longer valid.

The viscosity of material pulled between the parallel plates also limits the application of this theory. The influence of viscosity on flow properties of the material is the same as the effect of the rate of loading; i.e., the higher the viscosity of the material, the greater would be the restraint of deformation and flow. Bikerman (6) observed that material with intermediate range viscosities does not flow toward the axis of the whole system, as is predicted by the theory. Rather, it flows toward many centers spread all over the film. At further separation of the plates, filaments or threads start from these points. Bikerman's observation simply proves that the failure of the material is due more to tensile stresses than to shear stresses. As previously stated, this would happen when the flow is restrained by extremely viscous resistance of the material.

The applicability of hydrodynamic theory depends not only on the viscosity of the material or the rate of the loading, but also on the thickness of the material. Because according to this theory, the velocity of flow in the horizontal direction is a parabolic function of the film thickness, the flow in thin films is considerably less than in thick ones. In thin films, where the material is more restrained from the flow, tensile stresses are developed and failure occurs in tension (22). The experiments conducted by Bikerman (5) on an asphalt film of 1 μ thickness indicate that failure occurred by rupture at a much smaller load than predicted by the theory. Of course, his experimental result is also influenced by the viscosity of the asphalt.

It should be stated that the foregoing discussion on the applicability of the hydrodynamic theory in thin films holds true only for the case of testing in tension.

Theory of Potential Energy and Cavities.—According to this theory, when a material fails in pure tension, the strength is partly a function of secondary valence forces between adjacent molecules (18). Because with an increase in distance between molecules the repulsive forces diminish more rapidly than attractive forces, the attractive forces would primarily govern the strength of the material. The energy associated with attractive forces is inversely proportional to the sixth power of the distance between the adjacent molecules (17). Tensile rupture, however, occurs in the material when the applied force equals the maximum force due to the potential of the secondary bonds. This theoretical strength, which is a constant of the material, depends on the degree of the packing of molecules in that material (18). Materials with closely packed molecules are characterized by molecules of low potential energy and have higher theoretical tensile strength than materials with loosely packed molecules.

To explain the strength-thickness rule of materials with this theory, the influence of cavities and orientation of molecules on theoretical strength should be considered. Mack (18) has stated that because of these cavities, the rupture stress is lower than the theoretical value and varies with the number of cavities. Because cavities are associated with an increase in volume and are dependent on the tensile strain, it can be concluded that film thickness influences the observed rupture stresses. Furthermore, the change in the orientation of molecules at different film thicknesses influences the strength-thickness relationship.

The relationship obtained between tensile strength and film thickness, according to this theory, can be expressed by the following equation:

$$\sigma = A\left(\frac{\Delta h}{H_o}\right)^{-a} \tag{4}$$

in which

σ = tensile strength;
H_o = film thickness;
Δh = amount of deformation to failure, assumed to be constant in a given asphalt;

A = constant related to rheological properties of asphalt; and
a = constant related to composition and type of asphalt.

A similar equation can be obtained by relating the maximum stress and the strain:

$$\frac{\sigma_m}{\sigma} = \left(\frac{\epsilon}{\epsilon_m}\right)^a \quad (5)$$

In this equation, ϵ_m is the maximum strain at the maximum stress, σ_m, and ϵ corresponds to strain at stress σ. Eq. 5 can also be written as:

$$\frac{\sigma_m}{\sigma} = \left(\frac{h_m}{h}\right)^a \quad (6)$$

in which σ_m and h_m are maximum film strength and optimum film thickness, respectively. σ corresponds to film strength at any other film thickness, h. The constant a in these equations is positive when $h < h_m$ and negative when $h > h_m$. In the region where a is positive, the secondary bond forces are strong and probably cause orientation of the molecules. In the region where a is negative, however, the secondary bond forces diminish with increasing film thickness. The constant a is also a measure of the degree of packing of molecules in the film.

As Eqs. 4, 5 and 6 indicate, the film thickness influences the tensile strength of asphalt films. As the film thickness increases, the tensile strength increases to a maximum and then decreases with further increase in film thickness. In addition, the tensile strength and the strength-thickness relationship is affected by the electrochemical and the molecular forces in the asphalt. The constant a in those equations, as reported by Mack, varies from 1.484 for coal tar pitch to 0.253 for Venezuelan oxidized asphalt. Mack also indicates the optimum film thickness for the different materials studied varies from 25.8 to 51.4 μ.

Discussion and Limitation of Theory.—The theory of potential energy and cavities, according to Mack's deductions can be used to explain the behavior of thin films of asphalts subjected to tensile stresses. His theoretical and experimental observations indicate that when tensile strength is plotted against film thickness on a logarithmic scale, it increases linearly with film thickness up to an optimum thickness, then decreases linearly with further increase in film thickness. At this optimum film thickness, the constant a in Eqs. 4, 5 and 6 changes from positive to negative, indicating the occurrence of changes in the secondary bond forces. In films thinner than optimum, secondary bond forces are stronger and probably cause the orientation of asphalt molecules. In films thicker than optimum, the secondary bond forces diminish with an increase in film thickness.

According to the basic assumptions, this theory is applicable only when no flow occurs in the asphalt. The asphalt film behaves as a solid. It is known from the hydrodynamic theory that in very thin films where flow is restrained, the material would be subjected only to tensile stresses. Therefore, this theory might be applicable only to very thin films where, due to the restraint of flow, the shortcoming of the hydrodynamic theory is obvious. Moreover, it is assumed that the amount of deformation-to-failure (Δh) is a constant for a given asphalt.

Other Theories.—To explain the extraordinary behavior of materials in thin films, other theories such as those of oriented molecular layers, probability of flaws, and internal stresses have been suggested. The theory of oriented molecular layers (20) is based on the extent to which molecules in a liquid are oreinted when they are in contact with a solid. In thin films, the oriented layers may extend well into the material, whereas in thick films, such layers only occur in a limited depth of film. From this, it is expected that thin films would be stronger than thick ones. The theory of probability of flaws (3) relates the tensile strength of a thin film to the number of flaws in the specimen. This theory states that there is a greater chance of finding severe flaws in a thick film than in a thin film. The third theory is the theory of internal stresses (21) which suggests that internal stresses developed in the specimen are responsible for the behavior of materials in thin films.

The applicability of these theories to materials such as asphalts is limited. It is indicated that the range of surface forces of solids which affects the orientation of molecules in an asphalt film is not quite significant (7, 9, 13, 14, 16, 18). Similarly, theories of probability of flaws and internal stresses are not applicable to asphalts which by their internal viscous flow neutralize any developed stresses (8, 14, 22).

Factors Influencing Strength-Thickness Rule

Because many of the factors influencing behavior of other materials might identically affect the behavior of asphalts in thin films, a review of these is quite important. The factors listed in this section are, however, limited only to those influential factors encountered in the literature, i.e., type, viscosity, and surface tension of asphalt; type and surface roughness of adherends (materials bonded by adhesive film); specimen arrangement; shape and size of specimen; rate of loading; and temperature.

MATERIALS

The bituminous material used in this investigation was a paving grade asphalt produced by Shell Oil Company. The properties of the asphalt are as follows:

Penetration at 77 F	72
Ductility at 77 F	150 cm +
Specific gravity at 60 F	1.015
Flash point COC F	600
Spot test	Negative
Percent soluble in CCl_4	99.86
Avg. molecular wt (20 samples)	1,056

APPARATUS AND TESTING PROCEDURE

The asphalt specimens were prepared by a standardized procedure. A small amount of the asphalt was placed between two aluminum blocks of known area and weight. Test blocks were carefully cleaned with n-pentane and accurately weighed to the nearest 0.0001 g on an analytical balance. Test blocks and asphalt were gently heated to allow suitable flow to provide better adhesion and to eliminate any air bubbles which might be trapped in the asphalt. To obtain uniform film thickness, test blocks with the asphalt between them were placed under an apparatus which, by its head weight, kept the test blocks in a parallel position. After the films were formed, specimens were allowed to cool for at least one-half hour to reach room temperature. Excess asphalt was removed and the sides of the blocks were carefully cleaned with solvent. After weighing the prepared specimen, the weight of the asphalt was obtained by subtracting the weight of the test blocks from the total weight. Because the area of the blocks and the specific gravity of the asphalt were known, the thickness of the asphalt film could be calculated.

The specimens were then placed in a controlled-temperature water bath for a period of at least one-half hour to make sure that the asphalt reached the desired temperature. After this period, the specimens were placed on the testing apparatus which was surrounded by a small constant-temperature water bath.

Special apparatus was developed for use in testing the circular shape specimens arranged as butt joints. In this apparatus, cylindrical test blocks, 1 in. high and 1 in. in diameter, were used to hold the asphalt specimens. These aluminum blocks had matched surfaces machine polished, and could be screwed to two vertical rods connected to the platforms of the hydraulic machine. Special spherical head arrangements were provided for the connection of the rods to these two platforms (Fig. 1). To control the temperature of the specimens during testing, a small water bath made of Plexiglass was placed on the lower platform. To prevent leakage from the water bath, the

bottom rod passing through the bottom of the bath was sealed by a rubber membrane. A microscope equipped with a measuring rectile and adjustable hairline was mounted on the lower platform (stationary platform) to measure the deformation of the film (Fig. 1).

A Riehle hydraulic testing machine with a load capacity of 60,000 lb and a calibrated accuracy of 2 lb was utilized in this investigation. All tests were carried out with a constant rate of extension ranging from 0.005 to 1.0 in./min. In addition to a strain pacer that was an integral part of the machine, an Ames dial was connected to the machine to measure the speed of testing.

EXPERIMENTAL RESULTS

To study the tensile properties of asphalts in thin films and verify the hypotheses and theories, a laboratory investigation was conducted on thin asphalt films under controlled test conditions. The variables studied were selected from the available information related to the general behavior of materials in thin films. These variables were film thickness, rate of extension and temperature. All experiments were conducted over a range of film thicknesses from 10 to 1,000 μ and by varying one factor at a time while holding the other constant. The rates of extension studied were 0.005, 0.02, 0.1, and 1.0 in./min; the temperatures used were 32 F (0 C), 68 F (20 C), 77 F (25 C), 86 F (30 C), 95 F (35 C), and 113 F (45 C).

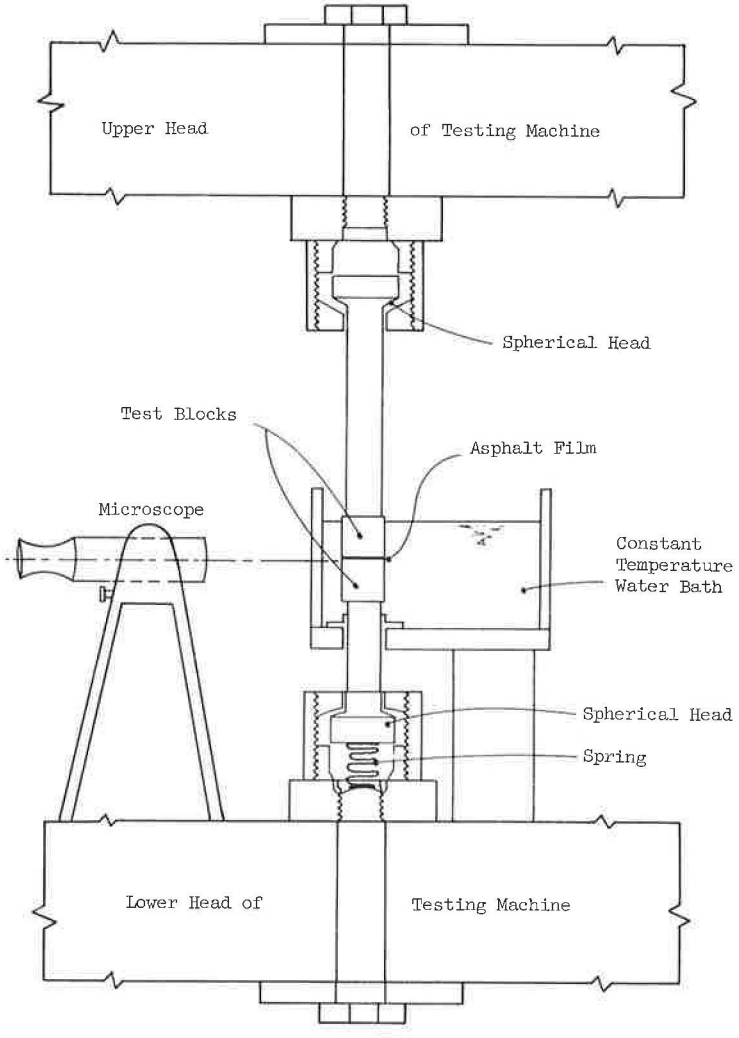

Figure 1. Schematic diagram of test apparatus for butt-type specimen arrangement.

It might appear that the consistency and type of binder were not considered as a variable in this investigation and, consequently, the conclusions would be seriously limited. The study did include these variables, but these data were not reported. The conclusions and theoretical considerations presented herein, however, were verified by the study of the different binders.

Load-Deformation Characteristics and Failure of Asphalt Films

The load-deformation characteristics of viscoelastic materials such as asphalts are known to be dependent on the rate of loading and the temperature (23). (Viscoelastic materials are those materials which, under various conditions, will act both elastically and plastically. The load-deformation characteristics of these materials are time dependent.) However, when the material is tested in thin films, the load-deformation characteristics, as indicated by laboratory test results, are also significantly influenced by film thickness (Figs. 2 and 3).

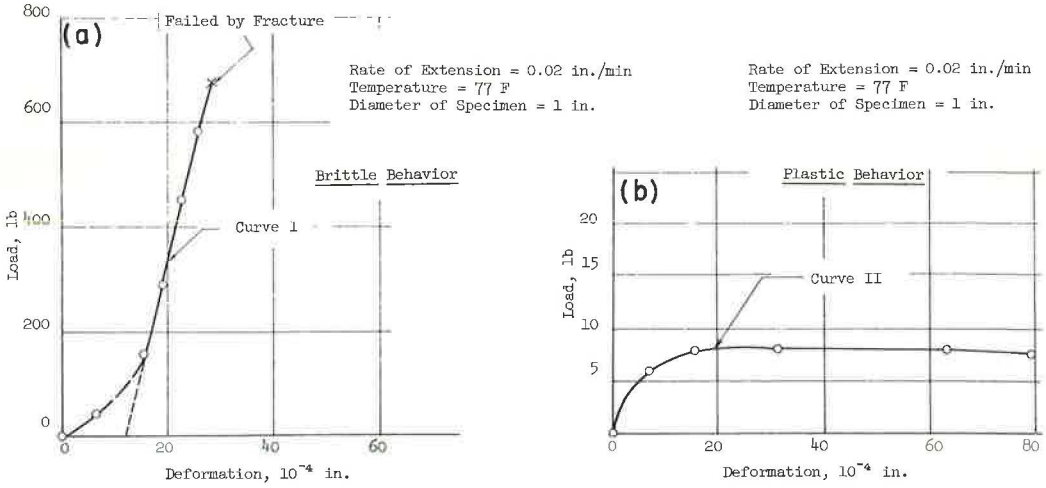

Figure 2. Typical load-deformation curves: (a) extremely thin (21.5 μ) asphalt film, and (b) extremely thick (1,490 μ) asphalt film.

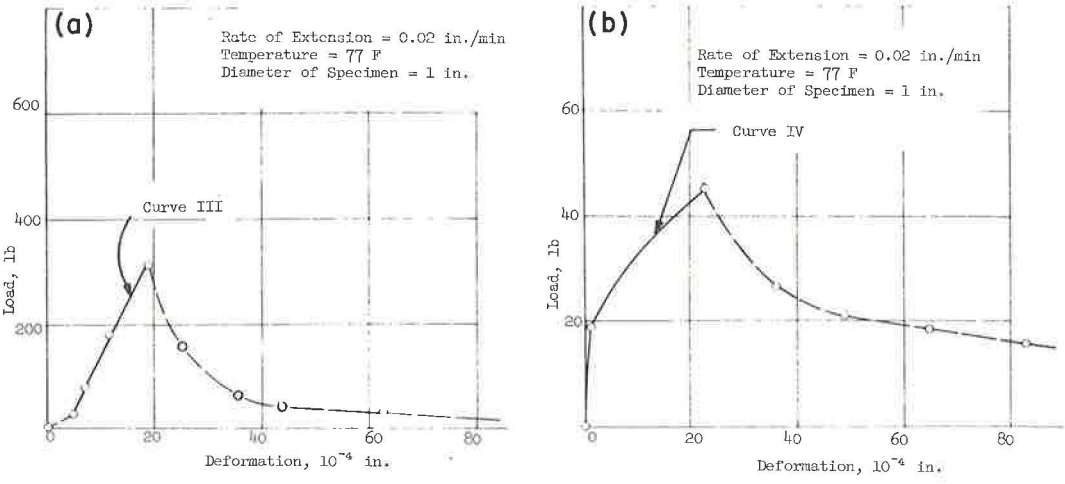

Figure 3. Typical load-deformation curves for intermediate asphalt film thicknessess: (a) 119 μ, and (b) 711 μ.

In Figure 2a, Curve I indicates that under the conditions shown, the asphalt present in a thin film (21.5 μ) behaved as a brittle material and the specimens separated instantaneously after the load reached the maximum. This type of behavior and linear load-deformation curve are characteristic of thin films of asphalt. The range of film thicknesses at which specimens fail by a brittle fracture depends on the test conditions and constitutes a "brittle" zone. The thickest film which may fail by brittle fracture is chosen as the limit of brittle fracture and is denoted by H_B.

Under identical conditions of temperature and rate of extension, asphalt behaves as a plastic material when tested in very thick films (1,490 μ). Curve II (Fig. 2b) indicates that, in contrast to brittle films, the load-deformation curve is not linear because after the load reaches the maximum, plastic flow occurs in the specimen. This type of failure, characterized by beginning of flow and necking in the asphalt films, was observed only in thick specimens. The range of film thicknesses at which such a type of failure was observed depends on test conditions and constitutes a so-called flow zone. The thinnest film which may fail by flow is chosen as the limit of "flow condition" and is identified by the notation H_F.

In Figure 3, two other distinct types of load-deformation curves are shown. Curve III (Fig. 3a) corresponds to the load-deformation curve of a relatively thin (119 μ) film of asphalt which is slightly thicker than H_B. This curve is a typical load-deformation curve obtained for films which failed predominately by tensile rupture. The load-deformation curves of these film thicknesses were linear, and there was a rapid decrease in load after the maximum load was reached. In contrast with very thin films, no fracture occurred in the film, and the specimen, after reaching the state of failure, could still carry a reduced load. Curve IV (Fig. 3b) is a typical load-deformation curve for films slightly thicker than H_F which fail predominately by flow. The load-deformation curves of these films were no longer linear. However, the load continued to decrease gradually after reaching maximum load. The behavior of such films is in transition between the behavior shown by Curve III and that shown by Curve II. Because flow and necking also occur to some extent, in these films this transition zone has been combined with the flow zone to differentiate between the failure by flow and failure by tensile rupture. That is, films thinner than H_F fail by tensile rupture, whereas those thicker than H_F fail predominately or entirely by flow.

In types of failure shown by Curve III (Fig. 3), when the material reached the state of failure, cavitation occurred in the film due to localized failure by separation. As a result of cavitation, filaments were formed which carried a reduced load for greater deformation. Fewer cavities and filaments were observed in thicker films than in thin films. In fact, in very thick films, represented by Curve II (Fig. 2), no filaments were observed; rather, the film flowed inward and necked to a single thread which broke after a very large deformation. When the filaments formed in thin films were broken and the test blocks were completely separated, a honeycomb pattern was observed on the surface of the film (Fig. 4). The depressions seen in the honeycomb pattern are associated

Figure 4. Failed specimens.

with the cavities or the small rupture planes in the film, whereas the ridges are formed by filaments receding to the surface. The size of these honeycombs as well as the number of such impressions in the surface depends on the thickness of the specimen. In thinner films, the size of honeycombs is smaller, whereas the number of these impressions increases as the thickness decreases.

Figure 4 shows the surface pattern of films after failure and separation of the test blocks. The film of Specimen 1, tested at low temperature and a high rate of extension, failed by brittle fracture. The film of Specimen 2 failed by tensile rupture and the honeycomb pattern may be seen on the surface. Specimen 3 consisted of a thick film which failed by flow and necking.

Amount of Deformation at Failure

The amount of deformation at failure, part of the load-deformation characteristics of the asphalts, requires a separate and more detailed investigation. The theoretical information available concerning the amount of deformation to failure (18) indicates that in the very thin films such a deformation is a constant for a given asphalt. This has been attributed to the molecular attractive forces of the asphalt and to the distance that molecules should be separated before rupture occurs in the film. In this regard, the experimental data collected in this investigation indicate that some unique relationships exist between the amount of deformation at failure and the variables studied. The amount of deformation at failure (Δh) is defined as the strain at maximum load. When corrected for intial curvature of the stress-deformation curve and plotted against film thickness, Δh appears to be less scattered and linearly related to film thickness (Fig. 5). (This initial curvature at small deformations is believed to result from seating and adjustments in testing apparatus.)

In Figures 5 and 6 the amount of deformation to failure has been plotted for different temperatures and rates of extension. These figures indicate a linear relationship between the amount of deformation to failure and film thickness. Moreover, the amount of deformation at failure seems not to be significantly influenced by the variables studied. Statistical analysis of these data indicates no significant difference in the amounts of deformation. Thus, for all practical purposes, the amount of deformation at failure

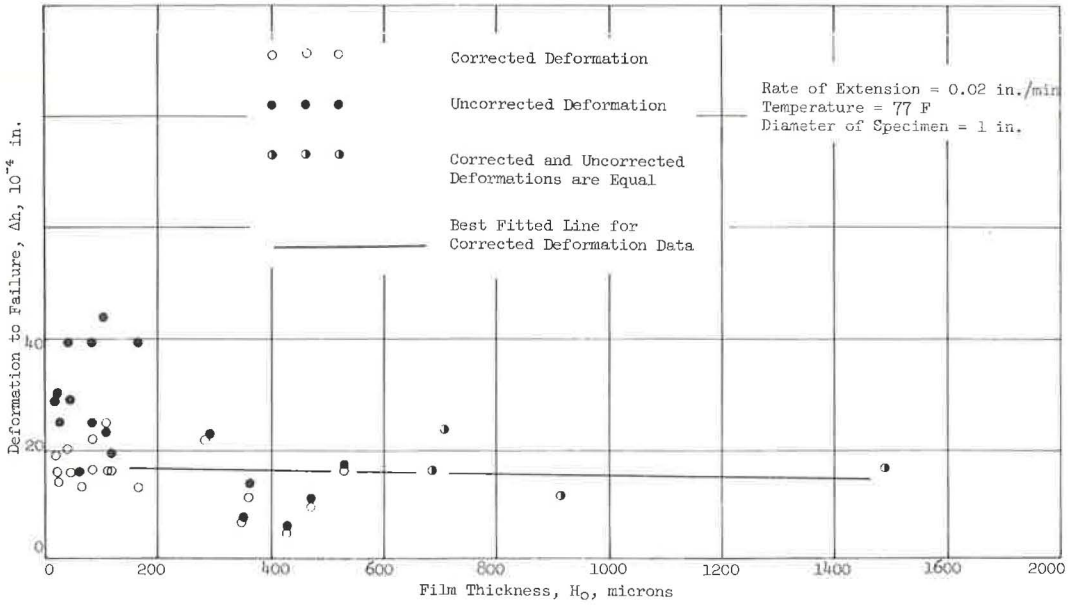

Figure 5. Relationship between deformation to failure and film thickness.

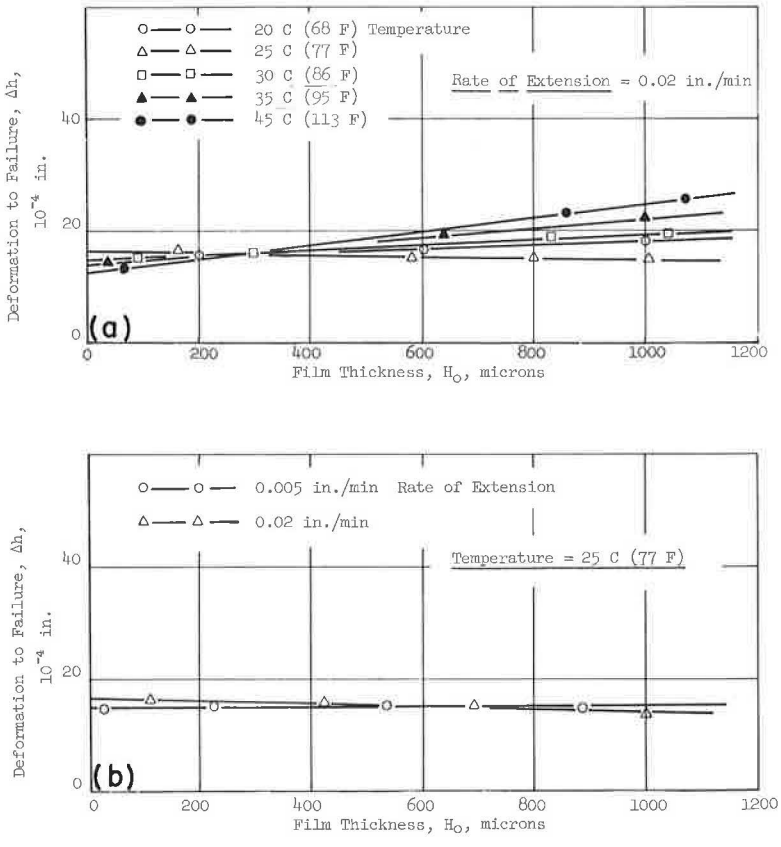

Figure 6. Calculated relationship of corrected amount of deformation to failure with film thickness: (a) effect of temperature, and (b) effect of rate of extension.

can be assumed constant regardless of film thickness, the rate of extension or the temperature.

Influence of Film Thickness on Tensile Strength

The shape of tensile strength-film thickness curves indicates a variation in the behavior of the asphalt at different film thicknesses. Figure 7, which is on an arithmetic scale, shows the relationship of tensile strength to film thickness at 77 F and 0.02 in./min rate of extension. According to this figure, the rule that "the thinner the film the higher the tensile strength" also holds true for asphalt films. In Figure 8, the same experimental data have been plotted on logarithmic scales. Lines A and B correspond to the predicted tensile strength by the hydrodynamic theory and the theory of potential energy and cavities, respectively. These lines will be discussed later. It is observed that there is a straight line relationship between the film thickness and tensile strength in the thick film range when data are plotted on these log-log scales.

When the experimental data plotted in Figure 8 are plotted on semilogarithmic scale (Fig. 9), a unique relationship is obtained. In this plot the upper curved portion of Figure 8 which corresponds to thin film range is represented by a straight line. This straight line, as will be explained later, corresponds to the range of film thickness at which failure appears to be predominately due to pure tensile stresses. The curved portion in Figure 9, however, corresponds to the thick film range where the asphalt films failed predominately by flow. Whereas behavior of thick films of asphalts can be predicted by the hydrodynamic theory, the behavior of asphalts in thin films can be

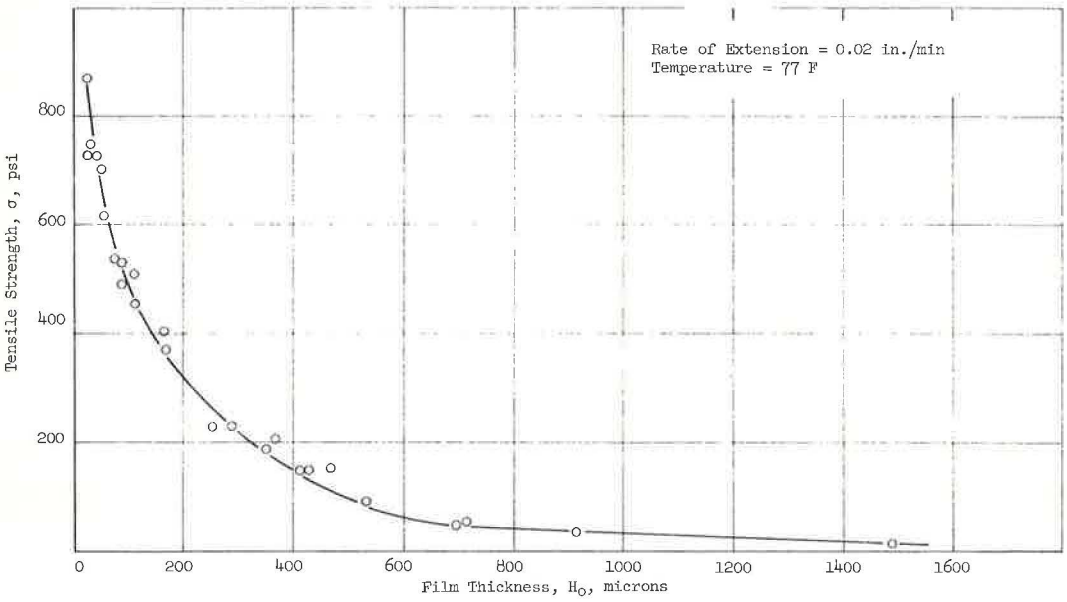

Figure 7. Influence of film thickness on tensile strength.

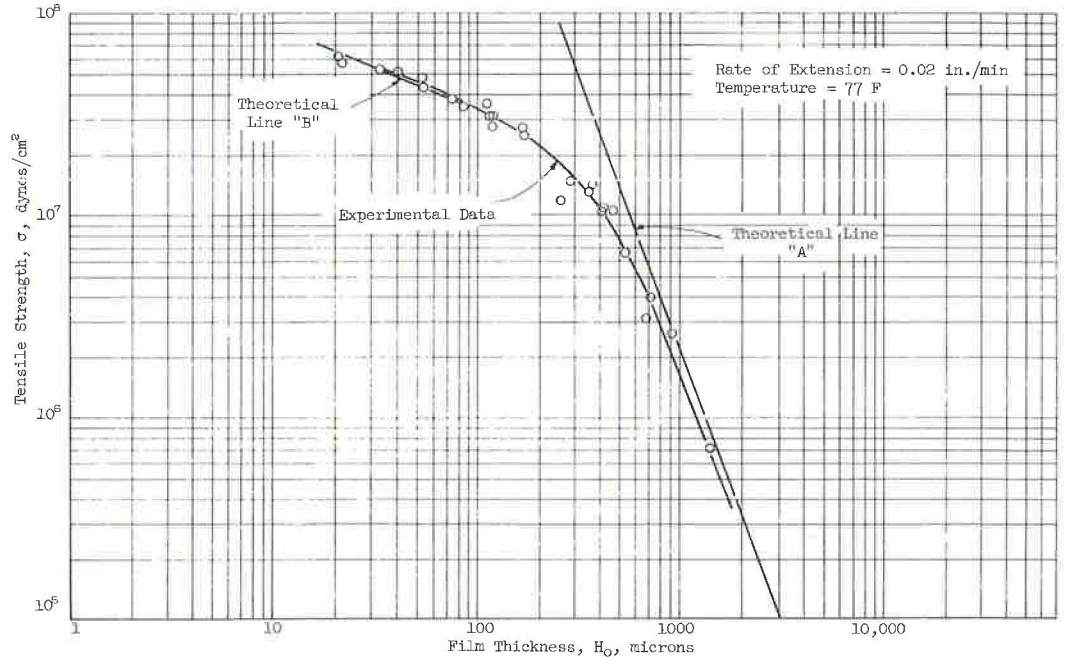

Figure 8. Influence of film thickness on tensile strength.

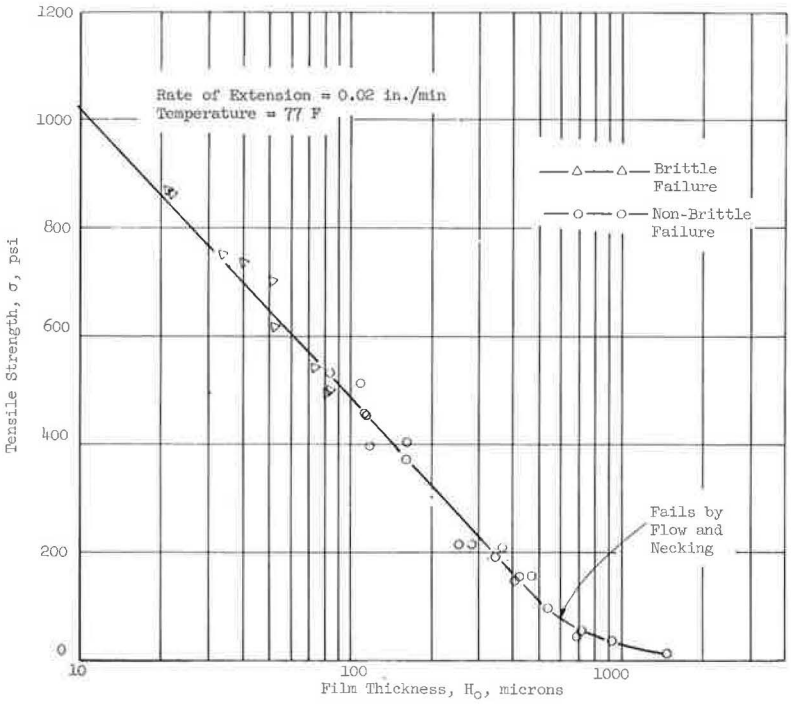

Figure 9. Influence of film thickness on tensile strength and types of failure.

predicted by a general equation derived for the straight portion of the curve on a semi-logarithmic plot. For example, the equation of the straight part of the curve in Figure 9 is:

$$\sigma = 1568.09 - 538.25 \log H_o \qquad (7)$$

in which

σ = tensile strength of asphalt film (psi), and
H_o = film thickness (μ).

H_o is limited by H_F and should only be smaller than or equal to H_F.

Influence of Rate of Extension on Tensile Strength

To study the influence of rate of extension on tensile properties of asphalt films, tests were conducted with different rates of extension, varying from 0.005 to 1.0 in./min and at a temperature of 77 F. The experimental data presented in Figure 10 indicate that the tensile strength is considerably influenced by the rate of extension. The higher the rate of extension, the greater is the tensile strength. Furthermore, the straight lines representing the relationship of tensile strength to film thickness in thin films are parallel for all rates of extension. This figure shows that the limit of brittle failure zone extends to the thicker film range as the rate of extension increases. The curved portion occurring in the thick film range of the strength-thickness relationship is also shifted to the thicker film range as the rate of extension is increased.

Statistical analysis indicates that the slopes of strength-thickness relationships for thin films are parallel to each other. The equation obtained for these series of lines is as follows:

$$\sigma = 1972.4\, \delta^{0.064} - 537.75 \log H_o \qquad (8)$$

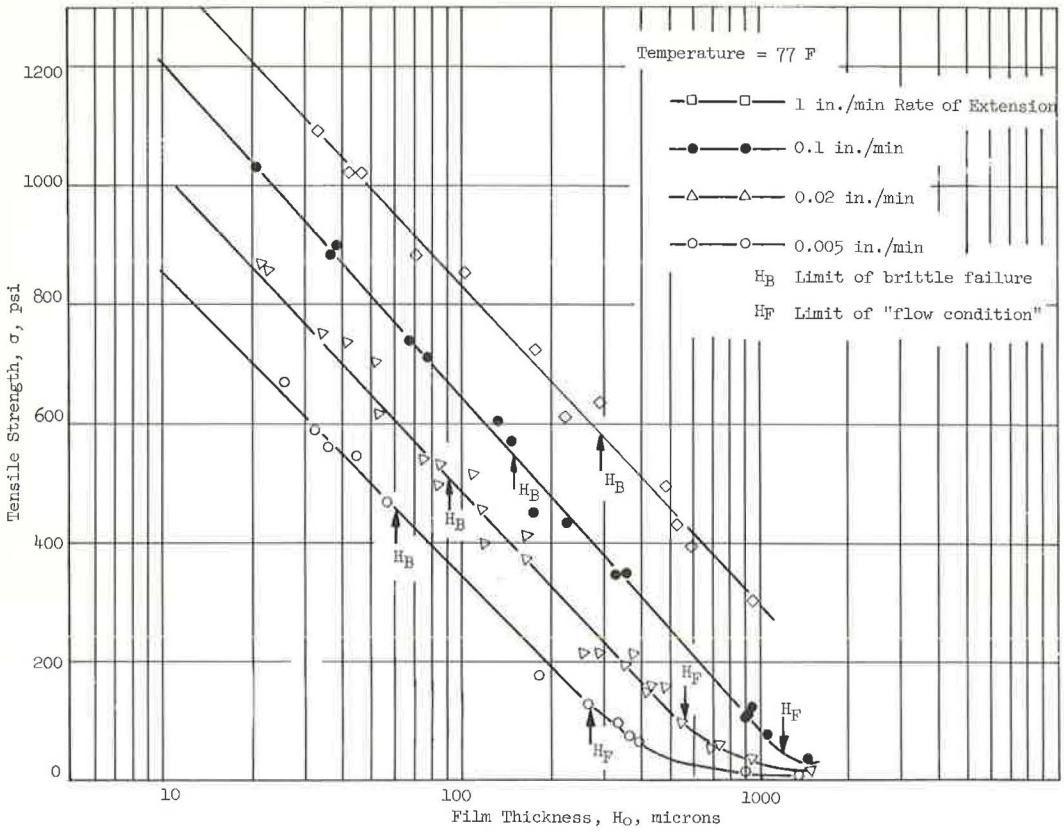

Figure 10. Influence of rate of extension on tensile strength.

in which

σ = tensile strength of asphalt in thin films (psi), and

$\dot{\delta}$ = rate of extension (in./min).

This numerical equation enables the prediction of the tensile strength of the asphalt in thin films at a temperature of 77 F. However, the general form of this equation might be used for all types of asphalts to predict the variations of tensile strength with film thickness and the rate of extension.

In Figure 10, the limit of brittle failure, H_B, and the limit of flow condition, H_F, are also plotted for different rates of extension. The asphalt in all films thinner than H_B behaves as a brittle material. All films thicker than H_F failed by flow. The film thicknesses at H_B and H_F are plotted in Figure 11. It is observed that as the rate of extension increases, H_B and H_F are shifted to the thicker film range. In this figure the lines representing H_B and H_F appear to be straight lines on a logarithmic scale.

Influence of Temperature on Tensile Strength

The effect of temperature on tensile properties of asphalt films was also studied. Tests were carried out over a temperature range of 0 to 45 C (32 to 113 F) with a constant rate of extension equal to 0.02 in./min. Figure 12 represents the relationship existing between the temperature and the tensile strength of asphalt for varying film thicknesses. Films of the same thickness have greater tensile strengths at lower temperatures. In this figure, it is also observed that the relationship existing between the tensile strength and the logarithm of film thickness is linear in the thin film range.

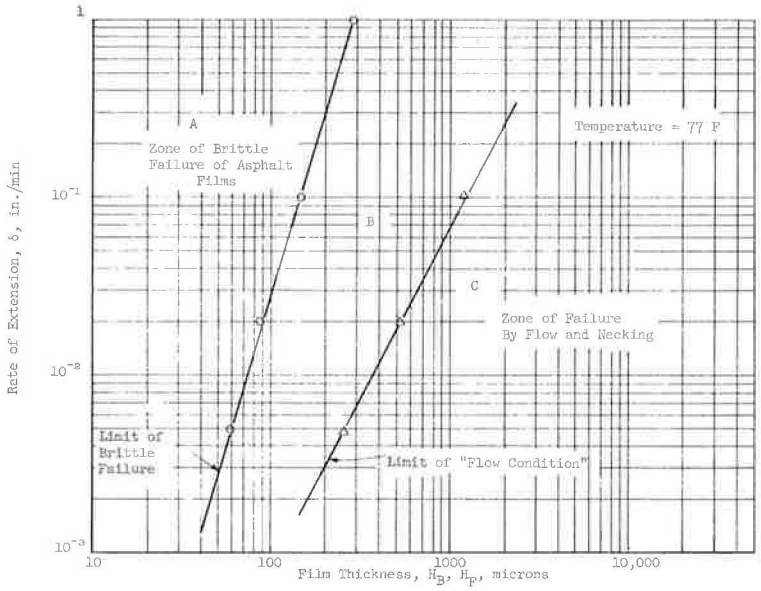

Figure 11. Influence of rate of extension on types of failure.

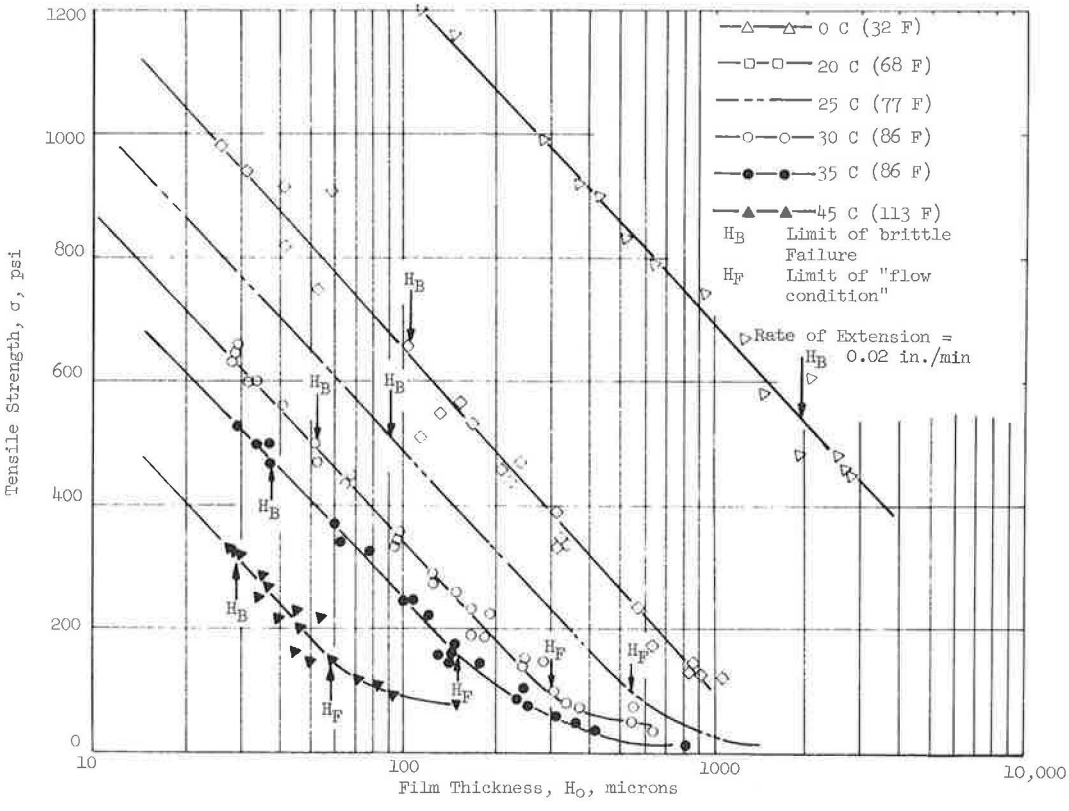

Figure 12. Influence of temperature on tensile strength.

The curved portions in the graphs corresponding to the different temperatures indicate the range of the film thickness at which the failure of asphalt is characterized by flow. The straight portion of the tensile strength-film thickness relationship corresponds to the range of film thickness at which asphalt films failed by either brittle fracture or tensile rupture. An analysis by covariance methods indicates that temperature significantly influences the location of these lines; however, the slopes of the linear portion of the lines are not affected by temperature and can be assumed equal.

In Figure 13, H_B and H_F are plotted for different temperatures. As temperature decreases, H_B is shifted to the thicker films. H_F is similarly affected by the temperature; that is, as the temperature decreases, the limit of "flow condition" extends to the thicker film range.

THEORETICAL EXPLANATION OF BEHAVIOR OF ASPHALT FILMS UNDER TENSILE STRESSES

In this section, an attempt is made to explain theoretically the behavior of asphalt films subjected to tensile stresses based on the concepts derived by the authors.

Explanation of Failure Mechanism

The experimental results clearly indicated that the failure of asphalt films subjected to tensile stresses could be placed in three distinct categories:

1. Asphalts in thick films, depending on the test conditions, behaved as a plastic material and failed by flow or shear.
2. Asphalts in thin films, depending on the test conditions, failed by brittle fracture.
3. Asphalt in intermediate film thicknesses failed by tensile ruptures which were characterized by the formation of small rupture planes (cavitation) and filaments.

The mechanism responsible for the occurrence of these different types of failure can be related to the extent to which the lateral deformation of the film is restrained

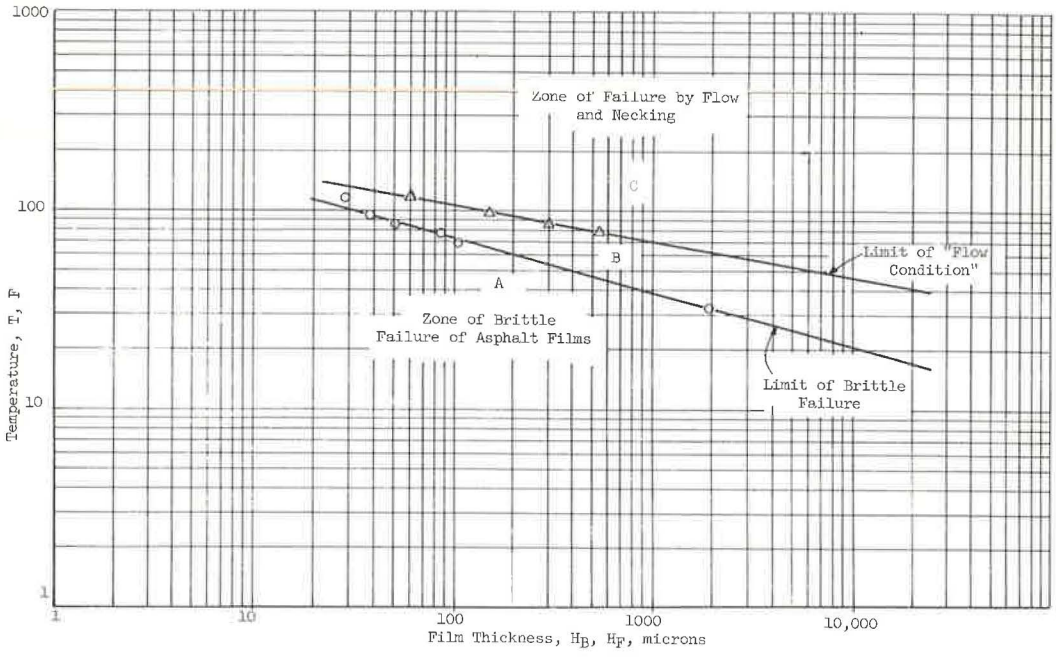

Figure 13. Influence of temperature on types of failure.

by the boundary conditions. To explain the failure mechanism, it is desirable that the failure of an asphalt specimen whose lateral deformation is not affected by the boundary conditions be examined first. When a long specimen (ratio of height to diameter more than three) is tested in tension, in addition to tensile stresses, shear stresses that can be quite large are also developed in the material as a result of lateral contraction of the specimen. Because the shear strength of asphalts, as well as other ductile and plastic materials, is smaller than its tensile strength, failure may be expected to occur because of shear stresses. However, in a shorter specimen where the material in contact with the boundary is prevented from deforming laterally, the relative amount of shear stress in the film decreases. This shear stress reduction can be attributed to transverse tensile stresses which are developed in the material as a result of the restraint of lateral deformation. When the transverse tensile stresses are superimposed with the simple tension that exists in a long specimen, a state of triaxial tension exists and results in a smaller shear stress in the asphalt. Therefore, as the lateral contraction is increasingly restrained with thinner films, the shear stress in a specimen is reduced and, thus, the tensile strength of the material is expected to increase. In a specimen which is considerably restrained from deforming laterally, the material would be subjected to more or less pure tensile stresses. In this condition, the failure of the specimen is by brittle fracture and is affected by the physical properties of the material such as flaws and cavities.

The three types of failure of the asphalt films observed in this investigation can be explained by this mechanism. In thick films, the amount of shear stress produced in the asphalt as a result of applied tensile stresses would be sufficient to cause the specimen to fail by flow or shear. However, as the film thickness decreases to an intermediate thickness, the transverse tensile stresses increase and the shear stresses in the specimen are reduced. The failure of specimens in these thicknesses, which is predominately due to tensile stress, is characterized by the formation of small rupture planes in the films. In very thin films where the lateral deformation is considerably reduced, the hydrostatic tension developed in the specimens would cause the films to fail by brittle fracture. The specimen, in this case, behaves more as a solid, and any flaws and cavities present in the material would cause stress concentration in the film which, in turn, would influence the fracture stress. Because the number of flaws in the material decreases with a decrease in film thickness, the tensile strength is expected to be higher for thinner films. In thick films, however, the stress concentration developed by the cavities and flaws are nullified by plastic flow. Thus, flaws do not significantly influence the tensile strength of thick films.

During the experimental work, three distinct types of failure were observed in the material: brittle fracture, tensile rupture and shear flow. Each type of failure occurred in a range of film thicknesses which constituted a failure zone. It was found that the brittle zone corresponds to the thin film range at which asphalt fails by brittle fracture as a result of excessive tensile stresses. In this investigation the limit of the brittle failure zone is represented by the notation H_B. The flow zone corresponds to the zone in which films fail predominately by flow and shear. Because the limit of this zone, in contrast to the limit of brittle failure, is not well defined, the thinnest film thickness at which the tensile strength plotted on semilogarithmic scale gradually levels off was assumed as the limit of flow condition, H_F. The experimental data indicate that the failure of films thicker than H_F is predominately or entirely due to shear stresses. The failure of films located between these two zones, however, is predominately by tensile stresses and is characterized by the formation of rupture planes or cavities in the specimens. In this type of failure, in contrast to brittle rupture, the specimen can still carry a reduced load after the maximum load has been reached.

This explanation for the failure mechanism can also explain the variation observed in the results of H_B and H_F. Figures 11 and 13 indicate H_B and H_F that are affected by the rate of extension and temperature. As the rate of extension increases, the film thicknesses which correspond to H_B and H_F are shifted to the thicker films. Likewise, the lower the temperature, the greater would be the thickness of the film at which these limits occur. Because asphalt is a viscoelastic material at higher rates of extension or lower temperature, the shearing resistance and, thus, the viscosity of the material

is increased. Therefore, the magnitude of the shear stress which would cause flow in a specimen tested at a slow rate of extension or at a high temperature would no longer be sufficient to produce a shear flow in the film. Thus, the H_F is shifted to thicker films where there is less restraint of lateral deformation and where sufficient shear stresses for failure can be developed in the specimen. Similarly, at high rates of extension or low temperatures, H_B is also shifted to the thicker films where the decreased tensile stresses resulting from the lowered restraint of lateral deformation are not sufficient to cause brittle fracture in the specimen.

Explanation of Load-Deformation Curves

The different load-deformation curves shown in Figures 2 and 3 are typical curves associated with different types of failure. The load-deformation curves corresponding to brittle failure are linear until an instantaneous separation of the film occurs as the load reaches the maximum. This type of load-deformation curve is observed in all films which fail by brittle fracture and behave more like a solid than a plastic. Curve I in Figure 2 is a typical load-deformation curve for this type of behavior. In very thick films, however, the load-deformation curves are no longer linear. In this type of load-deformation curve, shown by Curve II in Figure 2, after the load reaches a maximum, plastic flow occurs in the film. This type of load-deformation curve is observed in films which fail by flow and necking. Because in thick films the lateral deformation of the specimen is less affected by the boundary conditions, the nonlinear load-deformation curves and the plastic flow can be attributed to the presence of sufficient shear stresses in the asphalt to produce the characteristic flow.

In Figure 3, two other typical load-deformation curves are shown. Curve III is a typical curve for films failing by tensile rupture and formation of cavities. In this type of failure, the load-deformation curve is linear initially but, in contrast to brittle films, no instantaneous breaking occurs in the specimen. After the specimen reached the state of failure, the filaments which formed as a result of cavitation still can carry a reduced load, for greater deformation. This type of load-deformation curve was observed for all specimens located between H_B and H_F. For films slightly thicker than H_F, another distinct type of load-deformation curve is observed. The load-deformation curve obtained for such films is no longer linear, but still a slight drop of the load is observed in the specimen after the load reaches the maximum. Curve IV is a typical load-deformation curve for films slightly thicker than H_F. As it is observed, this curve is more similar to Curve II (Fig. 2), which was obtained for flow-type failure, than to Curve III. That is, as the film thickness increases, the shape of Curve IV approaches the shape of Curve II obtained for flow-type failure. Therefore, it can be concluded that the load-deformation curves for films thicker than H_F are predominately or entirely affected by the occurrence of flow in the specimen.

Explanation of Tensile Strength-Film Thickness Relationship

In explaining the tensile strength-film thickness relationship, different failure mechanisms observed in the asphalt films must be considered. Each of the three types of failure have significant influence on the behavior of the asphalt film subjected to tensile stresses. In other words, in the range of film thicknesses where the films fail by shear flow, the behavior of the asphalt film is different from the behavior in the range at which failure is characterized by brittle fracture or in the range where tensile rupture occurs.

In the flow zone, where the material fails predominately or entirely by shear flow, the hydrodynamic theory given previously was found to be in agreement with experimental results. In Figure 8, Line A has been drawn based on this theory and its equation is as follows:

$$\sigma^n = \frac{dh}{dt} \frac{A^{\frac{(n+1)}{2}}}{\pi^{\frac{(n+1)}{2}}} \frac{K(2n)^n (n+2)}{(3n+1)^n} \frac{H_o^{\frac{3n+1}{2}}}{(H_o + \Delta h)^{\frac{5n+5}{2}}} \qquad (9)$$

in which

σ = tensile strength of film (dynes/sq cm);

$\frac{dh}{dt}$ = rate of extension (cm/sec), which is equal to 8.46×10^{-4} cm/sec (0.02 in./min) in this case;

H_o = initial film thickness (cm);

Δh = amount of deformation to failure (cm);

A = area of specimen (sq cm);

n = constant related to non-Newtonian behavior of asphalt, which for this asphalt is 1.06708, obtained from the equation $\dot{\delta} = \tau^n/K$ (for Newtonian materials, n = 1); and

K = constant related to viscosity of asphalt (dynes-sec/sq cm), which for this asphalt is equal to 3.108×10^6 dynes-sec/sq cm).

Eq. 9 is similar to Eq. 3 presented previously. If in Eq. 3 the term related to force, F, is divided by area, A, to be in the form of stress, σ, and H is subdivided by H_o and Δh, Eq. 9 is obtained. Up to H_F, the part of the experimental plot which is approximately tangent and parallel to Line A (Fig. 8) indicates that the material, in thick films, tends to behave according to this theory.

In the equation derived from the hydrodynamic theory, if the rate of extension and the constants n and K, which are related to the type and viscosity of the asphalt, are known, the tensile strength of the asphalt in thick films can be predicted. The constants n and K in Eq. 9 were obtained from the results of shear tests conducted on the asphalt at 77 F.

The experimental results indicate that as the film thickness decreases, the difference between the theoretical tensile strength predicted by hydrodynamic theory and the observed strength increases. That is, in thin films, the failure of the asphalt films occurs at much smaller loads than those predicted by this theory. Because, in thin films, as a result of restraint of the lateral deformation, the magnitude of shear stresses decreases, a greater magnitude of tensile stress is required to develop sufficient shear stresses for producing flow in the film. However, when this tensile stress exceeds the tensile strength of the asphalt films, the failure occurs by tensile rupture before any appreciable flow can be produced in the film. Therefore, the failure can no longer be assumed to be a failure by flow, and, thus, this theory is invalid for thin films of asphalts. The experimental data indicate that H_F is the thinnest film thickness whose strength can be predicted by this theory.

In very thin films, where the lateral deformation of the specimen is considerably restricted, the asphalt films behave as solids and fail by brittle fracture. This type of failure is attributed to hydrostatic tension which is developed in the specimen as a result of restraint of lateral deformation. In films failing by brittle fracture, the cohesive strength of the material and the cavities and flaws present in the specimen influence the tensile strength of the film. The theory of potential energy and cavities which was given previously might predict the tensile strength of the films behaving as a solid. In Figure 8, Line B was based on this theory and its equation is as follows:

$$\sigma = A \left(\frac{\Delta h}{H_o} \right)^{+a} \tag{10}$$

in which, for the experimental data obtained at 77 F and rate of extension equal to 0.02 in./min,

A = a constant for these test conditions, equal to 4.782×10^7;

Δh = amount of deformation to failure (cm), the average amount of which assumed for the film thicknesses located in the brittle zone is equal to 41.4×10^{-4} cm; and

a = constant related to cavities and molecular forces of asphalt, which for films thicker than the optimum film thickness (see the assumptions of theory) is equal to 0.397.

In this equation, the constant A depends on the rate of extension, temperature and consistency of the asphalts. This constant, for tests conducted at 77 F (25 C) and 0.005 in./min rate of extension, is equal to 3.80×10^7. For tests conducted at 0.02 in./min rate of extension and temperatures of 20, 35, and 45 C, A is 5.65×10^7, 3.10×10^7 and 1.87×10^7, respectively.

To predict the tensile strength of thin films of asphalts by the theory of potential energy and cavities, certain assumptions should be made:

1. The relationship of tensile strength to film thickness for the very thin films (the films located in the brittle zone) is a straight line on a logarithmic scale. The experimental data plotted in the upper portion of Figure 8 indicate that such an assumption can be made without introducing any appreciable error.
2. As predicted by the theory, there is an optimum film thickness in the tensile strength-film thickness relationship. However, because no optimum film thickness was observed in any of the experiments conducted in this investigation, the validity of this assumption remains unclarified. Therefore, the experimental data plotted in Figure 8 corresponds to the right side of the optimum and the sign of the constant a, as was discussed previously, is negative.
3. A constant value needs to be assumed for the amount of deformation to failure. According to Mack's assumptions, the amount of deformation to failure (Δh) remains constant for a given asphalt. The experimental results indicate that the amount of deformation to failure is not significantly influenced by the test variables, and, moreover, its variation with the film thickness is very small. Therefore, an average value can be assumed for the amount of deformation to failure for the range of film thicknesses studied.

The experimental data plotted in Figure 8 indicate that as the film thickness increases, the deviation of the theoretical Line B from the experimental results becomes greater. Moreover, it is observed that for a range of film thicknesses thicker than the limit of brittle failure, the tensile strength-film thickness relationship can no longer be assumed to be linear on logarithmic scales. Therefore, this theory, similar to the hydrodynamic theory, is only applicable to a limited range of film thicknesses. Thus, according to the basic assumptions discussed previously, the theory of potential energy and cavities is only applicable to films which behave as solids.

In the explanation of the tensile strength-film thickness relationship, only the three different types of behavior which are observed in the experimental work were discussed. However, there is a fourth type of behavior predicted by the suggested failure mechanism, even though it has not been observed in the experimental results. According to the hypothesis given for failure mechanism, as the film thickness decreases, the restraint of deformation and the resulting transverse tensile stresses increase. Therefore, it is expected that in extremely thin films, the lateral deformation is completely prevented and purely tensile stress is developed in the specimen. In this case, the asphalt film which is subjected to equal tensile stresses in all directions (pure hydrostatic tension) would also fail in a brittle fracture. Because the number of flaws and cavities which might be present in the asphalt film has been considerably reduced in the extremely thin films, it is expected that the tensile strength might not vary with film thickness. That is, in extremely thin films the tensile strength would gradually reach an ultimate value and remain constant regardless of the thickness of the asphalt film. Therefore, the general form of the tensile strength-film thickness relationship would be that of an S-shaped curve. The difference between this fourth type of behavior and the behavior of films in the brittle zone which was previously discussed is due to the variation in the number of flaws and the degree that lateral deformation is prevented. Thus, it might be concluded that in extremely thin films, the tensile strength might reach an ultimate value determined by the cohesive strength of the asphalt molecules. However, the difficulties associated with preparing such extremely thin films in the laboratory make it impossible to study this fourth type of behavior.

SUMMARY AND CONCLUSIONS

The purpose of this investigation was to study the tensile properties of asphalts in thin films. Attempts were made to explain theoretically the behavior of asphalts, as well as to derive relationships for such behaviors. Two theories that seemed to predict the tensile properties of asphalts in very thin and very thick films were investigated. It was found that these two theories can closely predict the tensile strength of asphalts in very thin and very thick films. In addition, an hypothesis was developed which tends to explain the general behavior of asphalt films. Laboratory investigations were conducted, and the influences of a selected group of variables on the tensile properties of asphalts were determined in order to verify the suggested hypothesis and theories.

The data reported herein were limited to one type of asphalt and a selected number of influential factors. However, other types of asphalt have been investigated and similar results were obtained. Therefore, the conclusions drawn from this study are limited primarily to the test conditions used. The conclusions reached from this investigation are as follows:

1. The tensile strength of asphalts in thin films varies with the film thickness. The tensile strength decreases as the film thickness increases, and, finally, the tensile strength approaches a constant value that does not change as the film thickness is increased. For the type of asphalt studied, it is observed that the tensile strength-film thickness relationship for thin films of asphalts is linear on a semilogarithmic scale. In thick films, however, depending on the test conditions, the tensile strength gradually approaches a constant value that is quite small.

2. It appears that the hydrodynamic theory can be used to predict the tensile strength of thick films of asphalts. According to this theory, the tensile strength depends on the type of asphalt, viscosity, and the rate of extension. It is indicated that this theory can be used for those films of asphalts which fail by shear flow and necking. However, this theory is not applicable to very thin films of asphalts which fail predominately by tensile stresses. For such thin films, the tensile strength predicted by this theory is much greater than the observed strength.

3. The theory of potential energy and cavities, with certain assumptions, can be applied to very thin films of asphalts which tend to behave as solids. According to this theory, there is an optimum film thickness in the tensile strength-film thickness relationship which varies with the type of asphalt. However, in the type of asphalt studied in this investigation, no optimum film thickness was observed. Thus, to apply this theory it must be assumed that all experimental data are of film thickness greater than optimum. Moreover, this theory is only applicable for thin films of asphalts. For thick films, the tensile strength predicted by this theory is much greater than the observed strength.

4. It is believed that the restraining action of the boundary conditions produces transverse tensile stresses in the specimen which change the state of simple tension to a state of triaxial tension. This change, occurring gradually as the film thickness decreases, is partly responsible for the different types of behavior observed in the asphalt films. In addition, the flaws and cavities that might be present in the asphalt films also influence the behavior of the material. However, the influence of flaws and cavities on the behavior of specimens is more pronounced in thin films where the material behaves more as a solid than in thick films where asphalt behaves more as a plastic material. It appears that this hypothesis can explain the behavior of asphalts over a wide range of film thicknesses.

5. Three types of failure are observed in the asphalt specimens; these are brittle fracture, tensile rupture, and failure by flow and necking. Depending on the test conditions, brittle fracture occurs in thin films, whereas thick films fail predominately by flow and necking. The failure of intermediate film thicknesses is by tensile rupture which is characterized by the formation of cavities and filaments in the film. These types of failure observed in the asphalt specimens can be explained by the suggested theoretical failure mechanism.

6. It is indicated that the range of film thicknesses at which different types of fail-

ure occur depend on the variables studied. Thus, the limit of brittle failure and the limit of flow condition, which are the limits of different zones of failure observed in the asphalt films, vary with such variables as rate of extension, temperature, and size of specimen. As the rate of extension increases or the temperature decreases, the limits of brittle failure and flow condition are shifted to the thicker film range. The variations observed in these limits can be explained by the suggested theoretical failure mechanism. Furthermore, the equations derived from these limits might be used to predict the type of failure of an asphalt film.

7. Rate of extension and temperature significantly influence the tensile strength of the asphalt films. The tensile strength increases as the rate of extension increases or as temperature decreases. It is indicated that when tensile strength is plotted against film thickness or a semilogarithmic scale, the slope of the straight line relationship existing in thin films is independent of the rate of extension and temperature for a specific asphalt.

8. The amount of deformation at failure tends to remain constant in the asphalts studied. The amount of deformation at failure is practically a constant regardless of the thickness of the specimen. The amount of deformation at failure also does not appear to vary significantly with the rate of extension and temperature.

ACKNOWLEDGMENTS

This study was a part of Illinois Cooperative Research Program Project IHR-75, "Basic Properties of Seal Coats and Surface Treatments." It was undertaken by the Engineering Experiment Station of the University of Illinois, in cooperation with the Illinois Division of Highways and the U. S. Bureau of Public Roads.

On the part of the University, the general administrative supervision was by W. L. Everitt, Dean of the College of Engineering, R. J. Martin, Director of the Engineering Experiment Station, N. M. Newmark, Head of the Department of Civil Engineering, and Ellis Danner, Director of the Illinois Cooperative Highway Research Program and Professor of Highway Engineering.

On the part of the Division of Highways, the work was initiated under the administrative direction of R. R. Bartelsmeyer, former Chief Highway Engineer, and Theodore Morf, former Engineer of Research and Planning; and continued under Virden E. Staff, Chief Highway Engineer, and W. E. Chastain, Sr., Engineer of Research and Development.

Technical advice was provided by a Project Advisory Committee consisting of the following personnel: W. E. Chastain, Sr., and L. J. Weishaar, Field Engineer, Bureau of Local Roads and Streets, representing the Illinois Division of Highways, Frederick P. Walton, Assistant Construction and Maintenance Engineer; and A. E. Traeger, Area Engineer, representing the U. S. Bureau of Public Roads; and Edward E. Bauer, Professor of Civil Engineering, and Charles E. Taylor, Professor of Theoretical and Applied Mechanics, representing the University of Illinois.

REFERENCES

1. Askew, F. A., "Time and Tack." Paint Technology, 9 (106):217 (Oct. 1944).
2. Banks, W. H., and Mill, C. C., "Tacky Adhesion, Preliminary Study." Jour. Colloidal Sci., 8:137 (1953).
3. Bikerman, J. J., "Strength and Thickness of Adhesive Joints." Trans. Jour. Soc. Chem. Ind., 60T (Pt. 3):23 (1941).
4. Bikerman, J. J., "The Fundamentals of Tackiness and Adhesion." Jour. Colloidal Sci., 2:163 (1947).
5. Bikerman, J. J., "Adhesion." Surface Chemistry for Industrial Research, Chap. 5, p. 358, Academic Press, New York (1948).
6. Bikerman, J. J., "The Rheology of Adhesion." Rheology Theory and Application (ed. by F. R. Eirich), Vol. 3, p. 479, Academic Press, New York (1960).
7. Bowden, F. P., (In German). Physik. Z. Sowjetunion, 4:185 (1933).

8. Bruyne, N. A. De, "The Strength of a Joint Under Tension." Bull. 61, Aero Res. Tech. Notes, Aero Research Ltd., Cambridge (Jan. 1948).
9. Bulkley, R., "Viscous Flow and Surface Films." Res. Paper 264, Jour. Res. Nat. Bur. Std. 6:89 (1931).
10. Crow, T. B., "Some Properties of Soft Soldered Joints." Trans. Jour. Soc. Chem. Ind., 43:65T (1924).
11. Dietz, A. G. H., "Tension Testing of Adhesives." ASTM Spec. Tech. Publ. 194, p. 19 (1956).
12. Erb, R. A., and Hanson, R. S., "The Tensile Strength and Tacky Behavior of Polymer Liquids." Trans. Soc. Rheology, 4 (1960).
13. Herrin, M., and Jones, G., "Behavior of Bituminous Materials from Viewpoint of the Absolute Rate Theory." Proc. AAPT, 32 (1963).
14. Hoekstra, J., and Fritzius, C. P., "Rheology of Adhesives." Adhesion and Adhesives (ed. by N. A. DeBruyne and R. Houwink), p. 33 Elsenier Press, Houston (1951).
15. Koehn, G. W., "Behavior of Adhesives in Strength Testing." Adhesion and Adhesives, Fundamental and Practice, p. 120, Soc. Chem. Ind., London (1954).
16. Lennard-Jones, J. E., and Dent, B. M., "Cohesion at Crystal Surfaces." Trans. Faraday Soc., 24:92 (1928).
17. Lennard-Jones, J.E., "Cohesion." Proc. Phys. Soc. of London, 43 (Pt. 5): 461 (Sept. 1931).
18. Mack, C., "Physical Properties of Asphalts in Thin Films." Ind. Eng. Chem., 49:422 (1957).
19. McBain, J. W., and Lee, W. B., "Adhesives and Adhesion: Gums, Resins and Waxes, Between Polished Metal Surfaces." Jour. Phys. Chem., 31:1674 (1927).
20. McBain, J. W., and Lee, W. B., "Adhesives and Adhesive Action." 3rd and Final Rept. Adhesives Res. Comm., Dept. of Sci. and Ind. Res., London, p. 66 (1932).
21. Meissner, H. P., and Bauldauf, G. H., "Strength Behavior of Adhesive Bond." Trans. ASME, 73:697 (July 1951).
22. Mylonas, C., and Bruyne, N. A. De, "Theoretical Investigations of the Stresses in Joints." Adhesion and Adhesives (ed. by N. A. DeBruyne and R. Houwink), p. 91, Elsenier Press, Houston (1951).
23. Reiner, M., and Freudenthal, A., "Failure of a Material Showing Creep (A Dynamic Theory of Strength)." Proc. 5th Internat. Cong. of Appl. Mech. p. 228 (1938).
24. Reynolds, O., Phil. Trans. Roy. Soc. London, 177:157 (1886).
25. Scott, J. R., "Theory and Application of the Parallel Plate Plastometer." Trans. Inst. Rubber Ind. 7:169 (Aug. 1931).
26. Stäger, H., "Allgemeine Werkstoffkunde." Birkhauser, Basle (1947).
27. Stefan, J., (In German). Sitzungoberichte Kaiserl. Akad. Wiss., Wien, Math. Naturw. Klasse, Abt. 2, 69:713 (1874)
28. Strasburger, H., "Tacky Adhesion." Jour. Colloidal Sci., 13:218 (1958).
29. Wood, P. R., "Rheology of Asphalts and the Relation to Behavior of Paving Mixtures." HRB Bull. 192 pp. 20-25 (1958).
30. Wood, P. R., and Miller, H. C., "Rheology of Bitumens and the Parallel Plate Microviscometer." HRB Bull. 270, pp. 38-46 (1960).

Chemistry of Breaking of Asphalt Emulsions

A. O. BOHN
The Technical University of Denmark, Copenhagen

The amount of asphalt emulsion coagulated by contact with different aggregates is determined for a series of soap-stabilized asphalt emulsions. It is shown that the acid action of the stones is not as important in breaking as has so far been supposed. The decisive factor is the reaction between the emulsifier and the calcium ions which are displaced from the stones by contact with the emulsifier solution. The process is not concluded because the stone surfaces are blocked up by coagulated bitumen. The tendency for blockade is dependent on the type of aggregate and on the alkalinity of the emulsion.

• IF AN ASPHALT emulsion is brought into contact with an aggregate, in many cases some of the emulsion will coagulate, even without a simultaneous evaporation of water from the emulsion. This tendency for the emulsion to break in contact with an aggregate can be observed in an experiment by Weber and Bechler (1) in which bitumen coagulates on the stones in such a form that it cannot be removed by rinsing with distilled water. The amount of coagulated bitumen may be determined by weighing.

The measurement of the electrolyte stability of the bituminous emulsions has been used to characterize their breaking qualities. In the measurements (Myer's Test), a known amount of electrolyte, usually calcium chloride, is added to a known amount of emulsion, after which the amount of coagulation of bitumen is measured (2).

By measuring the electrolyte stability, information may be obtained about the quantity of emulsifier (2) or the breaking tendency of salts dissolved in the water on the road (3) and of calcium salts in the aggregate which are soluble in water (4, 5, 6, 7, 8). The importance of the water-soluble salts in the aggregate has been studied by extracting the aggregate with water, adding the extracts to the emulsion, and measuring the coagulation. It has usually been necessary, however, to choose extremely favorable conditions of dissolution (for instance, fine crushing of the aggregates) to obtain a sufficient quantity of salts to determine the coagulating effect of the aggregates.

Because the measurement of the electrolyte stability is a very convenient estimation method, the possibility of a connection between the electrolyte stability and the stability against aggregates has been empirically investigated. The results have been very contradictory: Nasini and Rossi (9) and Bohn and Mikkelsen (10) find good agreement, whereas Statens Vejlaboratorium (11) and Jekel (12), who work with a large number of emulsions, find poor agreement. All these investigators use factory-produced emulsions. McKesson (2) and Neubronner (13), who work with self-produced emulsions, have found very good agreement. However, both have produced their emulsions by varying the amount of the added soap. As the content of alkali in the emulsions is especially important for the breaking qualities (1), it would be reasonable to suppose that more information would be obtained by working with a series of emulsions where the content of alkali is varied, independent of the content of fatty acid.

WEBER AND BECHLER'S EXPERIMENTS

With a colloid mill four series of potassium oleate-stabilized emulsions are produced. Keppeler, Blakenstein and Borchers (14) have used such a series of emulsions

Paper sponsored by Committee on Characteristics of Bituminous Materials and Means for Their Evaluation.

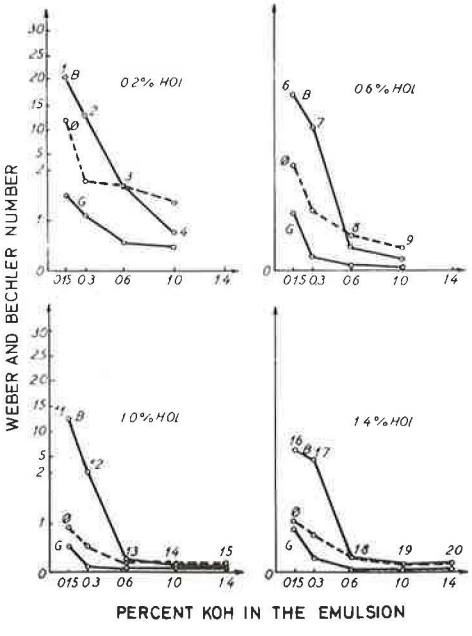

Figure 1. Weber and Bechler numbers (percent coagulated asphalt) for basalt (B), granite (G) and limestone (ø).

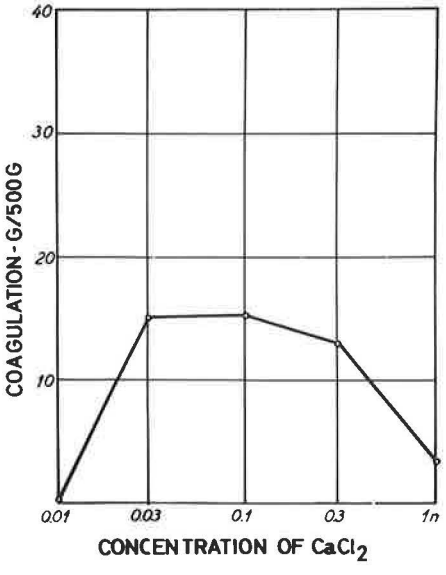

Figure 2. Myers test with 2.2 meq $CaCl_2$ per 500 g Emulsion 8.

for their experiments. All emulsions contained 50 percent bitumen with a penetration of 300. In the first series (Nos. 1 to 5), the content of oleic acid (HOl) was 0.2 percent, and the amount of KOH was 0.15, 0.30, 0.60, 1.0 and 1.4 percent, corresponding to normalities of 0.53, 0.106, 0.21, 0.36 and 0.50, respectively, calculated on the basis of the water phase of the emulsion. The second series (Nos. 6 to 10) contained 0.6 percent HOl; the third (Nos. 11 to 15), 1.0 percent HOl; and the fourth (Nos. 16 to 20), 1.4 percent HOl. Within the last three series, the content of KOH was varied as in the first series. The HOl contents of 0.2, 0.6, 1.0 and 1.4 percent correspond to the normalities 0.014, 0.043, 0.071 and 0.1, respectively, calculated on the basis of the water phase. To this can be added 0.027 from the acid content of the bitumen because the bitumen has an acid number of 1.5. Emulsions 5 and 10 broke immediately after production and were, therefore, omitted from the experiments.

Figure 1 shows the result of Weber and Bechler's experiments with three aggregates: a basalt (B) from the Faroes, a granite (G) from Hammeren in Bornholm, and a limestone (ø) from Øland. The figure indicates the amount of bitumen per 100 g aggregate which coagulate in a form that cannot be washed out with distilled water when 10 g of aggregate with the particle size 0.5 to 1 mm is reacted with 50 g emulsion for 1 hour with no evaporation. With increasing content of KOH in the emulsions, the breaking numbers will decrease.

An increase of the content of oleic acid will have the same result, although to a lesser degree. Both phenomena are in agreement with the observations of Keppeler, Blankenstein and Borcher (14).

The basalt numbers are always higher than the granite numbers. Øland limestone normally has a breaking tendency between ability to a higher degree when the content of alkali increases. Therefore, the Øland limestone curves, except for the last series of emulsions, cross the basalt curves as alkali content increases.

MYER'S TEST

The electrolyte stability has been determined by a modification of Myer's test. To compare it more easily with Weber and Bechler's experiments, 50 g of emulsion was

used, into which 0.22 milliequivalents (meq) calcium chloride solution were added dropwise from a burette with vigorous stirring. It was found that 10 g basalt under certain circumstances will give up this amount of calcium ions. After an hour the emulsion was filtered through a sieve with openings of 0.3 mm, and the coagulate filtered out was washed with distilled water, dried and weighed. The results are referred to 500 g of emulsion as in the Weber and Bechler experiments.

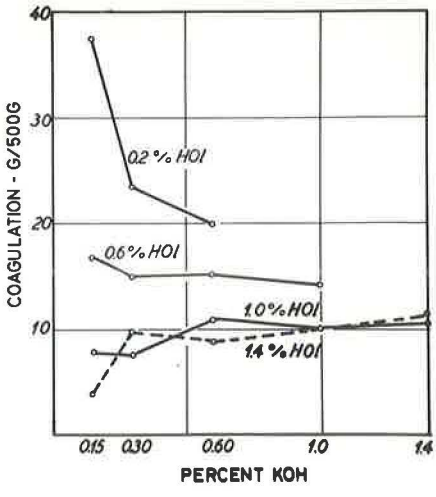

Figure 3. Myers test with $CaCl_2$.

As the results proved to be strongly dependent on the concentration of the calcium chloride solution, the experiments were made with the following addition of solution: 0.22 ml 1 N, 0.73 ml 0.3 N, 2.2 ml 0.1 N, 7.3 ml 0.03 N, and 22 ml 0.01 N. The results are shown in Figure 2. The maximum amount of coagulation occurs at 0.1 N concentration. That the coagulation numbers are low with the weakest calcium chloride solutions agrees with an increase in the electrolyte stability with thinned emulsions (20). The low coagulation numbers with concentrated calcium chloride solutions are due to the coagulation of the bitumen around the single drops of the calcium chloride solution which prevents the effect from spreading in the liquid.

The experiment was carried out with all emulsions at a concentration of 0.1 N. The results (Fig. 3) show that it is essentially the content of fatty acid in the emulsion which determines the stability. Only when emulsions with a fairly constant proportion of KOH to HOl are compared, do increasing Weber and Bechler numbers correspond to increasing Myer numbers.

ACID ACTION OF AGGREGATES AS BREADING MECHANISM

Williams (15) has shown that even acidic aggregates (that is, aggregates with a high content of SiO_2) will not give up hydrogen ions to water. But against alkali hydroxide solutions, most aggregates will work as an acid, and Weber and Bechler (1) have found the breaking to be due to the acid action of the stones. If an active stone was put into potassium hydroxide, the activity of the stone was considerably reduced. They explained this by the fact that the acid action of the stone (as they call it, the alkali adsorption ability) is neutralized. Furthermore, the stability of an emulsion is increased by addition of potassium hydroxide. Keppeler, Blankenstein and Borchers (14) state that if an active aggregate is put into a soap solution, the latter becomes turbid, probably due to precipitated fatty acid. They have also measured the acid action for a series of stones and have found good agreement between the acid action and the breaking numbers. Klinkmann (7) has proposed a theory according to which the alkali concentrates at the stone surface, causing the emulsifier soap to be salted out, resulting in coagulation. The alkali is bound, however, in the formation of salt, and as Nasini and Rossi (8) have pointed out, Weber and Bechler's alkali-treated stones give especially small breaking numbers. Nasini and Rossi also find rather good agreement between the acid action and the breaking ability of the stones; however, they do not see the acid action as the actual cause for breaking. Rather, without any experimental basis, they see the cause as the adsorption of sodium ions on the stone surface, resulting in a disturbance of the balance in the electric double layer.

STABILITY AGAINST ACIDS

As the acid action of the stones is said to be important, the stability of the emulsions against acids is determined by performing Myer's test with acetic acid. An amount of

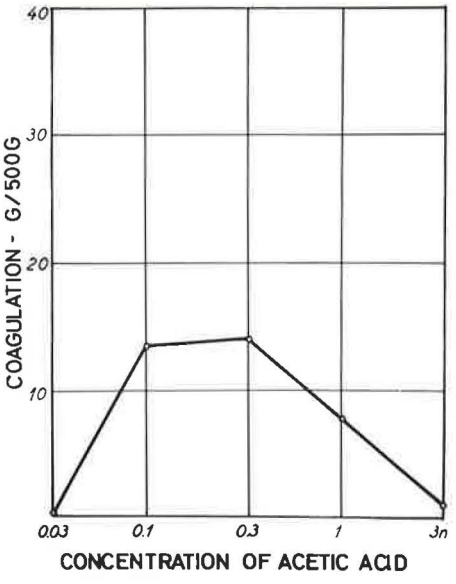

Figure 4. Myers test with 2.2 meq acetic acid per 500 g emulsion.

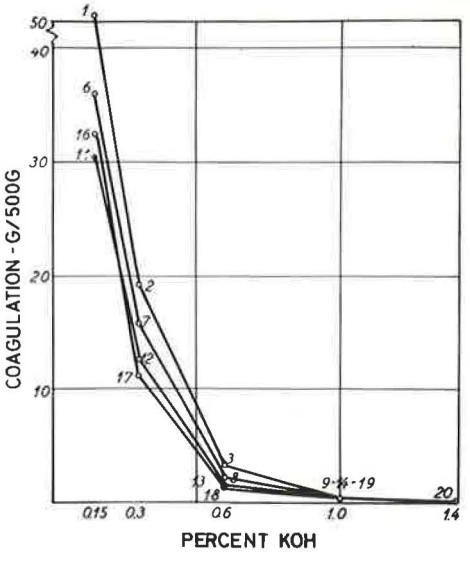

Figure 5. Myers test with acetic acid.

0.36 meq acetic acid was added in the form of 0.03, 0.1, 0.3, 1 and 3 N solutions to 50 g of Emulsion 12. As mentioned later, 0.36 meq is the amount of hydrogen ions which 10 g of basalt can give up under certain circumstances. The coagulation numbers shown in Figure 4 are quite similar to those for addition of calcium chloride (Fig. 2). The experiment was carried out using the emulsions at a concentration of 0.1 N. The results (Fig. 5) show good agreement with the Weber and Bechler numbers for basalt (Fig. 1). Again it is observed that the stability increases greatly when the content of potassium hydroxide in the emulsifier increases, whereas the stability increase with increase in oleic acid is more modest. The results differ greatly from the calcium chloride numbers in Figure 3.

DIFFICULTIES IN ACID-ACTION THEORY—CATION EMULSIONS

The measurements of the stability against H ions and Ca ions were in rather good agreement with Weber and Bechler (1) and Keppeler, Blankenstein and Borchers (14), suggesting that the acid action of the stones is decisive for breaking. There are, however, many phenomena which cannot be explained by the acid-action theory. For example, the Weber and Bechler experiments showed that the examined limestone usually was more stable than basalt in emulsions rich in alkali, whereas the opposite was true in emulsions poor in alkali. Also, Weber and Bechler have found that the ranking of breaking for a series of stones was dependent on the emulsion. These findings show that the acid action of the stones cannot alone be responsible for the breaking action.

Myer's experiment with HAc indicated that 3.6 ml 0.1 N HAc coagulated 36 g bitumen per 500 g emulsion when Emulsion 6 was used. This is more than, though of the same order of magnitude as, the Weber and Bechler number for basalt (17). Experiments with addition of 3.6 ml 0.1 N boric acid and 3.6 ml of a 0.1 N suspension of aluminum hydroxide, gave, however, the very small coagulation numbers of 0.23 and 0.13 g per 500 g emulsion, respectively. The acid-action theory thus forces us to conclude that the stone looked upon as an acid is almost as strong as acetic acid; this does not sound very probable.

The breaking process cannot be explained by the acid action of the aggregate in acidic cation emulsions. These emulsions come outside the scope of this investigation. Some experimental results will, however, be mentioned for a 50 percent emulsion made with bitumen 300 as binder and 1.3 percent cetyl pyridium chloride as emulsifier. The

TABLE 1

ACID ACTION OF BASALT AND GRANITE

KOH (N)	Basalt (meq/100g)	Granite (meq/100g)
0.3	5.1	0.46
0.1	3.63	0.35
0.03	2.11	0.23
0.01	1.11	0.19

emulsion had a pH of 5.6, and Weber and Bechler numbers of 6.5 and 1.6 were measured against basalt and granite, respectively.

Basalt and granite work as acids (against alkalis.) However, against acids they work as bases. The base action was measured under conditions corresponding to a Weber and Bechler experiment by pouring 50 ml 0.05 HCl over 10 g stone with the particle size 0.5 to 1.0 mm. After an hour the glass was inverted several times, and after centrifuging for 5 min, 25 ml was pipetted. After titration and deduction of the acid consumption in a control experiment, the result was indicated as milliequivalents OH per 100 g aggregate. For basalt and granite the base action was found as 2.67 and 0.73 meq/100 g, respectively.

If the KOH concentration is varied, the acid actions obtained (40 g 0.5 to 1 mm crushed stone in 100 g KOH for 1 hr) are as given in Table 1.

The most alkaline of the emulsions is Emulsion 15. The water phase has a KOH surplus corresponding to a concentration of approximately 0.4 N. The acid action decreases rather considerably at low concentrations. The acid action was correspondingly measured by pouring 50 ml 0.05 N KOH over 10 g stone. For basalt and granite the acid action was 3.02 and 0.39 meq/100 g, respectively.

In the same way as an anion soap-stabilized emulsion breaks on addition of acid, a cation soap-stabilized emulsion will break on addition of alkali. Vogt (16) has found that pH increases on addition of certain kinds of stone to an amine salt solution. The coagulation occurring simultaneously is larger, however, than the coagulation occurring on addition of an amount of ammonia corresponding to the base action of the stone. Vogt explains the breaking of the cation soap emulsions by a completely physical adsorption of the amine salt to the stone surface.

Calculation shows that an emulsion containing 0.2 percent oleic acid has 6 times as much oleic acid as is necessary for covering the emulsion drops, the average diameter of which is 2 μ with a monomolecular layer of oriented oleate ions.

The breaking by contact with aggregates can not be explained by the fact that these adsorb a monomolecular layer of oleate and thereby deprive the emulsifier films of their oleate ions because the specific surface of the aggregates is small in a surface treatment.

Fuerstenau (17) has studied the adsorption process by measuring flow potentials for the combination SiO_2-amine salt solution. He thinks that it is possible to explain certain bends in the zeta potential curve by assuming that at these concentrations, which are about a hundred times smaller than the critical concentration for the formation of micelles (CMC), "hemimicelles" are built at the quartz wall. Below this concentration, the amines are adsorbed one by one. This strong adsorption of amine salts to SiO_2 supports Vogt's theory of the amine salt adsorption of the stones as the cause for breaking.

CONTENT OF EXCHANGEABLE IONS IN STONES

Aqueous extracts of aggregates have, as earlier mentioned, only little coagulating action. However, the water phase in the emulsion holds electrolytes, and it would, therefore, be appropriate to examine the number of coagulating ions which can be displaced by treating the stones for 1 hr with different electrolytes. NH_4Cl or KCl was initially used as the electrolyte, and test conditions were relatively simple. The same exchanges are used in agricultural chemistry. Calcium was determined by titration with complexone by the method of Hildebrand and Reilley (18), and calcium + magnesium was determined by the method of Diehl, Goetz and Hach (19), who also used complexone. For basalt and granite, the Ca + Mg numbers were only about 10 to 15 percent higher than the Ca numbers.

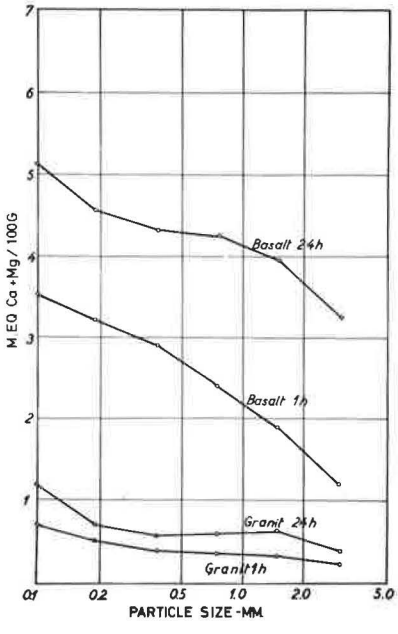

Figure 6. Dependence of displacement of Ca + Mg ions in NH_4Ac on size of aggregate.

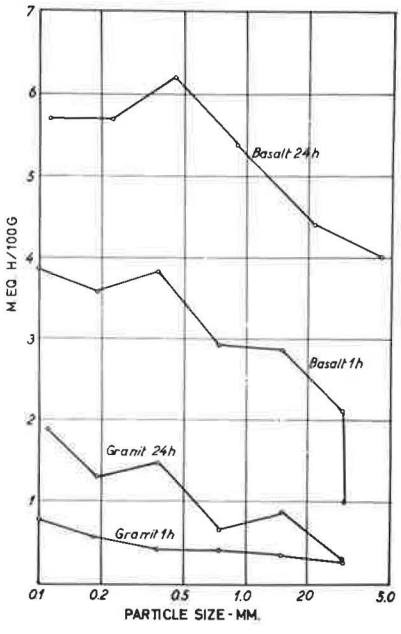

Figure 7. Dependence of acid action in KOH on size of aggregate.

Figure 6 shows the results of a series of experiments with granite and basalt in terms of the number of milliequivalents Mg + Ca ions displaced by the reaction between 100 g stone and 500 ml 0.1 N ammonium acetate at reaction times of 1 and 24 hr. Astonishing large amounts of Mg + Ca are dissolved; for example, for basalt with the particle size of 1 mm in a reaction time of 1 hr, 2.2 meq, the amount chosen in Myer's experiments, are dissolved. The ion exchange increases with increasing surface area, but by less than what would correspond to proportionality. Increasing the time from 1 to 24 hr increases the ion exchange 50 to 100 percent. Basalt is seen to be 4 to 6 times more active than granite.

Figure 7 shows the acid action measured in milliequivalents ions per 100 g stone after 1- or 24-hr reaction with 0.05 N KOH. The numbers are a little higher than the Ca numbers; for basalt with the particle size of 1 mm and with a reaction time of 1 hr, the acid action is 3.6 meq, the amount chosen in the earlier mentioned Myer's experiments with acetic acid.

Weber and Bechler's experiments have been made with the same aggregates and Emulsion 6. The result is seen in Figure 8. The curves are similar to the ion exchange curves, but the importance of the particle size is greater, without, however, reaching proportionality between surface and coagulation numbers. This is consistent with the observation of Martin and Hermann (20) that the coagulating tendency of soap-stabilized emulsions is rather low on small additions of electrolytes and then rises disproportionately strongly on larger additions of electrolytes. The Weber and Bechler numbers for 1 mm basalt are of the same order of magnitude as the earlier ascertained coagulation numbers on addition of 2.2 meq Ca or 3.6 meq H ions. However, it must be pointed out that the 3.6 meq H ions have been determined against an extraction liquid which was 0.05 N with regard to OH ions—Emulsion 6 does not contain that many OH ions.

With basalt of the particle size 0.5 to 1 mm, an experiment was conducted where the NH_4Ac concentration in the exchange liquid was varied from 1 to 0.05 N. The experiment showed that the amount of Ca + Mg exchanged during 1 hr decreased from 4.3 to 1.6 meq/100 g.

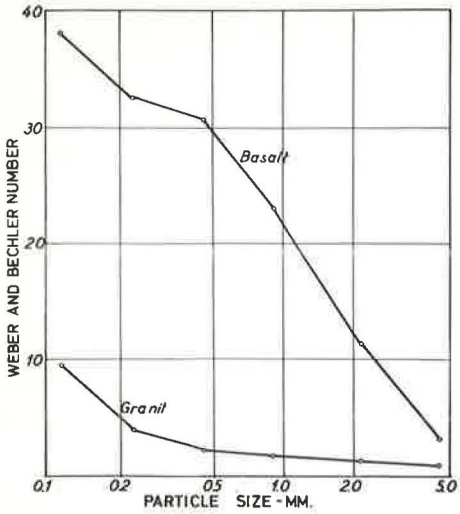

Figure 8. Dependence of Weber and Bechler numbers (percent coagulated asphalt) on particle size.

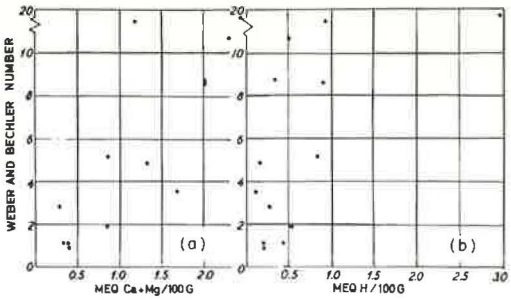

Figure 9. Dependence of Weber and Bechler numbers on (a) amount of exchangeable Ca + Mg ions and (b) amount of H ions.

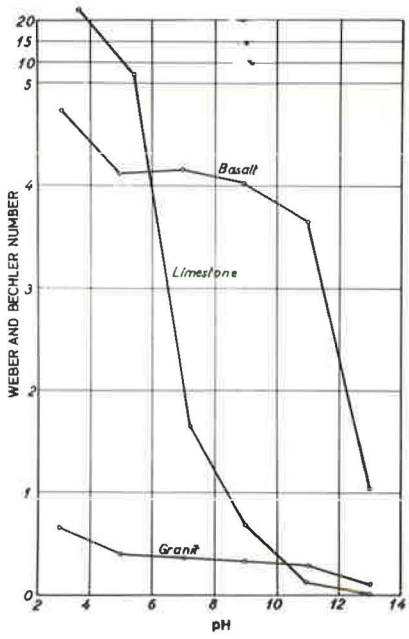

Figure 10. Dependence of Ca ion exchange on pH of exchange solution (KCl).

If the concentration of NH_4Ac is chosen as 0.1 N, and the proportion between the amounts of basalt and ammonium acetate solution is altered from 2:100 to 50:100, then the exchanged amount of Ca + Mg decreases from 3.37 to 2.49 meq/100 g. In a Weber and Bechler experiment, the ratio of stone to serum is 20:100. The observations are in agreement with those found in agricultural chemistry.

In Figure 9, the Weber and Bechler numbers are plotted for Emulsion 6 in reaction with 13 aggregates (four granites, four limestones, one diabase, one slate, one sandstone, one cleave stone and one basalt). In Figure 9a the Weber and Bechler numbers are plotted against the milliequivalents of Ca + Mg ions displaced by reaction for 1 hr with 0.1 N NH_4Ac, and in Figure 9b they are plotted against the milliequivalents of H ions removed by reaction for 1 hr with 0.05 N KOH. The correlation between Weber and Bechler numbers and ion exchange is bad, especially for the acid-action numbers. There seems to be no correlation between the mineralogical composition of the stones and the breaking ability. The limestones all give up rather large amounts of Ca + Mg ions, whereas the acid action generally is small.

Measurements are made with the 13 aggregates to see how many coagulating ions are dissolved in distilled water alone. An average of only 22 percent of the amount of Ca + Mg were found by reaction for 1 hr with NH_4Ac.

Figure 10 shows the pH dependence of the Ca ion exchange for Hammer granite, Faroe basalt and Øland limestone. As exchange liquid, 1 N KCl is used, with pH regulated by additions of HAc, NH_4Ac, or KOH or mixtures of these. The calcium exchange falls with increasing pH. It is strange that the fall is extraordinarily great for Øland

TABLE 2

AMOUNTS OF CALCIUM AND MAGNESIUM IONS DISPLACED IN 0.05 N POTASSIUM OLEATE

KOH Surplus (%)	pH	Ca+Mg (meq/100g)		
		Granite	Basalt	Limestone
0	9.6	0.18	1.03	0.23
10	10.1	0.17	1.08	0.24
30	11.1	0.17	0.90	0.20
100	11.9	0.11	0.79	0.17

TABLE 3

REACTIONS BETWEEN BASALT FILLER AND SOAP SOLUTION

Alkali Surplus (%)	pH Before Exper.[a]	pH After Exper.[a]
0	9.6	8.5
10	10.1	9.3
30	11.1	9.9
100	11.9	11.2

[a]Addition of basalt filler.

limestone, as this stone showed relatively large Weber and Bechler numbers in emulsions rich in alkali. Mattson and Larrson (21, p. 129) have determined by using bentonite that Ca is bound more strongly than NH_4 with increasing pH, which agrees with the results shown in Figure 10.

REACTIONS BETWEEN STONE AND SOAP SOLUTION

The Ca and Mg exchange was determined by letting 40 g 0.5 to 1 mm crushed stone react for 1 hr with 100 ml 0.05 N potassium oleate (KOl). The liquid was then decanted off and the crushed stone was rinsed with distilled water. The Ca + Mg ion content of the decanted liquid and the rinsing water was determined by the method of Leggieri (22), that is, by boiling the Ca + Mg soaps with hydrochloric acid, filtering off the oleic acid, and titrating the filtrate with complexone. To facilitate filtering off of the oleic acid a mixture of 25 percent stearic acid and 75 percent oleic acid was used for the experiment instead of pure oleic acid. This method could not be used with Øland limestone because small particles of limestone came into the rinsing water and resulted in calcium numbers which were too large. Therefore, the Ca oleate amount was determined turbidimetrically in a colorimeter by Lange's method.

The results of these determinations are given in Table 2. The amounts of Ca + Mg ions displaced in 0.05 N KOl is a little smaller than earlier found in 0.05 N NH_4Ac. The small amount of exchange, in spite of the poor solubility of the calcium oleate, may be because the potassium ions are bound in the ion atmosphere around the micelles, which diminishes their ability to displace Ca ions. It is also found that the exchange decreases with increasing pH, especially when considering that a 0.05 N KOl solution with 100 percent KOH surplus is 0.1 N with regard to K ions and, therefore, judging from the results with NH_4Ac, should give 1.5 times more Ca + Mg than 0.05 N KOl without any surplus of KOH.

As mentioned earlier, Keppeler, Blankenstein, and Borchers (14) declare that the turbidity which may be observed in a soap solution on reaction with an aggregate is due to precipitated fatty acid. This obviously cannot be correct: the precipitate must at any rate partly consist of calcium soap. To clear up this problem, 40 g aggregate, 0.5 to 1 mm, was again reacted for 1 hr with 0.05 N KOl. The stones were removed and rinsed, and the soap water and rinsing water were evaporated to dryness on a steam bath. The residue was extracted with boiling 96 percent alcohol, and the fatty acid was titrated potentiometrically with a glass electrode to pH 10. A control experiment was conducted without addition of stone. Results in milliequivalents per 100 g were 0.09 fatty acid and 1.03 Ca + Mg for basalt, no fatty acid and 0.18 Ca + Mg for granite, and -0.48 fatty acid and 0.23 Ca + Mg for limestone. This shows that in a reaction between a KOl solution and aggregate, only small amounts of fatty acid are disengaged, compared with the amount of Ca + Mg oleate precipitated. Øland limestone even binds fatty acid.

If 40 g basalt filler (particle size less than 0.076 mm) is added to 100 g 0.05 N KOl, pH decreases an average of 0.9 after 1 hr (Table 3).

EXPERIMENTS WITH AGGREGATES SUBJECTED TO CATION EXCHANGE

Table 4 indicates the result of measurements of acid action in KOH, Ca and Ca + Mg exchange in NH_4Ac, and Weber and Bechler numbers for Emulsions 6 and 8 in reaction with basalt which has been subjected to different cation exchange treatments. Calcium chloride treatment consisted of placing 200 g basalt in 0.5 liter 1N $CaCl_2$ for 30 min, then replacing the $CaCl_2$ solution with fresh solution. This is repeated seven times. The basalt was rinsed ten times for 15-min periods with 1 liter distilled water each time until the rinsing water was free of chloride. Then the stones were dried. Table 4 indicates that, whereas the Ca + Mg numbers have increased 20 percent, the Weber and Bechler numbers and the acid action are almost unaltered by the treatment.

The procedure with KOH was the same as that just described with $CaCl_2$; it was, however, necessary to use 5 N instead of 1 N solution to passivate the stones sufficiently. With the treatment, the acid action and the contents of Ca and Ca + Mg are reduced to approximately 20 percent of the original value. The Weber and Bechler numbers obtained with both emulsions are very small.

This experiment has produced both a reduction of the acid action of the stones on accountof the added OH ions and an exchange of the bivalent metal ions with monovalent ions. Therefore, there is a special interest in the next experiment, in which the basalt is treated with 1 N NaCl. The Na ions have a greater ability for ion exchange with the hydrogen ions of the aggregate than do the Ca ions; the acid action decreases to about half the original value. This is still a rather considerable acid action, and it is, therefore, surprising that the Weber and Bechler numbers are now practically zero. This should be a strong argument against the acid action theory.

The content of Ca + Mg is reduced still more than in the alkaline exchange liquid in the previous experiment. This is in agreement with the results of the measurement of the dependence of the exchange in KCl on pH: the Ca ions had relatively little tendency to be exchanged by monovalent cations at high pH.

An unsuccessful attempt was made to neutralize the acid action of the basalt by treating with $Ca(OH)_2$. In saturated $Ca(OH)_2$ solution, the OH ion concentration is so small that there is little reduction of acid action. The high Ca + Mg numbers show once more that Ca is strongly bound at high pH.

When basalt was treated with $MgSO_4$, the Weber and Bechler numbers were not very high; indeed, for Emulsion 8 the number was zero. The reason for this is that Mg in the emulsion containing OH ions is precipitated as $Mg(OH)_2$ which is less soluble than $MgOl_2$.

When basalt was treated with 1 N acetic acid (hydrochloric acid corrodes basalt strongly), the content of exchangeable Ca ions was reduced to 16 percent of the original value. At the same time the acid action increased so that H + Cawas about the same as before treatment. The Weber and Bechler numbers for Emulsion 6 were rather high.

TABLE 4

CATION EXCHANGE TREATMENTS OF BASALT

Treatment	H (meq/100g)	Ca (meq/100g)	Ca + Mg (meq/100g)	Weber and Bechler No.	
				Emul. 6	Emul. 8
None	3.12	2.29	2.63	19.1	0.85
$CaCl_2$	3.33	3.17	3.17	20.70	0.85
NaOH	0.62	0.51	0.55	0.82	0.02
NaCl	1.42	0.064	—	0.19	0.02
$Ca(OH)_2$	2.18	4.25	4.31	18.9	2.65
$MgSO_4$	4.43	0.25	2.95	18.0	0
HAc	4.80	0.37	—	13.61	0.17

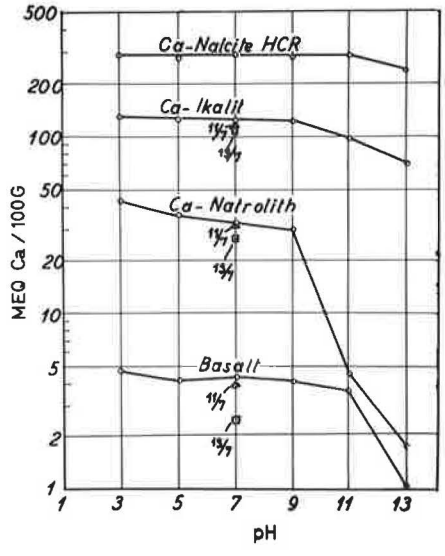

Figure 11. Dependence of Ca ion exchange on pH of exchange solution.

The hydrogen ions taken up by exchange were rather loosely bound in contrast to those after treatment with NaCl. The amount of fatty acid disengaged by the reaction between basalt treated with HAc and soap solution was also rather high, 0.80 meq/100 g, as compared with 0.09 meq/100 g for untreated basalt. The Weber and Bechler number for Emulsion 8 is very low. Emulsions rich in alkali are not sensitive to aggregates with great acid action when the content of the stones of exchangeable Ca ions is small.

EXPERIMENTS WITH WATER-SOFTENING ION EXCHANGERS

Some experiments were made with three anion exchangers with large exchange capacities. Figure 11 shows the pH dependence of the ion exchange expressed as milliequivalents Ca displaced by the reaction for 1 hr with 1N KCl for three water-softening ion exchangers in Ca form; the earlier measured numbers for basalt are indicated for comparison. The ion exchangers used were Nalcite HCR, an ion exchange resin produced by Dow Chemical Corp.; Natrolith, a product produced by burning an ion exchanging clay from Sweden; and Ikalit, a tuff from Iceland. Because of the high ion exchange capacities, only 2 g Natrolith, 0.2 g Nalcite HCR, and 0.6 g Ikalit were used with 100 g 1N KCl to determine ion exchange.

The curves show that the exchange capacities of the water-softening ion exchangers are up to 75 times greater than that of basalt, and also that the decrease of the exchange capacities with increasing pH is very different: quite small for Nalcite HCR, larger for Ikalit and much larger for Natrolith. The great decrease of the exchange ability might perhaps be due to a destruction of the material in the strongly alkaline liquids. The points marked 11/7 and 13/7 show the ion exchange in materials exposed for half the time to the influence of the exchange liquid at a pH of 11 and 13, respectively, and half the time at a pH of 7. Even the 13/7 points are not very much lower than the curves; therefore, destruction of the materials at high pH cannot be the main cause for the decrease of exchange capability.

In Table 5, the acid action, the Ca exchange and the Weber and Bechler numbers against Emulsion 7 for the anion exchangers are given. For the Ca form of the inorganic

TABLE 5

PROPERTIES OF WATER-SOFTENING ION EXCHANGERS

Ion Exchangers	H in 0.05N KOH	Solid/100 ml Liquid (g)	Ca in 1N KOl	Ca in 0.1N NH_4Ol	Solid/100 ml Liquid (g)	W-B No. Emul. 7
Ca-Natrolith	22.2	4	32	18.7	2	31.8
Ca-Nalcite	6.5	12	299	89	0.2	7.24
Ca-Ikalit	65.4	1.2	126	—	0.6	—
Basalt	3.12	40	4.4	2.63	40	14.8
H-Nalcite	143	1.5	—	0.14	2	57
K-Natrolith	8.3	4	—	0.9	2	0

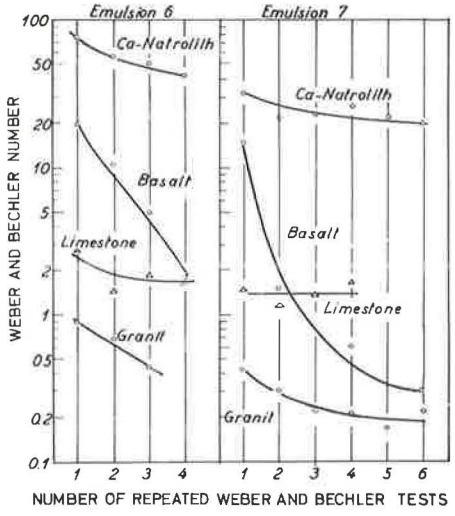

Figure 12. Blocking of stone surfaces by coagulated asphalt restrains ion reactions.

ion exchangers, the proportion between acid action and Ca exchange is nearly the same as for basalt, whereas the ion exchange resin Nalcite HCR has a minimal acid action considering the great ion exchange capacity. Wiklander (21, p. 138) mentions that the ranking of the displacement ability of the ions will be Ca > K > H for ion exchangers containing strong acid groups such as Nalcite HCR; this is in agreement with the fact that the acid action is small in Nalcite HCR when treated with $CaCl_2$. For ion exchangers with weaker acidic qualities, such as the inorganic ion exchanger Permutit, the ranking changes to K < Ca < H, which agrees with the facts that there still existed a great acid action in Natrolith and basalt after treatment with $CaCl_2$, and that a small Ca content existed in the basalt treated with acetic acid. However, it does not agree with Wiklander's experiences that the acid action for basalt and, as later shown, for Natrolith is reduced by treatment with alkali metal chloride, whereas it is not reduced by treatment with calcium chloride.

The Weber and Bechler numbers for Ca-Natrolith are only about twice the numbers for the basalt, although its ion exchange numbers and acid action are many times greater than that of the basalt. Also, Ca-Nalcite shows astonishingly small Weber and Bechler numbers, especially when considering its low specific weight. Ca-Nalcite has a relatively small acid action; therefore, a sample was made of H-Nalcite by leaching with hydrochloric acid; it had a great breaking ability. The superior breaking ability of H-Nalcite agrees with the previously mentioned displacement ranking: it is easier for the K ions of the emulsion to displace H ions than Ca ions.

The K-Natrolith in Table 5 was produced by leaching Ca-Natrolith with KCl. The acid action decreased considerably as in the earlier mentioned corresponding basalt experiment, whereas the Weber and Bechler number decreased to about zero as a consequence of the exchange.

Unfortunately, Ikalit proved to be unfit for determination of the Weber and Bechler numbers, losing all its strength and crumbling away due to drying out.

BLOCKING OF STONE SURFACES

Figure 12 shows the result of a series of Weber and Bechler number determinations on the same aggregate with Emulsions 6 and 7, in which the aggregate was rinsed free from bitumen with benzene in between the experiments. The Weber and Bechler number was 19.1 for Emulsion 6 and untreated basalt, in which the content of Ca ions exchangeable in 0.1 N NH_4Ac and the acid action against 0.05 N KOH were 2.63 and 3.12 meq/100 g, respectively. After the coagulated bitumen was removed, a Weber and Bechler number of 10.4 was measured on the same aggregate. This was repeated four times. The Weber and Bechler number decreased to only 1.8 after the fourth experiment. If the stones were again rinsed with benzene, 0.24 and 1.18 meq/100 g would be found for the exchangeable Ca ions and the acid action, respectively. In the experiments with Emulsion 7, which is richer in alkali, the Weber and Bechler number decreased still more with the number of experiments. At the same time the content of exchangeable Ca ions and the acid action decreased to 0.58 and 0.52 meq/100 g, respectively, after the sixth experiment. The Ca exchange occurs slower in the more alkaline emulsion; this agrees with the earlier mentioned dependence of the Ca exchange on pH.

The Øland limestone behaves quite differently from basalt: the breaking numbers change little in the repeated Weber and Bechler experiments, and the amount of Ca dis-

solved in NH_4Ac also stays constant. Whereas basalt has a breaking action in these experiments until the exchangeable Ca ions are used, the breaking ability of the Øland limestone will not change. The reaction between soap solution and aggregate does not have the character of ion exchange here.

Granite shows small Weber and Bechler numbers which decrease on repeating the experiments, as do the basalt numbers, but at a somewhat slower rate.

The Weber and Bechler numbers for Ca-Natrolith are high, but not as high as expected from the great ion exchange capacity because the coagulated bitumen also blocks up the stone surfaces. The Ca and H numbers decrease less with the number of experiments than in the case of basalt: from 18.9 and 22.2, respectively, for untreated Ca-Natrolith to 15.0 and 17.3 after the fourth Weber and Bechler experiment with Emulsion 6 and to 9.8 and 13.1 after the sixth experiment with Emulsion 7.

It may be added that the Weber and Bechler numbers are only increased by 8 percent when the time in the Weber and Bechler experiment with Emulsion 7 and basalt is increased from 1 to 4 hr, so that the facts shown on the curve cannot be explained by a longer reaction time.

ADHESION BETWEEN STONE AND BINDER—CONCLUDING REMARKS

From the preceding experiments, it appears that there is no simple connection between the ion exchange and the Weber and Bechler numbers. At most, a connection might be expected between the ion exchange and the amounts of bitumen coagulated in many repeated Weber and Bechler experiments accumulated by benzene extraction. That would be a very time-consuming operation and would have very little relation to what happens in practice.

The blocking-up of the stone surfaces with coagulated bitumen is closely connected with the problem which is highly discussed in the asphalt literature: the adhesion between asphalt bitumen and wet aggregates. Riedel and Weber (23) have tried to measure the adhesion by visually judging the displacement of bitumen from the stone surface on boiling with water. If the aggregate-bitumen combination passed this test, an attempt was made to use a displacement liquid with better wetting properties than water. Riedel and Weber repeated their boiling test with a series of soap solutions with increasing concentration, and used the concentration of the soap solution which just could displace the bitumen from the stone as a measure for the adhesion. Later Riedel and Weber found out that the differentiation became better when using a series of soda solutions with increasing concentrations. These experiments indicated that aqueous alkali solutions will more thoroughly prevent the contact of the stone-binder with a more alkaline solution.

This is certainly the cause contributing most highly to the decrease of breaking numbers in very alkaline emulsions. In the emulsions rich in alkali, the bitumen particles will be kept away from the stone surfaces. Therefore, the Ca ions displaced by ion exchange must preferably react to make insoluble Ca soap with the fatty acid ions which have not been adsorbed on the bitumen drops, but are distributed molecularly dispersed or as micelles in the dispersing medium. The decrease of the breaking with increasing alkalinity is supported by the fact that the Ca ion exchange decreases with increasing pH.

In emulsions with smaller alkalinity, the repulsion between the bitumen drops and the stone surface will be less, so that the Ca ions displaced by ion exchange will be able to precipitate Ca soap from the fatty acid anions which have been adsorbed on the bitumen drops. This may be counteracted to some extent by increasing the amount of fatty acid in the emulsion; the emulsions rich in fatty acid also proved to be more stable than the emulsions poor in fatty acid.

The earlier found correspondence between breaking and acid action is due to the fact that many aggregates (but not limestone) with high acid action also possess many exchangeable Ca ions. The experiments with basalt treated with NaCl and Natrolith treated with KCl show, however, that it is possible to make aggregates which, in spite of a rather high acid action, have a small breaking activity. By the alkali chloride treatment, the acidic action decreased somewhat; some of the most easily exchangeable hydrogen ions must have been displaced. The remaining hydrogen ions are bound so

TABLE 6

ADHESION TENSION MEASUREMENTS

Aggregate	Treatment	P (cm H_2O)	p (cm H_2O)	A (dynes/cm)
Basalt	Untreated	55.3	9.0	11.7
	NaCl completely		1.25	1.6
	NaOH completely		< 0.5	< 0.6
	NaOH partly		4.5	5.8
Granite	Untreated	60.8	7.5	8.9
	NaCl completely		0.75	0.9
	NaOH completely		< 0.5	< 0.6
	NaOH partly		4.5	5.3
Øland limestone	Untreated	63.9	11.5	13.0
	NaCl completely		11.5	13.0
	NaOH completely		9.5	10.8
	NaOH partly		10.0	11.2

strongly that they have not been able to disturb the hydrolysis balance of the soap sufficiently to cause coagulation.

Some of the hydrogen ions in the ion exchange resin Nalcite HCl treated with hydrochloric acid are bound so loosely that there is a certain breaking ability although the content of exchangeable Ca ions is zero.

It would be interesting to be able to judge the adhesive ability between asphalt bitumen and stone in contact with a soap solution. In the English immersion tray test (24), water (in this case, soap solution) is poured onto a layer of asphalt. A stone is put through the layer of water and pressed into the layer of asphalt. After 5 min the stone is removed and it is visually assessed if the stone is wetted with asphalt. An experiment with 0.5 to 1 mm stones, fixed by a small pair of tweezers, shows that all aggregates, with exception of the ion exchange resin Nalcite HCR (both H-, Ca-, and K-Nalcite), have insufficient adhesion. However, Nalcite showed the greatest disproportion between a great ion exchange capacity and a relatively small Weber and Bechler number.

The adhesion of the aggregates which did not pass this test (that is, basalt, granite and Øland limestone) was examined by the Bartell-Halberg displacement cell (25). The principle here is that a column of stone powder with a particle size of 0.10 to 0.15 mm is soaked with 67 percent solution of bitumen 300 in mineral turpentine with a viscosity of 225 cP at 25 C. After 15 min a certain minimal water pressure, p, in dynes per square centimeter is applied to attempt to displace the binder with water. The experiment is repeated with the stone column soaked with water, and a measurement is taken of the air pressure, P, which is just sufficient to displace the water from the stone column. Because the surface tension of the water is 72 dyne/cm, the adhesion tension, A, of the binder (the product of the water-binder interfacial tension and cosine of the contact angle) may be expressed as follows:

$$A = 72\ p/P \text{ dyne/cm} \qquad (1)$$

In the experiments, measurements were included of the aggregates after they have been treated thoroughly with NaCl and NaOH followed with rinsing with distilled water. In Table 6, the results are given for complete exchange. The results of measurements with stones treated with 0.05 N NaOH for 1 hr (200 g stone with 1 liter NaOH) followed by a thorough rinsing are also shown as partly exchanged. It is seen how the adhesion decreases with exchange with Na. NaCl is not as effective as NaOH. Riedel and Weber (23) have already ascertained the bitumen-displacing action of NaCl solutions. The reason must be found in the exchangeable Ca ions being replaced by Na ions, with reduced adhesive ability as a consequence. Nüssel and Buhs (26) have found that an emulsion

becomes more stable on addition of KCl. For the limestone which does not have ion-exchanging qualities, a treatment with NaCl or NaOH has little influence. This is in good agreement with the fact that the Øland limestone is the aggregate with the greatest blocking-up tendency against alkaline emulsions and with breaking numbers reduced least against emulsions where the NaOH surplus increased.

The conclusion must be that the breaking in a Weber and Bechler experiment is chiefly caused by the destruction of the emulsifier by formation of insoluble Ca and Mg soaps. The examined anion emulsions will convert the aggregates according to their greater or smaller ion exchange ability into aggregates with more or less diminished adhesion properties. At the same time, Ca ions are disengaged in an amount dependent on the pH of the emulsion, as well as on the ion exchange capacity, the content of calcium carbonate, and on the degree of the blocking-up of the stone surface by coagulated bitumen. These Ca ions will precipitate Ca soap both from the alkali metal soap which is present as an emulsifier film around the emulsion particles, and from the alkali metal soap which is found, principally in form of micelles, in the continuous phase. The coagulation which is measured will, therefore, be dependent on the amount of fatty acid anions, on the coagulating Ca ions available, and on the way these Ca ions distribute themselves between the fatty acid anions in the emulsifier film and in the micelles. This distribution is again dependent on the attraction between the stone and the asphalt bitumen that manifests itself in the measured adhesive ability which decreases with increasing content of KOH in the water phase.

The acid action of the stones or the adsorption of emulsifier (27), which earlier was thought to be the most important cause of the breaking, seems to be of less importance.

REFERENCES

1. Weber, H., "Über den Zerfall Bituminöser Strassenbau-Emulsionen am Gestein." Proc. World Petroleum Cong., Vol. G, pp. 669-673 (1933).
2. McKesson, C. L., "Modern Paving Emulsions, Types, Characteristics and Test Methods." Proc. ASTM, American Society for Testing, 31(Pt II):841-850 (1931).
3. Riis, A., "Contribution from the Danish Government Laboratory for Road Research on the Methods for Testing Asphaltic Bitumen Road Emulsion Employed in Denmark." Proc. World Petroleum Cong., Vol. G, pp. 630-641 (1933).
4. Kell, K., "Untersuchungen über den Zerfallswert der Bituminösen Strassenbau-Emulsion." Bitumen, 3:11-17 (1933).
5. Harsch, R., and Spotswood, E. H., "Relation of the Demulsibility Test to the Rate of Break of Asphalt Emulsion." Proc. AAPT, 12:184-205 (1940).
6. Caroselli, A., "Methode zur Bestimmung der Brechbarkeit von Bitumenemulsionen." Bitumen, 6:61-65 (1936).
7. Klinkmann, G. H., "Ueber die Brechung Bituminöser Emulsionen am Gestein." Asphalt und Teer, 33:842-841, 873-876, 893-896.
8. Nasini, A. G., and Rossi, C., "Sulla Rottura delle Emulsioni in Contatto con Solidi." Trabajos del IX Cong. Internat. de Quimica Pura y Aplicado, 2(384): 1-15 (1934).
9. Nasini, A. G., and Rossi, C., "Stabilita di Emulsioni Concentrati in Presenza di Elektroliti." Monografie Casa Editrice Tamtruzini, Milano (1940).
10. Bohn, A. O., and Mikkelsen, N. M., "Asfaltemulsioners Stabilitet." Dansk Vejtidsskrift, 20:130-139 (1943).
11. Meddelelser fra Vejlaboratoriet nr. 16 Vejkomiteen, G. E. C. Gad, København (1938).
12. Jekel, O., "Über den Zerfall Bituminöser Strassenbau-Emulsionen." Ö. P. I.-Veröffentlichung 10, Verlag für Fachlitteratur, Wien (1938).
13. Neubronner, K., "Über die Anwendung der J. Myer'schen Entemulgierungsmethode auf Kaltasphalte." Asphalt und Teer, 33:10-13 (1933).
14. Keppeler, G., Blankenstein, P., and Borchers, H., "Die 'Brechbarkeit' von Bitumenemulsionen und ihre Beeinflussung." Angew. Chem., 47:228-229 (1934).

15. Williams, H. G., "pH Determinations of Water in Contact with Stones." Jour. Soc. Chem. Ind., 62:269-312 (1963).
16. Vogt, J. C., "Considérations sur les Dopes et les Emulsions." Rev. Gén. des Routes et des Aerodromes, 28(319):55-65 (1958).
17. Fuerstenau, D. W., "Streaming Potential Studies on Quartz in Solutions of Ammonium Acetates in Relation to the Formation of Hemimicelles at the Quartz-Solution Interface." Jour. Phys. Chem., 60:981-985 (1956).
18. Hildebrand, G. P., and Reilley, C. N., "New Indicator for Complexometric Titration of Calcium in Presence of Magnesium." Anal. Chem., 29:258-264 (1957).
19. Diehl, H., Goetz, C. A., and Hach, C. C., "Versenate Titration for Total Hardness." Jour. Amer. Water Work Assoc., 42:40-48 (1950).
20. Martin, A. R., and Hermann, R. N., "Emulsions. Part II. Partial Coagulation of a Standard Emulsion in Sodium Oleate Solution by Salts of Some Bi- and Higher Valent Metals." Trans. Faraday Soc., 37:30-38 (1941).
21. Bear, F. E., "Chemistry of the Soil." Reinhold Publishing Corp., New York (1955).
22. Leggieri, G., "Sull'analisi dei Naftenati Metallici Mediante il Metodo dei Complessoni." Chimica (Milano), 10:287-288 (1955).
23. Riedel, W., and Weber, H., "Ueber die Haftfestigkeit Bituminöser Bindemittel an Gesteinen." Asphalt und Teer, 33:677-680, 693-695, 713-718, 729-732, 749-751, 793-798, 809-812(1933).
24. "Preventing of Wet-Weather Damage to Surface Dressings." Road Res. Lab., Road Note 14, 2nd Ed.
25. Hallberg, S., "The Adhesion of Bituminous Binders and Aggregates in the Presence of Water." Meddelande 78 Statens Väginstitut, Stockholm (1950).
26. Nüssel, H., and Buhs, A., "Bitumen Emulsionen. Neuere Fortschritte in der Kenntnis ihrer Eigenschaften." Bitumen, Teere, Asphalte, Peche und Verwandte Stoffe, 7:423-427, 444-449 (1956); pp. 15-17 (1957).
27. Vogt, J. C., "Nouvelles Recherches sur les Mécanismes d'Adsorption des Composés Superficiellement Actifs en Relation avec la Technique Routiére." Rev. Gén. des Routes et des Aérodromes, 30(337):45-60 (1960).